THE INVESTIGATION INTO THE CONDITION MONITORING OF TRIBOLOGICAL BEHAVIOUR BETWEEN PISTON RING AND CYLINDER LINER USING ACOUSTIC EMISSIONS

Nasha Wei

Supervised by

Professor Andrew D. Ball and Dr Fengshou Gu

07th November 2017

School of Computing and Engineering

University of Huddersfield

LIST OF CONTENTS

LIST OF FIGURES

The hard threshold method based LED results have been corrected as show in section 7.4 and 7.5 from the Figure 10-1 to Figure 10-2. The hard threshed results showed tiny consistent differences between two new lubricants in downward strokes whereas they

LIST OF TABLES

LIST OF NOMENCLATURE

A_e	*Contact spot of fully elastic area for a hemisphere*
A_o	*Total apparent contact area*
a_e	*Approximated radius of* A_e
$a_{J,k}$	*Approximation coefficients*
a_0	*constant at atmospheric pressure*
a_w	*Dilation index*
b	*Ring face-width*
b_w	*Translation index*
D	*Number of asperities per unit area*
$d_{j,k}$	*Detailed coefficients*
$d(x_{rE}, \tilde{v}_p)$	*The normalised correlation distance*
E_b	*Elasticity modulus for material of cylinder liner*
E_r	*Elasticity modulus for material of piston ring*
E'	*Effective elasticity modulus of the contact surfaces*
E'	*The Hertzian contact modulus*
$E1, E2$	*The Yong's modulus of the contact materials*
f_{asp}	*Asperity friction*
F_e	*Tension force of ring*
F_g	*Combustion gas force*

$F_n(h)$ *Probability density function of randomly variable h*

F_s *The stress force induced by the lubricants*

F_{TO} *The total applied load*

f_v *Viscous friction*

$f(t_w)$ *Continuous wavelet transform of a signal*

f(z) *Probability density function (PDF) of the asperity height z*

h *Film thickness*

$\mathrm{K_c}$ *The conversion rate of elastic strain energy to AE energy*

$\mathrm{k_e}$ *The energy conversion rate that the elastic strain energy converts to AE pulses;*

$\mathrm{k_m}$ *The energy conversion rate gained from the AE measurement system*

l *The rod length*

L_e *The elastic load on a spot*

L_n *The load projected on to the geometrical surface*

N *The total number of asperities*

N_d *The total number of data*

P *Pressure*

$\bar{P}$ *Average pressure*

p_{asp} *Asperity contact pressure*

p_g *The combustion pressure*

p_h *The hydrodynamic pressure generated in the film*

R *The radius of hemisphere*

r *The crank radius*

$r(x_r, v_p)$ *The normalised correlation between the envelope sequence* x_r *and the pston velocity* v_p

T_1, T_2 *Correlation parameter of the Vogel equation*

T_m *Mean oil film temperature*

T_e *The time to release the elastic energy for one asperity*

$\overline{T}_e$ *The mean release time of elastic deformation*

U *Speed of entraining motion*

U_{AE} *The energy of acoustic emission signal*

$\dot{U}_{AE}$ *The power of the AE energy excited by the friction power*

U_{ie} *The elastic energy stored in individual asperity contact*

$\overline{U}_{ie}$ *The mean elastic energy for per unit hemisphere joined area*

U_E *The total elastic energy stored in the asperity contacts*

$\dot{U}_E$ *The elastic energy release rate of asperity contacts*

$\dot{U}_s$ *The power of the fluid stress force*

$\dot{U}_f$ *The power of the AE energy excited by the friction power*

v1, v2 *The Poisson's ratios of the contact materials*

V_s *The rotational speed*

v_p *Piston or ring sliding velocity*

v_{x_p} *The speed with respect to crank angle*

v_p^{T} *The modified velocity*

W_{TO} *The total contact load*

W_A *The asperity contact force*

W_O *The film pressure force*

W_j	*The wavelet coefficients*
W_k	*The WPT spectra*
x	*Direction along the ring movement*
x_p	*Piston displacement from TDC*
x_r	*The envelope sequence reconstructed by wavelet coefficients*
z	*The height from the asperity surface to reference plane*
Z_p	*Constant independent of pressure*
α	*The angle of the con-rod made with the vertical*
β	*The asperity radius of curvature*
β_n	*viscosity–temperature coefficient.*
β_T	*Thermal expansion coefficient of the lubricant*
φ_x	*Pressure flow factors*
φ_s	*Shear flow factor*
φ_c	*Contact factor*
$\phi(s)$	*The Gaussian function representing the distribution characteristics of the asperity with respect its standard deviation s asperity heights*
$\psi^*(t_w)$	*The complex conjugate of function* $\psi(t_w)$
Ψ_{a_w,b_w}	*The mother wavelet function*
θ	*Crank angle displacement*
μ_{asp}	*The coefficient of asperity friction*
τ_{ij}	*Average shear stress*
η	*The dynamic viscosity*
ρ	*Lubricant density*

ρ_0	*Bulk lubricant density at ambient pressure*
δ_e	*The deformed distance during elastic deformation*
δ_p	*The deformed distance during plastic deformation*
σ_s	*The standard deviation of the asperity heights*
σ_1, σ_2	*The roughness of two engineering surfaces*
σ	*The composite roughness of the ring and liner*
ω	*Angular speed*
$\vartheta_j(i_{tr}, t)$	*The time varying threshold*

ABSTRACT

To improve engine operational performance and reliability, this study focuses on the investigation into the behaviour of tribological conjunction between the ring-liner based on a comprehensive analysis of non-intrusive acoustic emission (AE) measurement. Particularly, the study will provide more knowledge of using AE for online monitoring and diagnosing the performances of the conjunction.

To fulfil this study, it integrates analytical predictions of the theoretical modelling for the AE generation mechanism with extensive experimental evaluations. Moreover, effective signal processing techniques are implemented with a combination of the model based AE predictions to extract the weak and nonstationary AE contents that correlate more with the tribological behaviour.

Based on conventional tribological models, tribological AE is modelled to be due to two main dynamic effects: asperity-asperity collision (AAC) and fluid-asperity interaction (FAI), which allows measured AE signals from the tribological conjunction to be explained under different scenarios, especially under abnormal behaviours. FAI induced AE is more correlated with lubricants and velocity. It presents mainly in the middle of engine strokes but is much weaker and severely interfered with AEs from not only valve landings, combustion and fuel injection shocks but also the effect of considerable AACs due to direct contacts and solid particles in oils.

To extract weak AEs for accurately diagnosing the tribological behaviours, wavelet transform analysis is applied to AE signals with three novel schemes: 1) hard threshold based wavelet coefficients selection in which the threshold value and wavelet analysis parameters are determined using a modified velocity of piston motion which has high dependence on the AE characteristics predicted by the two models; 2) Adaptive threshold wavelet coefficients selection in which the threshold is gradually updated to minimise the distance between the AE envelopes and the predicted dependence; and 3) wavelet packet transform (WPT) analysis is carried out by an optimised Daubechies wavelet through a novel approach based on minimising the time and frequency overlaps in WPT spectrum. Based on these optimal analyses, the local envelope amplitude (LEA)

and the average residual wavelet coefficient (ARWC) are developed from AE signals as novel indicators to reflect the tribological behaviours.

Both the hard threshold based LEA and wavelet packet transform LEA values allow two different new lubricants to be diagnosed in accordance with model predictions whereas they produce less consistent results in differentiating the used oil under several operating conditions. Nevertheless, ARWC can separate the used oil successfully in that it can highlight the AAC effects of particle collisions in used oils.

Similarly, LEA shows little impacts of two alternative fuels on the tribological behaviours. However, ARWC shows significantly higher amplitudes in several operating conditions when more particles can be produced due to unstable and incomplete combustions of both the biodiesel and FT diesel, compared with pure diesel, indicating they can cause light wear.

Keywords: Acoustic Emission; Piston Ring; Cylinder Liner; Optimal Wavelet Basis; Wavelet Packets Transform; Tribological Behaviour; Alternative Fuels;

DECLARATION

I declare this Ph.D. thesis was carried out for the degree of Doctor of Philosophy at the University of Huddersfield. This dissertation represents my own work.

The contribution of any others to the research and to the thesis was consistent with the regulations of the University of Huddersfield.

For this thesis, which I am submitting to the University of Huddersfield, there is no similar thesis or dissertation which has been or is being submitted in any other University.

ACKNOWLEDGEMENT

I would like to acknowledge the Centre for Efficiency and Performance Engineering (CEPE) and School of Computing and Engineering at University of Huddersfield, UK to provide me excellent research environment in UK to finish this thesis. This work was financially funded by the Natural Science Foundation of China. I would like to give my grateful acknowledgements to the Taiyuan University of Technology Institute of Mechanical Engineering for their support during the work.

I would like to thank my main supervisor professor Andrew Ball for his guidance and sincere support during my research.

I am especially express appreciations to my co-supervisor Dr Fengshou Gu. his sincerely patient support and abundant experience guided me with a broaden vision in the condition monitoring fields field and provided me with a lot of valuable advises.

I would like to thank professor Tie Wang for provides me with an excellent experimental and research environment in Taiyuan University of Technology.

I would like to express my gratitude to my friends and associates in Huddersfield especially Dr Dong Zhen, Dr Xiang'e Tian, Dr Guojin Feng, Dr Ruichen Wang, Dr.Guoxing Li, Yuandong Xu and Xiaoli Tang for their professional advice and kind-hearted care in life.

My thanks are also to the research group members in the Taiyuan University of Technology Institute of mechanical engineering for their warm-hearted help and efficient cooperation.

Finally, I would like to express my appreciations to my parents and my husband for their long-term supporting and understanding of my study.

LIST OF PUBLICATIONS

[1] Wei N., Gu F., Wang T., Li G. ,Xu Y., Yang L., Ball A.(2015) "Characterisation of Acoustic Emissions for the Frictional Effect in Engines using Wavelets based Multi-resolution Analysis",In: 21st International Conference on Automation & Computing, 11th-12th September, 2015,University of Strathclyde,Glasgow, UK

[2] Wei, N., Gu, F., Li, G., Wang, T. and Ball, A. (2014) 'Characterising the friction and wear of the ring-liner system based on acoustic emission analysis'. In: 21st International Congress on Sound and Vibration, 13th - 17th July, 2014, Beijing, China

[3] Wei, N., Ball, A. and Gu, F. (2013) 'A Study of Alternative Fuels Potential Effects on the Combustion Engines using acoustic emission'. In: Proceedings of Computing and Engineering Annual Researchers' Conference 2013 : CEARC'13. Huddersfield: University of Huddersfield. p. 239. ISBN 9781862181212

[4] Towsyfyan H., Wei N., Gu F., Ball A.(2015) "Identification of lubrication Regimes in Mechanical Seals using Acoustic Emission for Condition Monitoring", In: 54th Annual Conference on NDT, 8th-10th September, 2015, Telford, UK.

[5] Osama A. Hassin, Nasha Wei, Hossein Towsyfyan, Fengshou Gu, Andrew D.Ball (2015) ''Journal bearing lubrication monitoring based on spectrum cluster analysis of vibration signals", In: 28th International Congress of Condition Monitoring and Diagnostic Engineering 10th Regional Congress on Non Destructive and Structural Testing, 1st -4th December, 2015 ,Buenos Aires, Argentina.

CHAPTER 1 INTRODUCTION

This chapter presents the background and research scope of this work. It first presents background and motivation for this research work, and then discusses the challenges for monitoring the tribological behaviour of the piston assembly under running condition. Finally, the research scope, methodology and objectives of this work are given.

1.1 Background and Motivation

1.1.1 Necessity for Monitoring the Tribological Behaviour of Piston Assemblies

Tribology, as named by Jost [1] in 1966, was defined as 'the science and practice of interacting surfaces in relative motion'. In an internal combustion engine system, the tribology behaviour is principally associated with friction, wear, corrosion, degradation on the surface, and energy losses as suggested in [2]. As prime power sources, IC engines are widely employed in different industries such as various means of transport and power stations. The fuel efficiency, reliability, stability, lifetime and environmental sustainability are the ultimate targets of engine industry. Remarkably, the improvement of tribological behaviour can be one of the most essential and rewarding approaches to accomplish the above targets. In addition, the recent crises of fuel depletion and environmental degradation have promoted more investigations into the possibility of using alternative fuels, instead of fossil fuels, which means that the substitute power sources are expected not only to show the better combustion performance with lower emissions but also maintain the acceptable tribological performance of using pure diesel.

Among various tribological conjunctions in an IC engine, the piston ring-cylinder liner system is the most important and complicated one. Its performance is decisive to maintain high combustion performance and low emissions. Tough working conditions with highly varying temperature, pressure, velocity and load can cause significant influences on its lifetime. Moreover, it is suggested that more than 30% of the petroleum is used to overcome friction in passenger cars [3], especially, the piston ring and cylinder liner are demonstrated to account for a substantial portion of engine friction losses [4]. Therefore, the tribological behaviour of the ring-liner system has been recognised as the most important aspect to affect the engine performance [5].

To gain sufficient understandings of the tribological behaviour of the ring-liner system, great deals of research works were carried out on developing more comprehensive models and detailed simulations. Considerable achievements in the tribological modelling and numerical simulation studies between the ring and liner were solved by the average Reynolds equation[6, 7] based on a general understanding of the piston rings operated in the mixed lubrication regime[8]. More extensively, numerous

sophisticated computing studies were conducted for the investigation into a wide range of practical impacts during ring-bore contacts such as piston ring profile, piston ring twist, blow-by, cylinder profile and thermal deformation, lubricant cavitation, and the conformability of the ring-bore contact. These models and findings have provided the insightful understanding of the operations for piston rings, which can subsequently be used to improve friction reduction of the piston assembly. Furthermore, a number of the other researchers [9, 10, 11] had added the wear process into the modelling of the ring-liner system to give a comprehensive understanding of the tribological process of rings and liners undergoing progressive wear. However, owing to the sophistication of engine tribology, it is difficult to combine all the important tribological parameters and factors in a model. Therefore, the experimental studies correlated with the tribological behaviour of piston rings and cylinder liners are crucial to reveal the piston tribological characteristics.

On the other hand, the piston ring lubrication is essential to the operational stability and lifetime of engines. Due to highly dynamic operating conditions of the ring-liner system, engine lubricants are subjected to different rates and hence degrees of deterioration during their service periods. Traditional oil quality monitoring is based on laboratory oil sample analysis at a given time interval, which is implemented with considerable deficiencies such as sample contaminations, high costs, and time-delayed results. Particularly, the traditional wear investigations of piston assembly generally need to dismantle engines for internal inspections after a long-term use.

Although some commercial sensors are designed for the continuous monitoring of the oil condition or oil quality, most of them are the insertion type which needs to be fixed in a single location of the system. Particularly, such sensors need to submerge into the oil channel which is fixed far away from the two sliding surface of the ring-liner. Hence, these sensors, which are located in a specific location, cannot give the accurate and timely information of ring-liner system under a nonstationary working condition in engines.

The complex mechanical apparatuses often break down accidentally without any relation to their life-cycle period [12, 13]. Wear processes of the ring-liner system are the most undesired failures of engines. The lubrication condition means the different states that the lubricant separates the two surfaces from direct contact to reduce the

friction and consequently wear. The proper lubrication condition helps to reduce premature failures and diminish the downtime of machines. To identify the significant changes which are developing to the faults in the ring-liner system, the online condition monitoring is a valuable technology for prognosis and condition monitoring based on health conditions. Particularly, the non-intrusive monitoring method can provide the comprehensive information of the ring and liner contact without any modification. Specifically, Acoustic emission (AE) is induced by the strain energy which is released spontaneously and rapidly during the deformation or fracture of materials [14]. The AE technology has been developed to diagnose the condition of engines and the friction wear process of the contact surface. Sporadic studies tried to relate the AE measurements of engines to the ring-liner wear or friction process.

All of the above investigations and achievements show a possibility to monitor the tribological process of the ring-liner system. However, there are no further understandings about friction and lubrication characteristics of the piston ring-cylinder liner to differ wear process in engines. Therefore, to monitor the tribological behaviour of the ring-liner online is necessary. That is mainly because that the real-time characteristics of the tribological process of the ring and liner contact can be used to identify the difference between the normal friction and lubrication condition and the early abnormal wear. Further, this is also a possible online approach to assess the tribological impacts of new alternative fuels on engines.

1.1.2 Challenges in Monitoring the Tribological Behaviour of the Piston Assembly under Running Conditions

Due to the complexity of the ring-liner tribology, the tribological factors and system dynamic factors such as contact force, sliding velocity, high temperatures and lubricant rheological properties such as viscosity varies nonlinearly in the engine system. This means that the tribological behaviour of the piston assembly is very complicated to be modelled and measured with sufficient accuracy that allows the true behaviours of the interactions between fluid and surface asperities to be understood adequately. Hence, there still some knowledge gaps in monitoring the tribological behaviour of the piston assembly using AE as shown in the following:

1. **Generation mechanism and modelling studies for tribological AE between two lubricated sliding surfaces in the piston assembly system are still ambiguous.**

   The piston rings work under a tough condition with highly varying temperature, pressure and velocity. The tribological behaviour of the ring-liner system is a complicated non-linear mechanical problem with regard to interdisciplinary fields. Although AE technology has been widely used to monitor the friction and wear [15, 16, 17, 18]. Most of these studies using AE were based on the experimental investigations in a design laboratory rig to reveal the AE generation regimes, rather than a real and complicated mechanical system, such as the engine. Hence, to decipher the AE generation mechanism during the friction and lubrication process of the ring-liner system, the theoretical modelling studies for the tribological AE in the ring-liner system are needed to be well studied.

   Mechefske et al. [19] investigated the wear process and wear situations with and without ZDDP additive, the results show the difference between oil with additive and the base oil. This indicates that AE can detect the presence of the protective tribofilm [20]. Particularly, Wang et.al [20] studied condition monitoring of oil lubricated hybrid sliding contacts using AE techniques, the experimental results showed a strong relationship between the AE RMS and the coefficient of friction level.

   However, there are sporadic investigations focused on the AE theoretical model in tribology processes. Sheng and Liu [21] developed the theoretical model of AE sensing process in the sliders and magnetic rigid disks system to demonstrate the variations of AE RMS amplitudes correlated to tribological factors and system dynamics factors such as contact force, sliding velocity and topographic parameters, particularly, the tested AE RMS values correlated to the lubricant thickness. Nevertheless, the AE theoretical modelling analysis of the AE generation regimes under the hydrodynamic lubrication condition was not reported. To fill this gap, a comprehensive AE theoretical modelling for the hybrid friction process need to be developed for the analytical predictions correlated to the experimental studies.

2. **Effective methods to detect the tribological AE of the ring-liner system for condition monitoring in engines have not been conducted sufficiently.**

   The previous experimental studies suggested in [22] and [23] demonstrated the possibility to detect the AE signals on the surface of the cylinder. However, the effective method to monitor the different lubrication and friction condition of the engine system were not conducted in-depth, further, specific condition monitoring approaches to detect the tribological impacts of the alternative fuels on engines were lack of the comprehensive investigation.

3. **Effective signal processing approaches are not reported for extracting the tribological features from noisy AE signals**

   Several signal processing approaches have been studied based on the burst type of AE signals with large amplitudes according to the signal energy or entropy, for the diagnostics of faults in valves and injectors. However, the AE signals induced by the tribological processes are significantly weaker than the responses to the excitations of valve movement, combustion process and other key events in engines. Wavelet techniques are effective in processing the non-stationery AE signals. The author [24] investigated the AE signals in the running engine test using different new oils to evaluate the friction and lubrication characteristics of piston assembly based on wavelet analysis with selected wavelet parameters.

   The problem is that the appropriate wavelet parameters are critically dependent on reliable and effective determination of the signal features. Hence, adaptive wavelet processing method is needed to extract the tribological AE accurately. However, there are no effective signal processing approaches reported for extracting the weak AE signals from the strong background noise. Therefore, an appropriate criterion and along with efficient implementation schemes to select suitable wavelet analysis parameters is very decisive in this study to obtain accurate and effective weak AE signals associated with engine tribological behaviour.

4. **The correlation between the AE signals and different lubrication conditions need a comprehensive understanding**

The lubrication oil can reflect the healthy state of the whole system and its key components. The lubrication oil is degraded when the oil protective properties are changed physically or chemically. However, most the oil monitoring sensors are designed intrusively which are costly and sophisticated in the measurement process.

AE testing, a special type of ultrasound method is designed to monitoring the inner generated waves owing to the material changes. The viscosity is usually believed as the one of representative indicator to evaluate the quality of lubricants[25]. Elamin and the co-workers [26, 27] reported the possibility to predict the quality of engine oil using AE RMS values owing to the AE RMS values influenced by oil viscosity. These studies demonstrated the capability to monitor the lubrication condition using AE.

However, the problems should be noted that the raw AE RMS values in a running engine contain too much information such as from valve impacts and combustion which cannot indicate the lubricating condition accurately. Moreover, the lubrication condition of engines is complicated with varying speed, load, pressure and temperature. Hence, there still need a comprehensive understanding to relate the AE sensing signals to the different lubrication regimes and the effect oil degradation for health condition morning of the engine system.

5. Potential impacts of alternative fuels on engine tribology are not fully understood for online diagnostics

Because of the environmental vulnerabilities of the fossil fuel such as global warming, smog and ozone depletion, ample investigations have been done focused on the emissions and working performance of engines fuelling alternative fuels. However, the tribological impacts of alternative fuel are still vague partly owing there are too many potential types of the alternative fuel which are hard to give the best choice. Especially, the tribological studies generally pay attention to the offline studies. Plenty of the researchers focused on the chemical and physical properties of the alternative fuel investigation, and the detrimental effect mainly on the teardown test after long-term use as reviewed in [28]. However, there is still lack of online methods to assess the

tribological impacts from using a wide range of alternative fuels in development so that a quantitative assessment of the impacts can be provided along with the combustion evaluation process.

1.1.3 Potential Signal Processing Techniques

To characterise the tribological processes using AE measurements under strong background noise in engines, effective signal processing techniques should be investigated to decipher the characteristics of the complicated AE contents in association with various lubrication regimens. From the signal processing point of view, AE signals from IC engines are typical nonstationary one of which the statistical properties including amplitudes and frequency values vary with time due to different sources such as valve impacts and combustion shocks [30]. On the contrary, there is also a wide range of stationary signals whose spectral contents are not changing with respect to time [29]. Based on this strict definition, nearly all of the condition monitoring signals from rotating machines are non-stationary. In a wide sense, the signals for a rotary system can be classified as cyclostationary signals and non-stationary signals in association with various faults.

The time-frequency analysis is an effective tool to characterise the features of nonstationary signals in the joint time-frequency plane to reveal the detailed patterns and diagnostic features for achieving more accurate diagnostics. Classical time-frequency analysis methods are the Short-time Fourier transform (STFT) and Wigner-Ville distribution [31, 32, 33].

Unlike the classical time-frequency representations, the wavelet transform (WT) uses a series of compactly supported waves, rather than the sinusoidal wave in STFT, to decompose a signal into different levels which correspond to different frequency bands. Wavelet based analysis has been successfully demonstrated to be particularly useful in the engine condition monitoring [34], as it is more effective and efficient to analyse non-stationary signals [35] which is the typical features of AE signals from IC engines.

The wavelet multi-resolution analysis (WMRA), firstly introduced by Mallat, is an efficient implementation of discrete wavelet transforms to separate the approximation signal into two parts with the different resolution by the different band passing filters at each level [36, 37]. Hence, WMRA reveals good frequency resolution around the low

frequency bands. That is beneficial to acquired AE features from a huge number of samples at MHz ranges.

Another more advanced is the wavelet packets transform (WPT) analysis which developed by Coifman, Meyer and Wickerhauser [38]. WPT is able to explore the target signals extensively for feature extractions by decomposing all the approximation and detail information into the desired levels or frequency bandwidths.

Specifically, WT techniques are also widely used for condition monitoring of many rotary mechanical systems such as gears[8, 39, 40], bearings[41, 42], diesel engines [43, 44, 45]. Especially, the authors [24] has investigated discrete wavelet transform(DWT) for the characterisation of the viscous friction using AE signals. Reference [46] applied wavelet packet decomposition to diagnose the failure of tribological systems using AE signal based on multi-resolution analysis theory. These key studies have demonstrated that wavelet analysis can be a more effective and efficient tool to be based on for extracting AE features induced by tribological interactions in engine systems.

1.2 Research Scope, Methodology, Aim and Objectives,

The aim of this research is to develop an online method to monitor the tribological behaviour of the ring-liner system based on the analysis of AE signals measured externally. The method can be applied to the online real-time monitoring of lubricity performance degradations such as changes in lubricant viscosity including oil shortages and abnormal wears for operational engines in the industry. Meanwhile, these capabilities can be based to assess the impact of alternative fuels on the tribological behaviour for engines tested with new fuels.

As one of the most important physical properties of lubricants, the viscosity is widely adopted to evaluate the quality of lubricating oils in different off-line methods [25]. Recently, researchers have noticed that AE signals from a running engine have observable changes in different frequency bands corresponding to oils with different viscosities, which was explored in recent studies of the authors and colleagues [24, 26, 27] and regarded as to the interactions between lubricant and micro-asperities in the hydrodynamic lubrication (HL) regimes. In addition, Douglas and the co-workers [23] demonstrated by a test with oil turning off that AE is effective to indicate the changes in

lubrication conditions. The changes of increased AE amplitudes was by the asperity contacts between the ring and liner owing to oil starvation in the boundary lubrication (BL) regimes. These experimental studies show promising results of using AE for monitoring tribological behaviours.

To consolidate these observations, a symmetric study of AE generation mechanisms will be one of the research scopes. It will allow AE signals to be insightfully interpreted and characterised in different lubrication regimes including not only the classical HL and BL regimes but also the mixed lubrication (ML) regimes. To address this subject, the dynamic behaviours of micro-asperities on two lubricated rough surfaces will be investigated based on the primary mechanism of rapid stress release process.

Subsequently, the research will be proceeded to further investigated to characterise AE signals under a wide range of engine operating conditions based on the generation mechanisms. This then will provide the fundamentals for developing effective signal processing methods to extract AE contents relating to tribological behaviours. In addition, AE technologies are deemed to be sensitive to not only to the tribological behaviour of interest but also various interferences such as combustion shocks, valve impacts and background noise. Principally, these interferences and noise need to be suppressed or eliminated in order to accurately characterise the AE content associating with tribological behaviour. In this perspective, wavelet analysis will be based on to process the non-stationary AE signals.

Having gained sufficient understandings of AE sources and AE signal characteristics, a symmetric experimental study will be carried out to verify the theoretical understanding and refine wavelet analysis methods for extracting tribological behaviour related AE contents. In particular, commonly used engine lubricants including both new and used ones with different viscosities will be tested based on a single cylinder engine to evaluate the detection sensitivity using AE signals and the performances of improved signal processing methods. Subsequently, two types of alternative fuels: biodiesel and F-T fuel which are more abundant locally will be also tested to assess their impacts on the tribological behaviours.

Therefore, to achieve the aim of this research, both AE generation mechanism and AE signature enhancement are regarded as two essential subjects to be addressed extensively, which will be carried out according to the following prioritised objectives:

Objective 1: To investigate and develop the AE generation mechanisms for the tribological effect of the piston ring-cylinder liner.

Objective 2: To develop frictional AE models for the AE characterisation analysis of the tribological behaviour of the ring-liner system.

Objective 3: To verify and evaluate AE characteristics through experimental studies based on an operating IC engine.

Objective 4: To develop wavelet based de-noising techniques to suppress interfering AE events and enhance tribological AE signals.

Objective 5: To develop AE based techniques to diagnose lubrication conditions, specifically, changes in lubricant viscosities.

Objective 6: To develop AE based techniques to diagnose any impacts of typical alternative fuels on tribological behaviours.

1.3 Organisation of the Thesis

Chapter 1 - This chapter firstly presents the background and motivation of this research work, and then discusses the challenges for monitoring the frictional behaviour of the piston assembly under running conditions. Finally, the aim and objectives of this work are given.

Chapter 2 - This chapter introduces the mechanisms and fundamentals of the piston-cylinder liner conjunctions and the acoustic emission from diesel engines. And the literature reviews of both the piton tribology and acoustic emission monitoring for engines are elaborated.

Chapter 3 – Based on the basic theory and review information of the mechanism of piston tribology summarised in Chapter 2, this chapter develops the models for ring-liner friction which allows numerical results to be obtained for accurately understanding the tribological behaviours and predicting AE effects relating to various frictions.

Chapter 4 - Based on micro asperity dynamics and hydrodynamic forces, this chapter investigates further details of AE mechanisms and develops analytic models for describing asperity-asperities collisions and asperity-fluid interactions that exist between lubricated rough surfaces under various lubrication regimes. In conjunction

numerical analysis in Chapters, these analytic predictions show the basics of AE in the time and frequency domain, the velocity, viscosity and load dependent characteristics. In addition, potential effects of particles are also foreseen, which paves the way for accurate AE signal processing.

Chapter 5 – Based on a single cylinder engine, this depicts test rig construction, AE measurement systems and methodology for acquiring AE data to verify the models and thereby to develop techniques of using AE for diagnosing tribological behaviours.

Chapter 6 - This chapter overviews signal processing methods and evaluate their suability for analysing AE signals which are found to be very nonstationary and large volume of data. By applying commonly used signal processing methods to typical AE signals, it has identified that wavelet can be the most effective one to reflect the weak AE content with efficient computations.

Chapter 7 - Based on WMRA with a hard threshold scheme, this chapter develops an effective mothed of feature extraction for reflecting tribological AE events. An optimal wavelet analysis is implemented based on the velocity dependent characteristics, which allows the establishment of diagnostic features from both envelope signals and their correlations with modified velocity of piton motion. Subsequently, the diagnostic performances of using these features are evaluated based on data sets from lubrication oil tests and alternative fuel tests, demonstrating that these features allows subtle changes in tribological behaviour to be identified successfully.

Chapter 8 - Based on WMRA with an adaptive threshold scheme, this chapter develops a novel mothed of feature extraction for reflecting tribological AE events. An optimal wavelet analysis is implemented based on the velocity dependent characteristics, which allows the establishment of improved diagnostic features from both envelope signals and residual signals of wavelet coefficient. Subsequently, the diagnostic performances of using these features are evaluated based on data sets from lubrication oil tests and alternative fuel tests, demonstrating that these new features allows abnormal tribological behaviour to be identified more accurately.

Chapter 9 – This chapter details optimal WPT analysis of the AE signals to utilise the narrowband filtration capability for suppressing the influence of random noise and hence for more accurate diagnostics. A novel scheme is developed to determine

optimally the decomposition level and wavelet orders based on minimising time-frequency overlaps. It results in multiple diagnostic features in different narrow bands, allowing subtle changes in tribological behaviour to be identified jointly for higher reliability and more insights into the changes.

Chapter 10 – This chapter summarises the conclusions and contributions of this research project, and the future work is given.

Finally, a block diagram of this research route is given in Figure 1-1 to show the relationship between main key methodologies explored in the project.

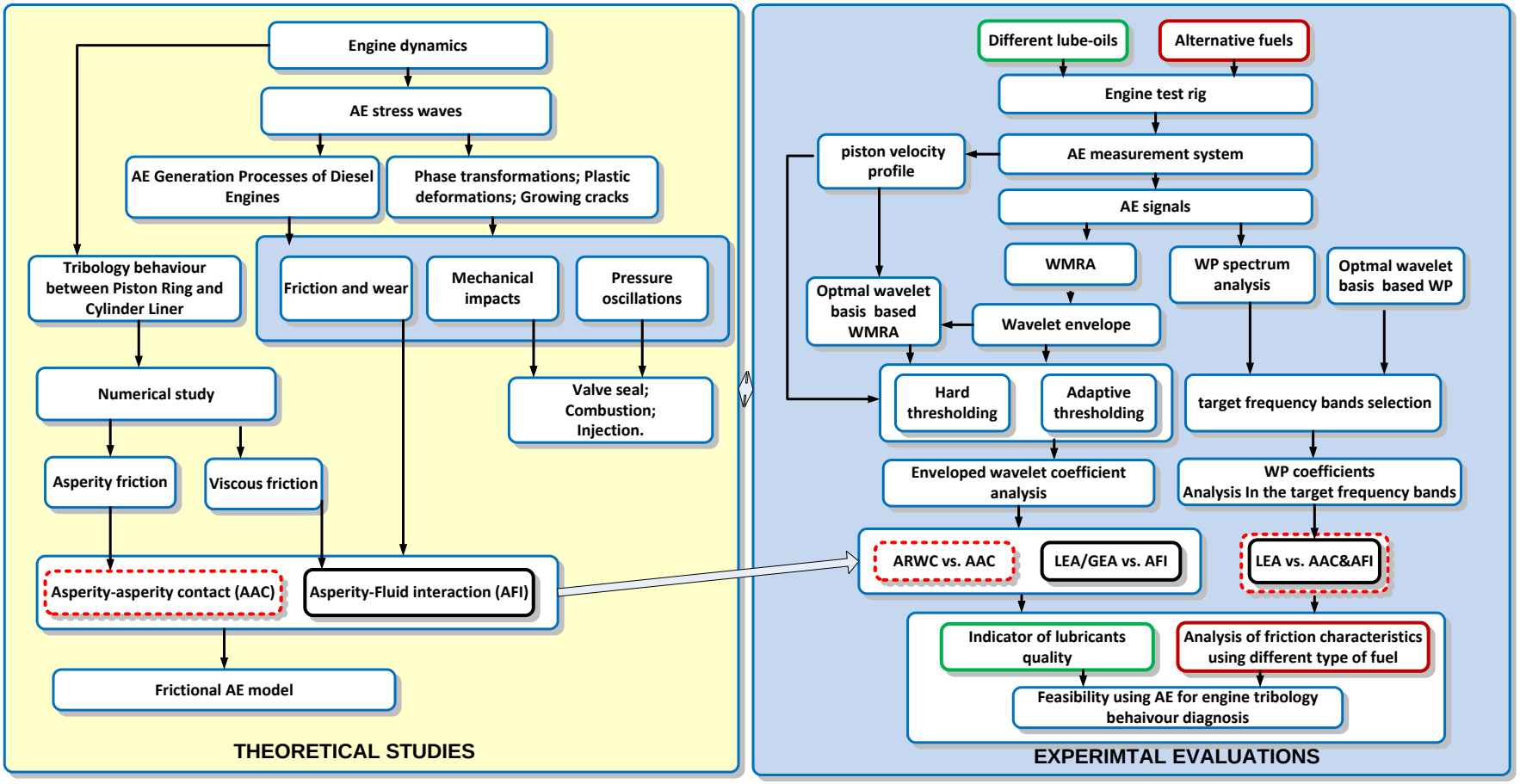

Figure 1-1 Block diagram of research route

CHAPTER 2 MECHANISMS AND FUNDAMENTALS OF ACOUSTIC EMISSIONS FROM THE PISTON RING-CYLINDER LINER TRIBODYNAMICS

This chapter reviews the basic theories and previous achievements in using AE for monitoring the tribological behaviour of the ring-liner system. It starts with a general analysis of the tribological behaviour. Then, it provides the overview of the fundamentals for AE generation and the potential AE mechanisms happening in an internal combustion engine. Finally, it elaborates critical valuations upon current progress in using AE technologies for engine diagnostics along with works relating to monitoring other tribological processes.

2.1 Introduction

The piston assembly is the core subsystem of engines. It exhibits a complex dynamic behaviour. This chapter detailed the basic theory and primary achievements in piston tribology and AE monitoring to provide theoretical support for the further research of this work.

On one hand, Section 2.2 gives a prelude understanding of the piston ring modelling research and analysis of the frictional behaviour between the ring and liner. This section aims to illustrate the mechanisms behind piston system motion and the fundamentals of the piston ring-cylinder liner system tribology in physics. Then a short review of some published works on the piston-cylinder system tribology is given. Finally, potential impact for alternative fuels on the piston-cylinder system is discussed.

On the other hand, the objective of Section 2.3 to 2.5 elaborates the mechanisms of AE in friction and discusses the possibility to detect the AE activities induced by tribological behaviour from engine base on both material laboratory studies and engine condition monitoring using AE.

2.2 Fundamentals and Mechanisms of the Piston Ring-Cylinder Liner Contact

2.2.1 Piston Ring and Cylinder liner Basics

The piston assembly is the heart of the internal combustion engine. [47]. The piston pack mainly aims to separate the combustion chamber from the crankcase by an effective labyrinth seal state using a series of metal rings. The piston pack is also designed to prevent the oil splashing into the combustion chamber, limit the amount of oil on the contact surface of the cylinder, and transfer heat from piston to cylinder. Piston rings are fundamentally categorised into two types: the compressing ring and oil control ring (or scraper ring). The piston and ring geometrical features are given in Figure 2-1. Usually, there are two sets of compression rings for ensuring the seal performance and one oil control rings for limiting and distributing the oil uniformly

over the cylinder liners. However, the top compression ring operates much extremer conditions: high temperature and pressure. So it will be concentrated more in this study.

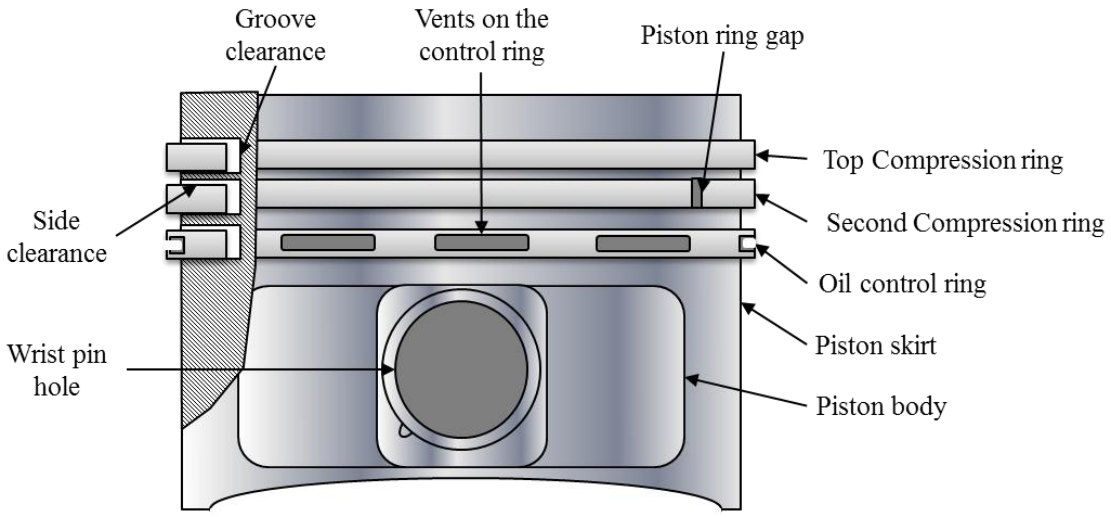

Figure 2-1. Piston and ring geometrical features

2.2.2 Piston Motions

In IC engines, the piston assembly moves up and down to convert the combustion energy into rotational energy of crankshaft. A schematic of crankshaft mechanism is shown in Figure 2-2., allowing for a better understanding of the motions between the piston assembly and cylinder liner with respect to the rotational motions of the crankshaft. Specifically, the piston displacement and velocity, given in Equation (2-4) and Equation (2-5) respectively, can be used to express the basic movement during a four-stroke engine cycle which equals to two revolutions.

Assume the crankshaft rotates at the constant speed ω, the position of the piston can be calculated as:

$$x = r\cos\theta + l\cos\alpha \tag{2-1}$$

where θ is the crank angle, r is the radius of the crank, l is the length of con-rod.

Take the angle between the con-rod and the vertical $as\ \alpha$:

$$l\sin\alpha = r\sin\theta \tag{2-2}$$

From Equation (2-2), it can be known that $\sin\alpha = \frac{r}{l}\sin\theta$

By using the trigonometric identity of :

$$\cos a = \sqrt{1-\sin^2 a} = \sqrt{1-\left(\frac{r}{l}\sin\theta\right)^2} = \sqrt{1-\left(n\sin\theta\right)^2} \tag{2-3}$$

where the ratio between the con-rod and crank radius: $n = l / r$.

Substituting Equation (2-1) the piston displacement is

$$x = r\cos\theta - l\sqrt{1-\left(n\sin\theta\right)^2} \,. \tag{2-4}$$

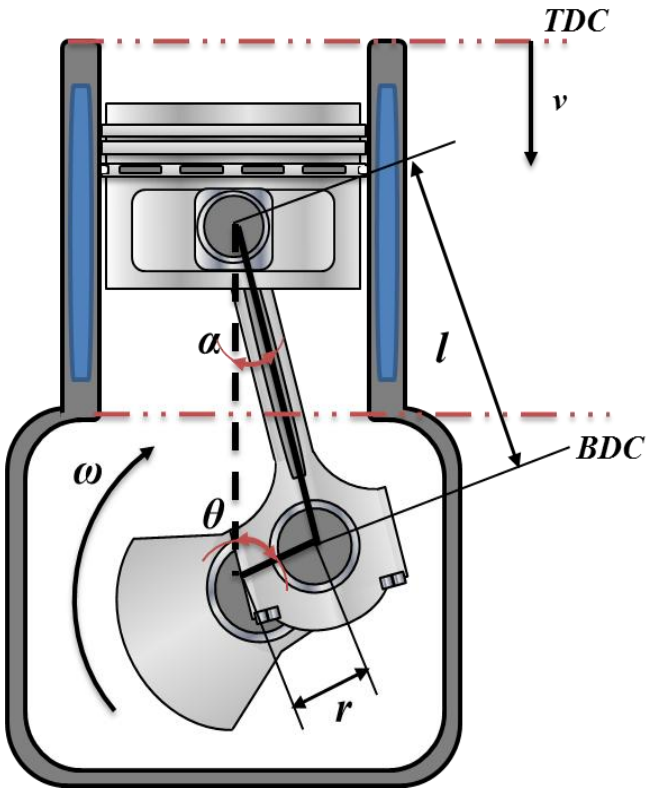

Figure 2-2. Schematic diagram of the crank-piston motion

The piston velocity $\dot{x}$ with respect to the crank angle θ can be given as the differential of the piston displacement from TDC:

$$\dot{x} = \frac{dx}{d\theta}\frac{d\theta}{dt} = -\omega\left(r\sin\theta + \frac{r^2\sin\theta\cos\theta}{\sqrt{l^2 - r^2\sin^2\theta}}\right) \tag{2-5}$$

2.2.3 The Surface Roughness of the Ring and Liner

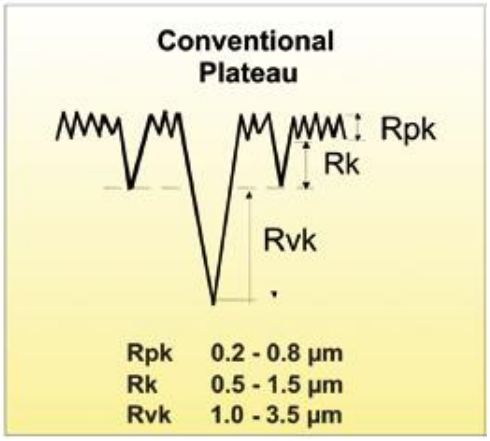

(a)

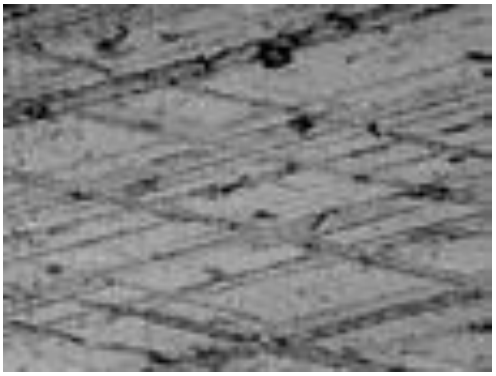

(b)

Figure 2-3. the representative liner surface, (a) a typical plateau honed cylinder, and (b) Laser microscopy imagery of liner[48, 49]

Surface roughness is an important factor used to specify the state of the machined surface of components[50, 51]. Ring and liner surfaces are finished to resist the friction and wear [52]. The cylinder liner surface is usually finishing by honing process. Honing is an abrasive machining process to produce a precision surface [53]. Figure 2-3 shows the typical surfaces of the liner[49]. The cylinder liner surface typically exhibits the plateau roughness and cross-hatching for oil preserving and high load-bearing capacity.

The sides of piston rings need to maintain a certain level of roughness as they slide against the cylinder liner, and the roughness of piston ring is used to ensure the smooth movement of the pistons in the cylinder while minimizing the abrasion caused by friction.

2.2.4 Basic Lubrication Regimes

Before discussing the friction and lubrication characteristics of the piston assembly, some fundamentals of lubrication theory are reviewed for further understanding the tribological behaviour relating to AE. When the specific loads or speeds on the two contacting surfaces vary, four different lubrication situations or regimes can be formalised in two fluid-lubricated surfaces, which are boundary lubrication, mixed lubrication, elastohydrodynamic lubrication and hydrodynamic lubrication as illustrated in Figure 2-4 with four schematic diagrams respectively.

The boundary lubrication, first introduced by Hardy and Doubleday in 1922 [54], is where a constant contact occurs at the high points of interact surfaces since the height of asperity on roughness surface is larger than the film thickness at the same point. Komvopoulos and the co-workers [55] stated that the primary steady state of boundary lubrication is ploughing, in which shear of the lubricant film between the sliding surfaces and adhesion between the asperities, although may occur, contribute less than ploughing to the overall friction force. Consequently, the two interfaces will generate more wear under boundary lubrication than the other three regimes mentioned above.

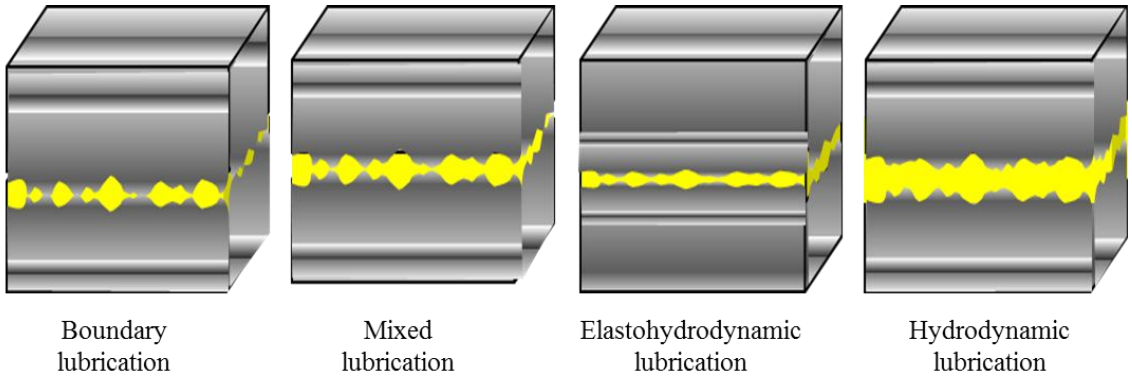

Figure 2-4. Film generation of lubrication regimes

Hydrodynamic lubrication indicates that a thick tribofilm generated at a sufficiently high velocity can prevent any surface contact each other. The theory of hydrodynamic lubrication was first published by Reynolds in 1886 [56]. This occurs between two surfaces moving relatively at a sufficient speed to generate a lubricating film. The hydrodynamic pressure generates when two contact surfaces moving towards each other [8], such as the piston ring sealing surface moving relative to the cylinder liner surface.

Elastohydrodynamic lubrication is caused by high load and high contact pressure to alter the film thinness between the contact surfaces. The viscosity of tribofilm increases rapidly with the high contact pressure, which is also correlated to the materials elastic properties and relative velocity. Elastohydrodynamic lubrication interfaces have very low friction coefficients due to thinner films reducing contacts between asperities.

Finally, the mixed lubrication regime is where boundary and elastohydrodynamic regimes both occur in interfaces.

In addition, chemical and physical actions in thin tribofilms affect the lubrication regimes. The chemical actions correlate to additives effects, such as the zinc dialkyldithophosphate (ZDDP) as one of most common anti-wear additives [57]. The physical actions mainly correlate to the viscosity variation of multi-grade lubricants containing the polymer that is decreased under high shear rate and increase at elevated pressure [47]. More sophisticated mathematical models have been developed to depict the lubrication behaviours associated with the physical actions in the field of engines [58]. The difficulty is to confirm these predicted behaviours experimentally because they occur under extreme conditions where existing testing systems are unable to measure them in real-time. Nevertheless, there are sustaining signs of progress in this area with new emerging testing and analytical techniques.

This work is mainly concerned with the piston-cylinder system lubrication. It is appropriate to have the general understandings of various lubrication regimes experienced by the piston assembly. The traditional Stribeck curve[59] has been proven to be useful for identifying boundary, mixed and hydrodynamic lubrication regimes for contacting surfaces[60]. The ideal contact model of the piston ring and cylinder liner is assumed with a sufficient tribofilm for lubrication during the reciprocating motions of the piston. However, a series of studies reported that boundary lubrication and surface asperity contact models should incorporate in the piston ring friction modelling [61] and simulating of wear [10] .

Therefore, the key lubrication regimes of automobiles is shown as a modified Stribeck diagram as shown in Figure 2-5 [57]. The friction coefficient value during hydrodynamic lubrication also has shown obviously ascending trend. [62]. The variation of friction between two lubricated surfaces can be correlated to the combined parameter of $\eta V_s/L_n$ as

shown on the abscissa, where η presents the dynamic viscosity, V_s specifies the sliding speed and L_n indicates the load applied on to the interacting surface.

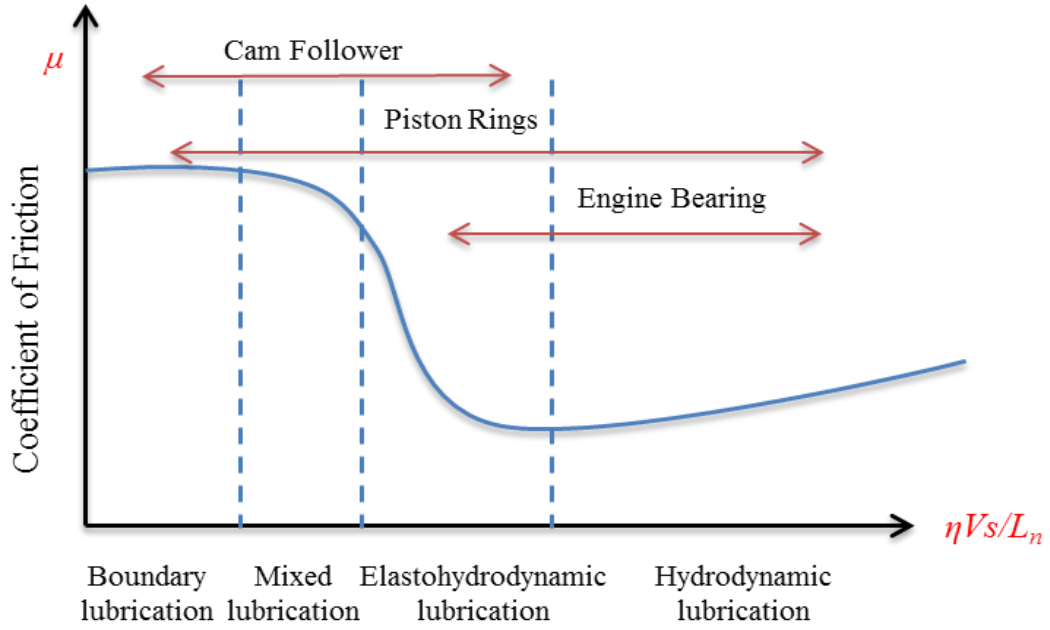

Figure 2-5. The modified Stribeck diagram [61]

2.2.5 Friction Loss of the Piston-Cylinder Liner System

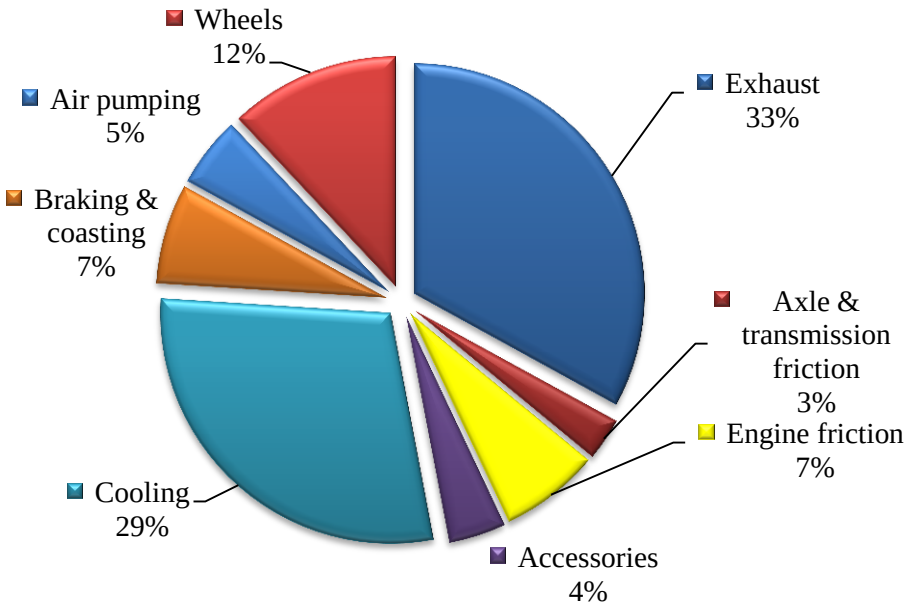

(a)

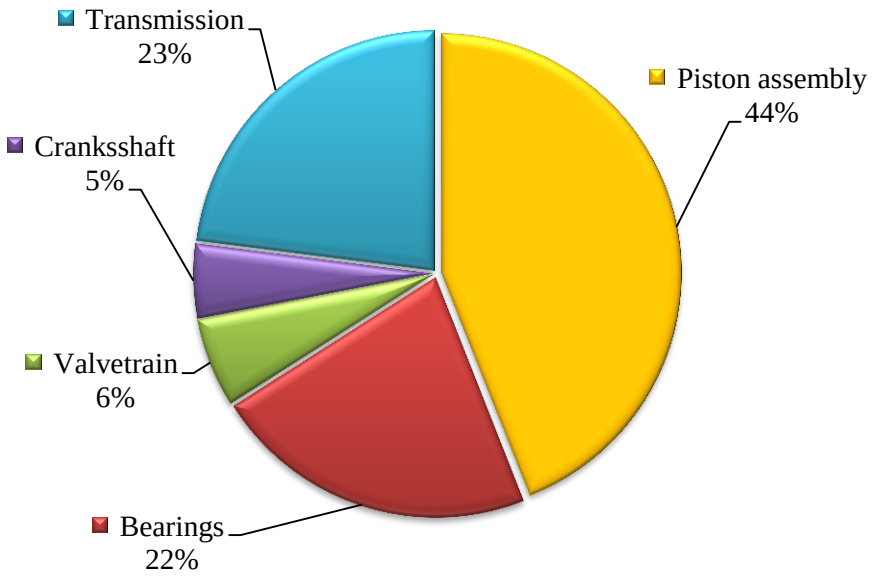

(b)

Figure 2-6. The percentage of energy consumption of the subsystem of the vehicle, (a) powertrain losses of the engine and (b) engine/transmission friction losses [47, 63]

As the highest share of the total friction loss in modern IC engines, friction influences between ring pack and cylinder wall has been drawn much attention for many years. McGeehan [64] reviewed that about 65% of the mechanical friction loss in an engine was caused by the piston and ring in 1978. In recent decades, this percentage of friction loss was declined as the technological innovation and improvement of the engine. Andersson [65] investigated that about 15% of the total energy was used to overcome the mechanical losses in the powertrain. Tung and McMillan [47] reviewed (the conclusion in the reference [66]) the total friction due to pistons assembly contributes for 44% in a modern engine, and the pie charts in Figure 2-6 [47, 63] displays The percentage of energy consumption of the subsystem of a vehicle. The pie chart of Figure 2-6 (a) depicts that nearly 15% of the energy is used to overcome mechanical losses, most of which are frictional losses; comparatively, the pie chart of Figure 2-6 (b) reveals that the piston assembly undoubtedly accounts for the most significant percentage of the friction loss.

Schwaderlapp et al. [67] reported that the energy consumptions percentage of the piston assembly was 43 % for SI engines and 31 % for diesel engines, which is the biggest share of parasitic losses for engines[67] (displayed in Figure 2-7).

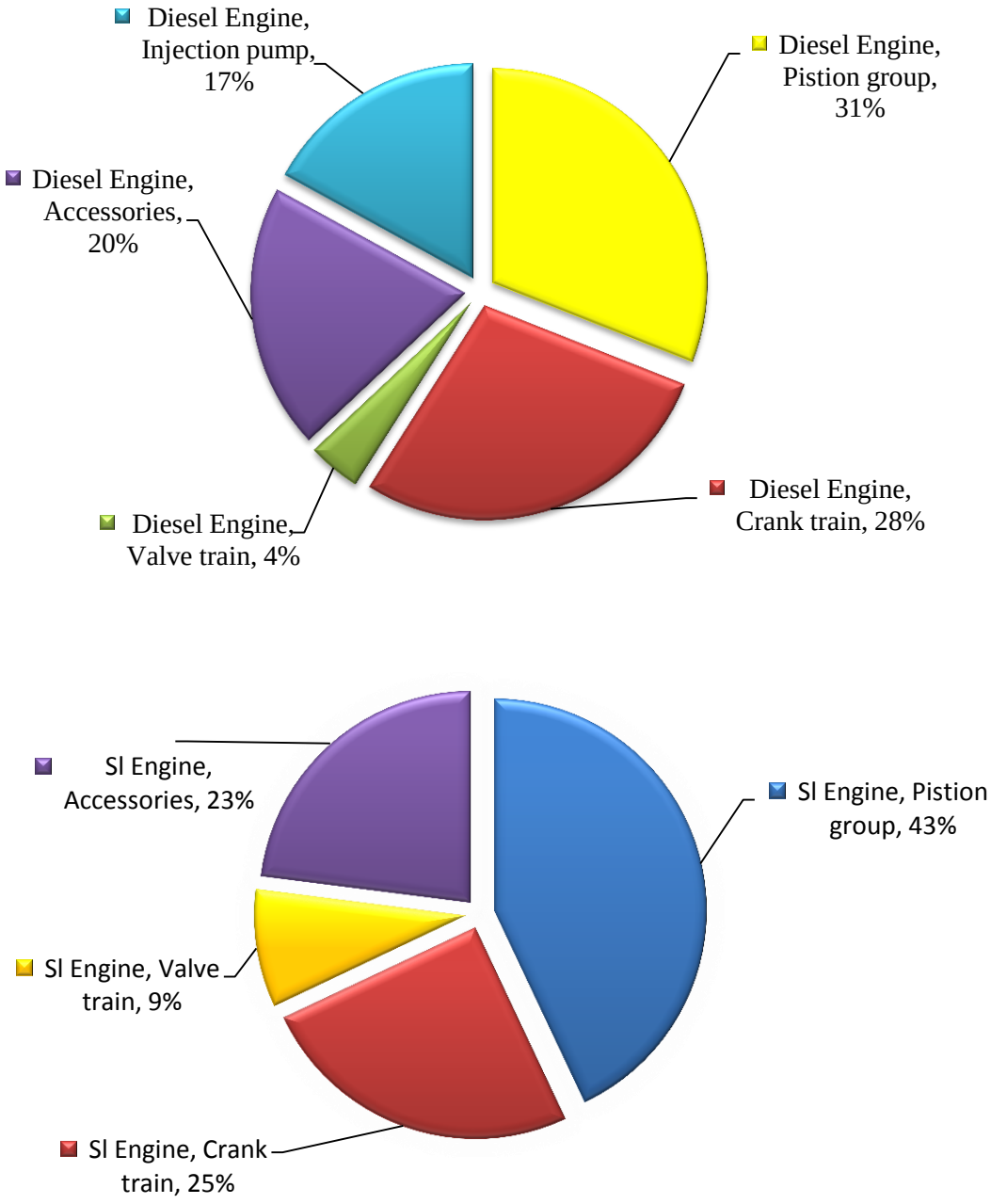

Figure 2-7. Distribution of friction losses of the diesel engine and SI engine (engine speed 2000 rpm) [67]

2.2.6 A Review of Key Published Works on the Piston-Cylinder Tribology

The elucidations into the lubrication models and friction properties of engines especially piston groups in the previous sections are the underpinning supporting an appreciation of the tribology of the piston assembly. Based on these illuminations, this section mainly reviews the published work of the piston tribology both in the modelling and experimental studies.

2.2.6.1 Predictive Methods for the Piston-Cylinder System Tribology

The piston ring pack is subjected to most severe working conditions with the rapid variation of velocity, load and temperature, leading to complicated tribological regimes. In the last decades, many works have been developed for an essential understanding of the tribology in piston groups.

The pioneering theoretical extension of the Reynolds theory from bearing lubrication to ring lubrication with the consideration of ring face as a convex and uneven shape can be back to the work of Cattleman [68] in 1936. Afterwards, Greenwood and Tripp [69] presented a comprehensive asperities contact model. Nadir Patir and Cheng [6, 7] proposed the average Reynolds equation and the average flow model to developed the investigations of mixed lubrication regimes of the piston groups [70, 71, 72].

Many investigations into the piston ring lubrication modelling are considering more practical factors, such as the non-axisymmetrical properties [73], the influence on deformed cylinder Bores [74, 75], the effects on the surface texture of the piston-cylinder system [76, 77], the blow-by and ring-twist effects[78] and cavitation [79, 80].

It is worth noting that the thermal effects reduce the lubricant viscosity of the tribofilm. Specifically, Radakovic et al. developed the numerical simulations of the performance of the piston considering the thermal effects[81]. Morris et al. [71] adopted the transient thermal into the piston tribology model and concluded to include the thermal effects in the modelling of the ring-bore contact.

Harigaya [82] established a numerical solution model to investigate the temperature and shear rate of the film thickness for multigrade oils and the heat transfer between the ring and the liner in engines. However, the oil viscosity and tribofilm thickness model for multigrade oils and the predictions made by these different models are still lack of experimental verification due to the difficulties in measuring the instantaneous temperatures, pressure and tribofilms with highly time-varying characteristics.

2.2.6.2 Friction Measurement Techniques for Piston-Cylinder System

To develop a further understanding of the mechanism of the piston assembly tribology and also to support the modelling studies of the piston assembly as mentioned above, the experimental measurement methodology was developed to mainly measure the friction force between the ring and liner. The method applied to measure the friction over the

complete engine cycle can be categorised into three approaches: the motoring teardown engine method, the floating liner method and the instantaneous mean effective pressure (IMEP) method.

Motoring an engine without the sealing components is a general method to measure the engine friction [83]. The engine crankshaft generally motored to rotate by an electric motor with a torque recording sub-system. To measure the total friction fore power accurately, the sealing components were removed which aims to motor the engine easily and reduce the non-friction power consumption interference. Hence, the tested torque represents the friction of the piston and the connecting rod. However, it is impossible to separate the piston friction from the rod friction because of a number of issues with motoring teardown tests [83]:

- The effect of high cylinder pressures is not included.
- The test will not be operating at realistic temperatures compared to the fired engine. Hence, the tribofilm temperature is obviously low with the motored test without combustion process.
- It is not possible to truly isolate the contribution of each individual component. For example, if one ring is removed, it will allow more oil to flow to the remaining rings. This will change the status of overall tribological properties and friction effect.

Consequently, the difference in friction between motored and fired engine test roots from the effect of high gas pressure and the high temperature of combustion. Mufti and Priest [84] reported the friction loss under fired conditions is slightly higher than motored condition due to the high pressure and temperature of the combustion process. Although motored test could not reveal the piston friction accurately, it is still very useful to quantify the frictional changes of the piston assembly with a very small modification of the engine test bench. Particularly, Douglas et al. [23] conducted a motored engine test with the cylinder head removed to eliminate the AE events from injector and valve, hence, the remaining AE relates to the tribological behaviour of the piston ring/cylinder liner interaction.

Another method probably the most accurate method to quantify the friction power of the ring-liner system is the floating liner method. The floating liner method utilizes a floating

cylinder liner supported by load cells to measuring the piston assembly friction. The test rig separates the liner from the cylinder head and crankcase by additional elastic constraints to provide a free movement in the axial direction and measures the forces acting on the cylinder liner. Several studies of the floating liner engine have been conducted for piston rings friction [85], supporting the validation of a model for the lubrication of oil control rings[86] and sensitivity to resolve differences in friction characteristics between different lubricant oil [87]. However, these findings also represent an abnormal running condition compared with the firing engine test which suffered interference from vibration instability. On the other hand, the problem with this method is that the sophisticated modification is expensive and hard to balance the radial force and pressure effects acting on the liner.

The IMEP method is needed for accurate measurements of series of parameters which are cylinder pressure, connecting rod force, engine speed and crank position, along with the calculation of piston acceleration and inertial forces. The friction force is the evaluated results subtracted from the connecting rod force. The drawback shows that the frictional force is a small difference between pressure and connecting rod force which is easily affected by the error in the pressure measurements.

Overall, there are no means for online measurements of friction and tribological effects that can be applicable for condition monitoring.

2.2.6.3 Lubrication Condition Monitoring for the Engine System

The lubricants play a vital role in the engine system, to protect the moving parts from friction and wear, dissipate heat of the components and clean the particle contamination on the contact surfaces of components. Analysis of lubricating oil is an effective approach in judging machine's health condition and providing early warning of machine's failure progression [88]. As summarised in [89], the indicators to evaluate the degree of the oil degradation are mainly including viscosity, water content, number of particles, total acid number, flash point, spectrometric oil analysis program (SOAP) and so forth. Generally, the main sensor strategies to monitoring the oil performance can be classified into two major types[90]: (a) physical detection which giving information about oil condition in terms of viscosity, particles and debris, polarity, or dielectric constant; (b) chemical recognition of aged oil interfered with high temperature, moisture, fuel contents in engine oil, and other contaminants.

The online method can perform real-time information for avoiding the catastrophic component failure during operation. Hence, plenty of studies and sensor technologies have been developed online monitoring on lubrication performance as reviewed in [88] and [89]. However, most of the sensors in the lubricating-oil measurement system were designed as the intrusive system and cannot offer integrated information for the remaining lifetime of the lubricants. Moreover, the above lubrication oil health monitoring sensing techniques are costly in manufacture and maintenance or complicated in the operation and installation.

Ultrasound method is an attractive non-intrusive method in condition monitoring without any invasion. The ultrasonic method has the potential for monitoring the flow regime owing that this technology is sensitive to both flow velocity and particle size in the slurry transport systems suggested in [91].

The ultrasound method also has been used to detect the tribofilm thickness of bearing system as investigated in [92]. Xu et al. [93] reported the simulation investigations and physical model analysis results by using ultrasonic oil debris sensor to identify the solid debris and air bubbles. Li and Jiang [94] presented the theoretical analysis of the ultrasonic sensor to recognise the wear debris in the lubricating oil. Particularly, Mills et.al [95] developed an ultrasonic method to measure the lubricant film thickness between the ring and liner surface under the running condition. These achievements demonstrate the possibility to detect the lubrication performance by using the active ultrasound techniques.

Specifically, because all the basic oil degradation features can be correlated to the viscosity variation including oxidation, water/particle contamination and fuel dilution as summarised in [89], the viscosity is usually taken as the comparison standard of lubricating oil degradation. Further, AE testing, as a special type of ultrasound method, is actively studied for monitoring the engine conditions. To correlate the AE with the viscosity of the engine lubricating oil, Elamin and the co-workers [26, 27] reported the possibility to predict the quality of engine oil using AE RMS values owing to the AE RMS values influenced more by oil viscosity. Therefore, the AE can potentially offer the comprehensive information of the lubrication condition in a cost-effective and easy implementing way.

2.2.7 The Potential Impact of Alternative Fuels on the Piston-Cylinder System

Due to the contradiction between the growing demand for petroleum-based fuels and the crisis of petroleum reserves, the alternative fuels aim to produce with acceptable performance and sustainability of resources. Most of the existing research has focused on economics, power performance and emissions of alternative fuels.

However, some new potential impacts from alternative fuels, such as the unknown changes in friction loss due to power performance differences with diesel and unspecified effect to the lubrication degradation process, have not yet been fully understood and the research is still on.

It should be noted that sufficient lubricity of engine combustion fuels is essential to prolong the machine life, and good lubricity is also important to cut down the energy consumption by reducing friction of automotive parts such as fuel supply pumps and injectors [47, 96]. If the lubricity of alternative fuels is poor, it will generate more tribological impacts on the engines than fuelling diesel. Further, the alternative fuels also come with some unfavourable features such as poor thermal stability, poor lubricity, auto-oxidation, corrosion, wear etc.

This section introduces two promising alternatives: F-T (Fischer-Tropsch) fuel and bio-diesel based on the availability of local fuel resources in China. Their physical and chemical characteristics are reviewed for understanding the potential effect on the friction of the piston assembly.

2.2.7.1 F-T Fuel

Basic Physical and Chemical Characteristics of F-T Fuel

Fischer-Tropsch (F-T) fuel is made a type of synthetic gas (CO and H_2) through the Fischer-Tropsch processes using natural gas or coal as introduced in [97,98]. The physical characteristics of the F-T fuel are very similar to diesel, such as the density, viscosity and content of energy. Hence, it is easy to blend with diesel without any intermediate. Moreover, the F-T fuel has high cetane number, low sulphur and aromatic level, the F-T fuel also has better ignition properties and lower NOx and particle than diesel emissions as discussed in [97, 99].

F-T Fuel Potential Impacts on the Piston Tribology

many studies [97, 99, 100, 101] reported that the F-T diesel has lower emissions than diesel, the PM emissions are reduced dramatically fuelling F-T fuel.Sporadic studies considered some correlated factors to tribological impacts. Huang et al. [102] investigated that the engine fueling F-T fuel has an obviously higher rate of pressure rise than fueling diesel.

The loss of the lubricity of the low-sulfur diesel from the crude oil seemed to indicate that hydroprocessed sulfur-free F-T diesel has poor lubricity [103]. Ajayi and the co-workers [104] conducted two groups of scuffing tests on a ball-on-flat test rig using diesel and F-T fuel. The F-T fuel reveals poor lubricity due to a low scuffing resistance. Gill et al.[105] suggested that the main drawbacks of F-T diesel are poor lubricity and density. However, the tribological impacts of F-T diesel fuel have still not been studied.

Basic Physical and Chemical Characteristics of Bio-diesel

The biodiesel can be generally made from plants, animal fat or used cooking oils. The chemical and physical characteristics of bio-diesel are differentiated owing to different raw materials and preparation process[106]. The bio-diesel and diesel blends proved to have progressive effects on the emissions and power performance [107, 108]. The bio-diesel and diesel were showed to have similar thermodynamic properties owing to the bio-blends with a low percentage of bio-oil [2]. Moreover, the key properties of the bio-diesel such as the bulk modulus, heating value, density and viscosity which were reported to affect the performance, fuel economy and emissions of the engines as suggested in [109, 110].

Bio-diesel Potential Impacts on Engine Components

It should be aware that the different physical properties strongly affect the cylinder pressure, blends fuel lubricity, fuel pump performance, injection pressure, and injection rate. These effects will extend to affect the performance of the piston tribology.

Qi and the co-authors [111] investigated that the peak heat release rate and the peak rate of pressure rise were lower for bio-diesel than diesel, although the peak pressure and power output of bio-diesel were almost same to that of diesel.

Several studies [112, 113, 114] focused on the impacts of the fuel pump performance of bio-diesel fuels, and the fuel injection pressure is demonstrated to increase when fuelling biodiesel.

ASMA et al. [115] reported that the pure biodiesel has better lubricity than diesel. The lubricity of bio-diesel affect by the chemical composition and its percentage in the blends. Hu et al. [116] investigated that the unrefined bio-diesels showed higher lubricity properties than refined bio-diesels, and the lubricity properties of bio-diesel affect by the concentration of free fatty acids, monoglycerides, diglycerides. Furthermore, the lubricity of bio-diesel shows that coefficient of friction was reduced in the reference [118] using the diluted lubrication oil containing biodiesel. Nevertheless, there are still controversies in the friction and wear effects on engine fuelled by bio-diesel blends. Some researchers reported bio-diesel shows good lubricity to decrease the wear and friction in long-term use for hundreds of hours. Agarwal et al. [119] identified the wear, the piston carbon deposits and ring sticking were lower by fuelling 20% bio-diesel blends than diesel after long-term use. Fazal et al. [96] looked into the friction and wear characteristics of palm bio-diesel by four-ball wear machine, and results indicated that both wear and friction decrease with the increase of bio-diesel concentration.

On the contrary, other results from on-the-road use of bio-diesel for many thousands of miles showed that it is similar to bio-diesel blends and conventional diesel in wear and or other issues with teardown the engines[120, 121]. Sundus and the co-authors [28] reviewed different tribological aspects of bio-diesel; moreover, they also summarised the downsides of the high viscosity of bio-diesel such as the poor atomization of the injector, plugging of the fuel filter. Furthermore, on the chemical view, bio-diesel is a mixture of methyl or ethyl esters with long-chain fatty acids [122], the corrosion reactions of bio-diesel were deliberated and discussed in [122, 123] and [124] to investigate the impacts correlated to the wear.

2.3 Acoustic Emission Technologies

2.3.1 Introduction

The term acoustic emission is used to describe both a technique and the phenomenon upon which the technique is based [125]. The acoustic emission phenomenon is spontaneously related to the deformation processing of materials. The technique of acoustic emission (AE) could detect the elastic wave generated from the rapidly released strain energy by using piezoelectric transducers. A prominent merit of AE is that it can be

used to monitor condition during running states whereas other conventional NDT methods have to test the condition of material at interrupted status. AE has the higher signal to noise ratio than vibration signal to restrain the influence of the background noise. On the other hand, the frequency range of AE is usually from 100 kHz to 1 MHz or even broader. Depending on the detectability for a wide range of the high-frequency band, AE technology is broadly used to evaluate the material features, structures or condition monitoring of the mechanical system.

2.3.2 General Features of AE Signals in Mechanical System

Features of AE signals are composed of the amplitude, duration, signal energy, and counts. Figure 2-8 illustrates a typical AE signal and the typical feature parameters.

During an AE testing, the signal from different source shows different shapes. A sharp shape signal is sourced by an impulse event such as mechanical impact, cause short-rise and quick-decay signals illustrating as Figure 2-9 (a); whereas a long, drawn-out shape signal is considered generated a series of consecutive events or pseudo-continuous events with very short intervals, such as frictional sliding, shown as slow-rise, slow-decay signals in Figure 2-9 (b).

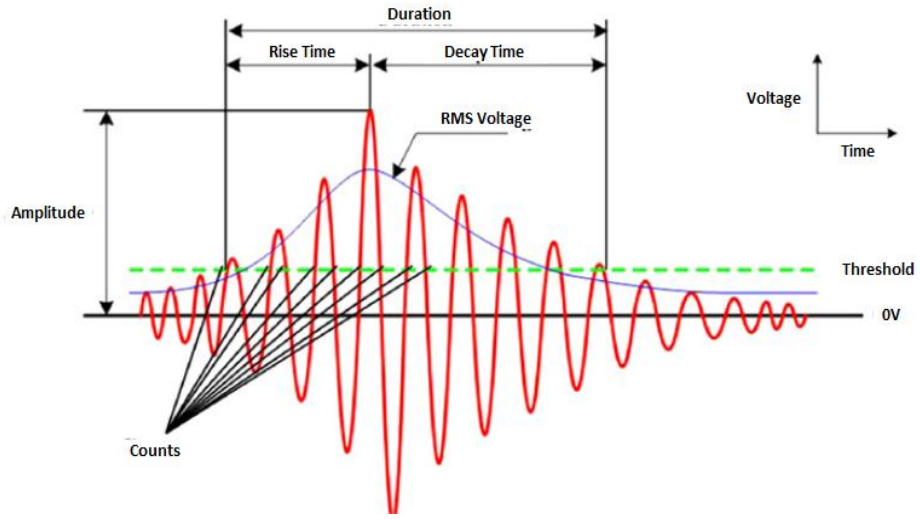

Figure 2-8. AE signal feature parameters (time domain)[126]

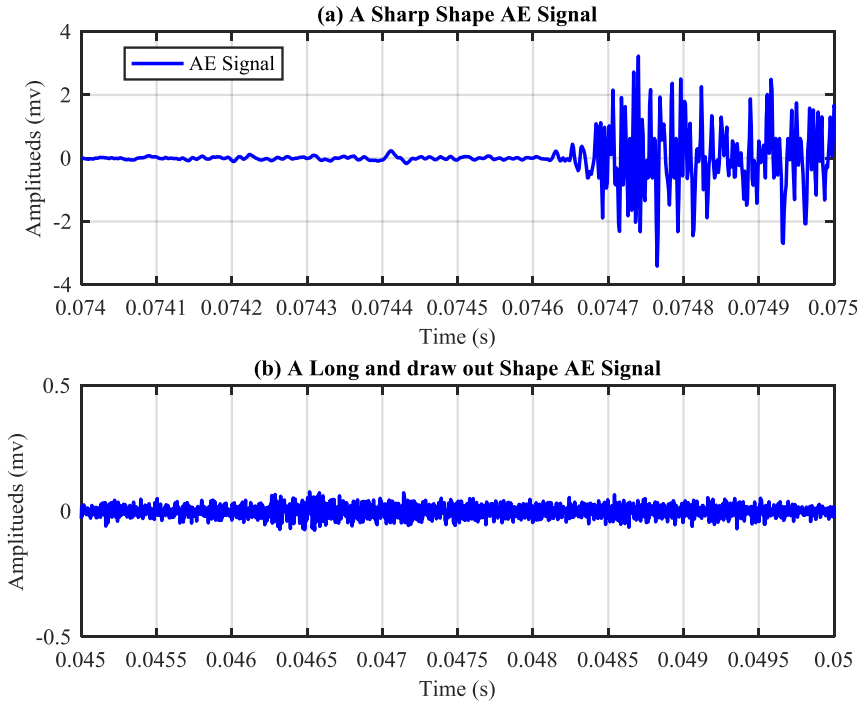

Figure 2-9. Signal shapes of the different source

2.4 Sources of Acoustic Emission in a Friction Process

2.4.1 Mechanism of Acoustic Emission Generation

In the perspective of materials and solid structures, acoustic emission is the short pulse of kinetic energy sourced from the internal structure variation of the material represented as an elastic wave. In addition, recently high-frequency acoustic vibrations appearing when gases and liquids effuse from holes in vessels and pipelines are considered as acoustic emission as well as the acoustic signals accompanying the friction of solids [127].

At the current stage of studies, the elastic waves inside the structural materials which generate acoustic emission events are due to the following three phenomena associated with collective atom motions: phase transformations, plastic deformations and cracks. On the level of the atom, material dislocations release elastic waves which attribute to the slipping motion between atom planes, even the tiny displacement can be tested as distinguished AE signals [128].

Another detectable source of acoustic emission is the elastic deformation. The deformations of material are usually accompanied by the suddenly varying stresses or strains which diffuses elastic waves rapidly with burst type at the high rate [129].

In addition to that, there are many mechanical processes which give rise AE based on the fundamental sources reviewed, researchers in [125] and [130] also summarised that the continuous or pseudo-continuous AE events could be detected in various physical processes of following types:

- ✧ Flow;
- ✧ Leaks;
- ✧ Cavitation;
- ✧ Friction and wear;

However, the exact mechanisms of such sources, especially fluid-lubricated frictions, have not given yet in association with the primary AE generation regimes. Nevertheless, AE has been found to be very useful for condition monitoring of rotating machines and manufacturing processes including pipeline transportations.

2.4.2 Sources of Acoustic Emission in Sliding Contact

The friction and wear were caused by the synthesis impacts of material deformation, adhesion, fracture, heat and chemical process during sliding contact [131]. Friction is a set of phenomena occurring within the zone of contact between relatively moving solids resulting in the appearance of contact forces[127]. The sliding contact generates AE signals sourced from the elastic and plastic deformation [132]. Benabdallah and Aguilar [18] reported that the primarily pseudo-continuous AE activities are induced by the friction and wear processes with irregular high-amplitude AE busts which are caused by asperity collision or particle interaction.

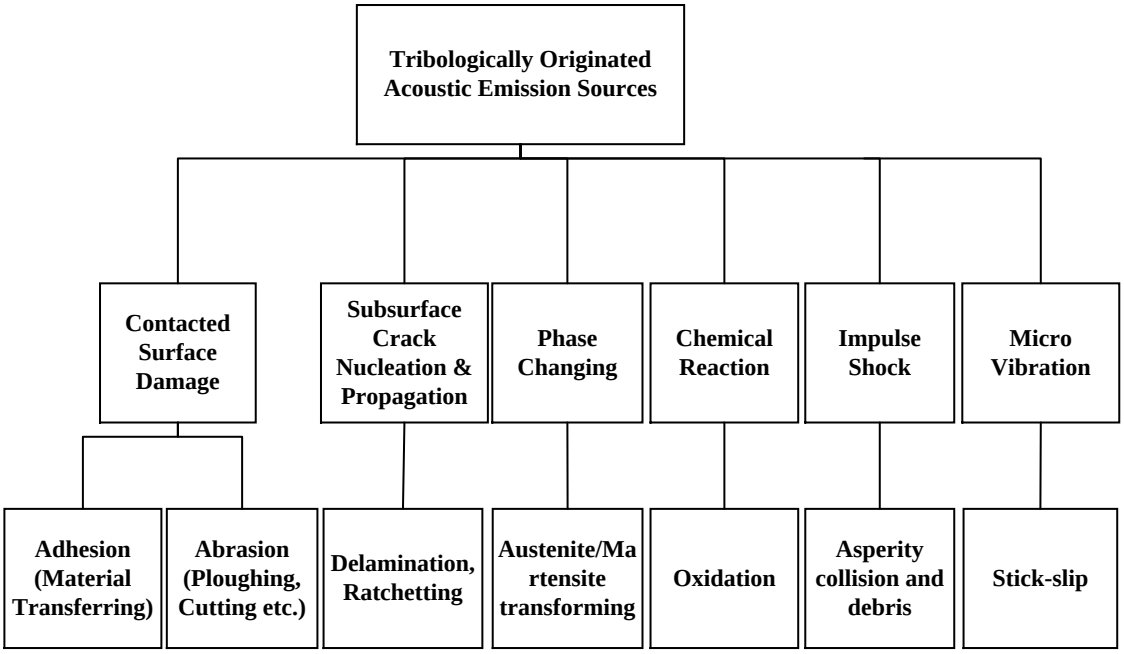

Figure 2-10 Possible AE sources from a tribological contact[133]

Specifically, Sun and the co-authors [133] summarised the possibility AE sources due to friction and wear between two metal surfaces (illustrated in Figure 2-10). Then, they demonstrated that AE correlated to the friction levels and wear rates in three distinct regions which is running-in, delamination/oxidation and oxidation [133].

2.5 Progress in AE Monitoring of Engines

2.5.1 Current Stage in AE Monitoring of Sliding Contact

In the early condition monitoring and fault diagnosis studies, friction is considered to be unwanted noise in AE testing. Then, most previous studies emphasised on the tribological behaviour during the manufacturing, for instance, cutting [134], turning [135, 136], milling [137, 138], grinding [139, 140].

Recently, friction behaviour has received sustained attention in AE testing and modelling for health condition monitoring. Parts of the publications provide the fundamental researches into the AE sources of sliding friction and wear processes. Aim to detect the tribological behaviour between sliding contact; some researchers have tried to find the relationships between AE and the tribological behaviour of contact surfaces by experimental approaches. Lingard et al. [15, 141] conducted a battery of tests on a

two-disc machine to identify the characteristics of the sliding friction and wear process using AE. It is indicated that the AE levels are correlated with the friction force and wear rate.

Jiaa et al. [16] investigated the wear process between two sliding surfaces based on AE, the results indicated that AE is the sensitive and effective technique to detect the wear behaviour. Benabdallah and Aguilar [18] revealed that there is a close relationship between friction coefficient and AE during the dry sliding process. It is demonstrated that the AE monitoring towards the slider to disk test rigs reveals that the sliding speed, acceleration and load can affect the AE RMS values [142, 143, 144], whereas it is not a significant difference in AE signals between the smooth and textured surfaces[145].

Particularly, Mechefske et al. [19] demonstrated AE can be used to differ the wear situations of the lubricated surfaces with and without ZDDP additive. Wang et.al [20] reported the experimental results showed a strong relationship between the AE RMS and the coefficient of friction level. The author and the co-workers [24] conducted a series of tests to demonstrate that AE signals on the cylinder surface were able to identify the viscosity variation of lubricants between the ring and liner. Therefore, these experimental results indicate the AE as a potential tool to detect the different lubrication regimes.

However, the tribological behaviour of contact surfaces is such complicated, there is still lack of correlation between AE characteristics and the physical models of contact progress. To fill this gap, sporadic theoretical models aimed to reveal the relationship between AE and tribological process. Sheng and Liu [21] established a theoretical model of the slider–disk interaction to include the major tribological effecting parameters such as contact forces, sliding velocity, topographic parameters and lubricant thickness. Baranov et al. [146] reported theoretical and experimental investigations on modelling AE under contact friction of solids and establishing the principal statistical properties of rubbing surfaces that affect the parameters of AE. Fan et al. [147] developed a theoretical AE model of the dry sliding process to depict the AE generation regimes during the early stage of the faults which is correlated to the asperity contacts.

In a real mechanical system, little changes under steady lubrication condition can indicate the early fault which may develop to a failure. However, most of the AE

modelling investigation in sliding contacts are focused on the friction and wear process induced by the asperity collisions. It should be aware that the shearing force induced by the viscosity of lubricants is an important part of the total friction force between the contact surfaces. Although Sheng and Liu [21] have summarised the film thickness as the key parameter of AE during sliding process, the AE generation mechanism under hydrodynamic lubrication has not been reported.

2.5.2 AE Sources from Physical Processes of Engine Operations

The AE responses from engines include burst and continuous signals that can principally source by the mechanical motions and fluid movements [127]. By following the primary AE generation mechanisms of inner structural surface interact reported in Section 2.4, the major AE sources in an engine are stimulated by the movement at movable connectors or oscillations due to joint clearances and fluid-structure interactions. A real engine system involves multi-physics processes. In general, the AE sources from engine can be summarised into three characteristic physics processes: friction and wear, rapid pressure oscillations and mechanical impacts.

2.5.2.1 Friction and Wear

Since the AE was gradually proven to be an effective tool to detect the friction and wear behaviour during manufacturing processes. Some researchers tried to detect tribological behaviour of engines using AE. Mishra et al. [148] presented that the main friction losses of piston groups were caused by the viscous friction. Douglas, Robertson and their co-authors from the research team of Heriot-Watt University, developed the latest remarkable investigation of AE mechanisms between the piston ring/cylinder liner interactions. Robertson et al. [149] aimed to verify the possibility to detect the ring and liner contacts on the body of diesel engines, and it showed that the simulated AE sources can be detected by AE sensors on the out surface of engine. Based on the above achievements, Douglas et al. [23] performed a sequence of experimental tests to relate the AE RMS to the ring and liner interaction under lubrication and dry contact conditions respectively. The test results suggested that the asperity contact, blow-by and hydrodynamic lubrication are the possible sources of the AE events acquired from engines.

It should be note that based on the mixed lubrication regimes between ring and cylinder liner surfaces, the piston ring is mainly subjected to the viscous friction due to the hydrodynamic lubrication condition. Moreover, the asperity contacts generally occur around the TDC and BDC that are usually at a lower speed near zero. Because the hybrid contact which means the surfaces contacted under lubricants has the lowest wear rates under steady state conditions[20]. Hence, aim to identify the AE generation regimes of the lubricated interaction surfaces in the ring-liner system, this work mainly focuses on the friction process induced AE under healthy working conditions.

2.5.2.2 Oscillations due to the pressure variation

Ghamry et al. [150] found the AE RMS value was well correlated to the cylinder pressure signals in both time and frequency domain. It is believed that the in-cylinder pressure is varied periodically which led to the contact force between the ring and liner varying cyclically. The normal force on the interaction surfaces of the piston groups, as an important AE source, are influenced by the oscillations of the cylinder pressure. Hence, the pressure variation can be taken as a factor to influence the AE response in engines.

2.5.2.3 Mechanical Impacts

The mechanical impacts can be considered as a collision between two or more components in a mechanical system. When two rough surfaces are in contact during a short time under compressions, it will initially generate impulsive shocks due to asperity collisions. Based on this mechanism, the AE responses could be motivated by engine components collisions with high fore in very short period. In particular, the typical impacts in an engine are the processes of valves sealing during the air intake and exhaust process and the fuel injections. Hence, many studies have been developed to diagnose the impacts of the valves opening and closing [152, 153] and the faults of injection [154, 155].

2.5.3 Studied AE Source from Engine

2.5.3.1 The Piston-Cylinder System Tribological Excitations

The tribological characteristics of interface interaction between the ring and liner are complicated owing to the sophisticated motion process and drastic combustion process. Generally, the input system energy is equal to the output energy plus dissipated energy.

most part of the energy to overcome the friction is transferred into thermal energy based on the basic theory of tribology, and the other energy loss links to deformation of asperity of interacted surfaces. Besides, the viscous friction under hydrodynamic lubrication also causes the loss of energy base on the theory of Stribeck curve. Therefore, the mechanical processes induced by the friction power can be categorized into elastic and plastic deformation, wear and viscous friction of engine tribofilm.

Shuster and the authors [19] firstly measured the friction and wear of the ring-liner system segments using AE RMS to correlate scuffing process to the AE signals.

Afterwards, Douglas et al.[23] conducted the engine running tests to demonstrate the semi-continuous AE signals possibly soured from the asperity contacts between the ring-pack and cylinder liner after turning of the lubricating oil supply. Subsequently, [156] in his Ph.D. thesis elucidated a novel condition monitoring method for monitoring extreme oil shortages in diesel engines using the AE RMS values.

These results demonstrated that the AE induced by the asperity collisions of the piston assembly can be identified on the engine body. Specifically, the AE amplitudes between normal and abnormal lubricating condition can be identified which is hopeful as an indicating tool to differ the tribology behaviour of the ring and liner.

Gu et al. [27] were trying to extract the meaningful information about engine lubricating conditions from the measured AE signals to correlate to the oil quality, which obtained results that confirm that it is feasible to use AE for monitoring subtle changes in engine lubrication conditions.

The authors in [24] further characterised online AE signals based on wavelet analysis for friction analysis, and also studied the impacts of engine tribological behaviours fuelling the substitute fuels using AE signals [157].

2.5.3.2 Combustion Oscillations

The pressure oscillations induced by combustion are the essential AE source which usually exhibits the high amplitudes and long duration of time. The signal mapping techniques were developed to identify the combustion AE activities in the engine automatically in [158]. Cavina [159] reported the AE signals can reveal the features of the combustion process and even some other impacts such as valves closing.

2.5.3.3 Valve Impacts

Valve impacts of engines generate strong AE activities with high amplitudes [160]. The valves open by pushing the stem with cam or cam follow and return back to the seat with a spring when the stem is not depressed. Gu et al. [153, 160] explored AE measurements to monitor and diagnose the clearance faults of engine valves.

2.5.3.4 Fuel Injection

Another important AE source is due to the high-speed fluid flows through nozzle orifices during the injection process. Characteristically, Gill et al. [161] deliberated the AE measurements were superior to vibration tests in detecting the injection process pump pressure of the needle valves. Reuben et al.[162] reported a detailed study into the effect injector discharge pressure has on the acoustic emission (AE) response of the injector body.

2.6 Key Findings of Chapter 2

This chapter has summarised the previous investigations of mechanisms and fundamentals of AE generations in engines focusing on tribological effects, and the current advances in engine condition monitoring and diagnosing using AE signals.

The AE technology has been demonstrated with laboratory rigs to be feasible to diagnose the friction and wear processes. Moreover, AE monitoring towards the slider to disk test rigs revealed that the sliding speed, acceleration and load can affect the AE root means square (RMS) values, whereas there is little difference in AE signals between the smooth and textured surfaces.

On the other hand, a simulated AE source on the liner can be detected on the liner surface of the diesel engine suggested in [149]. And then, Douglas et al. [23] developed a series of test on a motored engine and a running engine respectively. The interesting results showed the continuous AE linked to the asperity collisions of the ring/liner interaction surfaces when the lubricating oil supply were stopped.

Further, the key results developed by Douglas [23] suggested that the semi-continuous AE signals in the middle of stroke related to the ring and liner contact according to the AE experimentation on a motored engine without lubrication. Then, a running engine test was conducted on an engine with lubrication. In the engine running test, the

semi-continuous AE of the mid-stroke showed many low amplitudes but a similar trend as the AE signals in the motored test. Based on the ring and liner friction and lubrication regimes, the experimental studies indicated the ring and liner contacts under well-lubricated condition generate much weaker AE than the dry contacts. Therefore, these weak AE signals under the health working condition can be mainly attributed to the friction process of the ring/liner interactions. In addition, the different levels of the scuffing phenomenon were demonstrated to relate to the AE RMS values reported in [163].

Further, the author applied an advanced signal method of discrete wavelet transform (DWT) to analyse the characterisation of the viscous friction using AE signals, and also studied the potential impacts of alternative fuels on acoustic emission signals of cylinder [157], which produced positive results and demonstrated AE signals need to be processed thoroughly for enhancements of tribology related AE contents .

Hence, these studies provide a general background for expending findings into more accurate diagnostics of engine systems. It also shows that AE signals in line with adequate signal analytics allow more insight into tribological behaviours of engines to be characterised online in a non-intrusive way.

CHAPTER 3 MODELLING AND SIMULATING TRIBOLOGICAL BEHAVIOUR OF A PISTON ASSEMBLY

This chapter depicts the fluid-lubricated models in the conjunction between the conjunctions formulated by the ring-liner of CI engines and conducts a numerical analysis to understand the frictional characteristics, being one of the main tribological properties, under different operating conditions. It starts with developing relevant models for predicting the friction forces in the conjunction. Then, representative behaviours of tribofilms and two types of frictional forces due to viscous and asperity effects respectively are obtained and examined based on the single cylinder diesel engine under test. The behaviour of these forces and the tribofilms distribution in the conjunction provide a basis for developing models for tribological AE events.

3.1 Introduction

The piston ring-cylinder liner system exhibits the most multiplex tribological properties amongst other subsystems of engine owing to the impacts of combustion oscillation, unsteady gas, oil transportation and a complex dynamic behaviour between ring pack and cylinder liner contact. Numerous investigations are often carried out to gain sufficient details of the tribological behaviours. It has been widely recognized that the mixed lubrication regimes are prevailing between the piston rings and cylinder liner and realised that the less satisfied lubrication conditions often happen around the TDC and BDC during one engine cycle as the elaboration in Section 2.2, resulting in substantial wear.

This chapter firstly establishes the lubrication models for the piston ring-cylinder liner conjunction according to commonly adopted the average Reynolds equation, then the numerical results are obtained based on the testing engine to understand possible AE generations and characteristics arisen from viscous and asperity frictions, which are well-known tribological behaviours.

3.2 Total Friction of the Piston-Cylinder Liner

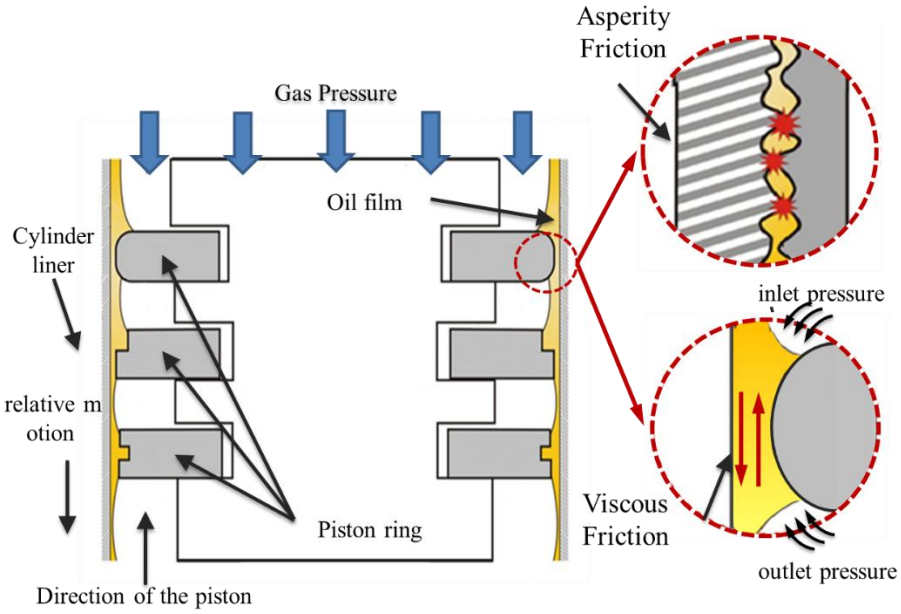

Figure 3-1. The friction and lubrication characteristics of the piston groups

Based on the mixed lubrication regimes, the total friction force of the piston assembly result from the viscous shearing force of the hydrodynamic film and the asperity friction when the asperities of two horizontal surfaces contact with each other as illustrated in Figure 3-1.

Yuanzhong [73] and MISHRA[148] conducted the total friction force of the ring-liner system is composed of viscous friction and asperity friction force as stated

$$f = f_v + f_{asp} \tag{3-1}$$

Where the f_{asp} is asperity friction force (N) which can be obtained by an integration of asperity pressures along the external surface of the piston ring:

$$f_{asp} = \mu_{asp} \int p_{asp} dx \tag{3-2}$$

And the f_v is the viscous friction due to the gradient of fluid flow obtained as

$$f_v = \int \tau_i dx \tag{3-3}$$

p_{asp} is the asperity contact pressure and μ_{asp} is the coefficient of asperity friction. τ_i is the average shear stress.

The viscous force is the shear stress sourced by entraining process of the oil and the pressure gradient can be expressed as follow owing to the converging and diverging process between the ring and the liner [148].

$$\tau_i = \frac{h}{2}\frac{p_h}{\partial x} + \frac{\eta}{h}U \tag{3-4}$$

For the numerical calculation, the piston ring force equilibrium condition is applied in the radial direction aiming to find a possible constraint as investigated by Rahnejat e.t. al [63] as illustrating in the Figure 3-2. At any instant of time, the total applied load F_{TO} acting on the piston ring from the piston groove clearance side to the ring inner surface is generated by the tension force F_e and combustion gas force F_g achieving the sealing effect; the reaction force is the total contact load W_{TO} equals to the sum of the

asperity normal force W_A correlating to the asperity contact pressure p_{asp} and the film pressure force W_O relating to the film pressure p_h .The equation is giving below,

$$F_{TO} - W_{TO} = (F_e + F_g) - (W_A + W_O) = 0 \tag{3-5}$$

$$W_{To} = \iint (p_h + p_{asp}) dxdy \,. \tag{3-6}$$

$$F_{To} = F_e + F_g \,, \tag{3-7}$$

In addition, the gas force F_g equals to:

$$F_g = b\,\mathrm{P}_g \,, \tag{3-8}$$

where b is the Ring face-width, $\mathrm{P_g}$ is the combustion pressure.

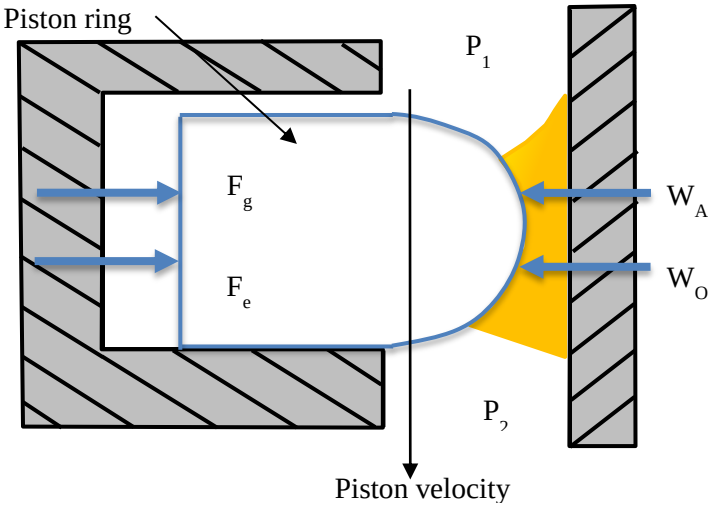

Figure 3-2. The force equilibrium on the piston ring applied in the radial direction

Particularly, the fluid model is under rich lubrication. In addition, the particle effects, the cavitation effects, piston slaps, ring flutter, twist, or tilt and waviness of cylinder are not taken into account in this model in order to just understand the interactions between the fundamental influence factors: velocity, load, viscosity and roughness and also for more efficient computation.

3.2.1 Rheological Relationship of Lubricants

The load carrying capacity of lubricant tribofilm is a key feature affecting the tribological performance of conjunction. The dynamic lubricant properties are resulting in the change of oil density, viscosity, temperature and the hydrodynamic pressure generated in the film.

Due to temperature variation and shear heating of the lubricant film between the ring and liner surfaces, the effective viscosity of lubricants varies with the temperature of the tribofilm. Additionally, the tribofilm viscosity can be estimated by using the liner surface temperature [164]. The viscosity of lubricants can be simply fit by the Reynolds viscosity equation [63]

$$\eta_0 = \eta_i \exp\left\{-\beta_n [T_1 - T_m^k]\right\} \tag{3-9}$$

where $T_m^k = \dfrac{p_g^k \Delta T}{p_{g\max}} + T_2$ is the variable of mean tribofilm temperature according to the liner temperature which is assumed to vary with the combustion pressure P_g. P_{gmax} is the max value of $p_g(x)$, ΔT and T_2 are the parameters to predict the tribofilm temperature base on the liner temperature. η_i is the corresponding viscosity at some representative temperature T_1. In this work, η_i is the measured viscosity at 100℃. The term β_n is the gradient of viscosity variation with temperature rise which equals $T_1 - T_m^k$ in a log near plot [63], and $\beta_n = 0.01$.

The dynamic viscosity of lubricant correlated to the pressure and temperature variations is given by combining the Reynolds equation [165] and Houpert's equation [166]as follows

$$\eta = \eta_0 \exp[(\ln \eta_0 + 9.67)(1 + 5.1\times10^{-9} p_h^{z_p} - 1)] \tag{3-10}$$

where p_h is the hydrodynamic pressure generated in the film. and Z_p is constant independent of pressure and is defined below [167]:

$$Z_p = \frac{a_0}{5.1\times10^{-9}(\ln\eta_0 + 9.67)} \tag{3-11}$$

where a_0 is constant at atmospheric pressure.

Besides, D. Dowson and G. R. Higginson [168] proposed the density-pressure relationship with modification to consider the thermal effect[169],

$$\frac{\rho}{\rho_0} = (1+\frac{0.6p_h}{1+1.7p_h})[1-\beta_T(T_m(x)-T_0)] \tag{3-12}$$

where ρ_0 is the lubricant density under temperature T_0, β_T is the thermal expansion coefficient of the lubricant.

Hence the lubricant viscosity can be accurately predicted by combining the viscosity, temperature, pressure and density as mention above.

3.2.1 Viscous Friction

The investigation of viscous friction corresponds to the pressure of hydrodynamic tribofilm. The mathematical model in this study is adopted the average Reynolds Equation developed by Nadir Patir and H. S. Cheng modified Reynolds equation [6, 7]. The surface roughness is taking into account with a series of flow factors. The corresponding expression is [170],

$$\frac{\partial}{\partial x}\left(\varphi_x\frac{\rho h^3}{\eta}\frac{\partial p_h}{\partial x}\right) = 6\,\mathrm{U}\,\varphi_c\frac{\partial}{\partial x}(\rho h) + 6U\sigma\varphi_s\frac{\partial}{\partial x}(\rho h) + 12\varphi_c\frac{\partial}{\partial t}(\rho h) \tag{3-13}$$

where U is the sliding speed. φ_x is the flow factor of pressure; φ_s is the factor of shear flow. The expressions of the above two factors were studied by Sutaria B.M. e.t. al [171] shown as:

$$\varphi_x = 1-0.9\exp(-0.56\mathrm{H}),\ as\,\mathrm{H}\to\infty, \varphi_x\to 0.\ , \tag{3-14}$$

$$\varphi_s = \begin{cases} 1.12\exp(-0.256\,\mathrm{H}) & H>5 \\ 1.899H^{0.98}\exp(-0.92\,\mathrm{H}+0.5\,\mathrm{H}^2) & H\le 5 \end{cases} \tag{3-15}$$

φ_c is the contact factor of Gaussian distribution of roughness heights fitted into an equation by Wu [170]

$$\varphi_c = \begin{cases} \exp(-0.6912 + 0.782 - 0.304\mathrm{H}^2 + 0.0401\mathrm{H}^3) & 0 \le H < 3 \\ 1 & H \ge 3 \end{cases} \tag{3-16}$$

The film shape at position x varying with the ring face profile which is approximated by a parabolic shape suggested in [148] can be expressed as

$$h = h_n + \frac{e}{(b/2)^2} x_j^2 \tag{3-17}$$

Where e is global in-plane ring deformation, h_n is the nominal clearance of two contact surfaces. b is the piston ring width.

3.2.2 Asperity Friction

The asperity contact needs to be considered in the piston ring-cylinder system since it occurs between any parts of rough surfaces in close contiguity with an insufficient film of lubricant. This model is calculated contact pressure between two rough surfaces based on the statistical methods, the pressure distribution firstly proposed by Greenwood and Tripp [148] is

$$p_{asp} = \frac{16\sqrt{2}\pi}{15}(\eta\beta\sigma)^2\sqrt{\frac{\sigma}{\beta}}E' F_{2.5}(\lambda) \tag{3-18}$$

where the β is the asperity radius of curvature and σ is the composite roughness of the ring and liner. E' is the equivalent elastic modulus of the contact surface which is $E' = \frac{2}{(1-\nu_r^2)/E_r + (1-\nu_b^2)/E_b}$. $F_{2.5}(\lambda)$ is the statistical function relating to the Stribeck's tribofilm parameter $\lambda = h/\sigma$, the function expression is

$$F_{2.5}(\lambda) = \frac{1}{2\pi}\int_{\lambda}^{\infty}(\mathrm{s}-\lambda)^{2.5}\exp(-0.5\mathrm{s}^2)\,\mathrm{ds} \tag{3-19}$$

For a convenient simulated calculation, Hu et al.[73] developed the following fitting formulas:

$$F_{2.5}(\lambda)=\begin{cases} A(\Omega-\lambda)^{z_1} & \lambda \le \Omega \\ 0 & \lambda > \Omega \end{cases} \tag{3-20}$$

where $\Omega=4, A=4.4068\times10^{-5}$, and $z_1=6.804$.

Assuming that the surface roughness can be expressed by

$$K^*=\frac{16\sqrt{2}\pi}{15}(\eta\beta\sigma)^2\sqrt{\frac{\sigma}{\beta}} \tag{3-21}$$

Thus average pressure of the asperity contact can be calculated as

$$p_{asp}=K^*E^{'}F_{2.5}(\lambda) \tag{3-22}$$

$K^*=5.318748\times10^{10}\sigma^{5/2}$ developed by Mishra e.t. al [148] has been used in this study.

3.3 Numerical Simulation

Table 3-1 Input parameters for the simulating calculation

Symbol	Name	value	Unit
σ_1	Roughness of cylinder surface (Ra)	0.8	μm
σ_2	Roughness of the piston surface (Ra)	0.2	μm
μ_{asp}	The asperity friction coefficient	0.1	-
h_e	Surface height of the piston ring	0.003	m
b	The axial height of the piston ring	0.003	m
ρ	oil density	890	Kg/m^3
E_1	Liner elastic modulus	$122x10^9$	Pa
E_2	Modulus of elasticity of the piston rings	$165x10^9$	Pa
a_0	Constant at atmospheric pressure	$2.2x10^{-8}$	m^2/N
$T_0, T_1, T_2, \Delta T$	Temperature parameters	40,100, 90,40	℃

r	Crank radius	0.06	m
l	Length of Connecting rod	0.205	m

In this work, a vertical single cylinder engine is adopted as a prototype for the friction simulation investigation, which is also based to carry out various AE tests and will be detailed more in Chapter 5. The input parameters for the simulating calculation are given in Table 3-1. The roughness values of ring and liner (Ra) were chosen based on the equivalent Ra values for surface finish grade numbers (ISO 1302:1992) according to the parameters in the reference [171], the direction of Ra is the normal direction of the piston ring movement.

The system variables are shown as follows,

- Operating speeds: 1000rpm, 1400rpm and 1800 rpm.
- Lubricants viscosity η_i at 100℃: 10W30 (0.0099 Pa s) and 15W40 (0.0147 Pa s) as shown in Table 3-2
- In-cylinder pressure (MPa): the combustion pressure Pg was measured from the test engine as detailed in Figure 3-5.

The flow chart of the calculation of total friction of the piston-cylinder liner is given in Figure 3-3, which realise key calculation steps as follows:

Step 1: Read input parameters of engine specifications, the combustion pressure *Pg* and the piston sliding velocity *U* and the tested viscosity of lubricant oil.

Step 2: Assume the initial minimum film thickness h_0 and the initial temperature field T of the tribofilm.

Step 3: The film shape *h* and the pressure distribution P_h are obtained by the simultaneous solution from the Equation (3-9) to Equation (3-17).

Step 4: Adopted the pressure convergence criterion which is $\frac{\sum_i^1 \sum_j^m \left| p_h^{k+1} - p_h^k \right|}{\sum_i^1 \sum_j^m \left| p_h^{k+1} \right|} \le 0.01$.

If the convergence criterion is not satisfied, the relaxation method is applied to reduce the error as $p_h^{k+1} = p_h^k + \varepsilon(p_h^{k+1} - p_h^k)$ (the relaxation factor ε is 0.5 under-.), and then repeat this step.

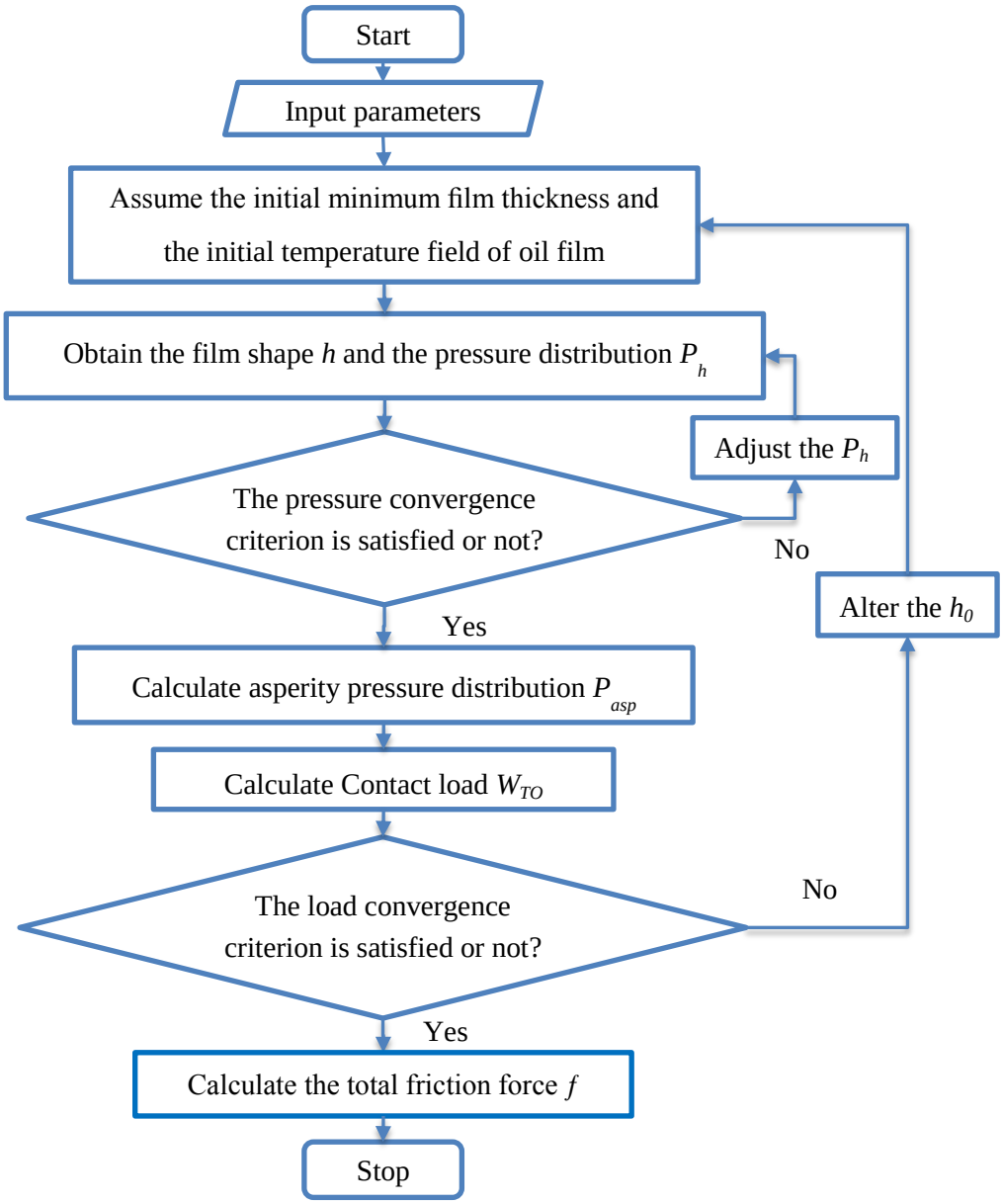

Figure 3-3. Numerical flow chart of the total friction of the Piston-cylinder liner

Step 5: Using Equation (3-18) and Equation (3-22) to calculate asperity pressure distribution $P_{asp.}$

Step 6: Calculate the contact load W_{TO} using Equation (3-6).

Step 7: Based on the force equilibrium condition, the load convergence criterion should be: $\left|(F_g+F_e)/(W_o+W_a)-1\right|<0.02$, the initial minimum film thickness is the ring bore nominal clearance (The minimum tribofilm thickness is determined by the force balance between applied load and oil pressure together with the mass continuity boundary

conditions at the edges of the ring [172]). If it is not satisfied, the clearance is altered to $h_n^{k+1} = h_n^k - \left\{ \gamma \left| (F_g + F_e)/(W_o + W_a) - 1 \right| \right\}$ (γ is the range from 10^{-8} to 10^{-9}). Then repeat the steps from 2 to 7.

Step 8: Calculate the total friction force f, using Equation (3-1), Equation (3-2) and Equation (3-3).

3.4 Evaluation of the Piston Ring Friction Forces

3.4.1 Viscosity Measurement Results of Lubricating Oil

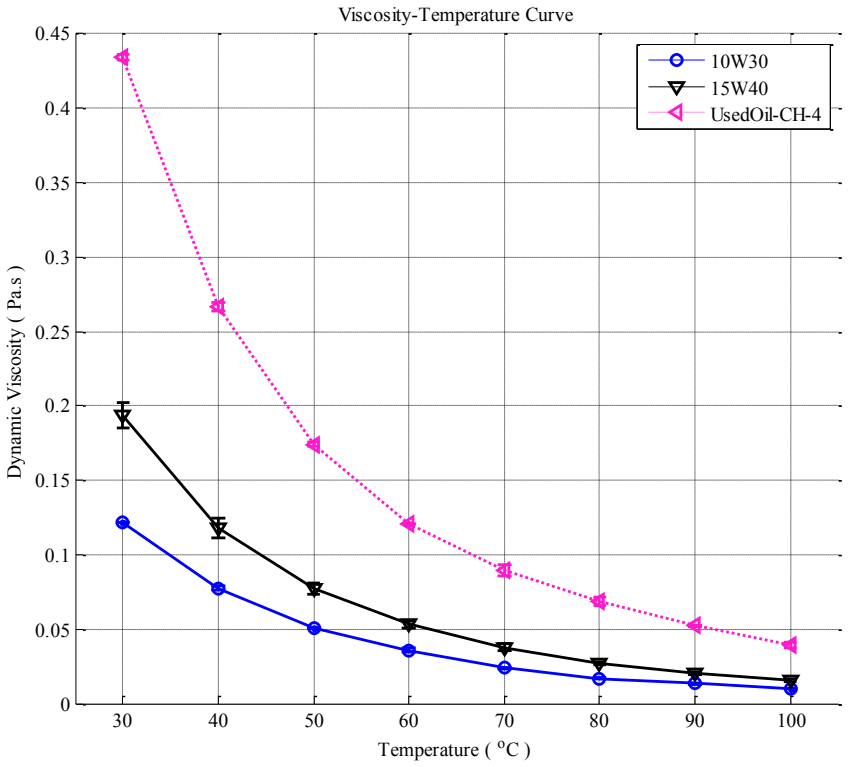

Figure 3-4. Measurement of viscosity-temperature characteristics for different lubricating oil

The viscosity of lubricating oil, one of an essential property in keeping a fluid film between sliding surface, can be defined as a parametre to represent the resistance to the deformation by shear force. The oil viscosity is temperature dependent and the effect of viscosity on the total friction force is significant. This research is adopted the testing lube-oil viscosity as the input parameter of the simulation results as shown follows, the detail measurement methodology was introduced in section 5.2.3 and 5.3.1 on chapter 5.

The viscosity-temperature characteristics for different lubricating oils are shown in Figure 3-4. Three types of oils were tested in this study. The first two types of oils are brand new. The SAE grade of the new oils is 10W30 and 15W40 respectively. They are mainly for the verification of the models and signal analysis tools. The used oils were from automotive diesel engines after the vehicle had operated for about 10,000km since previous maintenance. The performance level of the used oil is API CH-4, but the SAE grade is unsure due to collect from several vehicles. So they can be based to evaluate how AE responses measured from engine body can differentiate between them and from other two new oils.The viscosity values of all types drop significantly with temperature. The viscosity values depicted particularly under 40^{o}C and 100^{o}C as shown Table 3-2.

Table 3-2 Viscosity-temperature comparison of different lubricating oils

Type of oils	Viscosity(Pa s)	
	40^{o}C	100 ^{o}C
10W30	0.0764	0.0099
15W-40	0.0112	0.0147
Used-oil CH-4	0.2686	0.0404

3.4.2 Cylinder Inner Pressure Distribution and Variation

Aim to investigate the piston friction properties, the input cylinder pressure was measured from the firing engine test (as described in the section 6.3.1 on chapter 6) with a single cylinder test engine QCH1125. Particularly, the two groups of pressure data were measured under the different lubrication condition by using 10W30 lube-oil and 15W40 lube-oil respectively for friction force calculation. In Figure 3-5, to show the simulated results clearly, three selected input speeds for simulating are 1000 rpm, 1400rpm and 1800rpm respectively which are the low speed, medium speed and high speed in the engine running test as displayed in the chapter 5; two viscosity values are adopted from the dynamic viscosity test: which are 0.0099 Pa s (the viscosity value of 10W30 oil under 100^{o}C) and 0.0147 Pa s the viscosity value of 15W40 oil under 100^{o}C as the input parameter η_i as stated in section 3.3.

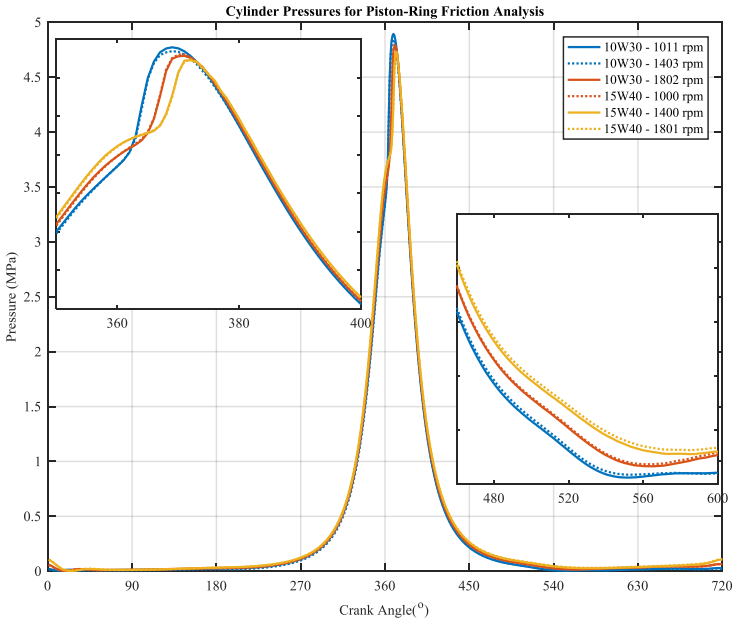

Figure 3-5 The cylinder pressures under 10Nm used for friction simulation

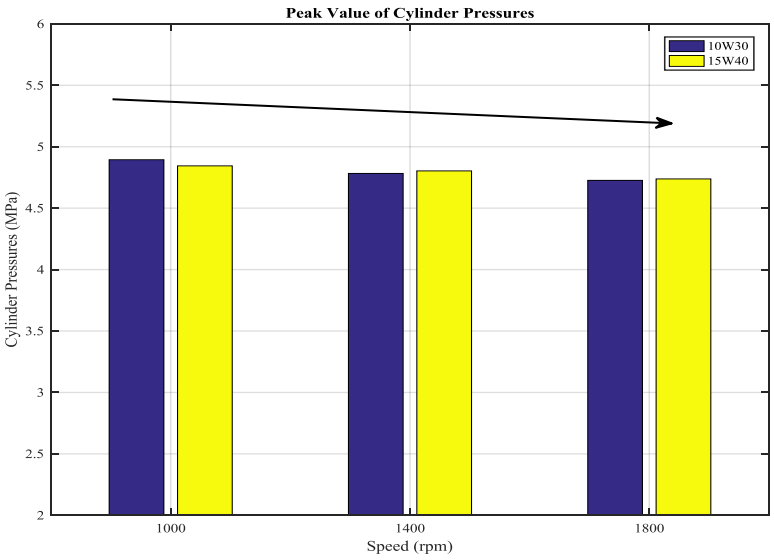

Figure 3-6 Max values of cylinder pressures

Under different viscosity values, pressure profiles are nearly same at the same speed the peak pressure decreased slightly as the engine speed increase. On the contrary, the pressure is enlarged with the engine speed increase during the other range except around the peak value. The bar chats Figure 3-6 displays the peak pressure value is generally decreased slightly with the increase of the engine speed and viscosity under 10Nm.

3.4.3 Minimum Film Thickness during a Working Cycle

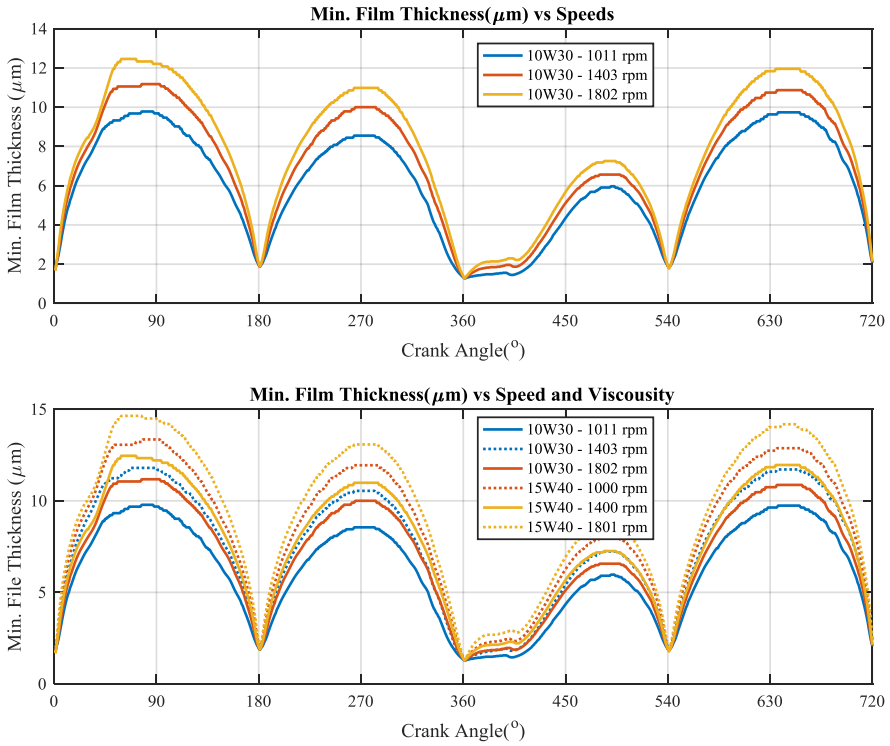

Figure 3-7 Simulation of film thickness under different speed and viscosity

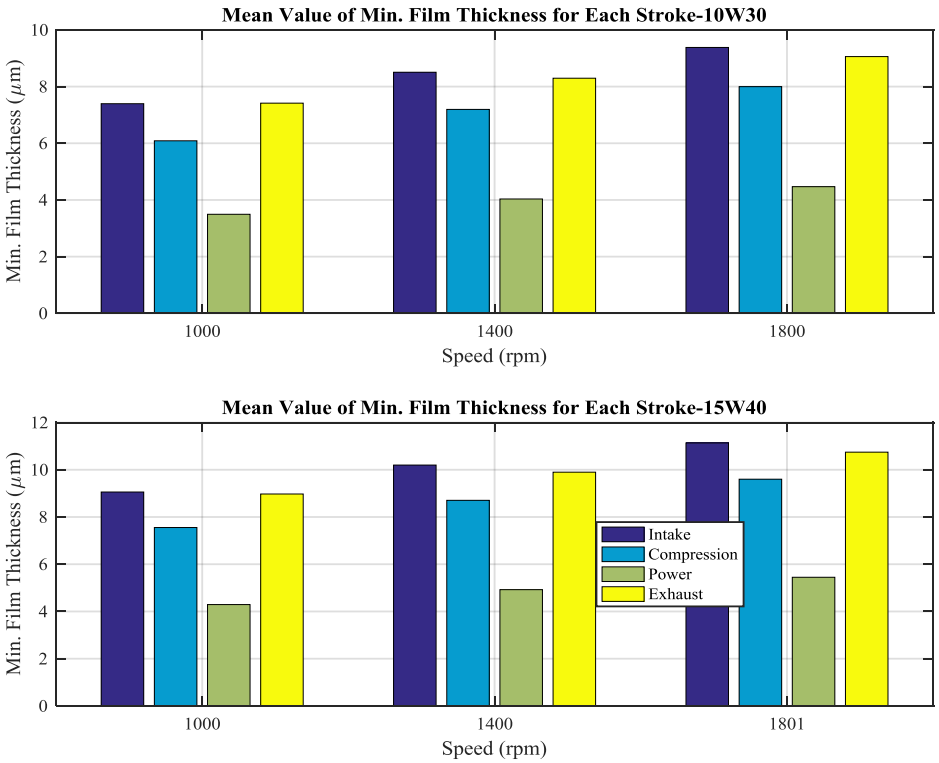

Figure 3-8 Mean values of minimum film thickness

The minimum film thickness is the minimum value of the film shape h as given in the equation (3-7). The minimum value of the film shape around the ring cycle is varied in one working due to the fore balance on the wage of the ring. It is simulated to exam the correlation to the engine speed, oil viscosity and pressure. In Figure 3-7, the value of min-film thickness was much lower during TDC and BDC, whereas the max value was during the mid of strokes around the degree of 90^{o}, 270^{o}, 450^{o} and 630^{o} related to the max piston speed around the middle stoke, and the thickness increased with engine speed and viscosity. Figure 3-8 is the bar chart of the mean value of min. film thickness for four strokes, the mean value clearly increases with the piston speed and viscosity of oil, and the lowest mean value is in the power stroke at each speed due to the high pressure of the combustion.

3.4.4 Numerical Results of Asperity Friction and Viscous Friction

The Figure 3-9 and Figure 3-11 show predicted results of asperity friction and viscous friction under different speeds and viscosity values. Asperity friction decreases with speed whereas viscous friction increases with speed during an engine cycle. The viscous force increased in the middle of the stroke mainly due to the max value of min film thickness with the sliding velocity increasing. In the power stroke, the max viscous friction is located after the TDC in degree 360° owing to the impacts of the combustion process.

In Figure 3-10, the mean value of viscous force in the compression and power strokes are significantly higher than the two other strokes owing to the higher cylinder pressure rising rapidly around the TDC before power strokes.

The bar chart for the mean value of asperity friction and BDC under different speed is illustrated in Figure 3-12. The asperity friction is extremely higher around the TDC before power stroke than others and the asperity friction values of BDC after power stroke also slightly higher than the BDC before compression. That is owing to the asperity interactions partly caused by the high value of cylinder pressure increasing sharply in the power stroke as shown in Figure 3-5. The TDC before exhaust strokes and the BDC before compression all display a decreasing with increasing the engine speed and oil viscosity, since a higher speed is helpful to formalise tribofilm and a more viscous lubricant has a higher load capacity. In other words, it is possible to reduce the

probability of the contact between the asperities on the sliding surfaces. The other TDC and BDC asperity friction show slightly difference between the three speeds compared with the TDC before power stroke.

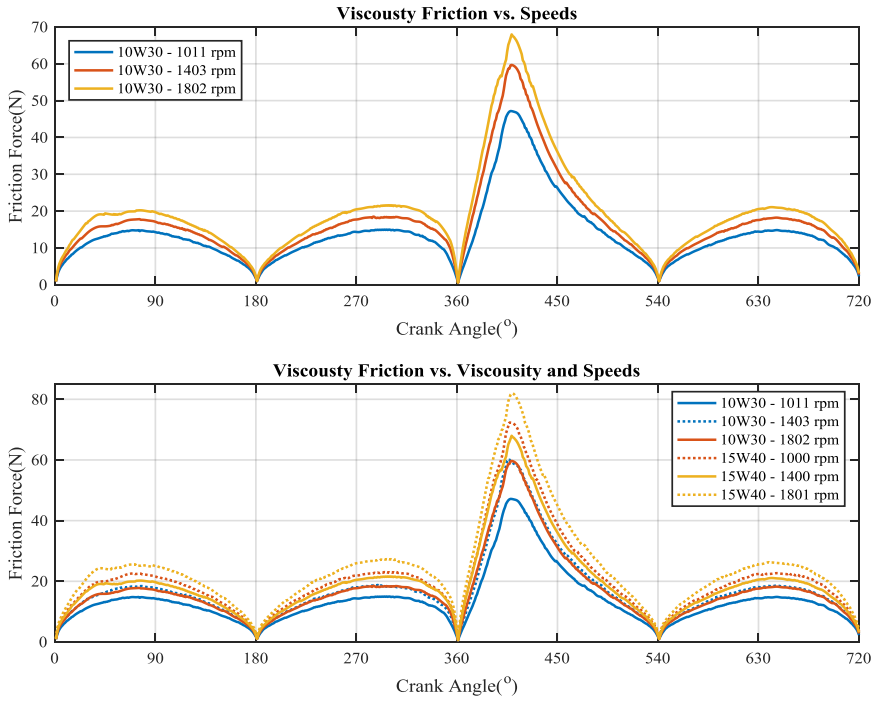

Figure 3-9. Simulation of viscous friction under different speed and viscosity

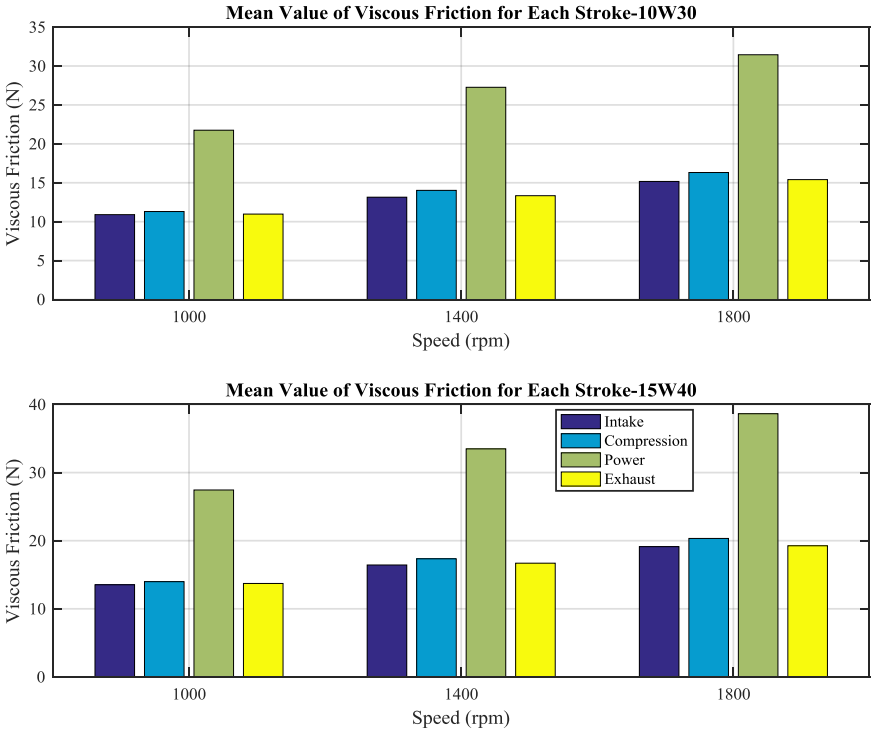

Figure 3-10. The mean value of viscous friction

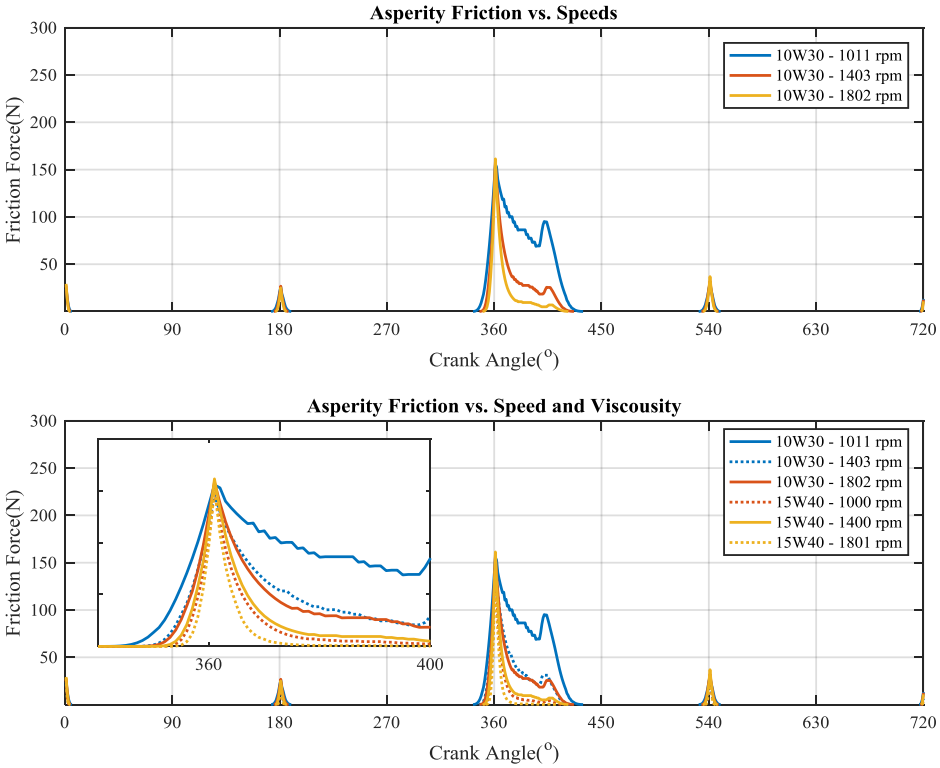

Figure 3-11 Simulation of asperity friction under different speed and viscosity

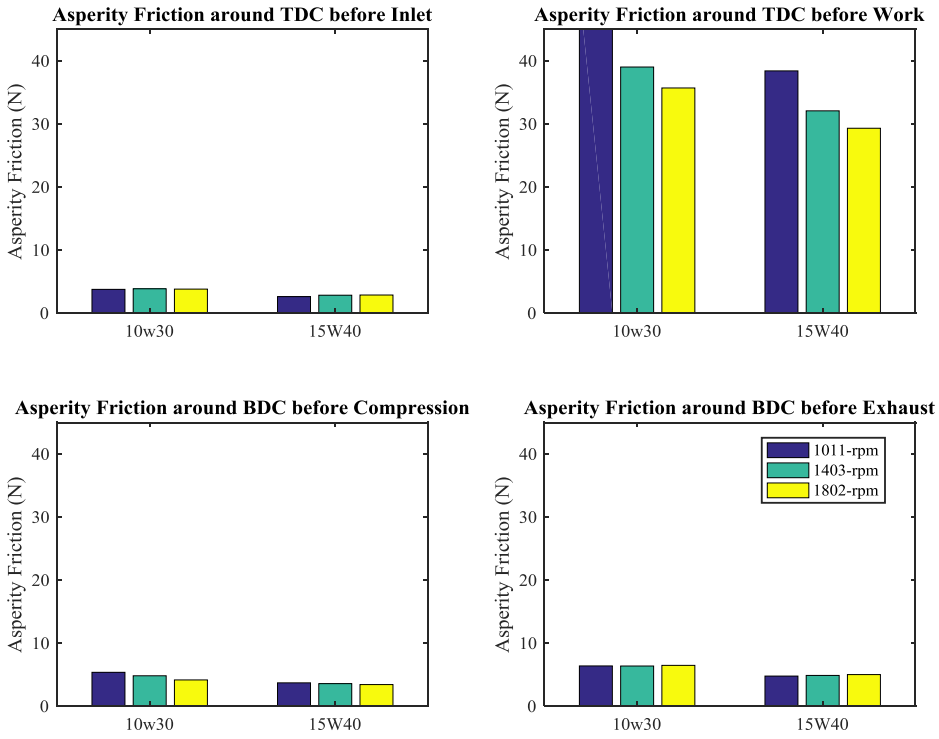

Figure 3-12 The mean values of asperity friction forces around TDC and BDC under different speed

3.5 Key Findings of Chapter 3

The key results developed by Douglas [23] investigated that the continuous AE in the middle of stroke correlated to the ring\liner contact when the lubricants have been stoped. Based on the ring and liner friction and lubrication regimes, these weak AE signals under the healthy working condition can be mainly attributed to the hydrodynamic friction regimes. However, the further investigations to correlate these weak AE to the friction process of the ring and liner were not in depth.

Aimed to verify the correlation between engine friction force and the AE responses from the cylinder outer surface; this chapter firstly develops a simulated model to compute the total friction force of the ring-liner system with the experimental parameters form the test engine.

The simulation results are calculated with the input data of in-cylinder pressure and dynamic viscosity data of the lubricating oil to evaluate the dynamic piston ring friction force. It can be found that the engine speed, viscosity of lube-oil engine load, as the key parameters of the engine system, are closely related to the friction process of the piston ring assembly according to the simulating results:

The value of minimum film thickness increases with engine speed and viscosity values whereas decreases with engine load. Moreover, the value is much lower in power stroke than others due to the high pressures and temperatures of the combustion process.

Asperity friction is more dominant around the TDC before power than the other TDC and BDCs. The values of asperity friction decrease with speed and viscosity values, whereas viscous friction shows in the middle strokes around the degree of 90 º, 270 ºand 630º related to the max piston speed around the middle stoke, whose amplitudes increase with viscous values and the engine speed. In the power stroke, the maximum viscous friction is located immediately after the TDC in degree 360 ºowing to the impacts of the combustion process.

This numerical analysis archives sufficient understandings to the high AE activities in the middle of strokes which are mostly relating to the viscous friction. However, it shows little information upon the effect of any asperity effect in the middle of each

stroke as the model is based on more perfect conditions in obtaining the numerical solutions.

CHAPTER 4 AE MECHANISMS BASED ON DYNAMICS OF MICRO ASPERITIES

This chapter elaborates AE mechanisms of fluid-lubricated rough surfaces based on an analysis of the dynamic behaviours of asperity-asperity collisions (AAC) and fluid-asperity interactions (FAI). It starts with formulating the AE generation from the asperity collision due to the compressive deformation of asperities when they are in contact. Then it derives the FAI AE formalisation based on the bending deformation of an asperity sheared by viscous fluid flows. Finally, the general characteristics of these two types of AEs caused by the tribological process of the ring-liner interaction are discussed, which provides fundamentals for effective AE signal acquisition and processing and thereby AE based lubrication diagnostics and monitoring.

4.1 Introduction

Non-intrusive technology has an unparalleled advantage in monitoring and diagnosing the tribology process of mechanical systems without breakdown. The AE technology attracts much attention in studies of the tribological features due to the direct relationship between AE phenomena and the deformation processing of materials.

However, the generation mechanism of AE induced by the friction process, especially lubricated surfaces, is still not fully understood so far. Therefore, this chapter explores the physical mechanisms of AE due to the friction between two rough surfaces subject to different lubrication regimes.

4.2 Acoustic Emission Energy

Prior work concerning the amplitude of AE signals contains information on the energy of AE source. The reference [23] suggested that AE energy of an original AE signal presented in the angular domain is estimated as the integral of the squared voltage signal in the angle domain to ensure an equal amount of data per engine cycle irrespective of engine speed:

$$E = \int_{de1}^{de2} A(\theta) d\theta \tag{4-1}$$

where $A(\theta)$ represents the amplitude of the AE signals in volts (mV), θ is the crank angle in degrees, E is the angle-domain AE energy, and $de1$ and $de2$ are the boundaries of the crank angle windows. Moreover, in situ studies demonstrated that the AE RMS values are shown a good correlation to the energy of AE signal induced by friction or wear [16, 20] .Consequently, this work employs the AE RMS value along with signal amplitude to evaluate the energy of AE during the friction process of interest.

4.3 AE induced by Micro Asperity-Asperity Collisions

The asperity contact during the sliding contacts was discovered as the primary source of acoustic emissions in a ball-on-cylinder test studied by Boness and McBride[173]. Later, the asperity contact behaviour between the slider and disk interface was studied using

AE [143, 174, 175], it demonstrated that the AE generation during sliding movements was correlated to the sliding speed, applied load and the topography of surface[23].

The basis of the research on the asperity contacts during the sliding process defined as the indentation of an elastic half-space by a rigid frictionless sphere [176] is investigated as an important role in sliding friction and wear processes. Komvopoulos and the co-workers [55] stated the boundary lubrication is accompanied with the asperities friction and wear. Particularly, reference [23] indicated that the AE events were related to asperity contacts and elaborated findings is for evaluation of lubricating oil feed rates with the lube oil turned off under abnormal running conditions.

These findings have prompted work focusing on AE modelling generated by sliding friction investigated by Y. Fan and his co-workers[147]. They developed the AE modelling during sliding friction based on the elastic deformation of asperities, and the model indicates that the AE energy is determined by the asperity contact load, sliding speed, and the surface topographic characteristics.

4.3.1 Energy Release of Asperity Collisions

4.3.1.1 Assumptions

During the sliding contact, elastic deformation means that the asperities are deformed when they collide, after the force is removed, the asperities return to their original shapes. If the applied force is sufficient to deform the asperities irreversibly, it is called plastic deformation. The adhesion and ploughing process is demonstrated to include the plastic deformation in the unlubricated friction process summarised by Rigney [177].

In the macroscale, the simulated results of the ring and liner contacts in chapter 3 manifest the asperity contact are mainly around the TDC and BDC. It indicates that the boundary lubrication regime is not the dominating lubrication condition. Additionally, wear is the most unwanted failure of the ring-liner. A variety of methods have been applied to diesel engines to reduce wear of the ring-liner system, such as the anti-wear additives of lubricants, honing liner surfaces and coatings. Hence, there is no significant wear between the ring and liner under the health working condition.

In addition, the plastic deformation is shown more close correlation with wear than friction under lubrication. Therefore, aim to identify the AE generation mechanism in friction process between the ring and liner with lubricants. In this study, the asperity

collisions between the ring and liner can be ideally assumed due to the elastic deformation.

Combined with the numerical simulation results between the ring and liner surfaces in Chapter 3 and the roughness of honed surfaces, the modelling for asperity collisions is based on the following assumptions:

- The asperities of real contact area are simply assumed as spherically tipped asperities with the same radius but the heights of asperities vary randomly;
- Asperities deform elastically i.e ignore the plastic defamation which probably more significantly occur when the surface becomes fatigued at the late service phases; and
- There is no adhesion at asperity contact.

As the foundlings in the prior investigation of AE in friction, the asperities entering are deformed when the solid surfaces in the relative motion and some share of this energy is registered as AE signals[127]. Generally, the two contact surfaces with different hardness often modelled consequently as a hemisphere against a rigid surface in the real rough surface contact.

To simplify the model of this process, all the asperity summits assumed with the same radius hemisphere R; z is the height from the asperity surface to reference plane; d is the rigid gap between the ring and liner surfaces. The critical interference δ can be described as the deflection of hemisphere in the contact area. The schematic diagram for contacting joint of rough surfaces and rigid surfaces are given in Figure 4-1. To discriminate the contact regimes of hemisphere result from the elastic deformation, the deflection of the hemisphere during pure elastic deformation assumed to be δ_e.

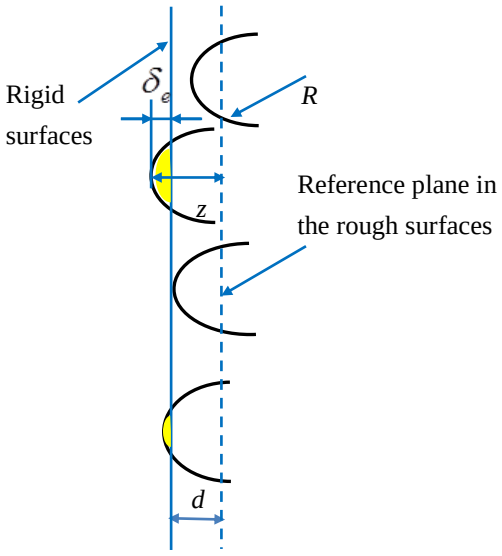

Figure 4-1 Contacting joint of rough surfaces and smooth surfaces [178]

The interact surfaces which the surface roughness are σ_1 and σ_2 can be simplified as the interactions between an ideal plane and a flat surface with roughness[147]

$$\sigma_s = \sqrt{\sigma_1^2 + \sigma_2^2}\,. \tag{4-2}$$

The deformed distance δ_e during purely elastic deformation assumed by Hertz solution is described as a tiny distance that cannot change the geometry significantly.

The probability of the height for the asperity surface from z to *z+dz* above the reference plane is

$$p(z > d) = \int_d^\infty f(z)dz\,. \tag{4-3}$$

where *f(z)* is the probability density function of the asperity height [147].

The total number of asperities in contact is defined as

$$N = D\int_d^\infty f(z)dz\,, \tag{4-4}$$

where D is the number of asperities in each unit area.

4.3.1.2 Energy Release Rate of Elastic Deformation

Based on the Greenwood model assumption, the elastic deformation of the hemispherical asperities are defined by the Hertz elastic solution[179]. The elastic load on a spot of contact area is the L_e [69], and the resulting equation is

$$L_e(\delta) = \frac{4}{3} E R^{1/2} \delta_e^{3/2} . \tag{4-5}$$

Hence, the elastic deflection is

$$\delta_e = (\frac{9}{16 E'^2 R})^{1/3} L_e^{2/3} . \tag{4-6}$$

where $\frac{1}{E'} = \frac{1-v_1^2}{E_1} + \frac{1-v_2^2}{E_2}$, E_1 and E_2 are the Yong's modulus of the contact materials; v_1, v_2 are the Poisson's ratios of the contact materials.

A hemisphere joined to the rigid surface can be stored elastic energy U_{ie} as [147]:

$$U_{ie} = \int L_e d\delta_e \tag{4-7}$$

Associated with the Equation (4-5), stored elastic energy (U_{ie}) can be expressed as

$$\begin{aligned} U_{ie} &= \int_d^\infty L_e d\delta_e = (\frac{9}{16 E'^2 R})^{1/3} \int_d^\infty L_e^{2/3} dL_e \\ &= \frac{3}{5} \cdot (\frac{9}{16 E'^2 R})^{1/3} \cdot L_e^{2/3} \cdot L_e = \frac{3}{5} L_e \delta_e \end{aligned} . \tag{4-8}$$

Since the interference of elastic deformation can be defined by

$$\delta_e = z - d , \tag{4-9}$$

the mean elastic energy for per unit hemisphere joined area is

$$\bar{U}_{ie} = \frac{3\int_d^\infty L_e \delta_e f(z) dz}{5\int_d^\infty f(z) dz} = \frac{3\int_d^\infty L_e (z-d) f(z) dz}{5\int_d^\infty f(z) dz} \tag{4-10}$$

The total elastic energy stored in the asperity contacts is

$$U_E = NA_o\bar{U}_{ie}, \tag{4-11}$$

where A_o is the apparent contact area;

Substituting the Equation (4-4) and Equation (4-10), the total elastic energy can be given by

$$U_E = \frac{3}{5}A_o DL_e\int_d^\infty (\mathrm{z}-\mathrm{d})\,f(\mathrm{z})dz\,. \tag{4-12}$$

The time to release the energy for one asperity is given by

$$t = \frac{2a}{v_p}, \tag{4-13}$$

where a is the radius of the contact area of one hemisphere, and the *v* is sliding velocity. For a hemisphere, the shape for contact spot of a fully elastic area is approximated as a circle; hence the contact area A_e which is given by the reference [180] as

$$A_e = \pi\delta_e R\,. \tag{4-14}$$

Therefore, the sliding distance can be represented as radius a_e,

$$a_e = (\delta_e R)^{1/2} \tag{4-15}$$

The release time of a unite sliding distance can be

$$T_e = \frac{2a_e}{v_p} = \frac{2(\delta_e R)^{1/2}}{v_p} \tag{4-16}$$

Putting Equation (4-3), the mean release time of elastic deformation is

$$\bar{T}_e = \frac{2\int_d^\infty R^{1/2}\delta_e^{1/2} f(\mathrm{z})dz}{v\int_d^\infty f(\mathrm{z})dz}\,. \tag{4-17}$$

The release rate of elastic energy can express by substituting Equation (4-12) and Equation(4-17),

$$\dot{U}_E = \frac{U_E}{\bar{T}_e} = \frac{3A_o DL_e \int_d^\infty (\mathrm{z}-\mathrm{d})\, f(\mathrm{z})dz \cdot v\int_d^\infty f(\mathrm{z})dz}{10\int_d^\infty R^{1/2}\delta_e^{1/2} f(\mathrm{z})dz} = 0.3A_o DL_e vR^{-1/2} \frac{\int_d^\infty (\mathrm{z}-\mathrm{d})\, f(\mathrm{z})dz \int_d^\infty f(\mathrm{z})dz}{\int_d^\infty (\mathrm{z}-\mathrm{d})^{1/2} f(\mathrm{z})dz} \tag{4-18}$$

Since the most machined surfaces have nearly Gaussian distribution, this work adopts a Gaussian distribution to calculate the asperity height standardized distribution function $\phi(s)$ as

$$\phi(s) = \frac{1}{\sqrt{2\pi}\sigma_s} \exp(-0.5s^2), \tag{4-19}$$

where $s = z/\sigma_s$, σ_s is the standard deviation of the asperity heights.

Reference[147] defines that the probability density function is

$$F_n(\mathrm{h}) = \int_t^\infty (s-h)^n \phi(s)ds, \tag{4-20}$$

where the standardized variable $s = z/\sigma_s$, σ_s is the standard deviation of height distribution and $h=d/\sigma_s$. $\phi(s)$ is the standardized height distribution.

Substituting the Equation (4-18) and Equation (4-20), the release rate of elastic energy can simplify to

$$\dot{U}_E = 0.3Np_e vR^{-1/2} \frac{F_1(\mathrm{h})}{F_{1/2}(\mathrm{h})}. \tag{4-21}$$

4.3.2 AE Modelling for Asperity Collisions

Fan et al [147] elaborated the conversion efficiency of the elastic strain energy which is converted to AE signals. Define the conversion rate of elastic strain energy into the measured AE energy is given by

$$K_c = k_e k_m. \tag{4-22}$$

where k_e is the energy conversion rate that the elastic strain energy converts to AE pulses which can be detected by the AE sensor; k_m is the energy conversion rate gain from the AE measurement system.

In friction of rough surface contact, the elastic interaction and impacts of surface micro-asperities can be considered to be the AE source. Therefore, the energy released rate of AE generated by the asperity contact can be taken as follows

$$\dot{U}_{AE\_asp} = K_c 0.3 N p_e v R^{-1/2} \frac{F_1(h)}{F_{1/2}(h)} \tag{4-23}$$

Based on above AE analytic models, the AE energy from AAI is promotional to the sliding speed of the two contact surfaces and normal force vertically on the contact area of the piston ring and bore. In addition, it is also influenced by the parameters of material characteristics for two contact components.

4.4 AE Induced by Fluid-Asperity Interactions

The model developed in Section 4.3 shows the AE generation due to asperity collisions. It can be used to explain most AE activities occurring in the boundary lubrication and mixed lubrication regimes in which asperity contacts are presented. However, for the hydrodynamic lubrication regimes when the two sliding surfaces are fully separated by tribofilms there such as that of the middle of engine strokes, are little asperities in contact. It is therefore not possible to use the asperity collision model to describe the AE signals observed in hydrodynamic lubrication regimes.

Particularly, the experimental studies of [27] indicated the possibility to predict the quality of engine oil using AE RMS values owing to a clear difference between used oil and three new oil types. The results showed the feasibility to use AE for engine lubrication condition monitoring. Further, the authors [24] also observed experimentally that the continuous and strong AE events exhibit in the middle of each stroke in a single cylinder engine and the intensity of these AE events is proportional to engine speed and oil viscosity. Furthermore, numerical studies [95], detailed in Section 3.3, shows that the lubrication in the mid-stroke is predicted to fall into hydrodynamic regimes where

little asperity contact happens. These findings show inconsistency with the AE model based aspect collisions. Moreover, little literature has been found in modelling the FAI for AE generation. Therefore, this section provides further AE mechanisms and modelling for the AE events occurring in hydrodynamic lubrication regime.

According to the fluid shearing effect or viscous friction generation between fluid layers and the liner boundary in the hydrodynamic lubrication regime, the pressurised fluid flow will shear rough surfaces of the liner and ring, leading to instantaneous bending deformation of asperities on the surfaces and formalising AE waves. Based on these understandings and the way in modelling the AE generation from the compressive deformation during asperity collision, a novel model will be developed to describe the FAI AE based on the dynamic bending deformation process of asperities under fluid shearing.

4.4.1 Energy Release of Asperity Bending Deformations

The typical plateau honing finish is used in current cylinder liners manufacturing as shown in Figure 2 3 (a). When the liner surface submerges in the film, the shearing force of lubricants is generated during the sliding to bend the asperities of liner surface owing to deep grooves. For ease of developing asperity bending deformation induced AE, the following simplifications are made:

(a) The asperities submerged in the tribofilm are simplified as a cantilever with a spherical tip which the asperity height is assumed as z with constant equivalent width w to represent the randomness of asperities for most machined rough surfaces with adequate running-in. The heights z thus are characterised by a Gaussian distribution $\phi(s)$ using Equation (4-19);

(b) The liner surface is focused as it much softer than the ring;

(c) The deformation along a line along the direction corresponding to ring width is examined and other parts along the circumference of the liner are assumed to be similar Gaussian heights.

(d) In addition, other potential effects such as fluid cavities, turbulences and gas blow-by are not considered.

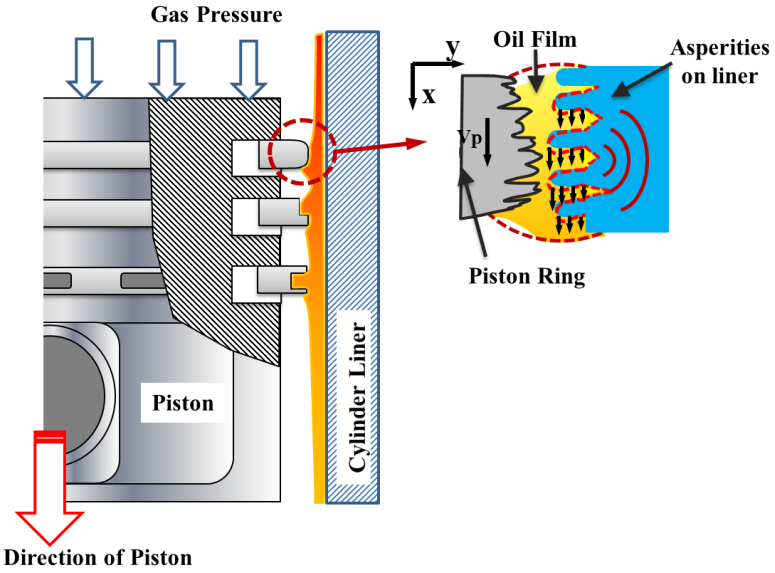

Figure 4-2 Elastic bending deformation of asperities on the surface of the cylinder liner

When the piston ring slides downward along the rough surface of the liner, the elastic bending deformations of asperities on the liner can be induced by the viscous shear stress τ_y, as shown in the magnified schematic of Figure 4-2.

During the hydrodynamic lubrication regimes the fluid has a pressure field, the pressure gradient along ring width $p(x,y,t)/\partial x$; the velocity distribution of fluid flows can be taken as a velocity field $v(x,y,t)$; and the nominal film thickness field can be shown as $h(x,y,t)$. These can be obtained by solving the average Reynold equation [22, 23] under given boundary and operating conditions including the contact load due to ring expansion and gas pressure. Therefore, the viscous force is shown in Equation (3-4) can be expressed as.

$$\tau(x,y,t)=\frac{h(x,y,t)}{2}\frac{p(x,y,t)}{\partial x}+\frac{\eta(x,y,t)}{h(x,y,t)}v(x,y,t), \qquad \text{(4-24)}$$

where η is the dynamic viscosity of lubricant and h is the nominal film thickness.

For a single asperity with a random height z and constant width w_i is assumed to have an equivalent width w, the sharing force applied to the asperity can be expressed as

$$F_i = \int_0^z w_i \tau(x, y, t) dy \tag{4-25}$$

It will bend the asperity and result in bending deformation energy for one asperity:

$$U_i = \frac{F_i z^3}{3E_l I_i} \tag{4-26}$$

where I_i is the bending moment. The bending deformation of the asperity is reclaimed immediately after the ring passes the asperity, provided that the damping effects can be ignored. When the piston moves at a velocity of v_p, the time duration for the bending and reclamation of one asperity is

$$t_b = \frac{b}{v_p} \tag{4-27}$$

and thus the energy release rate is:

$$\dot{U}_s = \frac{U_i v_p}{b} \tag{4-28}$$

As a result of this rapid bending process, an instant disturbance on the cylinder liner will be induced by a portion of the energy, which will exhibit as an AE burst. If the number of asperities per unit length is N_s, the expected number of bent asperities across ring width *b*

$$N_d = N_s \int_0^b f(z) dz, \tag{4-29}$$

The total deformation energy U_s:

$$U_s = N_d U_i = N_d \frac{F_i z^3}{3E_l I_i} \tag{4-30}$$

The total energy release rate $\dot{U}_s$ along the line is:

$$\dot{U}_s = \frac{U_s v_p}{b} \tag{4-31}$$

Substituting Equations (4-24) - (4-30) into (4-31) yields the energy rate in a more specific expression:

$$\dot{U}_s = \frac{v_p N_d z_i w_i}{3bE_l I_i} \int_0^z [\frac{h(x,y,t)}{2} \frac{p(x,y,t)}{\partial x} + \frac{\eta(x,y,t)}{h(x,y,t)} v(x,y,t)]dy \qquad (4\text{-}32)$$

It shows that AE intensity is directly proportional to viscously and velocity whereas less dependent on pressure or load. That allows a better interpretation of AE activities in HL (hydrodynamic lubrication) regimes and provides the basis for lubrication monitoring.

It can be seen from Equation (4-32) that the release rate of elastic bending energy due to the interaction between fluid and surface asperities is proportional to the material and geometry characteristics of the ring-liner but also the sliding velocity, lubricant viscosity and fluid pressure or contact load. This allows a rigorous interpretation of the AE generation during hydrodynamic lubrication and consistent with the observations that the AE events are stronger in the middle of stroke where the speed of the piston is maximal.

Moreover, based on the proportional relationship between the bending energy rate and viscosity it is possible to use AE signals to monitor the lubricant conditions which is mainly reflected by viscosity changes.

4.4.2 AE Signal from Flow Induced Bending Deformations in Asperities

Similar to the AE signal generated by the compressive deformation of asperities which is studied in Section 4.3.2 and [147], the strength of AE signal due to the interaction between fluid and asperity can be obtained by weighting the energy release rate k_b which is smaller than unity as most bending energy is converted into frictional heat. Furthermore, there are a large number of asperities that can be under bending deformations across entire ring surface at any time instants and the velocity of the piston is time-varying but with high orders of continuity. Considering the high density of asperity bending and the sufficient continuity of the piston velocity and oil pressure, AE signal from FAI process will exhibit pseudo-continuous (or stationary) with superimposed burst excitations due to sporadic high-amplitude during the period of HL regimes, and thereby be expressed approximately by considering the contact area of ring surface and energy released rate as

$$AE_b(t) = \pi d_r b k_b \dot{U}_s \tag{4-33}$$

Where d_r is the diameter of the piston ring.

Substituting the Equation (4-32) into (4-34),

$$AE_b(t) = \frac{\pi d_r k_b v_p(t) N_d(t) z_i w}{3E_l I_i} \int_0^{z_i} [\frac{h(x,y,t)}{2} \frac{p(x,y,t)}{\partial x} + \frac{\eta(x,y,t)}{h(x,y,t)} v(x,y,t)] dy \tag{4-34}$$

Equation (4-34) gives a more comprehensive description of the AE from FAI. Like the AAC induced AE in Equation (4-23), the intensity of FAI induced AE is found to be more promotional to the sliding speed between the two contact surfaces, similar to that described by the integration term of Equation (4-23). However, it is related to pressure or loads the pressure gradient or less influential by the loads. Moreover, it shows a direct connection between AE amplitudes and lubricant viscosity. This provides the theoretic basis for lubrication diagnosis.

It is also influenced by the parameters of material characteristics including surface quality for two contact components, which shows that worn and local defected surfaces can be also reflected by AE responses.

4.5 General Characteristics of AE from Ring and Liner

As shown in previous studies, the lubrication of ring-liner consists of the three classical regimes: BL, ML and HL. With the two AE models developed it is possible to explain AE characteristics in these three regimes more clearly. Obviously, AE behaviours in BL and HL can be explained mainly be the AAC and FAI models respectively. For the ML regime, as it presents both asperity collisions and flow shearing, so its AE can be predicted by both the AAC and FAI models jointly. As both AE models are developed based on deformation energy it is sufficient to linearly add together these AEs from both models to represent the total AE in ML regimes. Therefore, these two models are sufficient to describe AE behaviours for the entire process of the ring-liner lubrication under different engine operating conditions.

4.5.1 AE Signals in the Time Domain

To evaluate the capability of using AE for engine lubrication diagnostics, a more rigorous understanding of AE variation during a full engine cycle is examined analytically based on the models developed.

As aforementioned, FAI AE can exhibit stationary behaviour in HL regimes when the velocity, contact load and viscously are high. This can be the main behaviour when the piston moves around the middle of an engine stroke with the highest speed. Considering the load during the power stroke is higher and the tribofilm thickness is lower, AE can be generated by both the FAI and AAI, leading to higher amplitudes compared with that of other three strokes. This amplitude distribution across strokes agrees with the viscous friction forces, predicted in Chapter 3 and observed from engine AE measurements [23, 24]. Especially, it can be used to detect the changes in lubricant viscosity which is commonly used to indicate lubricant deterioration.

At all dead centres of the piston motions, the velocity is turned to zero, and therefore two AE models result in zero AE amplitudes. This is very different from the maximal amplitudes of asperity friction forces in Chapter 3, showing the limitation of AE at dead centres for diagnostics.

However, immediately the piston moves away from the dead centres, AAC induced AE can be significantly high because of the solid-solid impacts from the contacted asperities, compared with the soft-solid impacts from FAI generation mechanisms. These characteristics of these AE events can be useful to indicate the early and abnormal wear at the top and bottom of a linear where the early wear occur frequently due to BL. In the meantime, it also allows the performance of anti-wear additives to be evaluated. The protective film developed by anti-wear additives in the lubricant is often used to limit the direct surface contact between the piston rings and cylinder liner [181].

4.5.2 AE Spectrum Characteristics

To characterise further AE contents between rings and liner, the basic features of its spectrum can be also understood based on the models, which will help to analyse the AE signals more effectively.

By taking the collision of a single pair of asperity as a timing impulse with a short duration t_a, its Fourier spectrum in the frequency domain will spread across a very wide frequency range as the time is very short. Comparatively, the time duration for a single pair of asperity collision in AAC is much shorter than FAI according to Equations (4-13) and (4-27), due to $a<<b$, which results in following relationship for these two characteristic times:

$$t_a = \frac{2a}{v_p} << t_b = \frac{b}{v_p} \tag{4-35}$$

Correspondingly, a characteristic frequency relationship will be

$$f_a = \frac{v_p}{2a} >> f_b = \frac{v_p}{b} \tag{4-36}$$

This means that the impulse of an asperity pair is much closer to an ideal pulse. Consequently its spectrum can present in a much wider band, compared with dynamic bending process of FAI. Overall, these general features predicted for AE from the ring-line conjunction provide a basic leadership for acquiring and analysing AE signals more effectively from an operating engine.

4.5.3 Additional AE from Deteriorated Oils

These two analytic models provide critical fundamentals to understand AE responses during in an ideal tribological process. For an operating engine, various solid particles can be produced and dissolved into lubricants and adhered to the frictional surfaces, which is more significant when the lubricants are deteriorated by various reasons such as after a long-terms of operation, poor combustions due to inadequate fuelling and leakages. In these cases, more solid particles from combustion residuals and early wear debris can be the common consequences. The existences of solid particles in oil reduce the lubricity and increase wear, which should be avoided.

Apparently, these particles will also affect AE formulations. In addition to the influences of oil viscosity, these additional particles will collide with surface asperities in a similar way with two asperities and lead to short burst AE waves. In this sense, the AAC model can be also based on to explain such AE activities. Particularly, for light contaminated lubricants, they may show smaller AE amplitudes compared with the direct asperity-asperity collisions because the hardness of particles such as soot are

much smaller and the relative speed also lower. However, it can have higher amplitudes compared with FAI because of direct solid collisions. With an accumulation of contaminants, such AE activities will be more significant. Therefore, monitoring them allows the performances of tribological behaviours and hence the conditions of lubricants to be assessed, which is one of the fundamentals of AE based diagnostics.

4.6 Key Findings of Chapter 4

This chapter develops and elaborates the models for describing the AE responses from the tribological conjunction of the ring-liner according to dynamic elastic deflections of micro asperities.

The AE behaviours in BL and HL regimes can be explained mainly with AAC and FAI models respectively. For the ML regime, as it presents both asperity collisions and flows shearing, so its AE can be predicted by the AAC and FAI models jointly. As both AE models are developed based on deformation energies it is sufficient to linearly add together these AEs from both models to represent the total AE in the ML regime. Therefore, these two models are sufficient to describe AE behaviours for the entire process of the ring-liner lubrication under different engine operating conditions.

The simulation results show that around all engine dead centres: TDC and BDC in an engine cycle, the boundary and mixed lubrication conditions contain more asperities undertaking dynamic compression. However, because of very low relative velocity, this AAC induced AE responses are less significant. According to the simulated results, significantly higher velocity leads to hydrodynamic lubrication around the middle of each stroke in which little asperity collision can occur but the higher AE activities arise mainly from asperity bending deflections driven by fluid shearing forces. This asperity–fluid interaction induced AE are more proportionally connecting to the relative velocity and oil viscosity but less dependent on the load.

More specifically, in the time domain, FAI induced AE will exhibit a quasi-continuous behaviour as the dynamic deflections on millions of asperities are stimulated by the velocity of the piston which is more continuous in the middle of a stroke. In the frequency domain, FAI induced AE can start from a lower frequency (tens of Kilohertz) and spread in a narrower band as the impulse period is associated with ring height;

whereas the AAC induced AE can have extremely wide bands as its characteristic time relates to asperity sizes which are far less than ring height.

It worth noting that these models of AE occurrences are developed based on an idea lubrication conditions. In reality, AE can be also affected by combustion residuals or soot, wear debris, unstable flow turbulence, fluid cavitation, localised elastic and dynamic deformations, etc. These effects can exhibit more significant when lubrication condition become poorer with engine service period or inadequate combustions. Therefore, these understandings can be based on to achieve early diagnosis, especially, the increased AE activities due to more collisions between solid particles in oil and asperities on surfaces can be a good indication of oil accumulation of contaminants. However, these factors can make AE responses very complicated and the analysis of AE signals should be carried out carefully to determine such effects reliably.

CHAPTER 5 FACILITY AND METHODOLOGY FOR EXPERIMENTAL STUDIES OF AE FROM ENGINES

This chapter details the experimental facilities, and the test methodologies are established to verify various models and simulations for performing high-performance diagnostics. It starts with the setup of hardware of the testing engine, instrumentation and test systems. Then, it develops a specific procedure for conducting AE tests when the engine operates with different lubricating oils and alternative fuels. In addition, auxiliary tests such as lubricant viscosity and particle distribution measurements are also detailed.

.

5.1 Objectives of the Experimental Research

Most of the previous experimental studies of the piston tribology were focused on the non-firing engine test with considerable modifications of engines; however, these test results can not reveal the real engine working condition with the high cylinder pressure and temperature under the combustion process. On the other hand, the previous investigations about AE generation during the friction and wear progression were generally conducted on a slider to disk laboratory rig. Although several works (have been discussed in section 2.5) show the possibility to investigate the ring and liner contacts in diesel engines under running conditions. However, the mechanism of the ring-liner tribology characteristics were not fully explored with subtle changes in engine lubrication.

In this work, two types of the experiments were conducted on diesel engine test rigs with AE acquisitions throughout the course. One is for the running test to detect the AE actives; the purpose of the firing test is to decipher the frictional AE activities under real engine working condition, which can be a prelude to realise the online monitoring of the piston tribological condition with AE without any modifications to engines. Another is for the motored test, and the main purpose of the motored test is to confirm the content of AE signals correlated with engine frictions. It will be achieved by comprising AE signals between motored test without accessories and engine test at different speeds.

Since the AE signals often coincide or overlap, particularly in multi-cylinder engines, it is difficult to identify the AE signatures correspond to the source actions[23]. Hence, this initial experimental study was conducted on the engine test rig which has only one cylinder in order to gain sufficient details for the ring\liner contacts for supporting AE applications to multiple cylinder engines.

5.2 Configuration of Test Rig and Data Acquisition System

5.2.1 The Configuration of Test Rig

Experimental works have been conducted on two types of single cylinder engines to assess the viability of using AE measurements as the basis for the tribological characteristics monitoring and diagnosis of a piston assembly system. Firstly, a series of

preliminary tests have been conducted on a vertical single cylinder compression ignition direct injection (CIDI) engine of QCH1110II model. The use of a single cylinder engine is for its less background noise from the other cylinders, compared with the multiple cylinders engine. Based on these experimental studies, further experimentation was investigated on a new single cylinder CIDI engine of QCH1125. The key specification is given in Table 5-1. The eddy current dynamometer and controller system DW 160 (form Chengbang, China) were couple with the test engine to controlled the test rotation speed and load. The Figure 5-1 illustrates the valve timing and fuel supply timing diagram. Schematic diagram in Figure 5-2 shows the schematic diagram of the engine testing system and position of AE sensor.

Table 5-1 the main specification of testing engines

Manufacturer	Anhui Quanchai Engine Co., Ltd., PR. China	
Cylinders number	one	one
Combustion system	Direct injection, vertical type	Direct injection, vertical type
Model	QCH1110II	QCH1125
Bore/stroke	115/110 mm	125/120 mm
Volume of displacement	1.093 L	1.473 L
Compression ratio	18:1	18:1
Rated power	14.7/2400 kW/r/min	20.6/2200 kW/r/min
Max. torque	67/1920 Nm/r/min	67/1920 Nm/r/min

The AE sensor is located on the cylinder outer surface near the cylinder head as presented in Figure 5-2. Since the transmission speed of AE waves is fast in the same medium and the weak AE frictional signals are easily attenuated through the water jacket. The sensor is arranged near the metal part of the cylinder as the vertical cross-section chart shown in Figure 5-2. In addition, this location is also subjected to little interference from the cam and crankshaft bearing because of a long transmission distance.

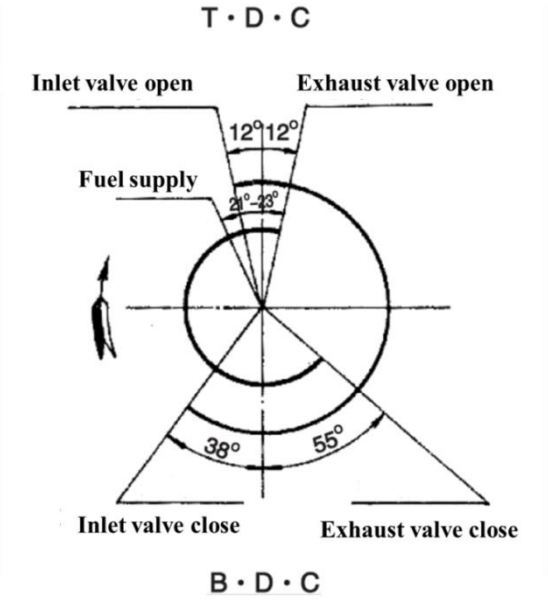

Figure 5-1 The valve timing and fuel supply timing diagram

Especially, the motored test was also conducted on the same test rig for the running test. To suppress the interference AE events, the valve and fuel injection pump are removed. The engine was motored by an electric motor which the specification is giving in Table 5-2. The output torque and speed of the motor was tested by a torque measurement system (Figure 5-8), the specification of the torque measuring instrument is listed in Table 5-3.

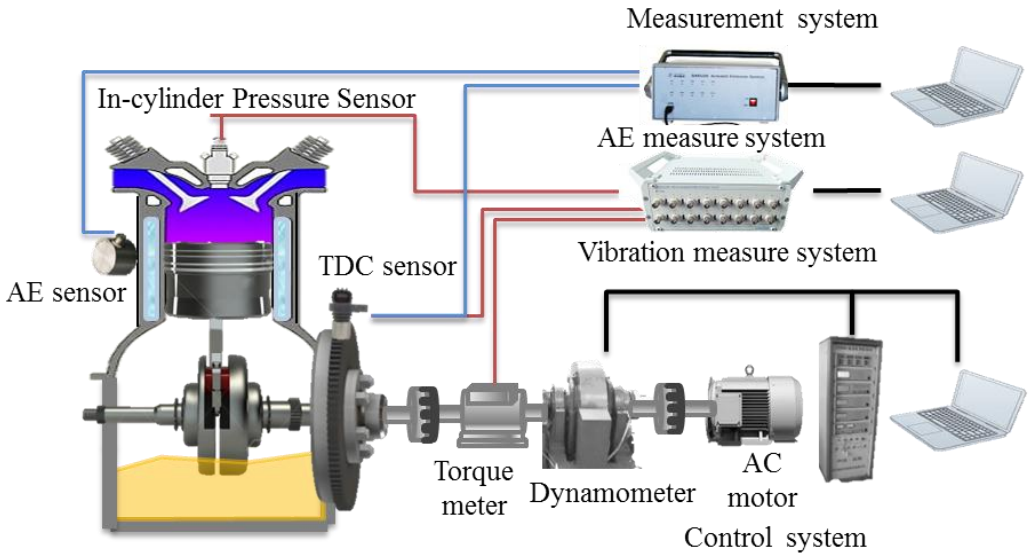

Figure 5-2 System schematic diagram of the engine measurement system and control system

Table 5-2 Specification of the motor

	Motor
Manufacturer	Shanxi Electric Motor Co., Ltd
Type	Y2-160M-4
Output (kW)	11
Electric Current (A)	22.6
Rated Speed (r/min)	1460
Efficiency (%)	88
Power Factor	0.84
Rated Torque (Nm)	71
Max. Torque (Nm)	78
Weight (kg)	120

Figure 5-3 Photo of torque measurement system

Table 5-3 Specification of the torque measuring instrument

Manufacturer	Sichuan Chengbang Measurement & Control Technology Co., Ltd	
Type	NC-3	
	Torque measurement	Speed measurement
Signal amplitude	RMS 0.2V - 20V AC	RMS 0.2V - 20V AC
Frequency range:	10kHz ±5kHz	2Hz-100kHz
Input impedance:	10kΩ	10kΩ
Sampling time:	1ms-5s	1ms-5s
Measurement accuracy:	±0.1% F.S	±0.5% below 50Hz and ± 0.1% ±1 above 50Hz

5.2.2 Measurement Instrumentation

During this research, the AE signal, engine rotating speed, in-cylinder pressure and crank angle position measured and recorded by the following measurements instrumentation.

5.2.2.1 AE Sensor Selection and Calibrations

Figure 5-4 SR800 broad-band acoustic emission sensor

Broad-band sensors usually have a good the potential to deliver extra information, but, unfortunately, most of the best information is at the low end of the spectrum, just where the noise problems are, thus, high-frequency resonant sensors are recommended for most practical structural monitoring[182].In this work, an SR800 AE sensor (in Figure 5-4) from Soundwel Technology Co., Ltd is mounted on the external surface of cylinder body to measure the AE responses, where it is more accessible in reality for achieving online monitoring of the engine lubrication. The specification of acoustic emission sensors SR800 was listed in Table 5-4 and the frequency characteristic curve of the AE sensor was given in Figure 5-6.The sensor has a good frequency response and high sensitivity in the band from 20kHz and 400kHz according to the calibration chart. Especially the band can cover the lower characteristic frequencies from 20kHz to 50kHz, estimated by (4-36) from FAI when the testing engine operates in the range from 1000rpm to 2000 rpm. AE signals for each type of test cases were acquired under steady operating conditions. The length of a data record is nearly 1s, sampled continuously at a rate of 800 kHz, which covers over 100 of engine working cycles for sufficient average and thus obtaining reliable results. In addition, a top dead centre (TDC) reference signal is also recorded along with the AE signals so that the angular domain analysis can be implemented to associate AE signals with key engine events. In total, the tests have resealed in nearly 1 Tera-bytes of data

Therefore, SR800 AE sensor as illustrated in Figure 5-4 from Soundwel Technology Co., Ltd was selected in this work. The specification of acoustic emission sensors SR800 is

listed in Table 5-4 and the frequency characteristic curve of the AE sensor is detailed in Figure 5-6.

Figure 5-5 Specification of acoustic emission sensor

Model	SR800
Dimension (mm)	Φ19×15
Operating Temperature (℃)	-20-80
Connector	M5－KY
Connector location	Side
Operating Frequency (kHz)	10～800
Resonance Frequency (kHz)	600
Sensitivity Peak (dB)	> 70

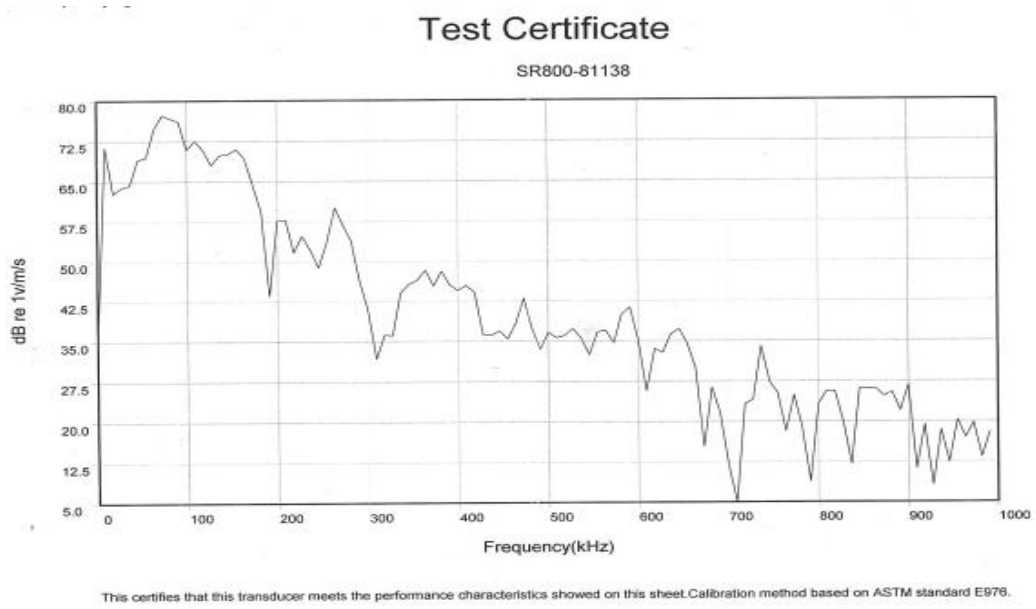

Figure 5-6 Frequency characteristic curve of the acoustic emission sensor SR800

According to the calibration plots, the frequency response shows three bands: 0-200kHz, 200-300 kHz and 300-700kHz, in which their gains drop clearly. In addition, there are many local peaks in each band. This basic frequency characteristic will be also taken into account when performing data analysis.

5.2.2.2 AE Senor Test Location and Amplifier

Figure 5-7 The AE sensor on engine surface

The AE sensor has been fastened on the outer surface of cylinder as shown in Figure 5-7. The sensor is located near the cylinder inner surface, thus, it is comparatively far from the interference sources such as the valves landing and combustion.

An AE measurement system SEAU2S with two channels was used to acquire the AE signals in this research. The output signal of AE sensor is sometimes as low as a few microvolts, for such a weak signal, the signal intensity will be reduced with a long-distance transmission. Hence, a preamplifier needs to enlarge the original sensor signal several times before transmission and then transmitted through the high-frequency coaxial cable to the signal acquisition unit. The commonly used magnification is 40dB. The specification and photo of the preamplifier for acoustic emission acquisition system in this work are given in Table 5-4 and Figure 5-8 respectively.Concurrently, an encoder signal was sampled to mark the top dead centre (TDC) position to align the AE signal with the speed of the engine for further analysis in the angular domain.

Table 5-4 The specification of the preamplifier for acoustic emission acquisition system

Model	PAI
Gain (dB)	40
Dimension (mm)	116*36*30
Operating Temperature (℃)	-20～60

Noise (dB)	＜26
Output Range Response (V)	±10
Operating Frequency (kHz)	10～2000
Voltage (V)	28V DC
Rated Load (Ω)	50

Figure 5-8 The illustrative photos of preamplifiers

5.2.2.3 AE Measurement System

Figure 5-9 Acoustic emission acquisition system

The AE measurement system in this study is composed of AE sensor, pre-amplifier, AE detector and PC, as shown in Figure 5-9.Acoustic emission detector is a very important part of the acoustic emission detection system. Its main role is to pre-amplifier through the analogue voltage signal through the A/D into a discrete digital signal, which can be collected by the software and stored on the computer. The acoustic emission detector used in this experiment is SEAU2S-1016-08 acoustic emission detector of Beijing

Shenghua Industrial Technology Co., Ltd. The waveform sampling length is up to 128k sampling points at 16-bit precision.

5.2.2.4 The Other Measurement Sensors and Instruments

The in-cylinder pressure was gained by Kistler 6052c pressure sensor which was plugged into the cylinder head as shown in Figure 5-10. Specifications of pressure sensor Kistler 6052C are listed in Table 5-5.The signals from the pressure sensor were passed through a Kistler Types 4618A2 charge amplifier which used to amplify the signals before feeding them to the Analogue-to-Digital Converter (ADC). The crankshaft position was measured by crankshaft position sensor 39180 (Hyundai Mobis) to associate the AE signals with the crank angle position. This crankshaft position sensor is an electromagnetic device located on the flywheel as given in Figure 5-11 to monitor the rotating speed of the crankshaft for each revolution. The relative angle between the testing position and the TDC position on the flywheel was measured before the tests. Hence the TDC information can be combined with the AE signals to mark the timing of the valves, injection and combustion of the test engine according to the valve timing and fuel supply timing diagram (Figure 5-1) of the testing engine.

Figure 5-10 Pressure sensor for cylinder pressure

Table 5-5 Pressure sensor specifications of Kistler 6052C

Type	units	Kistler 6052C
Measuring range	bar	0-250

Overload	bar	300
Sensitivity	pC/bar	≈–20
Natural frequency (measuring element)	kHz	≈160
Linearity, all ranges (at 23 ℃)	%/FSO	≤±0,4
Acceleration sensitivity (axial)	bar/*g*	<0,0002
Acceleration sensitivity (radial)	bar/*g*	<0,0005
Operating temperature range . min.-max	℃	–20-350
Sensitivity change in the temperature range: 23- 350 ℃	%	≤±2
Thermal shock error (at 1500 1/min, pmi = 9 bar) Δp (short time drift)	Bar	≤±0,5
Insulation resistance at 23 ℃	Ω	≥1013
Shock resistance	*g*	2 000
Tightening torque	N ṁ	1,5
Capacitance, without cable	pF	5

Figure 5-11 The location of crankshaft position sensor

5.2.3 Measurement of Viscosity-Temperature Characteristics

The viscosity-temperature characteristics of different lube-oil measured by the SV-10(the specifications of the viscometer SV-10 is listed in Table 5-6) sine viscometer and

heated by the 1331 temperature-control magnetic heating stirrer as shown in Figure 5-12.

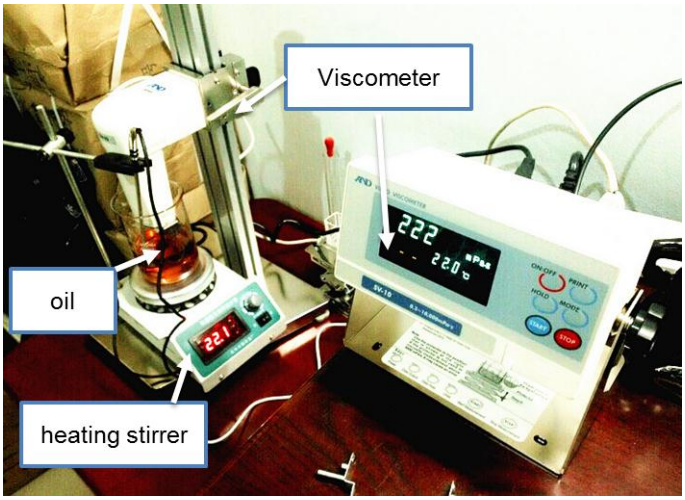

Figure 5-12 The measurement of oil viscosity

Table 5-6 Specifications of the viscometer SV-10

Vibration Frequency	30Hz
Viscosity Measurement Range	SV-10: 0.3 - 10,000 mPa・s (cP)
Accuracy (Repeatability)	1% of Reading (Full Range) (S.D. , 20 - 30 ℃, No-condensation)
Operating Temperature (indoor temperature)	10 - 40 ℃ (50 - 104 F ℉)
Temperature Measurement	0 - 160 ℃ / 0.1 ℃(32 - 212 F / 0.1 F ℉)
Power Supply	AC Adaptor

5.3 Experiment Programmes

To detect the frictional AE signals on the cylinder body, a number of feasibility tests were conducted before the comprehensive test programmes as developed in the following. The previous trial tests were first performed to find the AE characteristics correlated to different working condition on the two running engines (QCH1110II and QCH1125), such as different speed, different load and under a constant condition for a period of 75 mints when the water and oil temperatures are steady. Then the engine was

tested by using two new lubricating oils with high and low viscosity value. The AE RMS value around the middle of stroke was extracted by using DWT as developed in [183], and the experimental results demonstrated that

- The AE signals obviously increased with the engine speed.
- There are no clear correlations between different load and AE RMS values.
- The AE RMS values slightly fluctuate under a constant working condition.
- There is a slight difference between the AE RMS values around the middle stroke using different lubricants under the same working condition.

In addition, each type of the test was repeated for at least three times.

Based on a number of trial tests as mentioned above, two types of running tests were conducted in this study, which are the tests with different lubricating oils and the tests with different alternative fuels. To verify proposed models and evaluate the performance of AE based diagnostics, the tests were performed carefully to acquire data reliably and accurately for investigating AE diagnosis performances with small or incipient changes in lubrication conditions and wide engine operation ranges. Further, motored tests were conducted to validate the AE signals induced by the friction process by removing the valves and injector pump.

Especially, each test run is controlled for a short duration when the engine is under steady operation (temperatures of both the cooling water and oil are stabilised to the specified the pacified ranges) to avoid potential occurrences of significant wear in the tested ring-liner. Particularly, the test for the used oils was conducted in final stages considering that its poor lubricity may lead to influences to the quality of other tests.

5.3.1 Tests under Different Lubrication Conditions

To examine the impacts from the variation of the engine operation and lubricating oil conditions, two types of new lubricating oils and used oils were tested under a wide range of operating conditions. The first brand new oils were selected in this test which the performance classification is CD and the SAE viscosity grade of the lubricants is 15W40 and 10W30 respectively. They are mainly for the verification of the models and signal analysis tools. The used oils (the performance level: API CH-4) were from an automotive diesel engine after the vehicle had operated for about 15,000km since

previous services. Unfortunately, it was not possible to establish the initial SAE grade of the used oil. However, the viscosity-temperature characteristics of these three different lube-oils were measured by the viscometer (in section 5.2.3) as given in Figure 3-4. The main difference of the two new oils is basically the viscosity value. Based on the analysis of FAI model in Section 4.4, the oil with higher viscosity induces more AE than the oil with lower viscosity value. Moreover, the oil viscosity is considered as the indicator of oil conditions.

Further, the AAC effect is recognised as an important source of AE which have been discussed in Section 4.3. When the oil is degrading, more asperity contacts generate due to the poor protecting function of the tribofilm. On the other hand, too more particles in lubricants affect the system health condition. During the sliding contact, the particle-asperity collisions can also induce the elastic deformation of asperities, and hence generate AE in the same way as AAC.

In this work, the viscosity value and the comparison of particle content in tested oils were measured. The used oil has the higher viscosity than the baseline oil (15W40) as shown in Figure 3-4 and contains significantly more particles as shown in Appendix A. Therefore, the purpose of testing these three oils aims to diagnose the normal and abnormal lubrication conditions due to different the oil viscosity values and the amount particles.

Table 5-7 shows the test operation conditions for different lubricants. The engine is warmed up for 15 to 20 min at 1000 rpm, each test being controlled for a short duration about 5 min when the engine is under steady operation to avoid clear wear occurrences, two groups of AE data were sampled under different loads(10 Nm and 40 Nm). The sample time for each test is about 30 s. Then the engine was rammed up to the next speed. Additionally, the temperatures of the cooling water and oil were measured by the controller system to ensure the stability of operation condition. In this work, all of the tests have been repeated twice for all the operating conditions (each type of lubricating oils and fuels). Each AE measurement was recorded at a sampling rate of 800 kHz for more than 100 engine cycles for sufficient averages and obtaining the reliable results.

Table 5-7 The testing operation conditions of AE measurements for different lubricating oils

Combustion	Lube oils	Engine velocity (rpm)	Load (Nm)	Duration (min.)

fuels		Warm-up at 1000 rpm	0	15~20
Standard diesel	10W30	1000,1200,1400,1600,1800,2000	10, 40	5
	15W40			
	Used CH-4			

5.3.2 Tests for the Impact of Alternative Fuels on Lubrication

To investigate the potential impacts of alternative fuels on engine tribology, three types of fuels were used in the experimental investigation, which are standard diesel, coal F-T fuel and bio-diesel.

Table 5-8 Main properties of different tested fuels

	Bio-Diesel	F-T fuel	Diesel
Density (20℃) (g/cm3)	0.88	0.76	0.83
Viscosity (20℃) (mm^2/s)	5.2	2.14	4.65
Cetane number	59	74.8	45
Lower heating value (MJ/kg)	39	44.2	42.6

The main properties of three types of fuels are presented in Table 5-8 and the test working conditions for different fuels are shown in

Table 5-9.

Table 5-9 The testing operation conditions of AE measurements for different fuels

Combustion fuels	Lube oils	Engine velocity (rpm)	Load(Nm)	Duration time (min)
		Warm-up at 1000 rpm	0	15~20
Standard Diesel	10W30	1000, 1200, 1400, 1600, 1800, 2000	10, 40	5
Bio-Diesel	10W30			
F-T fuel	10W30			

5.3.3 Motored Tests

Additionally, a group of motored tests were also conducted on the same test rig by driving the engine by an AC motor. To verify the AE characteristics induced by the friction behaviour, the valves and injection pump were removed to exclude the noise influences from combustion shock and valve impacts. Due to the speed limitation of the AC motor, the highest test speed was operated up to 1400 rpm .The motored test conditions are shown in Table 5-10:

Table 5-10 Engine operation conditions of the motored test

Fuel	Lube oil	Engine speed (rpm)	Load(Nm)	Duration time (min)
Standard Diesel	15W40	800,1000, 1200, 1400,	0	5

5.4 Key Findings of Chapter 5

Starting with the clarification of the main objectives of the experimental studies, this chapter presents the experimental facilities and the test methodologies in order to made for a rigorous evaluation of using AE for detecting and characterising weak events generated from the tribological effects of the ring-liner system, which allows for not only a verification of AE models and friction simulations but also for further diagnosis studies.

A single cylinder engine is adopted for efficient and economical test studies. Moreover, it allows the key AE characteristics of the tribological effects to be gained as it has less interfering events. Meanwhile, as its key structures are very similar to common multiple cylinder engines, results obtained made can also be widely applicable.

A broad band AE sensor is justified to have 800kHz frequency responses and 70dB gain for capturing the AE events from both the weak AAC and FAI effects and strong responses of key events. Based on the trial tests of both running and motored engines, the captured AE signals show high levels of AE activities in a mid- stroke to be predicted. This then has confirmed that the measurement system is suitable.

Moreover, all test cases were designed to induce subtle changes in lubrication conditions, which are realised under both different lubricating oils and alternative fuels. A reliable differentiation between these lubricating conditions using AE analysis is particularly significant for online diagnostics and in site early fault detection. Moreover, it will create sufficient challenges to developing effective signal analysis approaches for separating the weak AE events for the differentiation.

CHAPTER 6 SIGNAL PROCESSING TECHNIQUES FOR ENGINE AE ANALYSIS

This chapter overviews both the conventional and emerging signal processing methods which can be more applicable to analyse nonstationary AE signals. Then wavelet and wavelet packets transforms are detailed due to their efficiency and effectiveness in dealing with the signals from the tribological process of engine lubrication which exhibit strong nonstationarity and have large volumes. To evaluate the elementary performance of these techniques, representative raw AE signals are applied with these techniques respectively in finding critical features to show the key characteristics of the tribological AE that are estimated from the established analytic models and existing studies.

6.1 Raw AE Signals from Engine Body

Two raw AE signals acquired from the different lubricant tests using 15W40 under 10Nm at speeds 1000 rpm and 1800 rpm correspondingly are selected as the examples to discuss the AE signal characteristics in this chapter as shown in Figure 6-1. It can be seen from the figure that these two AE signals reflect the basic characteristics of AE responses from the engine: 1) high amplitude bursts with very short time duration due to combustion shocks and valve impacts which vary periodically with engine operation cycle; and 2) low amplitude contents appearing nearly full-time course due to tribological friction excitations of which the variation period is consistent with engine strokes. In addition, both these events are varying with engine speeds.

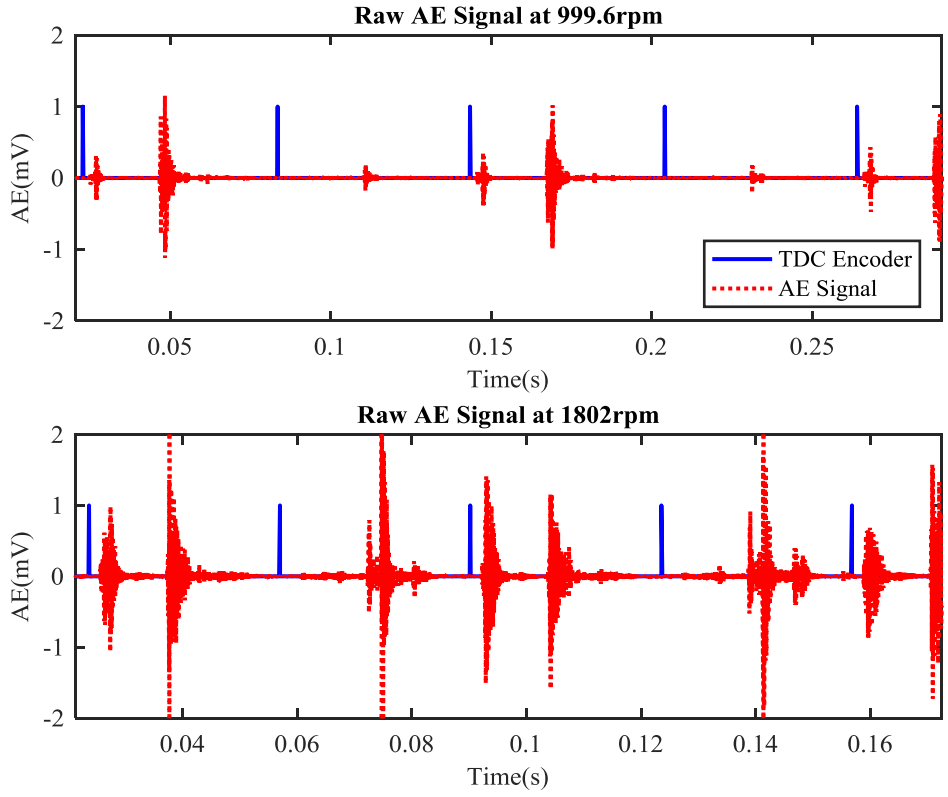

Figure 6-1 Raw AE signals from engine body at different speeds

From the signal processing point of view, these signals show strong non-stationarity. Conventional signal processing techniques such as waveform statistics and Fourier transforms are deemed to be less effective to extract the critical information of the non-stationarity that is more correlated to tribo-dynamics in conjunction with the engine

piston-groups. However, they can be implemented efficiently to give a general estimation of signls, which is very appalling from the standpoint of online applications.

In the meantime, there are numerous emerging signal analysis methods such as time-frequency representations and wavelet transforms which are intensively investigated to tackle the nonstationary phenomena in recent years. To determine which of them are more applicable to engine AE signals, their effectiveness is evaluated in finding the tribological features of interest in the following sections.

6.2 Conventional Signal Analysis

6.2.1 Typical Statistical Parameters in Time Domain Analysis

Time domain analysis principally displays the amplitude variation of the signal of a time series. The peak value, peak-to-peak (shorten as PK-PK), root mean square (RMS), skewness and kurtosis [30] are popular characteristic features to describe the signal statistics in the time-domain. Time domain analysis is the simplest way to examine the basics and trends of signals.

6.2.1.1 Peak Value and Peak-to-peak Value

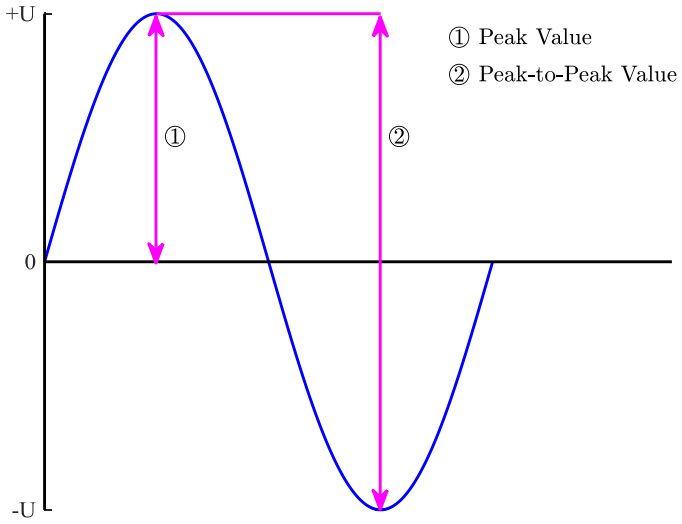

Figure 6-2 Peak value and the peak-to-peak value of a sinusoidal curve

Take the sine wave as example, the peak value and peak-to-peak value are usually determined by the positive and negative amplitudes as shown in Figure 6-2.

6.2.1.2 RMS

RMS value is a typical parameter to represent the raw signal amplitude level, which can be expressed as

$$V_{RMS} = \sqrt{\frac{1}{T}\int_{t_0}^{t_0+T} x(t)^2 dt} \tag{6-1}$$

where $x(t)$ represents the amplitude of the sampling signal at point *t*, *T* is the time period of the signal. Consequently, the RMS value of a discrete signal can be expressed as the following equation.

$$RMS = \sqrt{\frac{1}{N}\sum_{i=1}^{N} x_i^2} \tag{6-2}$$

where x_i is the discrete points of a signal and *N* represents the total number of the signal.

6.2.1.3 Kurtosis and Skewness

Kurtosis and skewness are representative of the signal distribution, which can characterise the location and variability of a data set. Kurtosis is used to describe the relative peakdness or flatness to the normal distribution of signal amplitudes. The kurtosis of a discrete signal x is:

$$Kur = \frac{\frac{1}{N_d}\sum_{i=1}^{N_d}(x_i - \bar{x})^4}{RMS^4} \tag{6-3}$$

Skewness is used to depict the asymmetric degree of a signal according to the mean value of this signal. Positive skewness shows the distribution with an asymmetric tail on right, negative skewness expresses the distribution with an asymmetric tail on left. Furthermore, the skewness of normal distributions is zero. The formula for skewness is expressed as:

$$S_k = \frac{E[(x_i - \bar{x})^3]}{RMS^3} \tag{6-4}$$

As illustrated in Figure 6-1, the amplitudes of AE signals at high speeds are higher than that at low speeds and consequently, more AE events will be generated at high revolution speeds. Hence, the RMS, peak value and peak-to-peak value of AE signals at

high speeds are greater than that at low speeds, which is clearly shown in Figure 6-3. However, the kurtosis indicates that AE signals at different speeds obey to a heavy tailed distribution, of which AE signals acquired at low speeds is distributed more peaked. Skewness values of the which given in Figure 6-3 at low and high speeds show that AE signals skew oppositely with respect to the piston speeds. Time domain parameters can demonstrate the tribological responses of the engine in a certain degree.

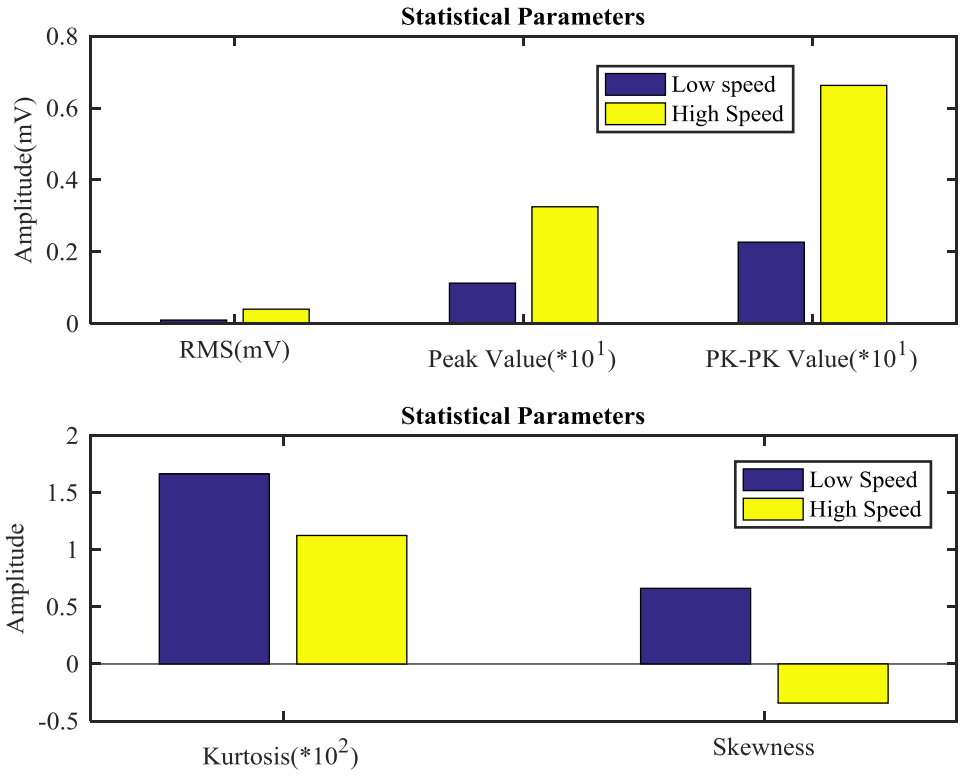

Figure 6-3 Signal parameters of the AE waveform

6.2.2 Frequency Domain Analysis

Frequency domain analysis reveals the spectral information of signals which is able to extract the interest frequency components to correlate with the oscillations of different engine components. In diagnosing and condition monitoring, the deviations of frequency spectra based on the machine baseline can also reflect the working conditions because some frequency information closely corresponds to the machine responses at different speeds and loads. Therefore, considering the complicated events of unknown origin, AE spectral analysis is more effective to investigate the source mechanism due to giving more particulars about machine working conditions[33]. Although AE signals

of engines are nonstationary, a series of events including combustion shocks, valve impacts, and tribological friction excitation are cyclical with engine cycles and the AE signal consists of some periodic components, which makes the conventional frequency analysis feasible.

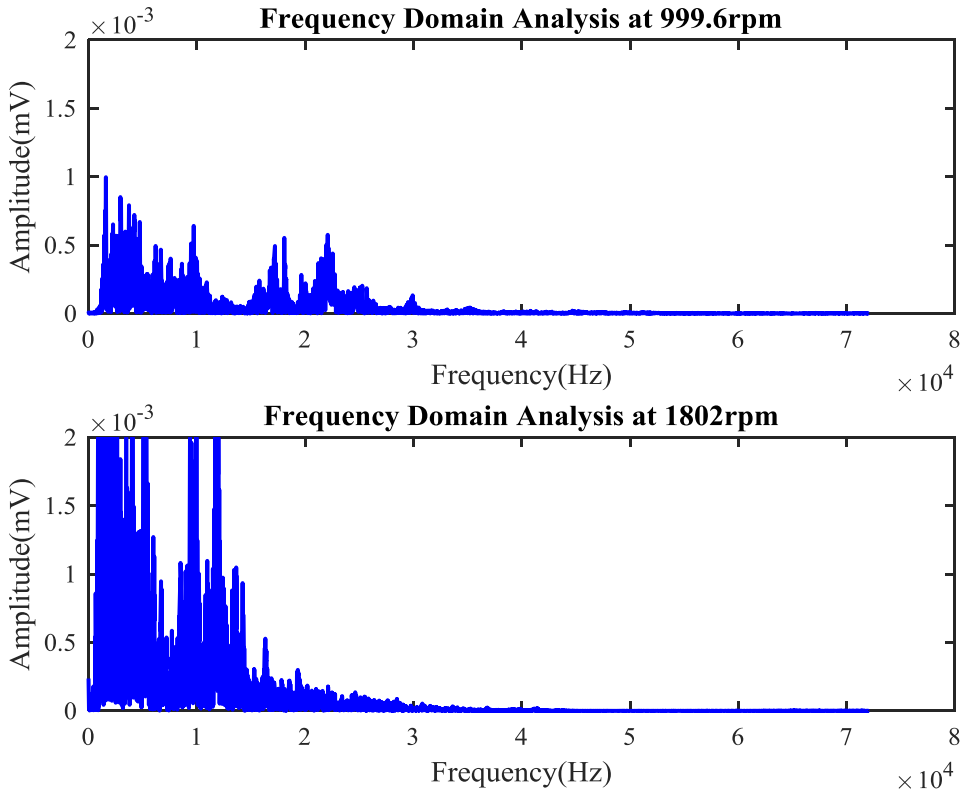

Figure 6-4 AE Spectra at different speeds

Figure 6-4 shows the amplitude spectra of AE signals at low and high speeds. Basically, AE events are concentrated in the low frequency band (<300kHz). Moreover, amplitudes for high speed AE are higher in a wide frequency band than that at a low speed. However, owing to the strong non-stationarity of AE signals, the large portion of frequency components vary with speeds and hard to know which of them more correlated to tribological effects, which makes the conventional frequency domain analysis inefficient for characterising the tribological dynamics between the ring-liner systems.

6.2.3 Time-Frequency Domain Analysis

Time-frequency analysis can exhibit the signal features in both frequency domain and time domain at the same time; hence these techniques can provide more information

about the time-varying characteristics of the frequency components. Consequently, the time-frequency analysis is suitable for analysing the nonstationary AE signals from mechanical systems.

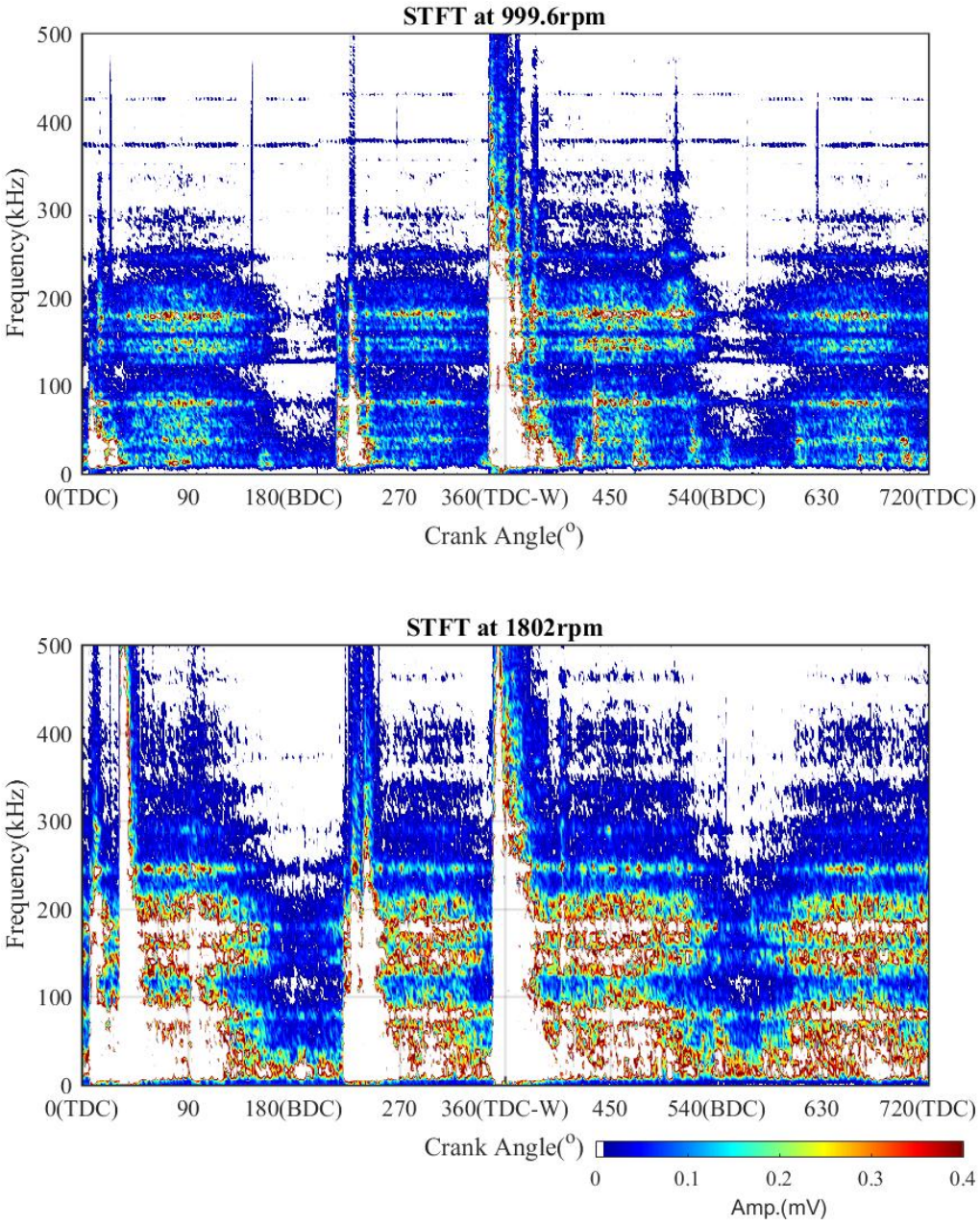

Figure 6-5 STFT analysis for engine AE signals

Short-Time Fourier Transform (STFT), as one of the most widely used time-frequency methods, divides an entire long time signal into short segments by an equal sized window which are considered to be stationary and can be applied with Fourier transform to obtain a successive series of spectra. Figure 6-5 shows the STFT results of

AE signals at low and high speeds, which are obtained with a data window size of 1024 and overlap ratio of 99% to resolve details of the time-frequency distribution of the AE responses. It can be seen that the AE events of combustion and valve impacts show the spread over the full frequency band, while the periodic features relating to the tribological effects are concordant across different strokes. Moreover, the increase of spectral amplitudes with engine speeds shows the high correlation between AE signals and tribological effects.

However, due to limited frequency resolution, the characteristic frequency bands of AE responses at high speeds cannot be recognised very well in the low-frequency range from 0 to 100 kHz, which makes STFT difficult to accurately characterise the signals and identify adequate diagnostic features. Moreover, another deficiency of STFT is the high consumption of computational resources and it needs large memory and high computation efforts to obtain and display the lengthy AE signals, which confines the full exploitation of high volumes of AE signals over different operating conditions and fault cases. In addition, this will also make it difficult for online application of AE based condition monitoring.

6.2.4 Angular Domain Analysis

Owing to the inevitable fluctuation in machine rotation speeds, responses of rotating machines are usually stochastic and uncertain so that the signals are difficult to be correlated with operating conditions and dynamic motions using the time domain signals directly. The angular domain ananysis is the most generally method processing the data of rotating machines, which is effective to identify system transient changes along with component rotation. The moving parts of internal combustion engines are integrated with the crankshaft and hence, it could correlate the AE events to the movements of engine components in the same crank angular position, which is a more effective approach than time domain analysis to eliminate the impacts of sampling point quantity in the time domain analysis. Moreover, the peak or RMS feature of the AE events also can be used in angular domain analysis to identify changes in engine conditions.

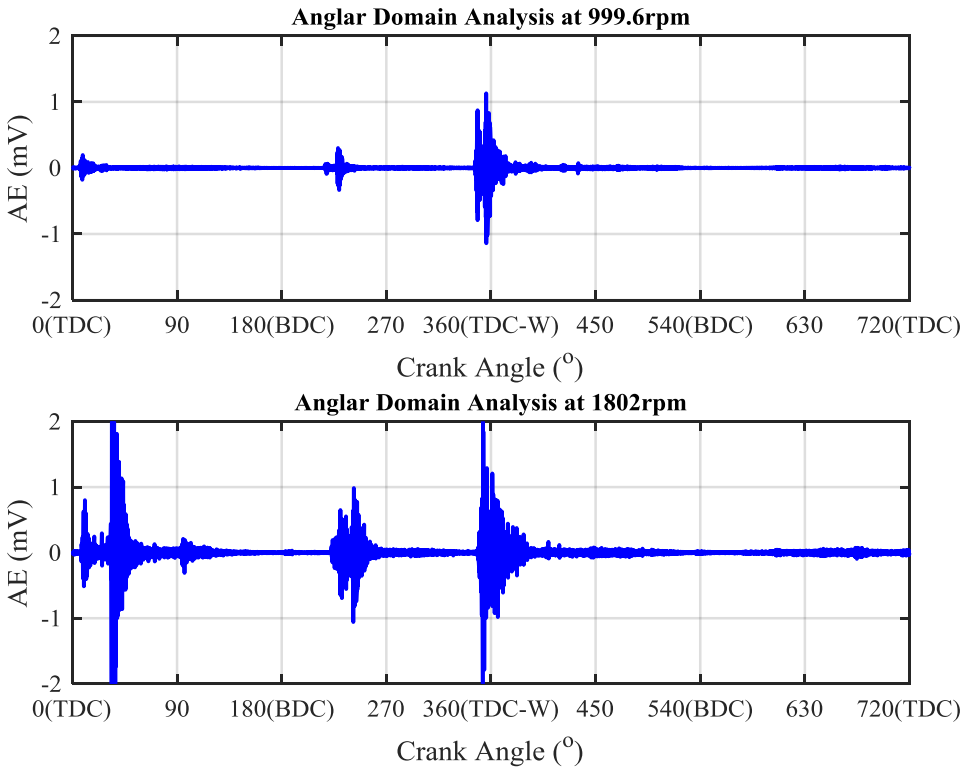

Figure 6-6 Angular domain analysis of AE signal under different speed

The simultaneously logged encoder signal is employed to estimate the engine speed by the crankshaft position sensor which located on the flywheel as given in Figure 5-11 to mark the rotating speed of the crankshaft for each revolution. According to the relative angle between the crankshaft position sensor location and the TDC position on the flywheel, AE signals are resampled into the angular domain correlated to the TDC information with the assumption of constant speed within one revolution of the crankshaft. Figure 6-6 presents the AE signals from the single cylinder engine in the angular domain at the speed of 900 and 1500 rpm respectively. As shown in Figure 6-6, four strokes happen periodically with a cycle of two revolutions, in which the power or composition stroke starts just after 360 degrees of the crank angle. The big AE events around 360^{o} are related to combustions, and the other two are induced by the valve opening and closing based on the valve timing of the engine. The exhaust valve is usually closed after the TDC of the inlet stroke and the inlet valve is closed a little later at the beginning of compression stroke. To sum up, it is easier to identify AE events according to engine working mechanism in the angular domain than that in the time domain.

The acquired AE signals in time domain were converted into angular domain by referring to TDC encoder signals. Thus, the different AE events corresponded to the movements of engines can be identified easily. Figure 6-7 displays two AE signals for one working cycle in angular domain at low and high speeds respectively. Obviously, there are strong AE bursts with large amplitudes which occur at the same crank angular position. Based on the engine operation process, the valve timing and fuel supply timing diagram are given in Figure 5-1. The crank angles of valve timing, injection timing and combustion are marked as short red bars at the top of Figure 6-7. It can be recognised that the AE events correspond to the impacts of exhaust valve closing (EVC), inlet valve closing (IVC), fuel injection and combustion in sequence. However, the exhaust valve opening (EVO) and inlet valve opening (IVO) cannot be captured due to the limitation of a long transmission path. Moreover, many others AE events cannot be identified evidently.

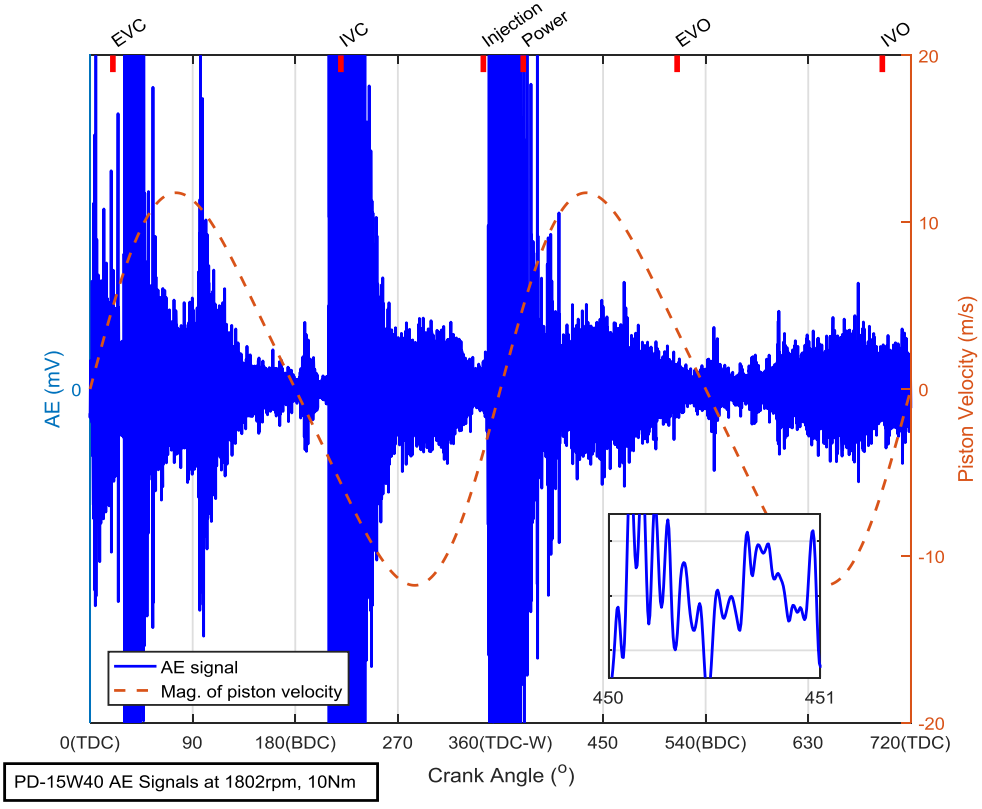

Figure 6-7 Typical raw AE signals on diesel engine body

To demonstrate the properties of weak AE events around the middle of each stroke in running tests as shown in Figure 6-7. A group of motored tests were carried out on the same engine of which the valves and injection pump were removed to exclude the

interfered AE activities from combustion and valves landing as the description in chapter 5. Figure 6-8 is shown the raw AE signals for one working cycle from a motored engine. In the motored test, the large AE bursts were excluded and the AE amplitudes are shown pseudo-continuing increasing primarily around the middle of each stroke. These amplitudes features of AE are similar to the motored test suggested in [23].

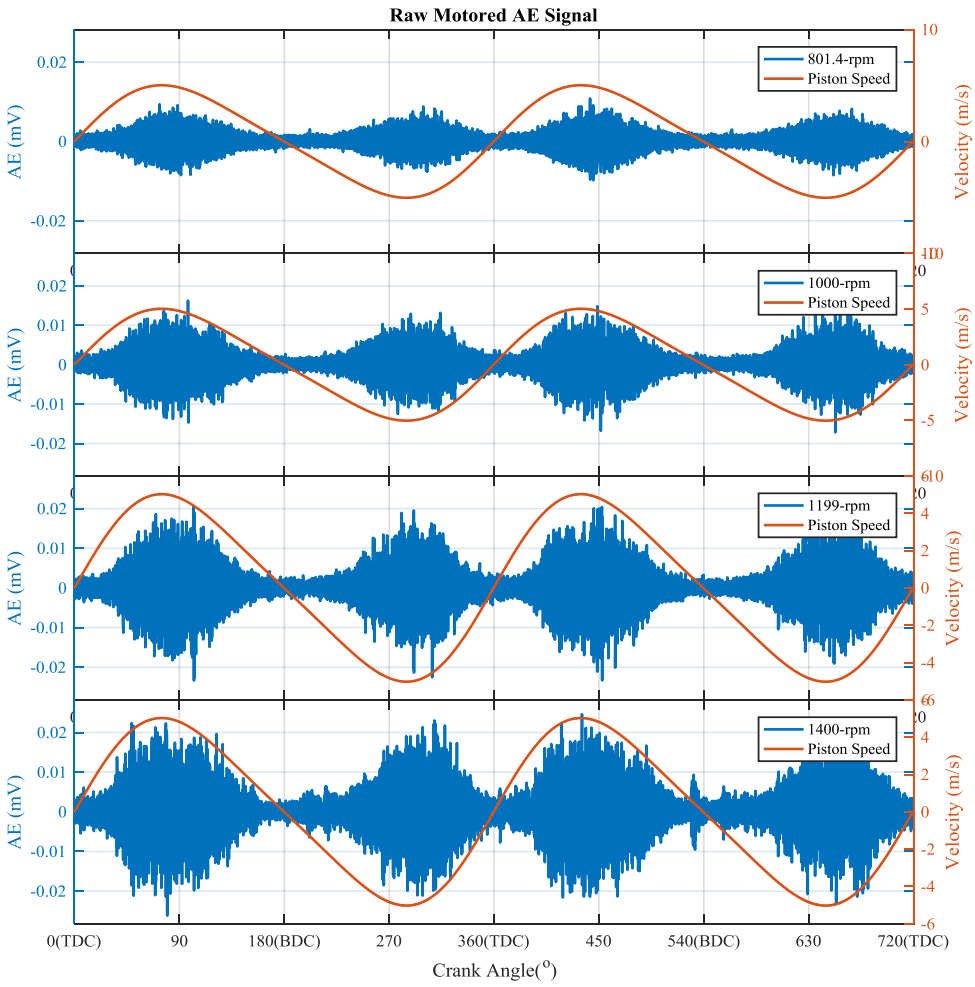

Figure 6-8 Raw AE signals from a motored engine

In Figure 6-8, there are pseudo-stationary AE signals in the middle of each stroke and some nonstationary AE bursts occurred randomly along with these stationary weak AE signals. Therefore, the profiles of the stationary AE amplitudes are similar to the positive contour of the piston speed. Without the interference of combustion and valves landing, the stationary waveforms of the two downwards strokes or upwards strokes are similar. Additionally, the AE amplitudes are evidently increased with the engine speed.

Moreover, it is also markedly that the amplitudes of the non-stationary AE bursts of which are increased with the engine speed present stochastically around each middle stroke.

Compared with Figure 6-8, the weak stationary AE signals and non-stationary AE bursts occurred locally in the same angular position which shows relatively lower amplitudes than the strong AE bursts as mentioned above. Overall, the weak local stationary AE signals and non-stationary AE bursts during the middle of strokes are considered to be due to the effect of the tribological dynamics of the ring-liner system.

However, the obvious AE events as a strong interference exhibit a broadband features with high amplitudes according to the STFT analysis displayed in Figure 6-5. Hence, conventional signal processing techniques are not effective and efficient to tackle the nonstationary AE signals for extracting the engine tribo-dynamics and consequently, more advanced analysis techniques for more accurate frequency and time resolution should be developed for weak AE signal processing.

6.3 Emerging Analysis Techniques: Wavelet Transforms

6.3.1 Wavelet Transform

Wavelet transform (WT) is a widely used tool for signal processing and condition monitoring [184]. The wavelet transform has a high-frequency resolution around low frequencies [30]. WT gives variable time resolution for different frequency bands while the short time Fourier transform (STFT) can only give constant resolutions[33] and therefore, the wavelet transform is useful for analysing nonstationary signals more effectively. In addition, the nonlinear frequency scales make WT analysis more efficient in processing the high volume of AE signals.

The general wavelet transforms are two types: continuous wavelets transform (CWT) and discreet wavelets transform (DTW). Both of them operate with the same principles and the choice depends on signals under analysis.

6.3.1.1 WT-based Multiresolution Analysis

The continuous wavelet transform of a nonstationary signal $f(t_w)$ can be express as

$$CWT(a_w, b_w) = \int_R f(t_w) \frac{1}{\sqrt{a_w}} \psi^* \left(\frac{t - b_w}{a_w} \right) dt_w \tag{6-5}$$

the mother wavelet function is $\psi_{a_w,b_w}(t_w) = \frac{1}{\sqrt{a_w}} \psi \left(\frac{t - b_w}{a_w} \right)$ $a_w, b_w \in R; a_w \neq 0$, where a_w is dilation index, b_w is time translation index, and $\psi^*(t_w)$ is the complex conjugate function $\psi(t_w)$.

As a discretization of the CWT, discrete wavelet transform (DWT) is. Its scale parameter is always discretized to integer powers of 2 so that the number of voices per octave is always 1, which has widely application in engineering due to its fast computational merits based on discretisation. The function of DWT can be expressed as

$$Wf(j,k) = \int_R f(t_w) \frac{1}{\sqrt{2^j}} \psi^* (\frac{t_w}{2^j} - k) dt_w . \tag{6-6}$$

The mother wavelet function of DWT presents as

$$\psi_{j,k}(t_w) = \frac{1}{\sqrt{2^j}} \psi (\frac{t_w}{2^j} - k), \tag{6-7}$$

and the father wavelet function of DWT is

$$\varphi_{j,k}(t_w) = \frac{1}{\sqrt{2^j}} \varphi (\frac{t_w}{2^j} - k). \tag{6-8}$$

where $a_w = 2^j$, $b_w = 2^j k$, $k = 1, 2, ..., N/2^j$ and decomposition levels $j = 1, 2, \ldots, J$. hence, the wavelet transform of $f(t_w)$ can be expressed as [22]:

$$a_{J,k} = \int f(t) \phi_{J,k}(t) dt \tag{6-9}$$

$$d_{j,k} = \int f(t) \varphi_{j,k}(t) dt \tag{6-10}$$

where $a_{J,k}$ is the approximation coefficients, $d_{j,k}$ is detailed coefficients.

The Daubechies wavelets, a family of orthogonal wavelet, are nominated by the study of Ingrid Daubechies[186]. The shapes of the wavelet and scaling functions of Daubechies wavelets for ‘db6’, ‘db9’, ‘db12’, ‘db16’, ‘db18’ and ‘db21’ are shown in Figure 6-9 respectively. Owing to the asymmetric shape of the AE signals in the middle of stroke (shown in Figure 6-7), the wavelet base in this analysis is selected as Daubechies wavelet with the asymmetric shape of the scaling and wavelet function for extracting the weak AE accurately.

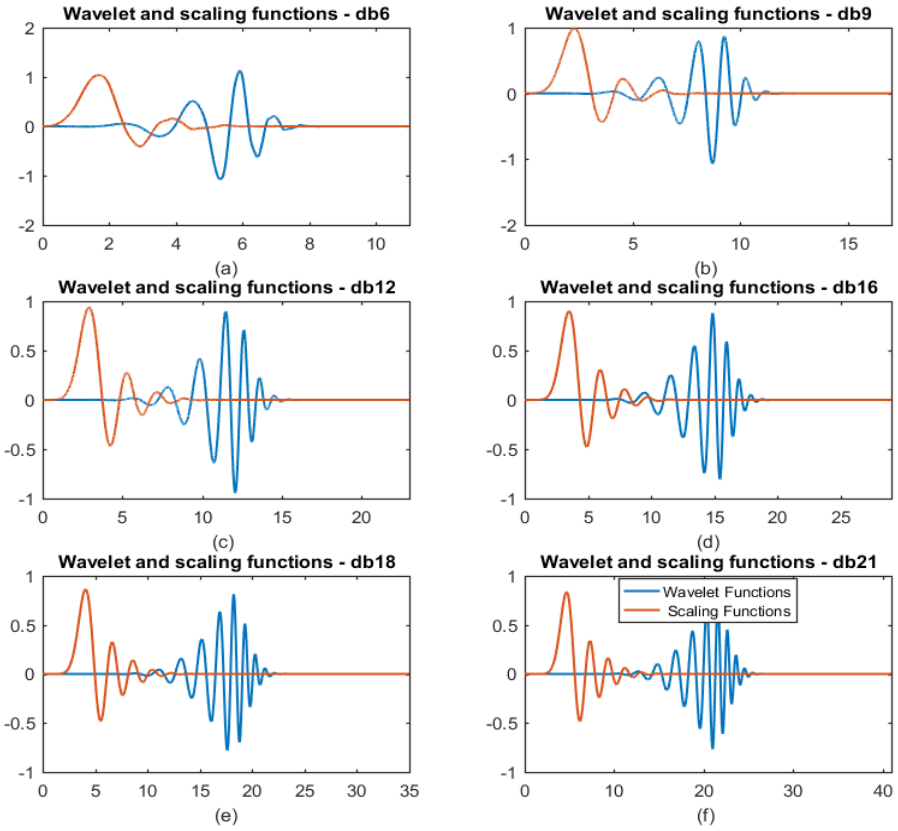

Figure 6-9. Wavelet and scaling functions of Daubechies wavelets at the order of (a)db6; (b) db9; (c) db12; (d) db18; (e) db6;(f) db21.

A Daubechies wavelet at the order ‘6’ or db6 for brevity is selected to analysis the AE signals processed by conventional methods in the last section. Based on the analysis in the angular domain (in Figure 6-6), the high amplitudes and wide-band frequency properties of the AE events induced by combustion and valve are clearly depicted by wavelet coefficients due to the good frequency resolution in Figure 6-10.

The theoretical model of the FAI induced AE in chapter 4 shows that AE intensity is directly proportional to viscously and velocity, consequently, it gives a better interpretation of AE activities in hydrodynamic lubrication (HL) regimes. Moreover, the

FAI induced AE can start from a lower frequency (tens of Kilohertz) and spread in a narrower band as the impulse period is associated with ring height based on the conclusions of Chapter 3 and Chapter 4. Therefore, in Figure 6-6, some of the ambiguous minor AE amplitudes in the middle of each stroke induced by the HL regimes. Based on WT, these AE signals show continuous weak amplitudes during the lower frequency band which verified the conclusion of the FAI induced AE.

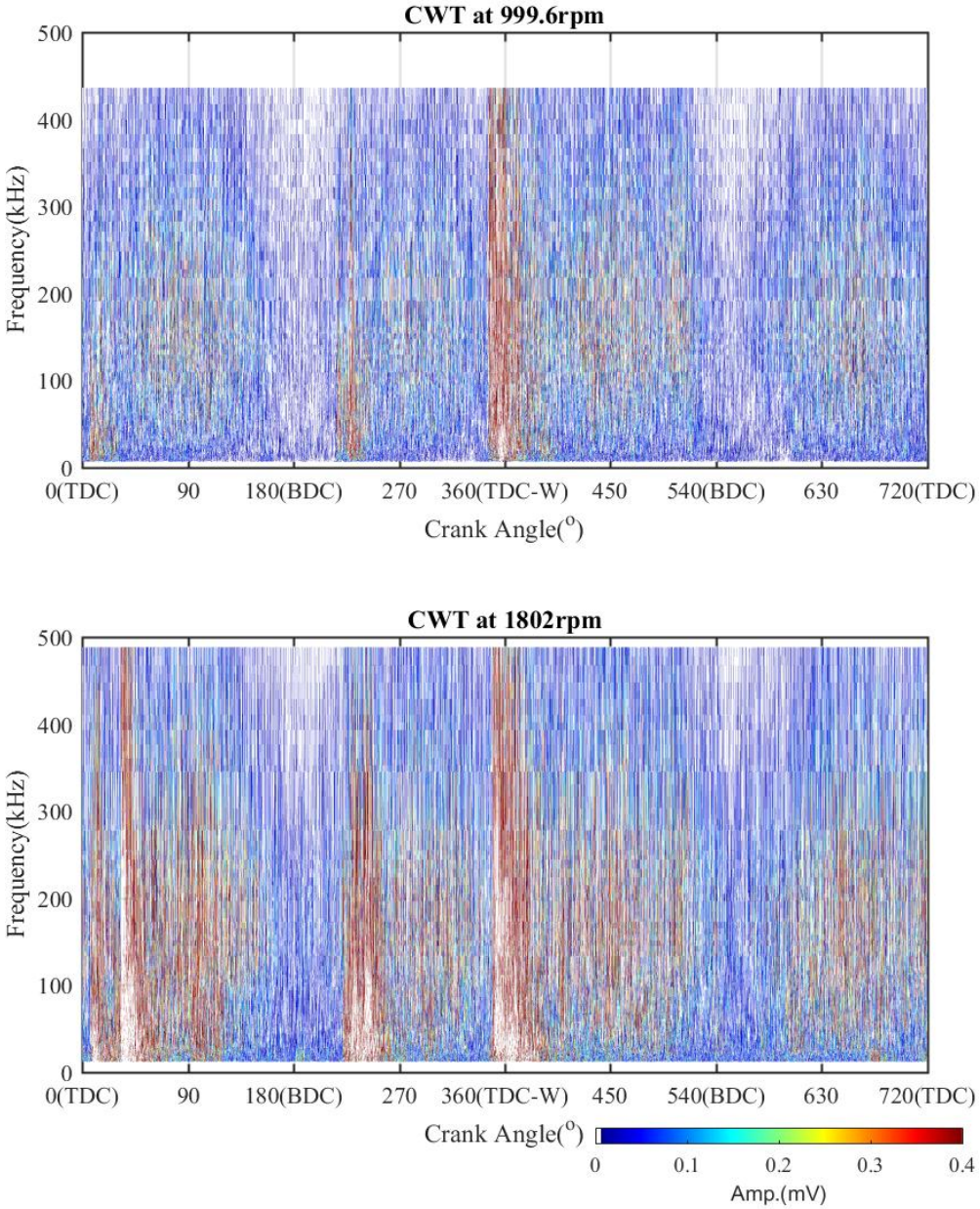

Figure 6-10 Angular-frequency domain analysis of AE signal based on wavelet transform under different speed

6.3.1.2 Wavelet Thresholding Analysis

Wavelet multi-resolution analysis (WMRA), the application of the DWT method, was firstly presented by Mallat [37]. WMRA can decompose the raw signal into a series of wavelet coefficients with different of resolution level. The generating function of the WMRA decomposed model can be expressed mathematically as [187]

$$\hat{f}(t_w) \approx \sum_k a_{J,k}\phi_{J,k}(t_w) + \sum_k \sum_{j=0}^{J-1} d_{j,k}\psi_{j,k}(\mathrm{t}_w) \tag{6-11}$$

Additionally, the approximated signal $A_J(t_w)$ and the detail signals $D_j(t_w)$ of the decomposed results can be presented as

$$A_J(t_w) = \sum_k a_{J,k}\phi_{J,k}(t_w) \qquad J,k \in Z \tag{6-12}$$

$$D_j(t_w) = \sum_k \sum_{j=0}^{J-1} d_{j,k}\psi_{j,k}(t_w), \qquad j,k \in Z \tag{6-13}$$

Based on an orthogonal wavelet, the wavelet coefficients separates into two parts by high pass filter $\tilde{H}(f)$ and low pass filter $\tilde{G}(f)$ in each level. Figure 6-11 illustrates a WMRA decomposition scheme with four levels. The WMRA only decomposed the approximation signal $A_J(t_w)$ into two parts for highly calculating efficiency, particularly, the detail parts of the wavelet coefficients $D_j(t_w)$ were generated by high pass filter $\tilde{H}(f)$ and the approximated parts of the wavelet coefficients $A_J(t_w)$ were generated by low pass filter $\tilde{G}(f)$ at every level *j*.

However, to acquire the target signals which have been denoised effectively, the signal data compression, and thereby signal enhancement, the determination of base wavelet types and decomposing levels are quite important. In this study, the selecting criterion of the above parameters will be discussed in Chapter 7 based on the friction behaviour of engines.

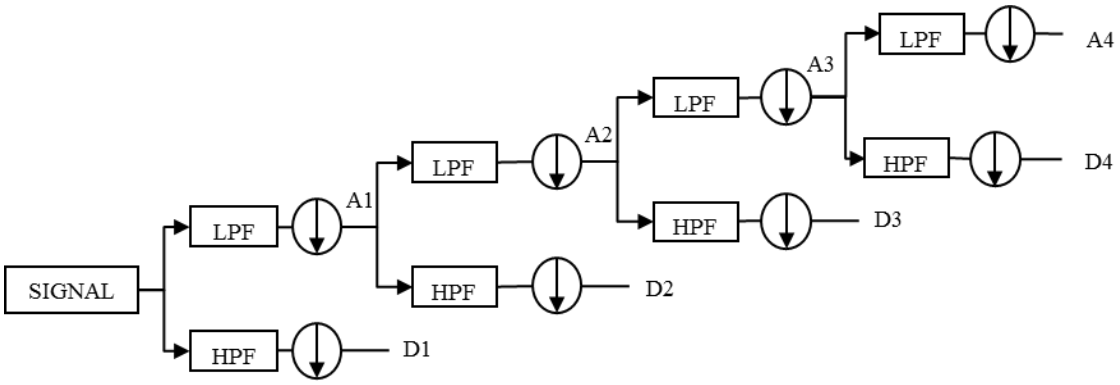

Figure 6-11 WMRA decomposition with 4 levels

6.3.2 Wavelet Packet Transform

6.3.2.1 WP Basics

The wavelet packet transform (WPT), shorten as wavelet packets (WP) or sub-band tree, is a more generalised decomposition in which discrete wavelet transform (DWT) is expanded at each decomposition level *j* by applying two filters as shown in Figure 6-12.

Based on the decomposition of DWT, the WP wavelet can be achieved by the following scheme

$$\begin{cases} W_{2n}^{j}(t_w) = \sqrt{2}\sum_{k=0}^{2N-1} h(k) W_n^j(2t_w - k) \\ W_{2n+1}^{j}(t_w) = \sqrt{2}\sum_{k=0}^{2N-1} g(k) W_n^j(2t_w - k) \end{cases} \tag{6-14}$$

where n=1, 2, 3 ⋯; k=1, 2, 3 ⋯2N-1; $W_0^0(t_w)$ is the scaling function $\phi(t_w)$ and $W_1^0(t_w)$ is the wavelet function $\varphi(t_w)$.The superscript j presents the j_{th} level of wavelet packets basis.

Consequently, WPT can deal with the nonstationary signals with a better frequency resolution compared with DWT at the same bandwidths regardless of high and low frequencies. Moreover, WPT only increases limited decomposition computation, which is much less than CWT and STFT and therefore, WPT is more applicable upon current computational resources.

6.3.2.2 WP Spectrum Analysis

The wavelet packet transform (WPT), developed by Coifman, Meyer and Wickerhauser, can decompose all the approximation and detailed information to the desired level [38], which is illustrated by the full wavelet packet tree down to level 3 in Figure 6-12. The orthogonal wavelet decomposition procedure separates the coefficients into two parts using high pass filter $\tilde{H}(f)$ and low pass filter $\tilde{G}(f)$. Consequently, WPT offers a thorough analysis of each node at the J_{th} level which contains complicated frequency components and can be divided into finer intervals or bands. In particular, the terminal nodes approximate bandpass filters of the form at the J_{th} level of the frequency axis can be expressed as $(nF_s/2^J, (n+1)F_s/2^J)$ $n = 0,1,2,3,\ldots 2^{J-1}$, where F_s is the sampling frequency. This finer band based representation makes WPT analysis significantly superior over DWT in that WPT allows more detailed characterisation of the content in the AE signals and hence provides more detailed features for differentiating small changes in the tribological behaviour.

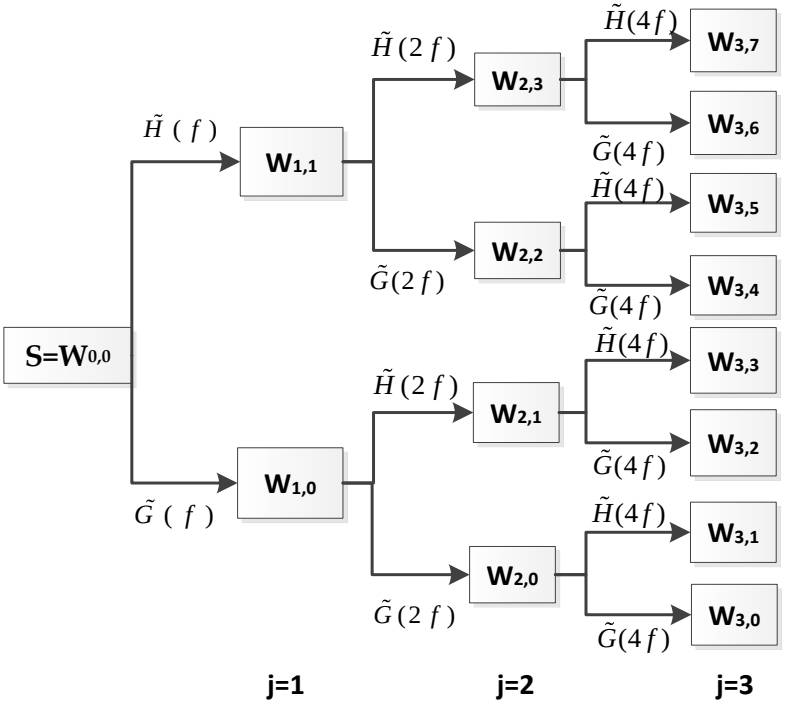

Figure 6-12 Wavelet packet decomposition tree at level 3

Wavelet packets are more superior at the frequency axis dividing and frequency resolution with respect to time series than DWT, and hence it provides in terms of metrics to identify singularities and edges at time-frequency analysis.

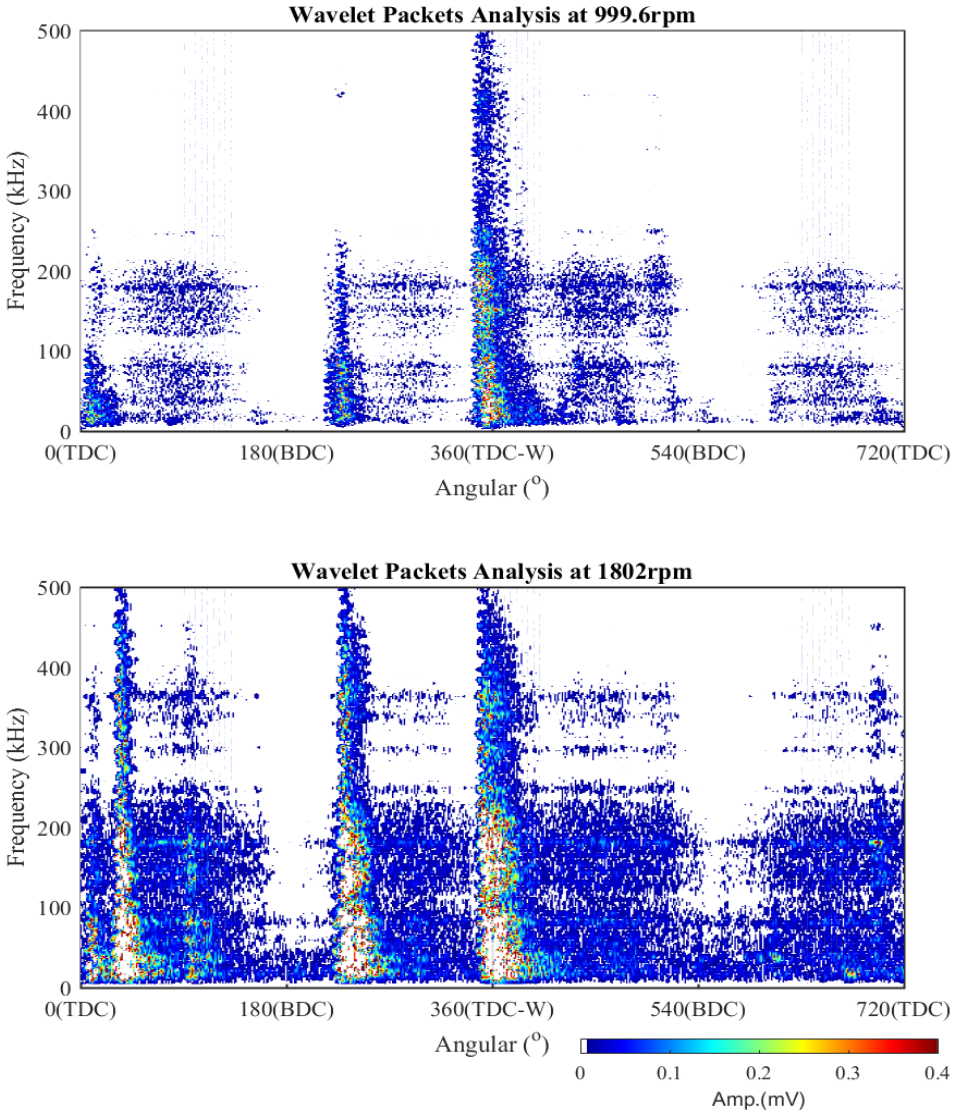

Figure 6-13 Angular-frequency domain analysis of AE signal based on wavelet packets under different speeds

The specific cases as mentioned above were analysed in angular-frequency domain by using wavelet packets and the results are shown in Figure 6-13. The wavelet base is 'sym9' at the decomposition level of 8. The distinct high amplitudes and the wide band of AE events are related to the combustion and valve impacts, which are shown both in the analysis results of wavelet transform and STFT. The continuous components located in the middle of each stoke with the much lower amplitudes than the distinct one. The broad-band characteristics in wake AE spectrums increase with engine speeds. These

demonstrated the wake AE signals around the middle of stroke which related to the HL regimes are shown slightly high amplitudes around several narrow bands based on WPT analysis method.

6.4 Key Findings of Chapter 6

Based on typical AE signals measured from the test engine, This chapter has evaluated the effectiveness of different signal processing methods in characterising and separating the weak AE responses to the tribological effect of ring-liner system. Conventional signal processing methods demonstrate that the engine AE signals are very nonstationary. Especially, in the angular domain, it has been known that AE content relating the tribological behaviours of ring-liner present very small amplitudes, which can be submerged by the various strong noises including the large AE bursts from air valve impacts, fuel injection smashes and combustion shocks.

STFT is effective to identify the interested weak AE features associated with frictional responses, but the time and frequency resolution are relatively low. Moreover, it consumes high computational resources, which makes STFT ineffective and inefficient to process AE signals with redundant contents of excitations and high volume of data samples.

The DWT and WPT methods are two emerging signal processing methods and they are superior to the conventional methods such as STFT due to the flexibilities of selecting time and frequency resolution along with their fast computation merits. Therefore, they are more preferred in this study to analyse the nonstationary AE signals for extracting the weak signatures correlated with tribological behaviour.

CHAPTER 7 DISCRETE WAVELET ANALYSIS AND DIAGNOSTICS OF THE TRIBOLOGICAL BEHAVIOUR BETWEEN THE RING-LINER

This chapter details the implementation of wavelet analysis of AE signals for diagnosing tribological behaviours of the ring-liner system. It starts with wavelet multiresolution analysis (WMRA) based on fast discrete wavelet transforms followed by the determination of an optimal wavelet and decomposition level. Then it develops AE diagnostic features from the envelope signals derived from the optimal analysis. Finally, the performance of diagnosing different types of lubricating oils and alternative fuels are evaluated with the derived features under a wide range of engine operating conditions.

7.1 Introduction

Previous researchers have elaborated the AE bursts with large amplitudes from IC engines corresponded to the valve sealing and combustion progress [16] [17] [18] [19]. The preliminary analysis carried out in Chapter 6 with conventional signal processing methods also confirms that such bursts are very distinctive in the AE signals from engine body. In addition, overall AE signals show a broadband frequency property.

However, the small or weak AE events between the large bursts have been less understood in association with engine tribology. According to the simulation results of viscous friction in Chapter 3 under different viscosities, the weak AE signals in the middle of strokes can be correlated with the viscous frictional behaviour whose amplitude is higher in the middle of engine strokes and increases with both engine operating conditions and lubricant viscosity values. In addition, the analysis in Chapters 4 also shows that AAI induced AE exhibits a proportional relation of AE amplitudes and the velocity as well as the viscosity. To verify previous simulations and the analytic predictions, wavelet analysis is implemented with optimising key analysis parameters in this chapter to extract the weak AE content occurred in the middle of the stroke and thereby to reflect the tribological behaviour relating more to the HL lubrication regime, which is denoted as HL-AE.

Among different approaches of wavelet analysis such as continuous wavelet transforms and wavelet packet transforms, the fast discrete wavelet with the multiresolution analysis is adopted firstly in this chapter because it is much more efficient in dealing with the large volume AE signals. Moreover, to extract the weak AE effectively, an optimal type of wavelets and levels of decomposition are investigated based on the piston velocity profiles. Then local envelope amplitude (LEA) is established as the diagnostic feature to show the performance of using AE in separating different lubricant oils and alternative fuels.

7.2 WRMA Optimisation with a Modified Velocity Profile of the Piston Motion

7.2.1 WMRA Analysis

Wavelet transform decomposes an AE signal into a few of sub-signals associated with the decomposition scales or levels to show the characteristics in the time-frequency domain. With those sub-signals, it is possible to separate easily the interested components from the random noise and other potential interferences. This method is also known as multiple resolution analysis which is abbreviated as WMRA. Especially, WMRA performs a good frequency resolution at low frequencies owing to that the approximation coefficients were decomposed into two parts by pass filters at each level. That allows the different AE bursts to be identified and excluded for characterising the AE activities relating more to hydrodynamic lubrication effects (abbreviated as HL-AE hereafter).

Moreover, because the number of sampling points at the high decomposition level is less than the raw signal, the frictional AE characteristics will be interfered in the processing process. Therefore, a robust de-noising scheme should be developed to exclude unwanted components including both random noise and localized interferences[188].

As one of the important applications, wavelet de-noising method has been investigated extensively for different types of signals. Usually, it selects interested wavelet coefficients with higher amplitudes based on a typically adopted hard or soft threshold scheme to exclude noise, and it is assumed that random white noise spreads across different levels in WMRA and become less significant.

However, for extracting the small HL-AE, the large AE bursts relating to key engine events are regarded to be noise and need to be removed or suppressed. Therefore, the selection is opposite to the conventional approach. The threshold value needs to be determined carefully so as to select the interested HL-AE accurately. Because of the complicated mechanisms of AE generation, AE amplitudes for both the large AE bursts and the small HL-AE might vary widely, which is hard to find out a stable magnitude for all operating and lubrication conditions. Therefore, to avoid an exclusion of the

useful information related to HL-AE, threshold values should be determined based on the maximum wavelet coefficients at different levels.

Before the determination of an appropriate threshold, the parameters of wavelet analysis, i.e. the maximal decomposition level and adequate wavelet, need to be dtermined so that the threshold can be estimated accurately.

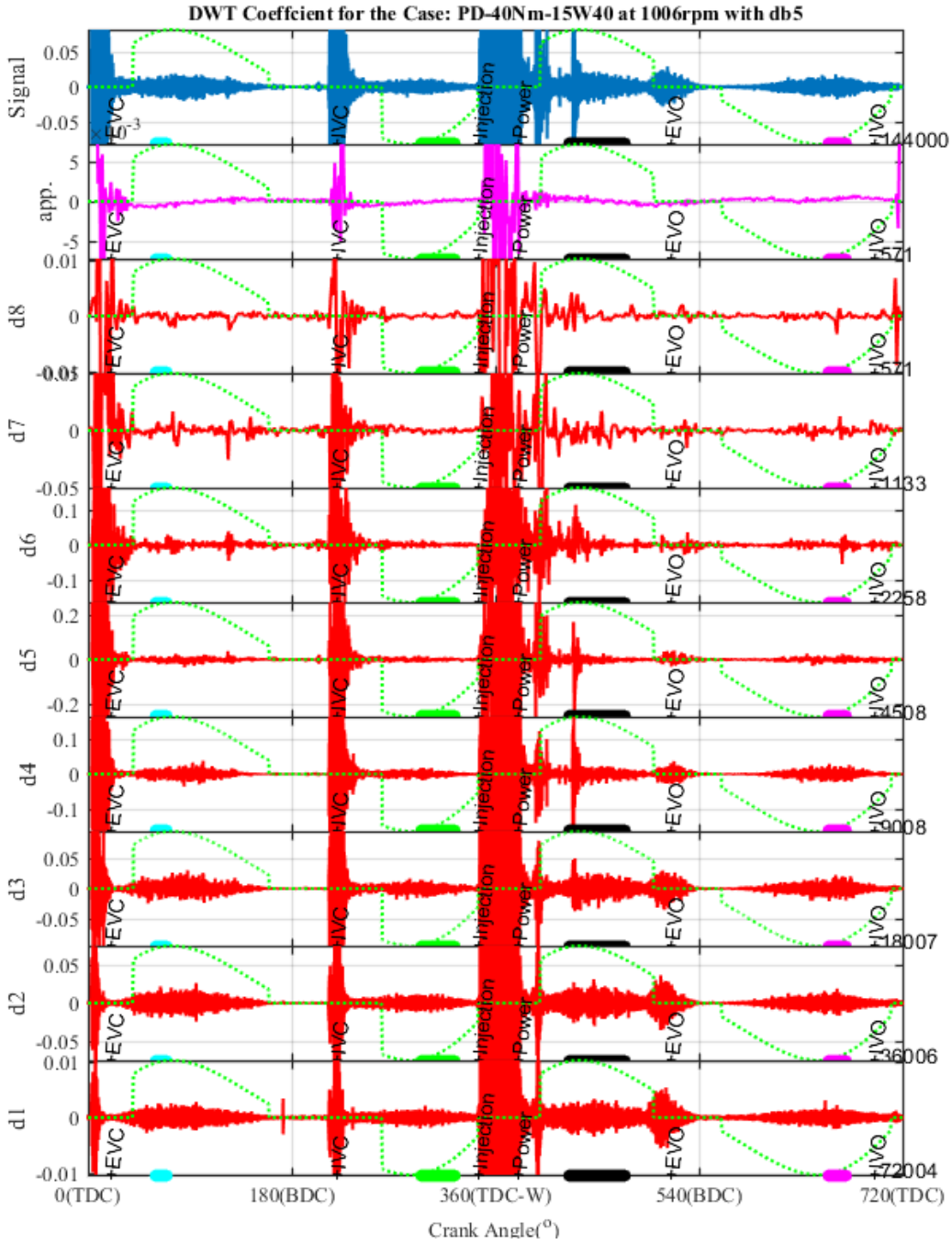

(a)

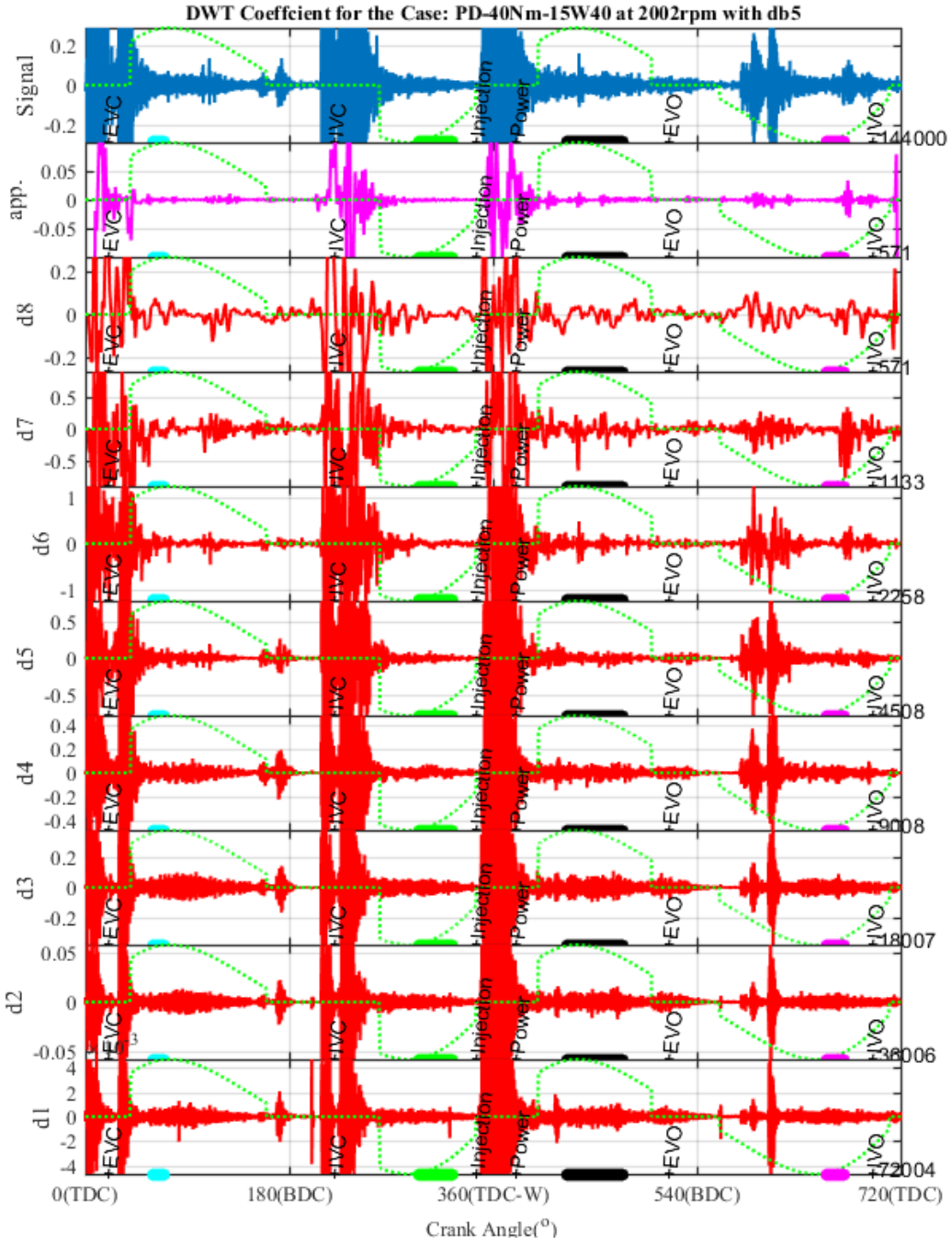

(b)

Figure 7-1 Wavelet decomposition of AE signal: (a) at 1000 rpm (b) at 2000 rpm

Figure 7-1 shows the typical raw AE signals at low and high speeds for one engine cycle, which has 144000 data points and measured from engine body. Moreover their DW decompositions are shown at successive wavelets levels (the reverse of scale parameter) up to J=8 with a wavelet base of order 5 from Daubechies family (db5).

Especially, the limits of Y-axis range is scaled at each level *j* by a factor of the doubled standard deviation $2\sigma_j$ calculated by

$$2\sigma_j = 2\sqrt{\frac{\sum_{k=1}^{K}\sum_{n=1}^{N_j} W_j^2(n)_k}{KN_j}} \tag{7-1}$$

where *n* is the time index, running up to N_j of the sample number for the wavelet coefficient signal at level *j* in an engine cycle; and the *K*=20 is the number of engine cycles. It is noted that the AE signals are for extreme operations i.e. the lowest speed (1000 rpm) and highest speed (2000 rpm) under high load (40Nm) and with the baseline lubricating oil of 15W40. Thus, more AE activities might be produced under the given lubricating oils, the determined threshold can be representative of other operations and lubrication cases.

Moreover, it can be also observed that key events of engine operation induced AE signals exhibit:

- Although the decompositions have more levels than those have been shown in Figure 7-1, HL-AE exhibits more observable at only lower levels from d1 to d5. At such lower levels, it is more likely to achieve a more accurate representation of the AE content. In contrast, the features of HL-AE at levers of d6-d8 appear to be redundant. Therefore, in terms of the extraction of HL-AE, the total decomposition level can be set to *J*=5.
- Large AE bursts of fuel injection, combustion, EVC and IVC activities are significant at all levels, which need to be excluded to avoid their influences in extracting the AE content from ring-liner conjunctions; EVO become more identifiable at lower levels; IVO is hardly identified because of its insignificant impacts between the seat and seal zone of the valve.
- A number of locally non-stationary AE bursts can be also seen at levels from d1 to d5. Typically, at d1 there is one burst in the middle of the compression stroke, and a number of bursts are very close to the middle of the combustion and exhaust strokes. As these locally non-stationary AE bursts present mainly in high-frequency bands (d1-d5), they are considered to be from AAC effect and

occur occasionally due to direct contacts between surfaces and solid soot particles. Certainly, these bursts are used to indicate the tribological behaviours. However, due to its unsteadiness and high amplitudes, it can result in unstable diagnostic feature values and affect diagnostic reliability. Therefore, it is better to be suppressed to a great degree in order to achieve the consistent diagnostic results.

Overall, these general characteristics achieved by WMRA will be the fundamentals for signal processing development and diagnosis implementations in coming chapters.

7.2.2 Optimal WMRA from the Correlation with Velocity of the Piston Motion

Based on above discussion, it can be determined that the decomposition level to be 5 is sufficient for analysis engine AE signals. For further confirmation this level, it is studied based on a correlation analysis approach by which an optimal order will be also determined.

Daubechies wavelet is one of them used widely in vibration and AE signal processing. In addition, there are many smaller wavelets available for different types of signal analysis. These wavelets are ordered according to an incremental integer number. Theoretically, the higher order number or vanishing moment, the more accurate it will approximate a signal. However, the higher order needs a greater amount of computation, hence, to affect the performance for the online implementation of AE based diagnostics.

As shown in Figure 7-1, the envelope of FAI induced weak AE content is very similar to the modified velocity profile of the piston motion which is also illustrated in the figure by the green line in each level. The modified velocity can be constructed easily based on the angular positions of each key engine events so that the large AE bursts can be excluded. This is also the analytic prediction made in Chapter 4 and numerically simulated in Chapter 3. According to this verified characteristic, a scheme is developed to quantitatively check the degree of similarity between the modified velocity and the envelope of wavelet coefficients.

Specifically, the normalised correlation $r(x_r, v_{p1})$ between the envelope sequence x_r reconstructed by wavelet coefficients which are shrunken by the modified velocity v_{p1}^{T} of the piston motion is calculated according to

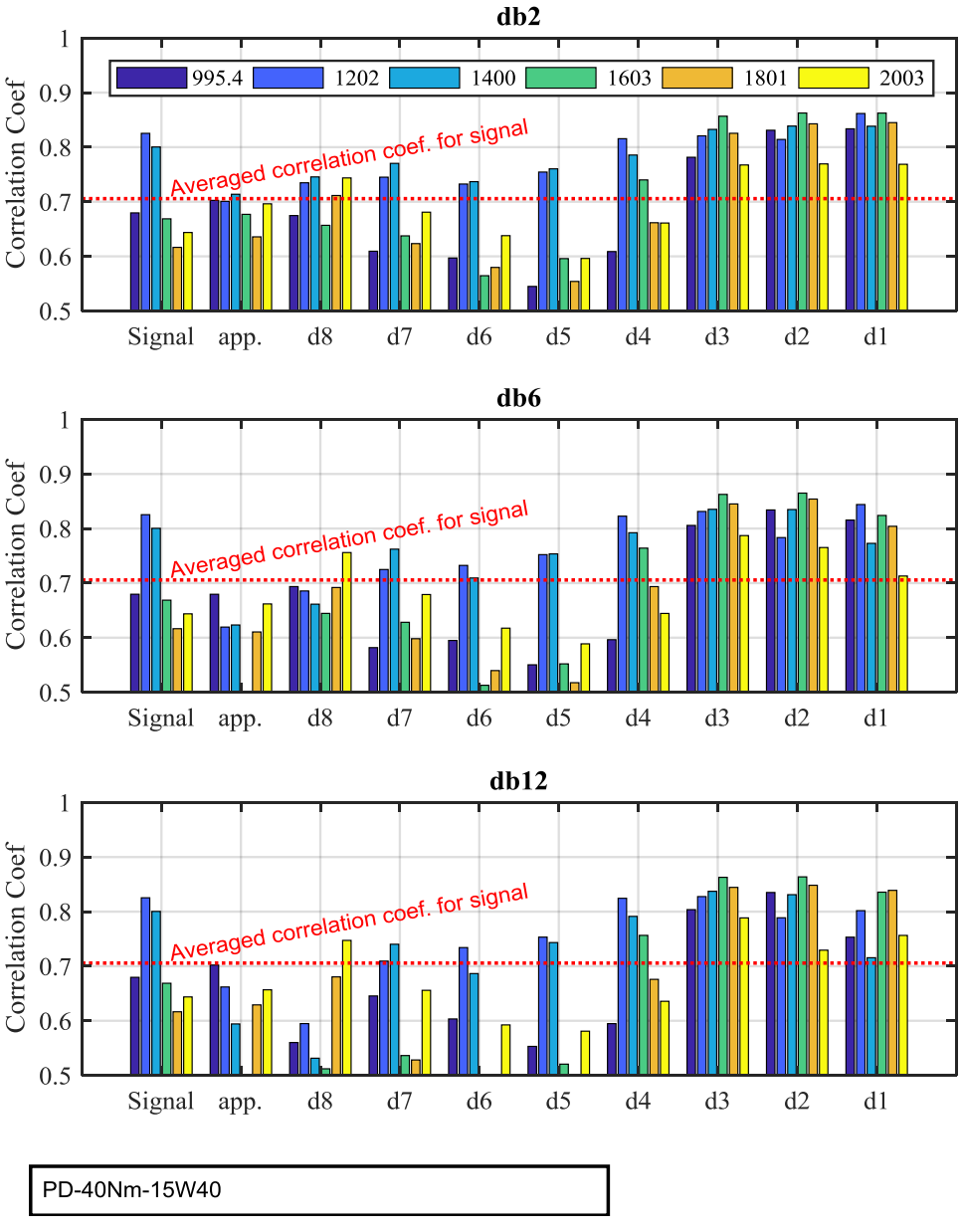

Figure 7-2 Average correlation versus different wavelet and operating speed under high load

$$r(x_r, v_{p1}) = \frac{\mathrm{sign}(v_{p1}) x_r v_{p1}^{\mathrm{T}}}{\sqrt{\mathrm{sign}(v_{p1}) x_r \, \mathrm{sign}(v_{p1}) x_r^{\mathrm{T}}} \sqrt{v_{p1} v_{p1}^{\mathrm{T}}}} \tag{7-2}$$

in which the 'sign' function is applied to convert the asymmetric envelope x_r into symmetric series or with zero mean. Obviously the closer $r(x_r, v_{p1})$ to the unit, the more similar between the two signals, and therefore show that the envelope is closer to the velocity profile and to better reflect the FAI effect. On the other hand, a smaller value of $r(x_r, v_{p1})$, such as close to zero, will mean that the data is too noisy and have less AE content of the FAI effect.

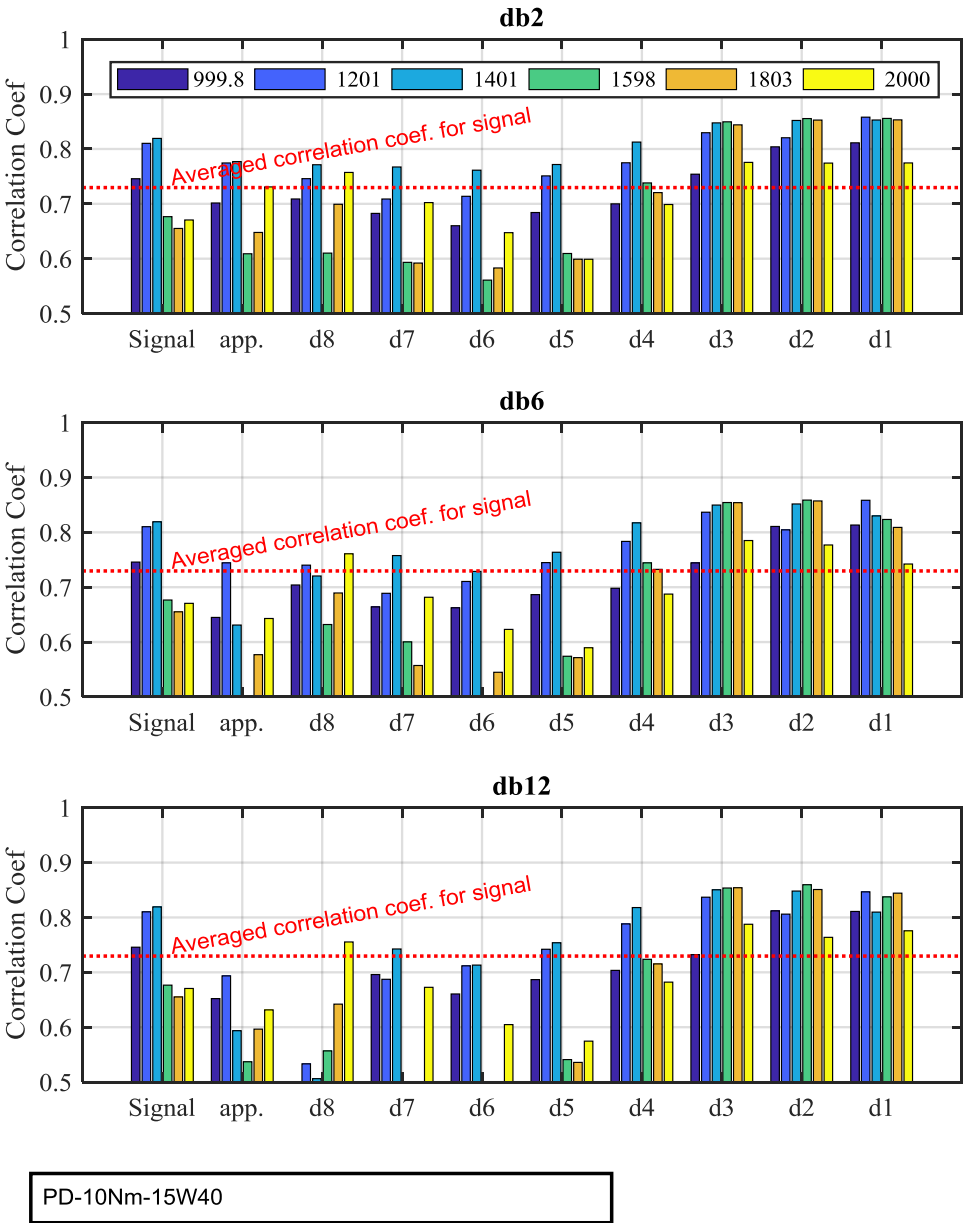

Figure 7-3 Average correlation versus different wavelet and operating speed under low load

Figure 7-2 and Figure 7-3 display the variation of average correlation amplitudes with decomposition levels and wavelet orders within a wide range of speeds and two values of loads. It can be seen that:

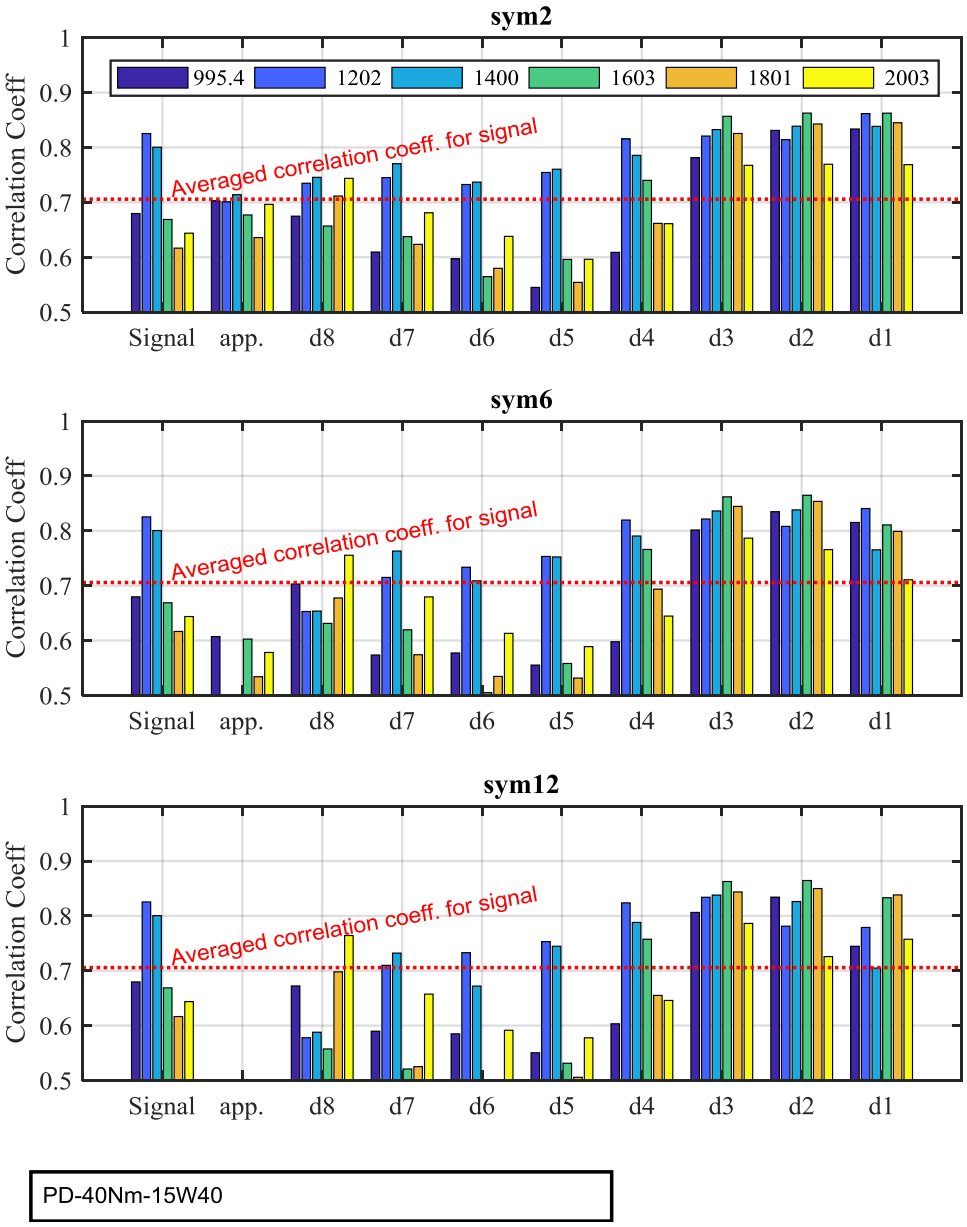

Figure 7-4 Average correlation versus different wavelet and operating speed under low load with Symlets wavelet

（1） Most of the correlation coefficients from d1 to d4 are higher than the raw signal's, it indicates that the similarity between the envelope of the wavelet coefficients from d1 to d4 and the modified profile of the piston speed are higher

than the similarity between the raw AE signals and the modified profile of the piston speed.

（2） Apart from at 2000rpm, correlation amplitudes from d1 to d4 exhibit high similarity under different speeds and loads. It indicates that the correlation amplitudes are nearly independent of operating conditions and can be useful for diagnostics.

（3） Hence, the FAI AE characteristics which are varied with the piston speed can be extracted by the wavelet coefficients from d1-d4 level with a higher signal to noise ratio. Therefore, the overall decomposition level just needs to go up to be d4, rather than d5 observed earlier in Figure 7-1.

（4） Moreover, the high amplitudes of correlation coefficients from d1 to d4 also confirm the observation of the high similarity between the weak AE content and the velocity profile, which are achieved from Figure 7-1. Importantly this critical achievement of observation shows that the setting of Y-scales is adequate and thereby it can be taken as the threshold to exclude the locally non-stationary AE bursts to a great degree.

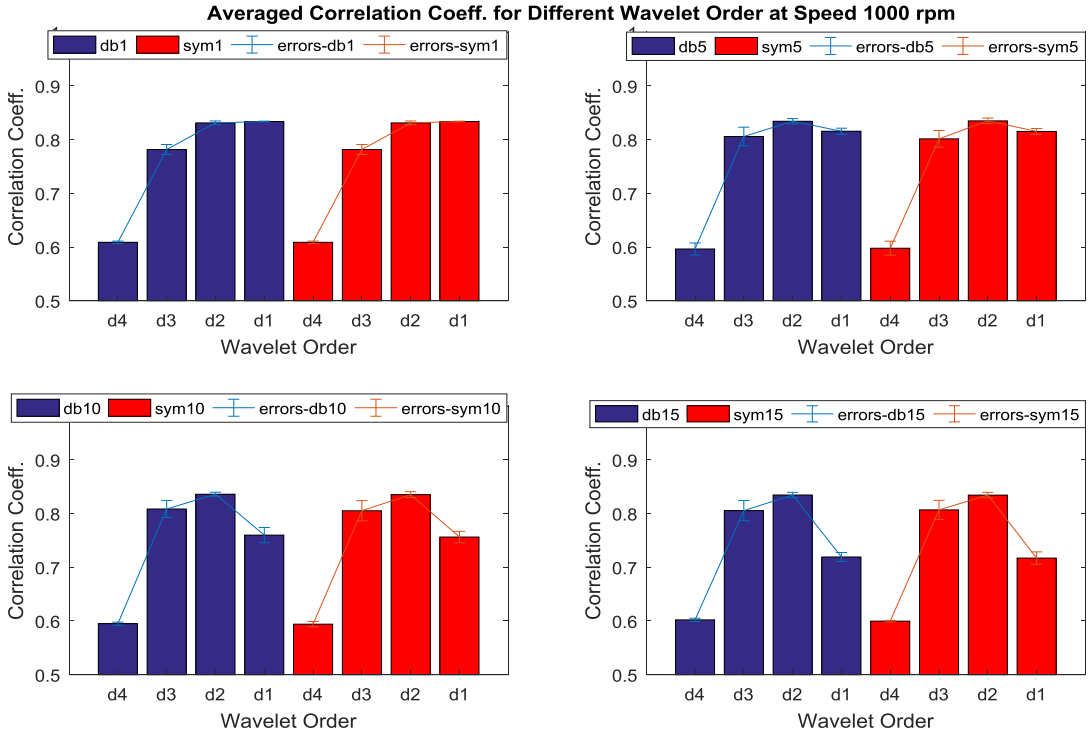

Figure 7-5 Average correlation coefficient versus different wavelet order at 1000 rpm under high load with Daubechies wavelet and Symlets wavelet

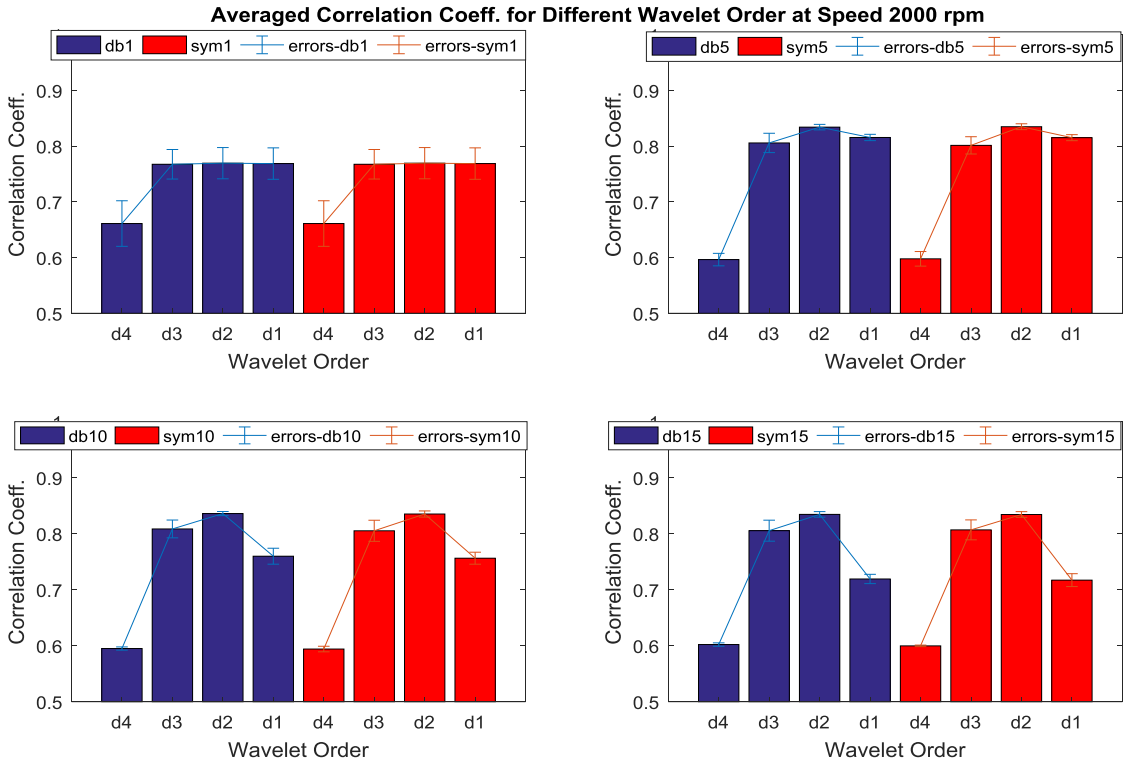

Figure 7-6 Average correlation coefficient versus different wavelet order at 2000 rpm under high load with Daubechies wavelet and Symlets wavelet

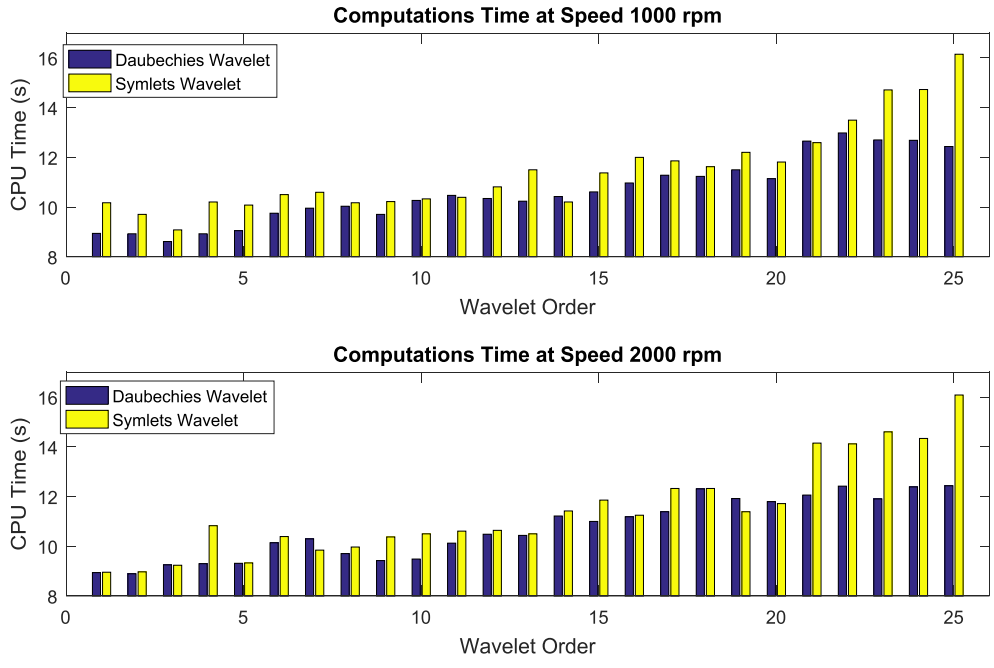

Figure 7-7 Computing cost versus different wavelet family and operating speed

In addition, the correlation analysis for the least asymmetric Symlets wavelet was also carried out to examine if it can perform better than the Daubechies wavelet. As shown

in Figure 7-4 Symlets wavelet produces very similar correlation amplitudes to Daubechies wavelet under the high load, compared with that of Figure 7-2. Particularly, to verify the similarity of these two wavelet families with the same order, Figure 7-5 and Figure 7-6 illustrate the average correlation coefficients of the level d1 to d4 decomposed by Daubechies wavelet and Symlets wavelet at 1000 rpm and 2000 rpm respectively. The correlation values of these two different wavelet families show very similar amplitudes and calculation errors when processing the AE signals from one same case.

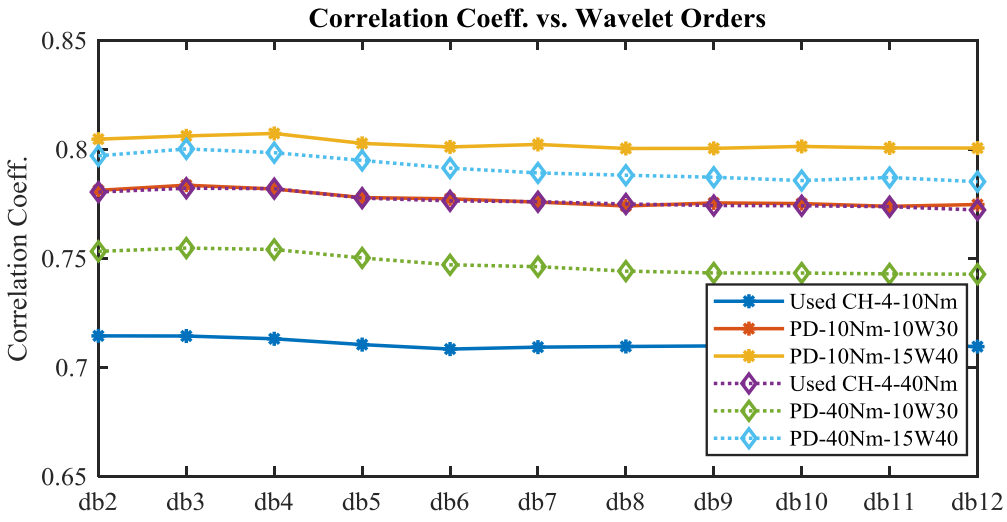

Figure 7-8 Average correlation amplitudes versus with wavelet orders

Moreover, the computations time of Daubechies wavelet and Symlets wavelet families with the order from 2 to 25 is given in Figure 7-7 at different speeds under high load (40Nm). The calculation time of the Symlets wavelet is generally longer than the Daubechies wavelet, especially on the high order. Considering that the Symlets wavelet will consume more computations time, it is not adopted in the study.

Further, the calculation time of Daubechies wavelet is increased generally with the order increasing in

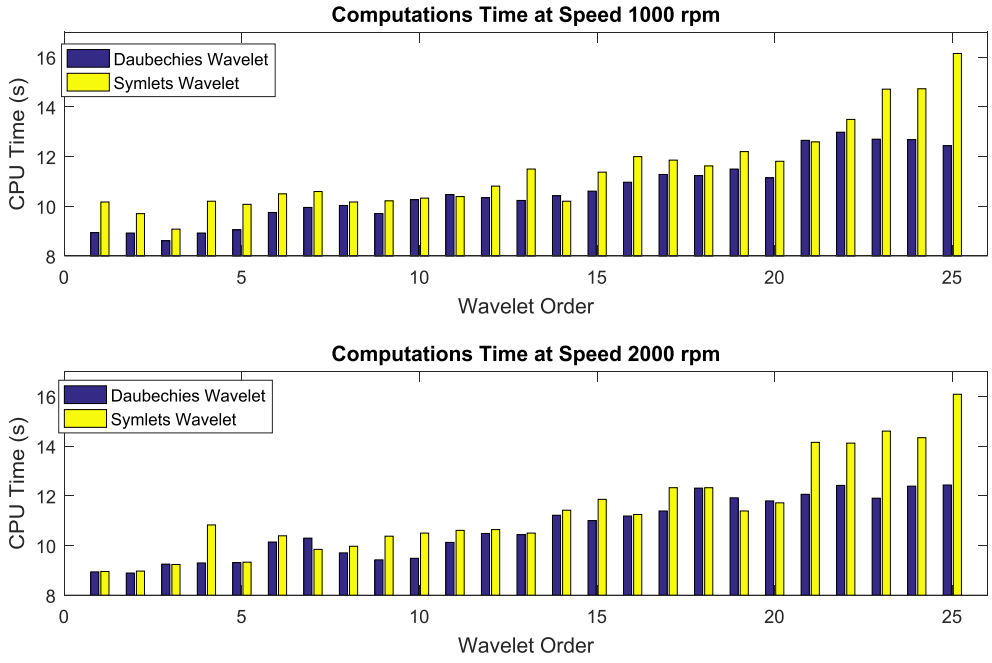

Figure 7-7. So a lower order can be used for higher computational efficiency. Specifically, as shown in Figure 7-8, the average correlation amplitudes for different wavelet orders show slight variations but it can be found that ‘db4’ is the maximal for all the cases explored. Considering a slight better smooth effect at the high order, the wavelet decomposition order is selected as ‘db5’ for the further WMRA analysis in this study.

7.3 Diagnostic Features from a Hard Threshold based Envelope

The above analysis shows that AE events induced by valve impacts, fuel injection and combustion reveal the broadband characteristics in all of the decomposition level based on WMRA. As shown in Figure 7-1 the wavelet decomposition results for the locally stationary AE activities are very weak compared to the large bursts AE events. In addition, both of them vary with engine operations. Hence, an adaptive wavelet threshold de-noising method is developed to separate the weak events with optimal wavelet base and decomposition level selection.

A thresholding scheme is the most commonly used method for implementing wavelet based de-noising [188]. Mallat et al.[189] firstly removed the white noises from signals, in which those signals with smaller magnitudes than the set threshold, and the others with larger magnitudes than the preset threshold are reserved (hard-threshold case) or shrunk (the soft-threshold case) [190]. The wavelet threshold de-noising usually selects the target signal which is concentrated on some of the wavelet coefficients, whereas the noise spreads throughout all of them. Therefore, wavelet threshold de-noising technique is a powerful tool to increase the SNR and thus develop reliable fault features for a wide class of nonstationary signals in rotating machinery fault diagnosis[191].

However, as the tribological AE amplitudes are much smaller compared to the interfering large AE bursts (fuel injection, combustion shock and valve impacts), it is not possible to apply the conventional de-noise scheme to highlight the tribological AE. Otherwise, it would outlook largely the diagnostic information tribological as the tribological AE with small amplitudes could be taken as noise and removed out. Therefore, the de-noise was implemented in this study by an inverse way in that the small amplitudes of wavelet coefficients are selected to reflect FAI effects while the large coefficients from combustions, valve and injection are rejected.

To evaluate using AE responses to diagnose tribological behaviours, AE signals are de-noised with a hard threshold-based approach, which is summarised as following key steps:

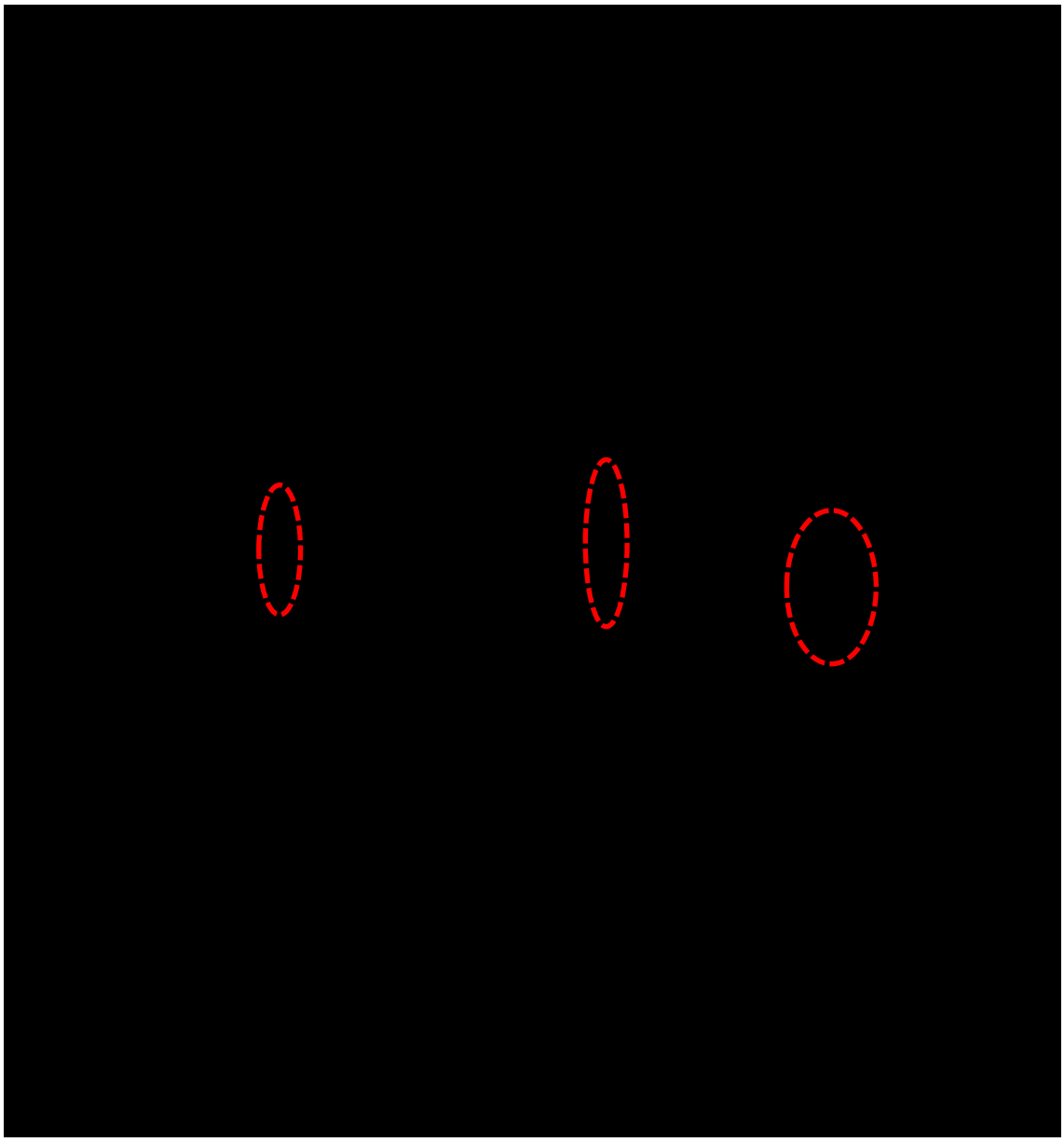

Figure 7-9 Average envelop calculation and illustration of local envelop amplitudes (LEA)

1) Exclude large AE bursts by setting the AE data samples to zeros in the angular intervals where the modified velocity are of zeros, as illustrated in Figure 7-9 (a) and (b).

2) Apply forward DWT to multiple AE signals (K=20 for the limited memory of the PC used) from single operating condition into wavelet domain, which is achieved with analysis parameters: J=4 and ‘db5’ wavelet.

3) Apply the hard threshold obtained by Equation (7-1) to suppress any possible locally non-stationary AE bursts in the middle of the strokes;

4) Perform inverses DWT to reconstruct the AE signals with only coefficients shrined at d1 to d4;

5) Calculate the average envelope sample signal of the 20 reconstructed signals to enhance the similarity to the velocity profile, of which a raw envelope signal is illustrated Figure 7-9 (b).

6) Apply a low-pass filtration to the averaged envelope signal by a wavelet filter in which only the approximate coefficients are selected during the inverse transform, which is implemented with J=12 and db12 wavelet for achieving a better smoothness or suppressing any spikes of the envelope signals.

As shown illustrated Figure 7-9 (c), the constructed envelope enhances significantly the locally stationary AE content in the middle of the stroke and can be used for more accurate diagnosis. Interestingly, two downward strokes: suction and power exhibit very similar profile and of similar magnitude, showing very consistent tribology behaviour. However two upward strokes: combustion and exhaust show very dissimilar profiles. The AE amplitudes during the exhaust stroke have very high magnitudes, which may indicate the effects of instantaneous temperature and combustion residual products. This dissimilarity is not consistent with the fiction forces predicted by conventional models in Chapter 3, showing that significant investigation needs to be carried out to take into account combustion residuals and temperature rises into the model.

Moreover, the effects of the locally non-stationary AE bursts still not suppressed sufficiently. As highlighted with oval circles in Figure 7-9 (b) and (c), these can still make significant contributions to the final envelope.

To reduce these influences, diagnostic feature parameters are calculated within four angular intervals illustrated by the horizontal thick colour bars in Figure 7-9 (c) with respect to the four strokes. Specifically, an average envelope amplitude is calculated in each angular interval, which then results in four diagnostic features to show AE magnitudes in four strokes respectively. As shown in Figure 7-10, the average amplitude reflects the general characteristic of the envelope for indicating the tribological behaviour of interest because it avoids, to a great degree, the inclusions of

potential effects of the locally non-stationary AE bursts. In particular, AE amplitudes are significantly different between the compression and exhaust strokes when the piston moves downwards. This can be an indication that more AE contents due to AAC effects occurring in the exhaust stroke because the thickness of tribofilm is significantly lower due to the decreased viscosity at higher instantaneous temperatures on the surfaces of the cylinder liner and piston rings. In contrast, AE magnitudes are the lowest during the compression stroke as its lubrication is dominated with HL regimes because the temperature is blown down by the flow of fresh air during the previous intake stroke to the lowest amongst the four strokes, which causes the least effect on the change in oil viscosity. This also means that the AE is mainly due to FAI effects and exhibit the lowest AE amplitudes during the compression stroke. Similarly, because of this temperature effects in other two engine strokes: intake and power strokes when the piston moves downward, their tribological behaviours are also mainly in ML regimes and produces higher AE amplitudes due to more pronounced AAC effects.

In addition, as these AE feature parameters are from just a small portion of the envelope, they are known as local envelope amplitude (LEA) in order to contrast to the average amplitude that is calculated from an entire lobe of the envelope in an entire stroke. The latter is denoted as the global envelop amplitude (GEA) and will be established in next chapter.

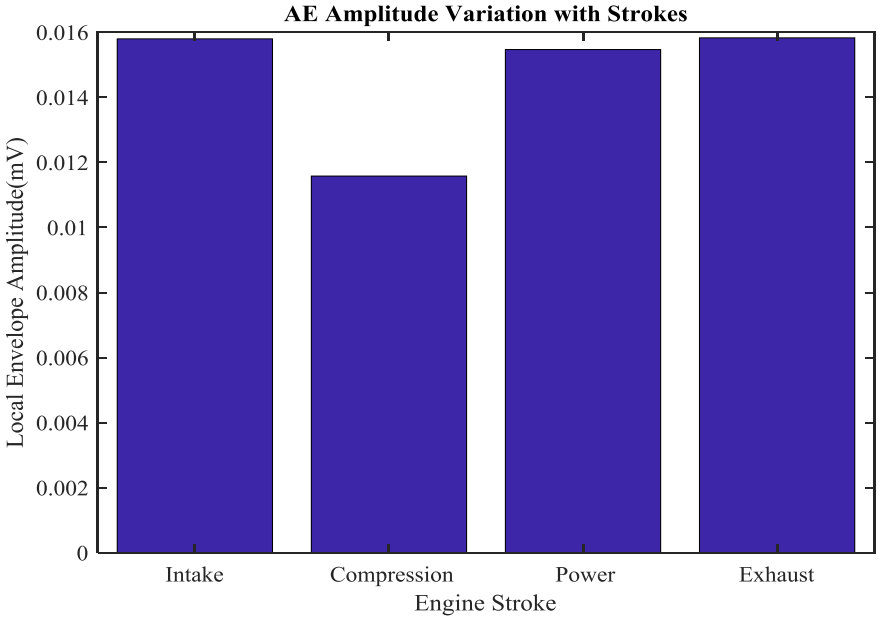

Figure 7-10 Local Envelope Amplitude (LEA) in different strokes

7.4 Diagnosis of Different Lubricating Oils

To evaluate the performance of using the proposed diagnostic parameters for oil diagnostics, LEA values were calculated from AE signal for three different lubrications oils across different speeds and loads and then were examined to check whether they can appear in a way similar with tribological behaviours. This was carried out after evaluating the detectability of using an averaged correlation coefficient.

7.4.1 Diagnosis using Correlation Coefficient Amplitude

Section 7.2 has found that wavelet coefficients at levels of d1 to d5 show higher degree of correlation with the modified velocity of the piston motion, average correlation coefficients thus were calculated from different operating conditions with the attempt to utilise direct results to indicate the difference between tested lubricants. As shown in Figure 7-11, this correlation amplitude allows the baseline oil of 15W40 to be differentiated consistently from 10W30, which can be based to show the analytic predictions that the higher viscosity oil produces higher FAI effects.

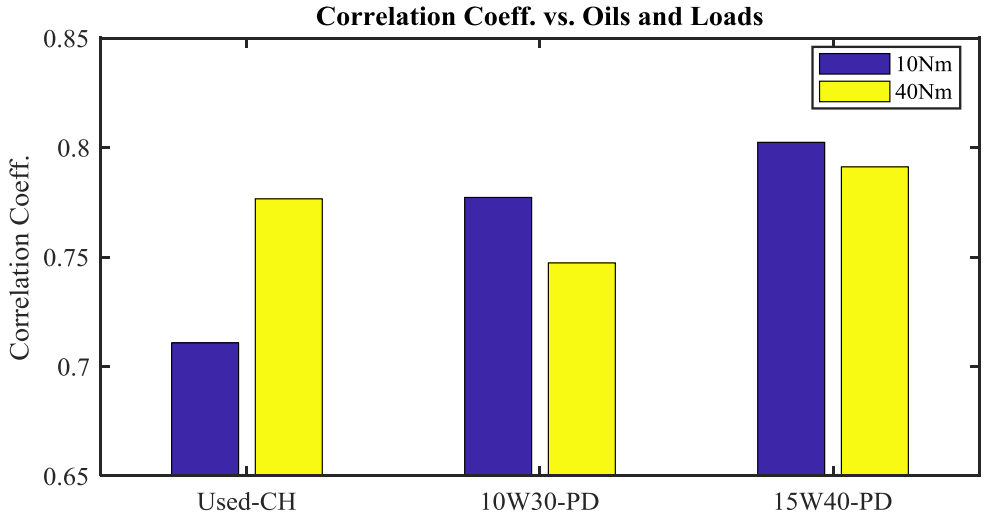

Figure 7-11 Wavelet decomposition of AE signal on the engine body

However, the lower correlation amplitudes are unable to give adequate explanations to the differences from the used oils as its viscosity was measured offline higher than 15W40, and neither do the differences between loads. This less success of diagnostics,

therefore, shows that this simple correlation analysis is insufficient and further processing such as the hard threshold based de-noising AE signals must be carried thoroughly to reduce any noise effects including that of locally non-stationary AE bursts.

7.4.2 Diagnosis with Local Envelope Amplitude (LEA) from a Hard Threshold Approach

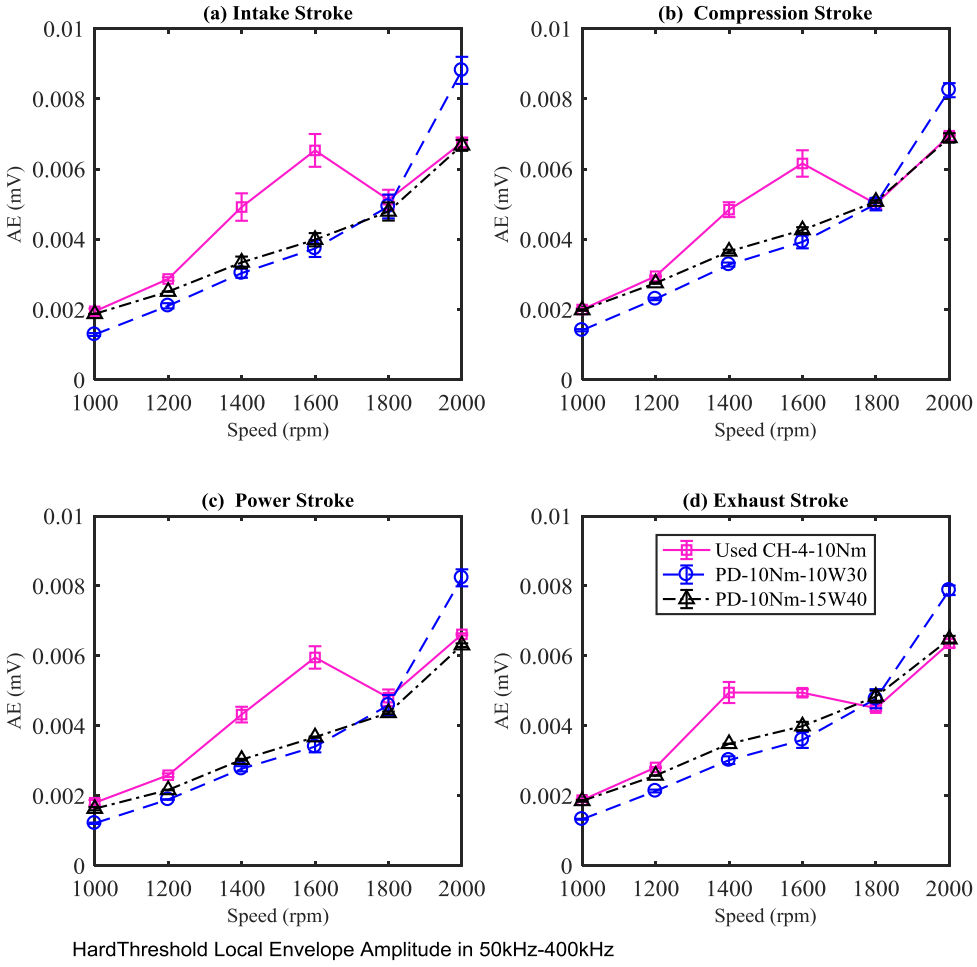

Figure 7-12 Diagnosis of different lubricating oils with LEA under low load

Figure 7-12 presents LEA values with incremental speeds under low load for four engine strokes respectively. For the baseline lubricant of 15W40, LEA values exhibit clear increases with engine speeds in all strokes. This indicates the characteristic of the speed dependence predicted analytically based on AAC and FAI models and numerical simulations based on viscous and asperity frictions, and thereby shows the potential for

detecting abnormal tribological behaviours using LEA values from AE envelope signals formulated by the wavelet coefficients selected using the hard threshold.

For the low viscously lubricant of 10W30, LEA also shows an increasing trend with speed. However, its amplitude is clearly lower than that of 15W40, which are particularly distinctive for the intake and power strokes (the downward piston motion) at all speeds tested. These differences are well agreed with the predictions and therefore confirm that LEA values can give a tiny separation between the two new lubricants. However, LEA values in upward strokes do not show very good separations. This can indicate more the effect of higher instantaneous temperatures.

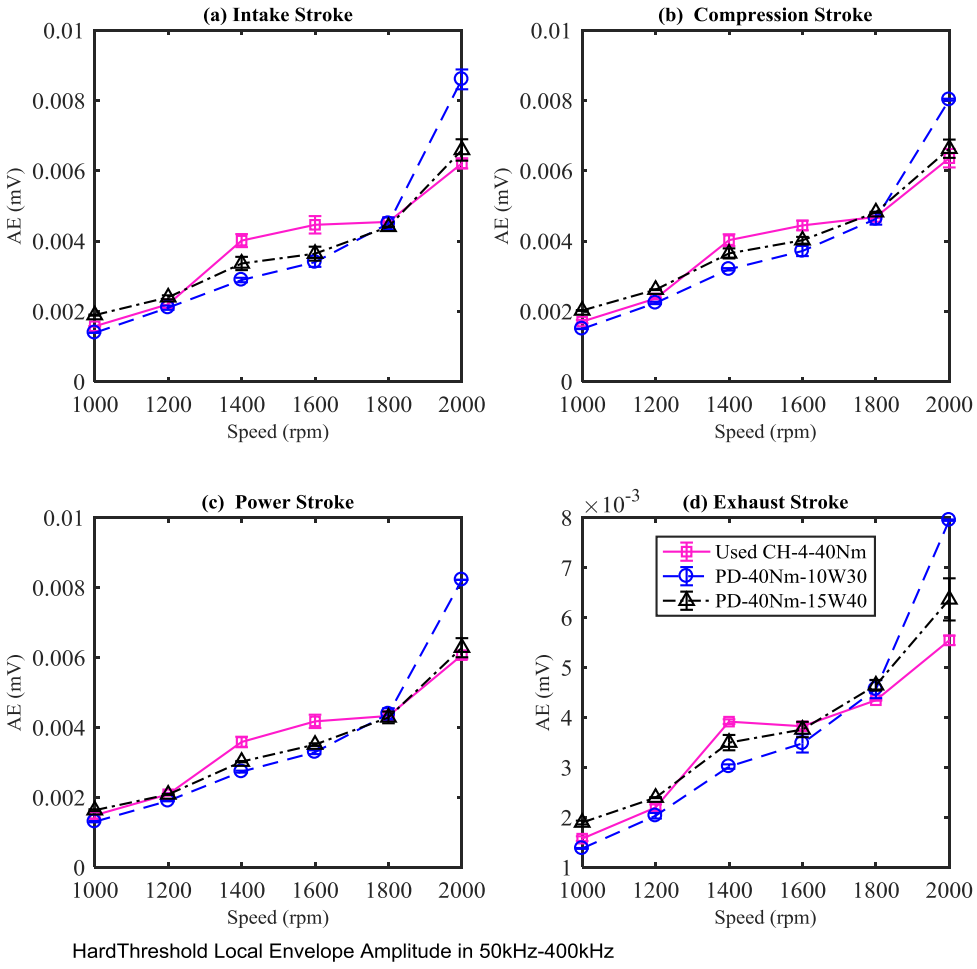

Figure 7-13 Diagnosis of different lubricating oils with LEA under high load

Having confirmed the capability of making the small differences between two lubricants, LEA is further evaluated for differentiating the used oil. As shown in Figure 7-12, LEA values for the used oils are generally higher compared to 15W40 and

10W30. This agrees with higher viscosity values measured offline before the test. Especially, the significantly higher LEA in the compression and exhaust strokes allows the deteriorated oil to be identified without any double. In addition, LEA values show more oscillations with speeds. This may indicate that the oil is more deviated from the properties of Newtonian fluid because of various influences such as dissolved water, combustion particles and various contaminants. Overall, it shows that LEA extracted from AE signals yields a satisfactory separation between different lubricants.

For high engine load, LEA values in Figure 7-13 show similar amplitudes to the low load one, confirming that FAI effects are not very much dependent on loads. Moreover, it also gives very similar performances in differentiating two new oils in the intake and power strokes, and less in the compression and exhaust strokes (the upward piston motions).

However, LEA for the used oil shows lower values in the compression and power strokes. This is not very agreeable with FAI effects due to the higher viscosity of the used oils. Because non-Newtonian effects exhibit more in the used oil, these decreases can be understood that the adhesive strength at higher temperature due to higher engine loads decreases more significantly and thus the FAI effect is not consistent with the offline viscosity. Nevertheless, higher LEA values in the upward piston motions allow an acceptable separation of used oils from the baseline one.

Therefore, a conclusion can be drawn that LEA of AE signals is possible to reveal the changes in oil viscosity and allows two new oils to be separated in accordance with tribological FAI effects during downward piston motions. In addition, the used oil can be identified in the upward motion strokes whereas it cannot be separated during the downward piston motions. This less consistent diagnosis will be further analysed in future studies.

7.5 Impact of Different Alternative Fuels

Having confirmed that LEA values from AE signals are very sensitive to changes in tribological behaviours, they are based on to evaluate whether any impacts can be induced by using the other two alternative fuels tests. Figure 7-14 and Figure 7-15 show the comparison of LEA between different fuels under two engine loads respectively. In

principle, as LEA behaviours for the two alternative fuels are very similar to the two lubricants during all four strokes, it means that they hardly produce any negative influences on tribological behaviour based on the FAI predictions.

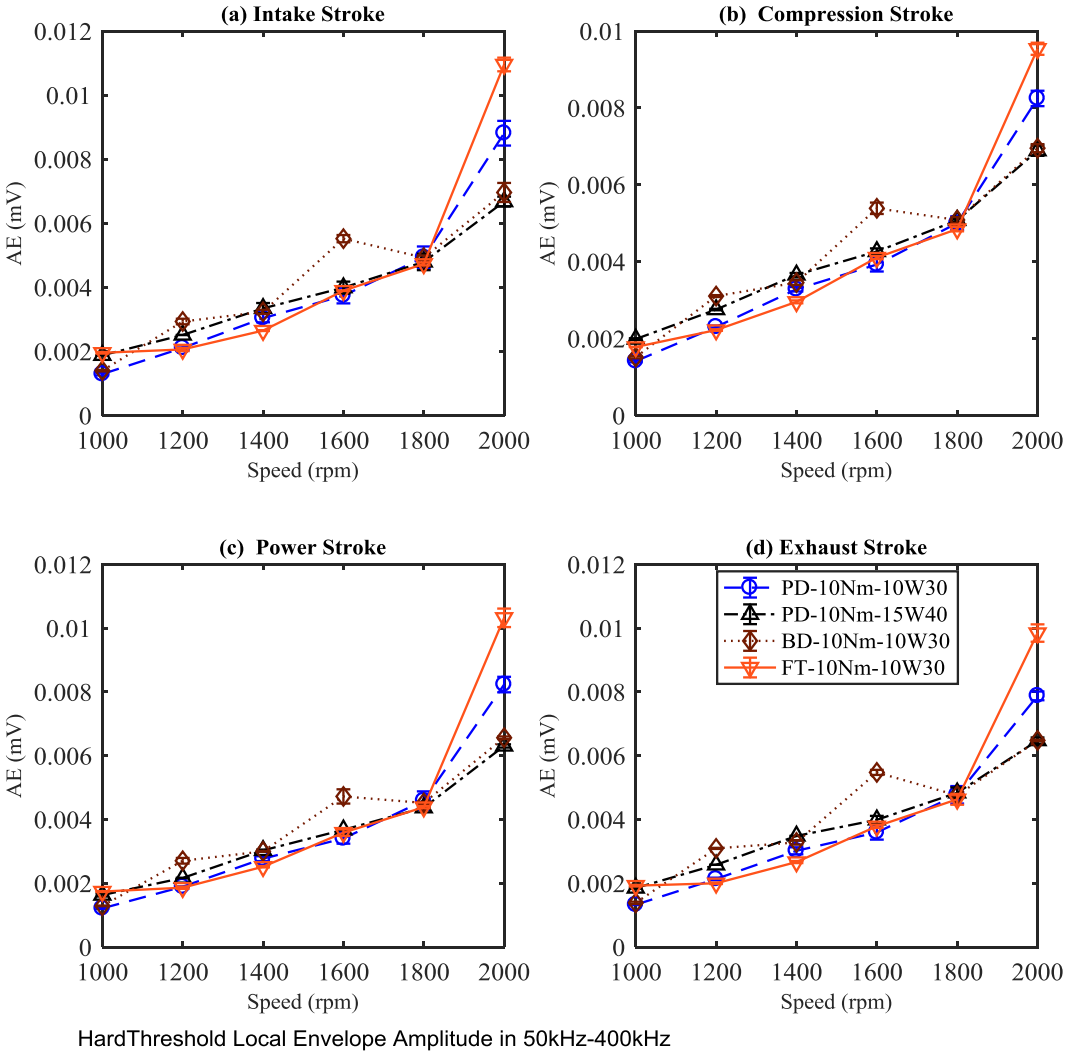

Figure 7-14 Impact of different fuels with LEA under low load

However, burning biodiesel produces a slight higher AE at several speeds such as 1600rpm, compared with that of 15W40 oil. In addition, the increasing trends during the downward piston motions show slightly more oscillations with speed. This can be an indication of more occurrence of AAC induced AE activities due to unsteady combustions in such particular speeds, which will be clarified in next chapter that it is possible to separate AE contents between FAI and AAC effects.

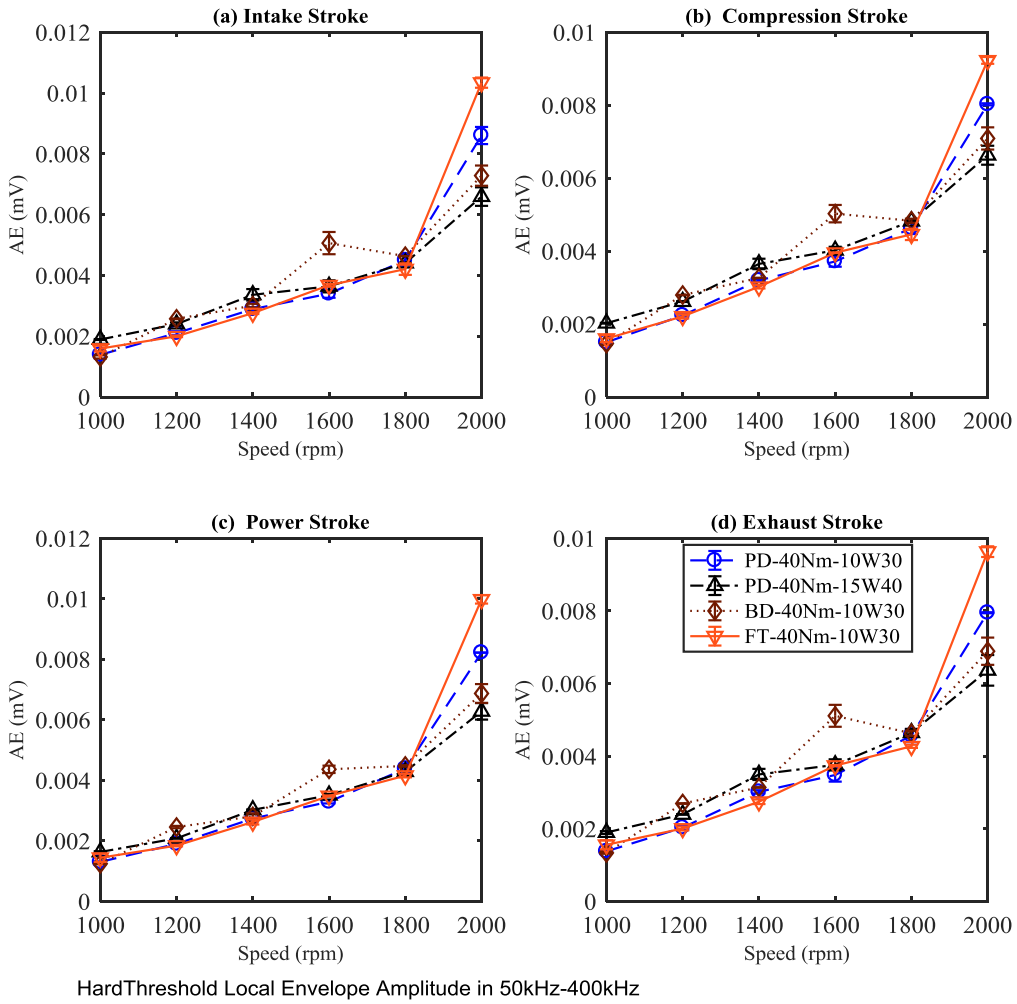

Figure 7-15 Impact of different fuels with LEA under high load

7.6 Key Findings of Chapter 7

To effectively apply wavelet analysis to AE signals, this chapter has addressed the key issues of determining optimal wavelet analysis parameters: wavelet types, wavelet scale or decomposition levels and wavelet orders. Then the optimal analysis results in a cleaner envelope from the noisy AE signals and subsequently is based on to diagnose different engine lubricating oils and alternative fuels.

Among many different types of wavelet available, Daubechies and Symlets wavelets that are widely applied to analyse vibro-acoustics signals, have been evaluated by a correlation analysis between the extracted AE envelope and modified velocity of the

piston motion, which leads to that an optimal wavelet transform can be achieved with a wavelet basis of ‘db4’ and a decomposition level of 4.

The average correlation amplitude allows differences between two new lubricants to be made consistently, but not enough accurate because of the influences of various noises and the potential interference with localised AE bursts of medium strengths.

The hard threshold based wavelet coefficient selection approach has reduced the noise greatly, particularly the locally non-stationary AE bursts being rejected largely with the twice standard deviation of the wavelet coefficient at each level. Thus the local envelope amplitudes show satisfactory diagnostics in making consistent differences between two new lubricants in downward strokes whereas they separate the used oils better in the upward strokes.

LEA values for the two alternative fuels exhibit very similar behaviours to the two lubricants during all four strokes. So they hardly show any negative influences on tribological behaviour according to the AE contents induced by FAI effects.

CHAPTER 8 WAVELET ANALYSIS WITH AN ADAPTIVE THRESHOLD AND DIAGNOSTICS OF TRIBOLOICAL BEHAVIOUR

This chapter details the further wavelet analysis of typical engine AE signals. It starts with developing an iteration scheme for WMRA which uses an adaptive threshold to select optimally FAI induced weak AE content subject to constrains a modified velocity profile of the piston motion. Then, it uses the extracted cleaner envelope of wavelet coefficient to establish an AE diagnostic feature using the global profile of the envelope, denoted as (GEA), and an improved LEA which uses a small portion of the envelope signal. Moreover, a novel diagnostic feature derived from residual signals derived during the adaptive process is also developed to reflect the effect of AAC in the tribological process. Finally, the performance of diagnosing different types of lubricants and alternative fuels are evaluated under a wide range of engine operating conditions.

8.1 Introduction

Hard threshold based wavelet coefficient selection shows positive results for making the satisfactory diagnosis on tribological conditions for different test cases. However, many medium AE responses closed to the middle of each engine strokes are removed based an empirical hard threshold value. Thus it leads to diagnostic results highly related to the speeds and less consistent with model prediction, in Chapter 7, where the characteristics of FAI induced AE are more affected by lubricant viscosity and speed but less to load.

To improve the diagnostic performance, therefore, this chapter develops a more comprehensive approach to suppress more the locally non-stationary AE bursts from AAC and to maintain the weak AE contents from FAI effects. In principle, the approach will select wavelet coefficients in an optimising scheme which is governed by the general characteristics of AE characteristics and mechanisms. In this way, it can maximise AFI effects for more accurate diagnosis of different lubricants.

8.2 Optimal Selection of Wavelet Coefficients

As shown in Chapter 7 the diagnostics produce sufficiently good results. Especially the correlation coefficient based diagnosis also shows a consistent result. Both of these achievements yield a further understanding that the correlation relationship between the week AE and the modified velocity should be utilised more comprehensively. In Chapter 7, the correlation has been involved in the early phase of the WMRA for trimming the raw signal and lead to good success, therefore, it is worth to apply the correlation characteristics to other key stages of wavelet analysis such as trimming both the wavelet coefficient sequences and the envelope signals as they all should exhibit a waveform in accordance with the velocity profile of the piston motion to a great degree, which is achieved by the predictions of analytic models.

To realise these understandings, an optimisation scheme is subsequently designed to calculate these two waveforms in an adaptive approach, which is summarised as following key steps:

1) Exclude the large AE bursts by setting the AE data samples to zeros in the angular intervals where the modified velocity are with zero values, as illustrated in Figure 7-9 (a) and (b).

2) Apply the forward DWT to multiple AE signals (K=20 for the limited memory in the PC used) from single operating condition into the wavelet domain, which is achieved using analysis parameters: J=4 and 'db5', the same as that in the hard threshold-based approach. This results in threshold wavelet coefficients W_j at different levels. As an example, the blue plot in Figure 8-1(a) shows the wavelet coefficient obtained at j=4. Clearly, it consists of several distinctive local bursts that might be less relating to FAI effects but more to AAC effects.

3) Calculate a maximum threshold value based on Equation (7-1) but with an overdetermined factor of 5 rather than 2 to ensure the inclusion of local busts in the wavelet coefficient, specifically

$$5\sigma_j = 5\sqrt{\frac{\sum_{k=1}^{K}\sum_{n=1}^{N} W_j^2(n)_k}{KN}} \tag{8-1}$$

4) Set a large iteration number such as $Itr_{\max} = 50$ and calculate the increment of the threshold for each iteration at level *j*:

$$\vartheta_j(i_{tr}) = \frac{i_{tr} \times 5\sigma_j}{Itr_{\max}} \tag{8-2}$$

A high value $Itr_{\max}$ can achieve slow convergence, which can be easily adjusted by several trail runs.

5) Calculate the time varying threshold based on the modified velocity $\tilde{v}_p(t)$

$$\vartheta_j(i_{tr}, t) = \frac{i_{tr} 5\sigma_j}{Itr_{\max}} \tilde{v}_p(t) + \frac{5\sigma_j}{2Itr_{\max}} \tag{8-3}$$

6) Apply $\vartheta_j(i_{tr}, t)$ to wavelet coefficient to select those lower than the threshold at the iteration, which runs for W_j at all levels in the wavelet domain, and results

in cleaner W_j^S as shown by the pink plot in Figure 8-1(a), demonstrating that it has excluded the locally non-stationary AE bursts largely.

7) Perform inverses DTW to reconstruct the AE signals with only coefficients selected by corresponding thresholds at d1 to d4;

8) Calculate the average envelope sample signal $\bar{x}_{rE}$ of reconstructed signals for 20 engine cycles to enhance the similarity to the velocity profile, of which an interim envelope signal is illustrated Figure 8-1 (b) at j=4.

9) Apply a low-pass filtration to the averaged envelope signal by a wavelet filter in which only the approximate coefficients are selected during the inverse transform, which is implemented with *J*=12 and db12 wavelet to achieve a better smoothness envelope signals.

10) Calculate the normalised correlation distance $d(x_{rE}, \tilde{v}_p)$ between the smoothed envelope and the modified velocity by:

$$d(\bar{x}_{rE}, \tilde{v}_p) = 1 - \frac{\bar{x}_{rE} \, | \tilde{v}_p^{\mathrm{T}} |}{\sqrt{\bar{x}_{rE} \bar{x}_{rE}^{\mathrm{T}}} \sqrt{| \tilde{v}_p \, \| \tilde{v}_p^{\mathrm{T}} |}} \tag{8-4}$$

11) Repeat steps from 5) to 10) until it goes to the iteration number at the minimal $d(\bar{x}_{rE}, \tilde{v}_p)_{\min}$, which means that the reconstructed envelope signals are the most similar to the modified velocity with the similar heights in the four of main lobes, as shown in Figure 8-1 (b) and (c).

12) Then continue the steps from 5) to 10) for additional 10 iterations in order to select more wavelet coefficients to enhance the content more with FAI effects. These iterations thus make the envelope more biased or less similarity to the velocity profile in that the second lobe of the envelope corresponding the compression stroke is smaller than others shown in Figure 8-2 (c), but is much closer to the observation form the raw AE signal or its corresponding coefficients such as that shown Figure 8-2 (a). Moreover, the locally

non-stationary AE bursts in the suction and exhaust strokes are still excluded successfully.

13) Complete the iteration. The envelope signal $\overline{x}_{rE}$ and the selected wavelet coefficient W_j^S determined using this iteration approach are of optimal ones in the sense that they reflect more FAI effects and thus can be based on for implementing diagnostics of the tribological behaviours.

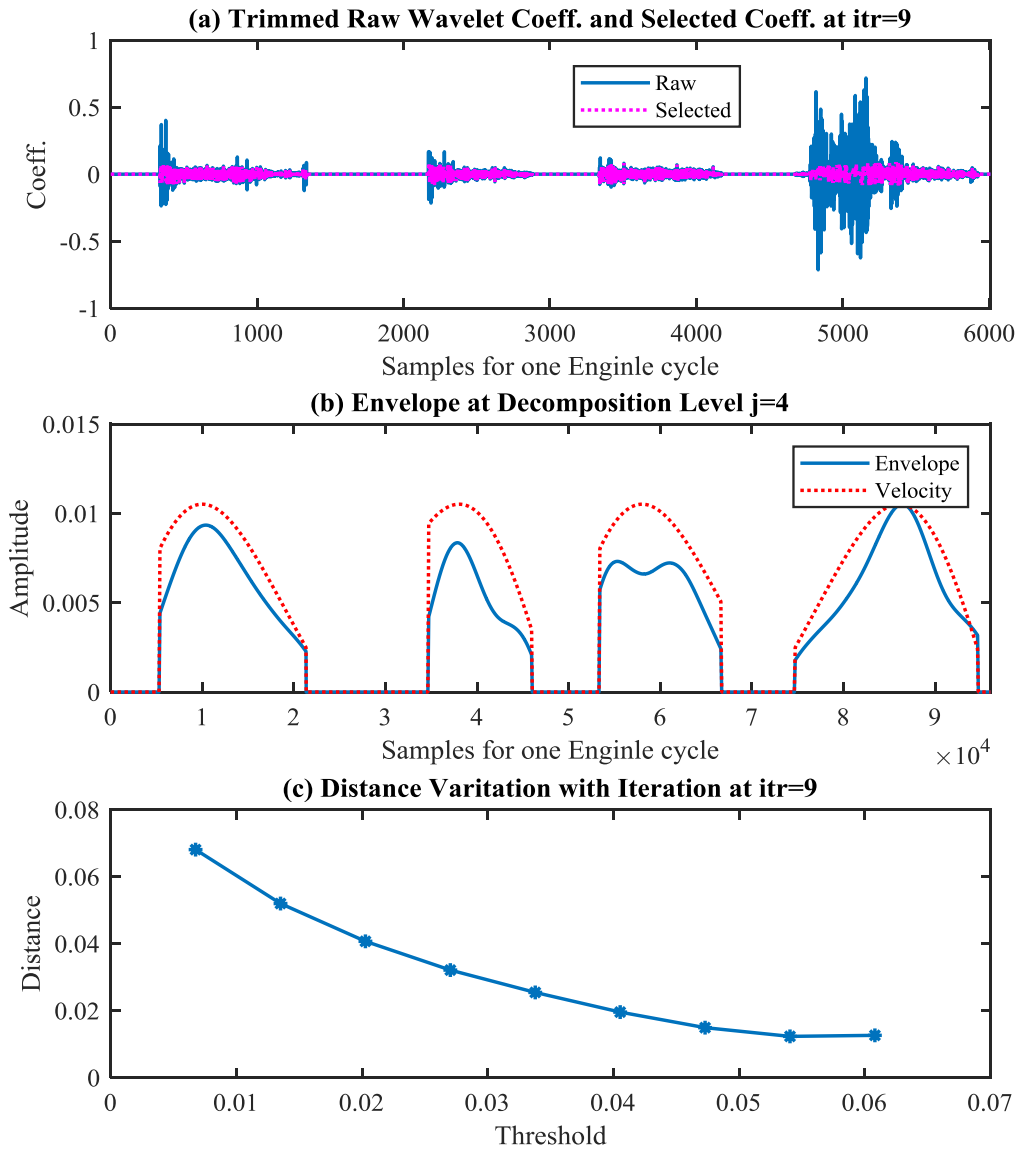

Figure 8-1 Envelope from selected wavelet coefficient at the minimal distance in Step 11)

As shown in Figure 8-3, envelope signals obtained by this approach are cleaner and highlight more clearly the differences between different lubricating oils in accordance with their viscous values.

In addition, adaptive operations have also been evaluated by different cases, showing very stable convergence performance for all the datasets investigated and proved to be robust for large variations of the amplitudes of locally non-stationary AE bursts.

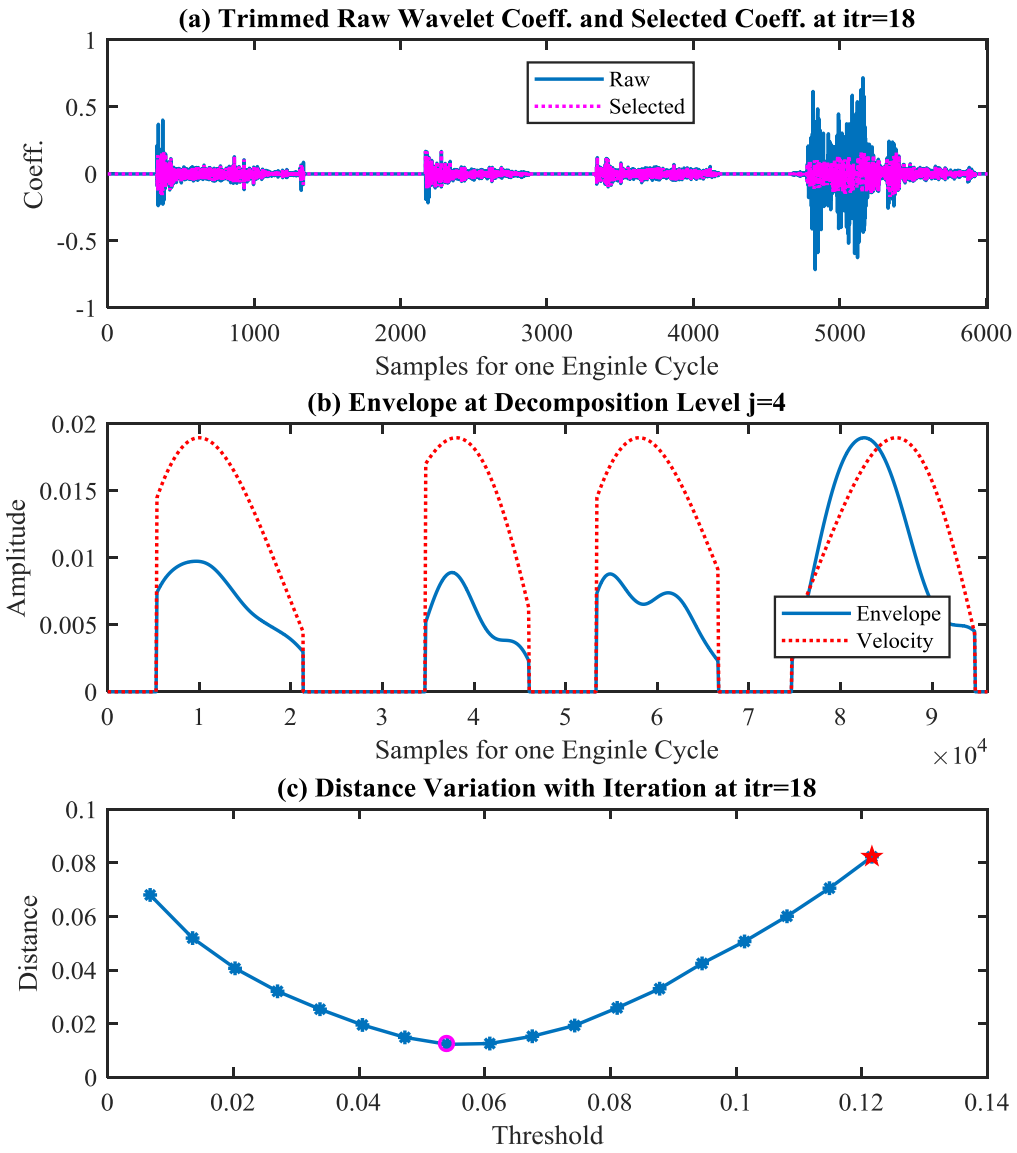

Figure 8-2 Biased envelope from selected wavelet coefficient at further 10 iterations in Step 12)

Figure 8-3 Optimised envelopes for different lubricating oils

8.3 Diagnostic Features from Adaptive Threshold based Envelope Extraction

With applying this adaptive threshold approach to AE signals, three diagnostic parameters can be obtained to reflect effectively tribological behaviours corresponding to ML and HL regimes.

The first one is the local envelop amplitude (LEA) for diagnosing the tribological behaviour relating more to FAI. It is calculated in the same way as that in Chapter 7 and named as improved LEA because the envelope is obtained from the wavelet coefficients with minimal influences from the locally non-stationary AE bursts.

The second one is also for the reflection of AAI effects mainly. It includes one entire lobe in each stroke. As the envelope is cleaned substantially it has minimal effects of the locally non-stationary AE bursts and all of them can be used to obtain to obtain a single indication by averaging the envelope lope in each stroke, rather than just a small portion of the envelope. For brevity, this indicator is known as global envelop amplitude (GEA), in contrast to LEA.

The third parameter can be obtained by subtracting between two sets of wavelet coefficients W_j at Step 2) and W_j^S at the final step. Specifically, it is calculated by

$$ARWC = \frac{1}{4}\sum_{j=1}^{J=4}\sqrt{\frac{1}{N_j}\sum_{1}^{N_c}(W_j - W_j^S)^2} \tag{8-5}$$

where N_j is the sample number per stroke at level *j*. It is obvious that this average of residual wavelet coefficient (ARWC), or the difference between the raw wavelet coefficients and the adaptively selected ones, can represent better the overall contents of the locally non-stationary AE bursts in AE signals, thus a higher ARWC reflecting more AAC effects and hence the asperity induced friction. As shown in Figure 8-2 (a), the locally non-stationary AE bursts left at the end of the iteration are clearly localised and can be regarded as intermittent asperity collisions due to various reasons such as combustion debris inside lubricants, instable motions of ring packs, local dynamic deformation of the liner, etc.

With these three diagnostic features obtained, the tribological behaviours can be more comprehensively evaluated under different conditions, such as different engine speeds, loads, lubricants and fuels.

8.4 Diagnosis of Different Lubricating Oils

8.4.1 Diagnosis with Improved LEA

Improved LEA from adaptive threshold approach selects slightly fewer wavelet coefficients in constructing final envelopes, compared with the hard threshold method. LEA values obtained from these underestimated envelopes thus reflect more the effect of FAI induced AE content and expected to give better diagnostics in differentiating different types of lubricants.

Figure 8-4 and Figure 8-5 present improved LEA values with incremental speeds under low load and high load for four engine strokes respectively. They exhibit smother trends with speeds compared with that of Figure 7-12 and Figure 7-13 because substantial removals of the locally non-stationary AE bursts which appears in a random manner. As a result, the effect of FAIs has represented more accurately, as FAI can induce only small and locally stationary AE activities, in contrast to AAC that can lead to higher local bursts due to direct asperity contacts at higher sliding velocity.

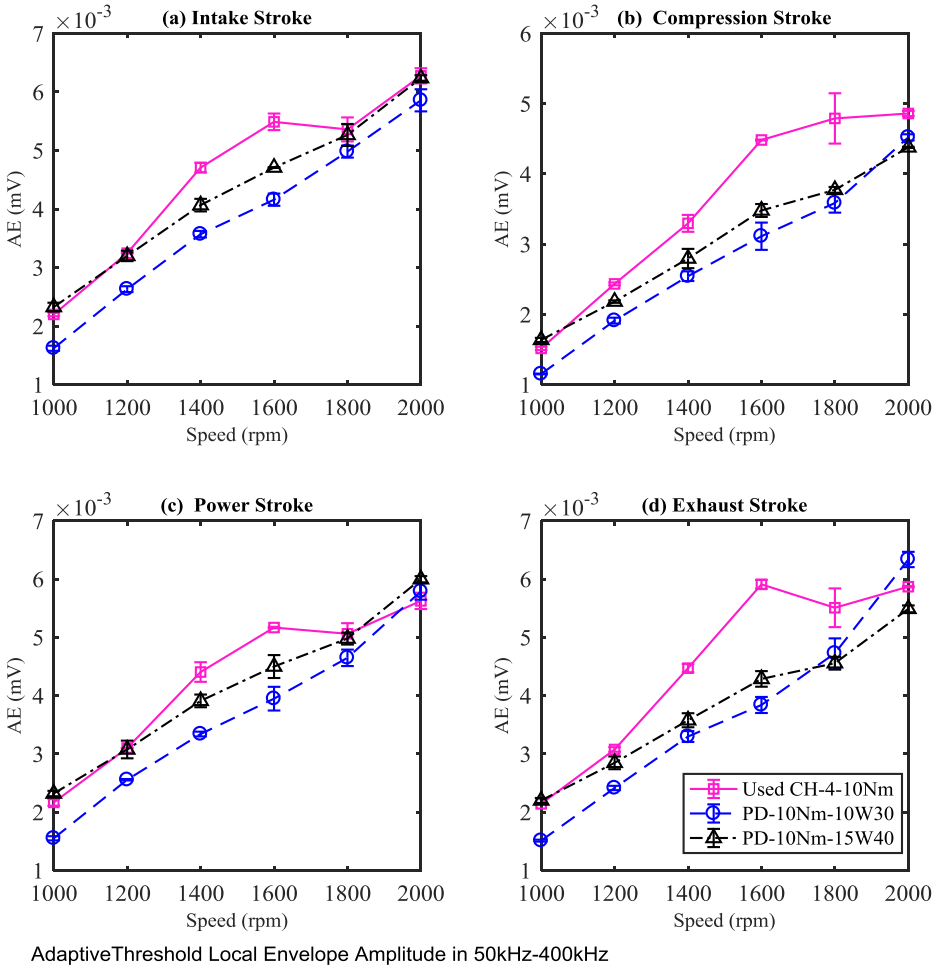

Figure 8-4 Diagnosis of different lubricating oils with LEA from adaptive threshold under low load

Specifically, LEA values also exhibit cleaner increases with engine speeds in all strokes for both the baseline lubricant of 15W40 and the lower viscosity one of 10W30. This indicates better the characteristic of speed dependency predicted analytically based on FAI models and numerically based on viscous and asperity frictions, and thereby shows consistent and steady differences between tested lubricating oils, being the potential for detecting abnormal tribological behaviours using LEA values of AE envelopes.

The detection performance of these more consistent LEA values is very similar to that of Figure 7-12 and Figure 7-13. However, as all the speed trends have less statistical fluctuations, the separation results appear more reliable. Especially, it can be confirmed that the reduction of viscosities is more significant under the high load and higher speeds (>1800 rpm) as LEA values exhibit drops after their increases at lower speeds.

This also allows for an explanation that the differences of LEA values between two new lubricants become smaller at high operating conditions.

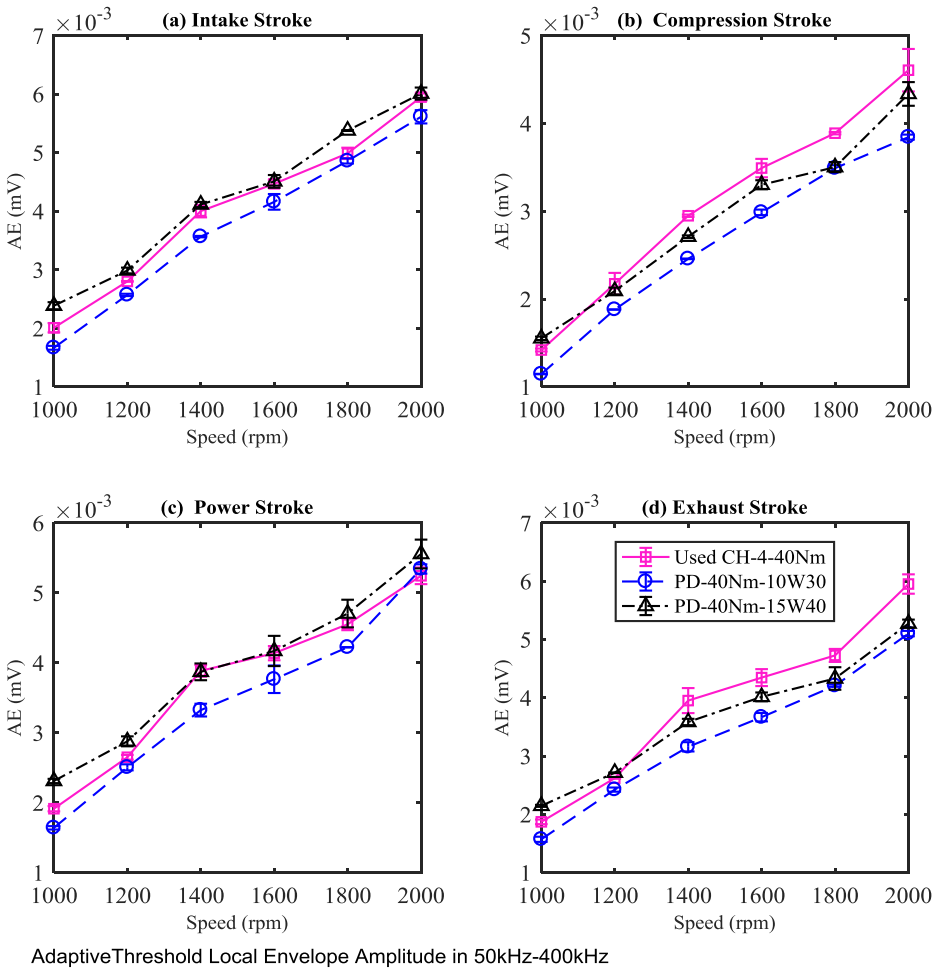

Figure 8-5 Diagnosis of different lubricating oils with LEA from adaptive threshold under high load

Overall, it shows that LEA values extracted from the enhanced AE envelope signals can achieve a more reliable diagnostic result in differentiating different lubricating oils.

8.4.2 Diagnosis with GEA

Figure 8-6 and Figure 8-7 presents the diagnostics of using GEA in differentiating different lubricating oils. In general, the speed trends are very similar to LEA presented in Figure 8-4 and Figure 8-5. So they also give agreeable separation between the lubricants tested and can be used for oil diagnostics.

In addition, this agreement also shows the high effectiveness of the adaptive approach in highlighting FAI induced AE contents.

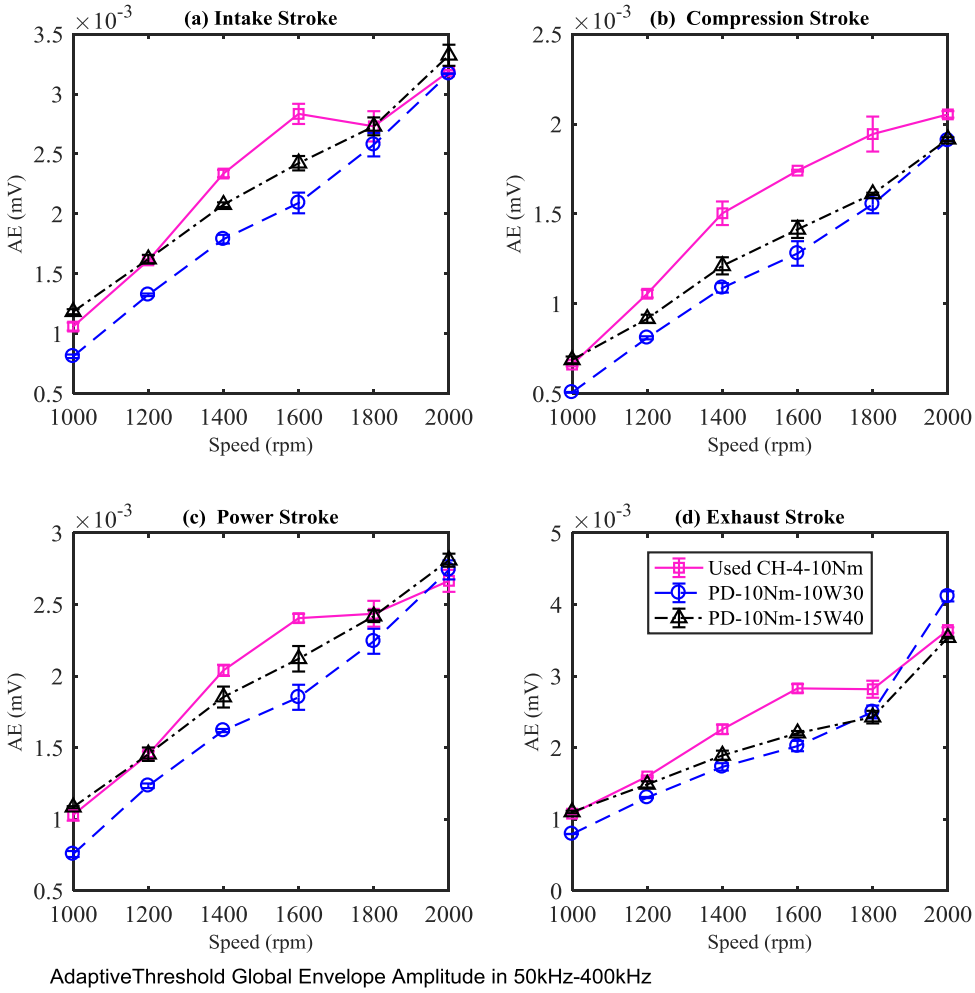

Figure 8-6 Diagnosis of different lubricating oils with GEA from adaptive threshold under low load

However, at the high operating condition of 2000rpm, the separation is slightly worse with GEA values. Moreover, LEA values are obtained within a narrow angular interval where the SNR is predicted and observed higher. So LEA is probably more reliable than GEA which is from a wide angular interval in which more noise can be included at the two ends of its lobe. Therefore, LEA will be based on in the following contents.

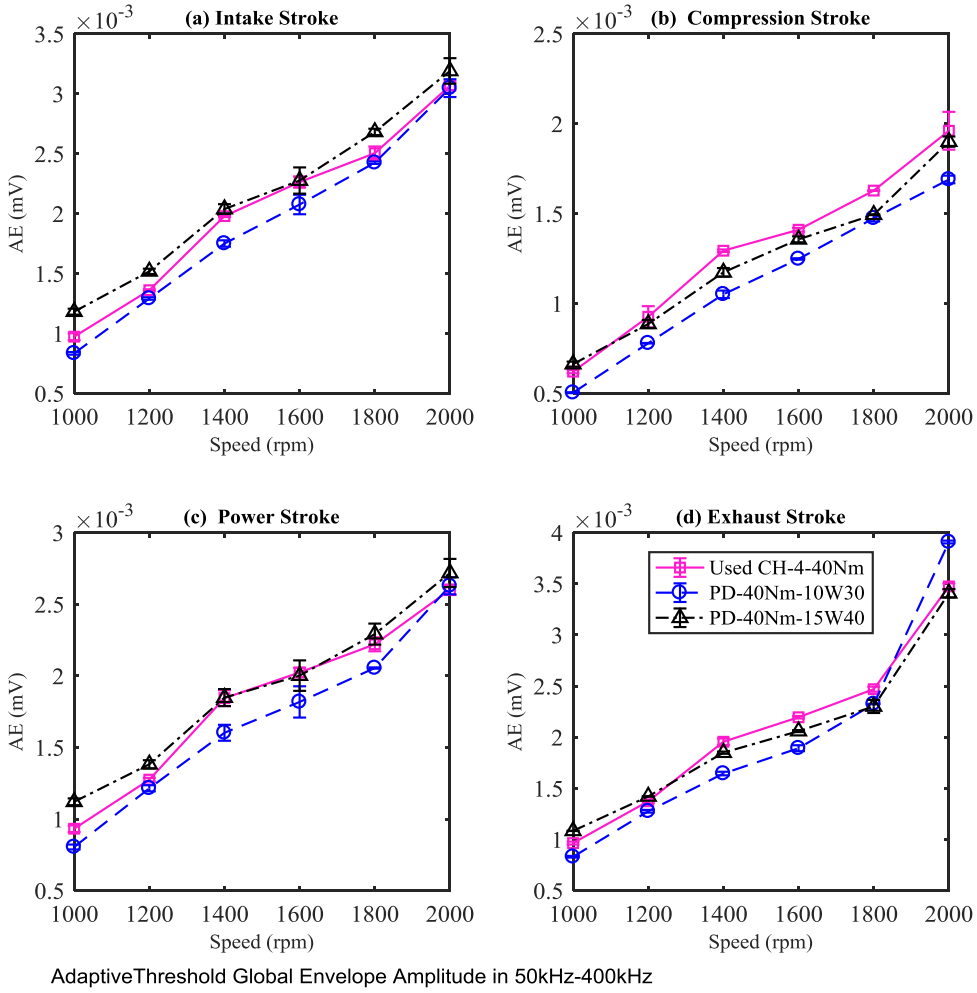

Figure 8-7 Diagnosis of different lubricating oils with GEA from adaptive threshold under high load

8.4.3 Diagnosis with ARWC

Figure 8-8 and Figure 8-9 present the results of using ARWC to diagnose the tribological behaviours of the ring-liner conjunctions for both low and high loads respectively. For the two new lubricating oils, their ARWC values all show nearly quadratic increases with speeds and present amplitudes close to each other at corresponding speeds. In addition, both trends also exhibit a smooth increase. These can indicate that AAC effects are relatively smaller and more uniformly occur for both oils. Especially, ARWC for the low viscosity oil (10W30) are slightly lower at low speeds, indicating that it is less interrupted by flow motions of less viscous oil, whereas it becomes higher at high speeds, indicating that more AAC activities happen due to the reduced tribo-film thickness which is resulted from by viscosity decreases at high

instantaneous temperatures. Furthermore, the ARWC trend for 10W30 lubricant also shows more fluctuations with speeds under the high loads, as shown in Figure 8-9 (b-d). It also indicates the AAC effects can happen more frequently when instantaneous temperatures are higher under higher loads due to reduced tribofilm thickness by the increased load.

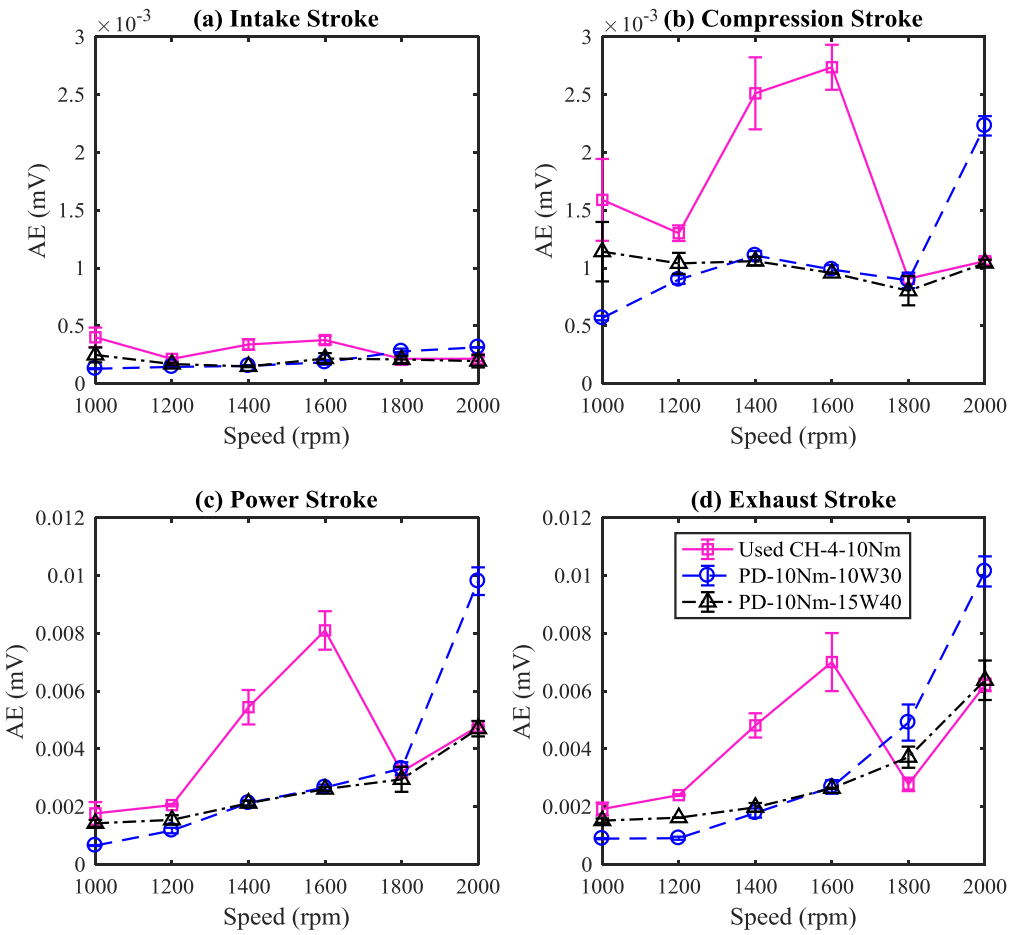

Figure 8-8 Diagnosis of different lubricating oils with ARWC under low load

In the meantime, the solid particles of sizes close to the clearance between two asperities will lead to the collisions between two sliding surfaces, as discussed in Chapter 4. These collisions act as AE sources from the interactions between asperities and particles which deformed the asperities during the sliding process. Similarly, these AE activities due to the asperities deformation on the liner surface transmits through the solid structure to the out surface of the cylinder. Therefore, the interactions between solid particles in the used oil and the surface asperities generate AE activities very

similar to the AAC effects. Although the oil filter can remove the most of parts of the contaminants and particles from engine oil. Some particles may still adhere to the surfaces to increase the probability of AAC effects. In separating the used oils from new lubricating oils, ARWC show significantly higher amplitudes at the middle engine speeds. These indicate that there exist strong AAC activities happening at such speeds. Because the trends are highly fluctuating, these AAC effects are regarded to be induced mainly by the interaction between solid particles in the used oil and the surface asperities. As shown in Appendix A, the used oil contains significantly more particle contents of larger sizes. Especially, these solid particles can be brought by unsteady oil flow streams into the lubrication conjunction and adhered to the surfaces non-uniformly from time to time, leading to occasional occurrences of AACs. As shown in Figure 8-10 these medium AE bursts do not always appear in every stroke and repeat with successive engine cycles, rather present only in some of the strokes when the conjunction contains more particles. It can be seen in the figure that AAC induced locally non-stationary AE bursts to happen more significantly in the inlet, power and exhaust strokes of the third cycle, and only observable in the inlet and power strokes of the first cycle, whereas there are hardly seen in the second cycle. This confirms that the unsteady interactions between the solid particles and asperities.

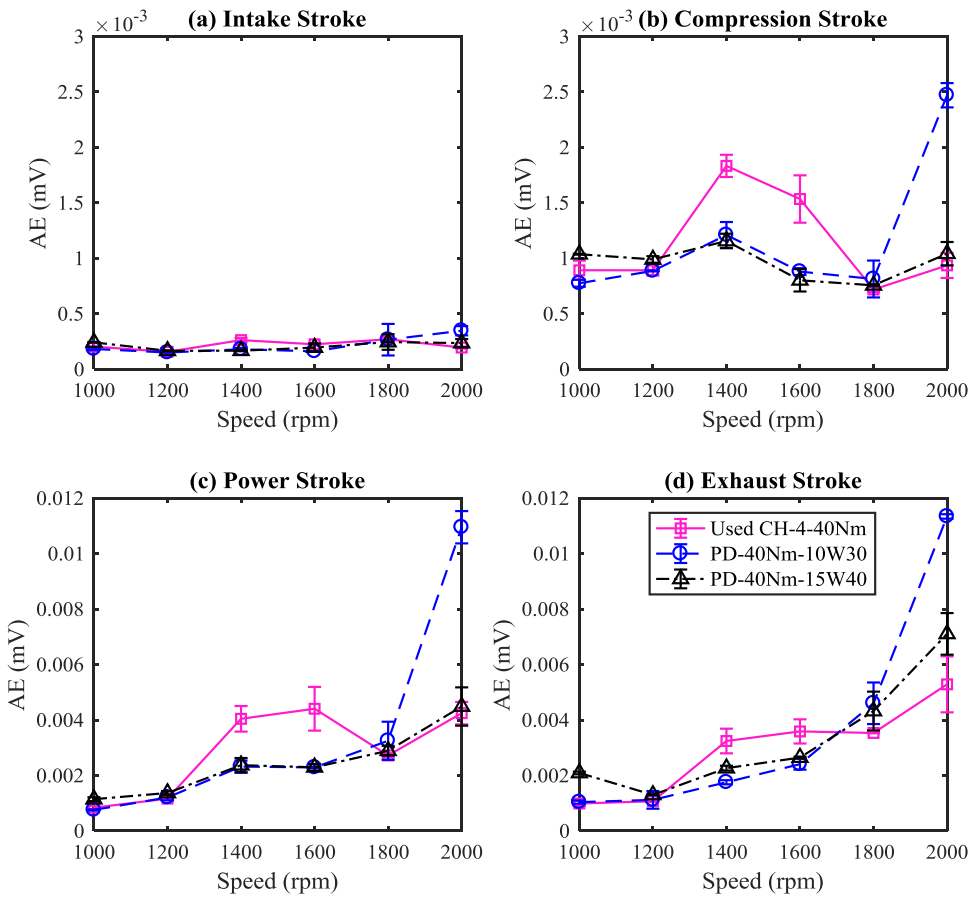

Figure 8-9 Diagnosis of different lubricating oils with ARWC under high load

Furthermore, as engine speeds are further higher (2000rpm) solid particles are less brought into the conjunction and adhered to surfaces due to mainly the reduced viscosity of the oil at high instantaneous temperatures and increased tribofilms due to increased sliding speed. As a result, the AAC effects are not significant anymore, thus ARWC showing low amplitudes at high engine speeds, as shown Figure 8-8 and Figure 8-9.

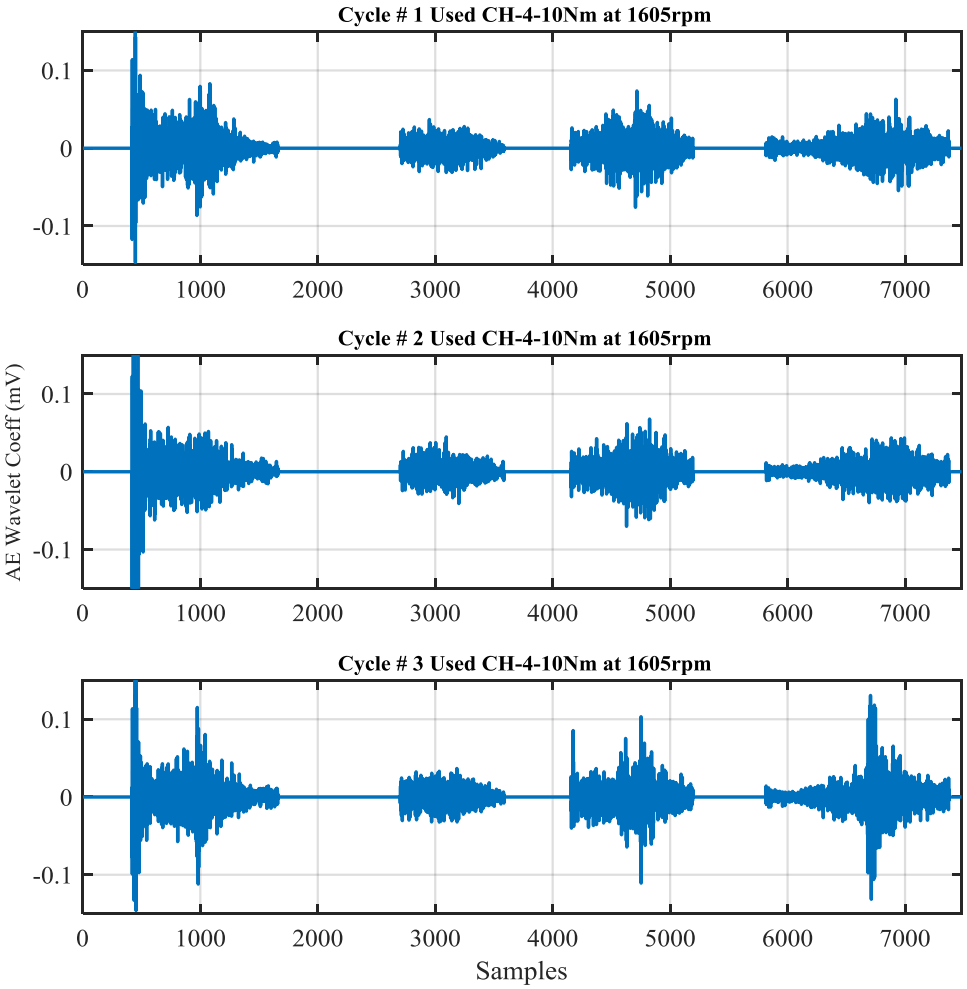

Figure 8-10 Unsteady occurrences of locally non-stationary AE bursts around the middle of strokes for the used oil

Overall, ARWC feature gives the more accurate indication of AAC effect, allowing abnormal tribological behaviours to be identified reliably. As AAC effects are closely relating to surface wear, it is more useful than FAI in the point of engine lubrication condition monitoring.

8.5 Impact of Different Alternative Fuels

With more powerful diagnostic features: improved LEA and ARWC established, the impact of different alternative fuels on tribological behaviour is evaluated further in this section.

8.5.1 Diagnosis with Improved LEA

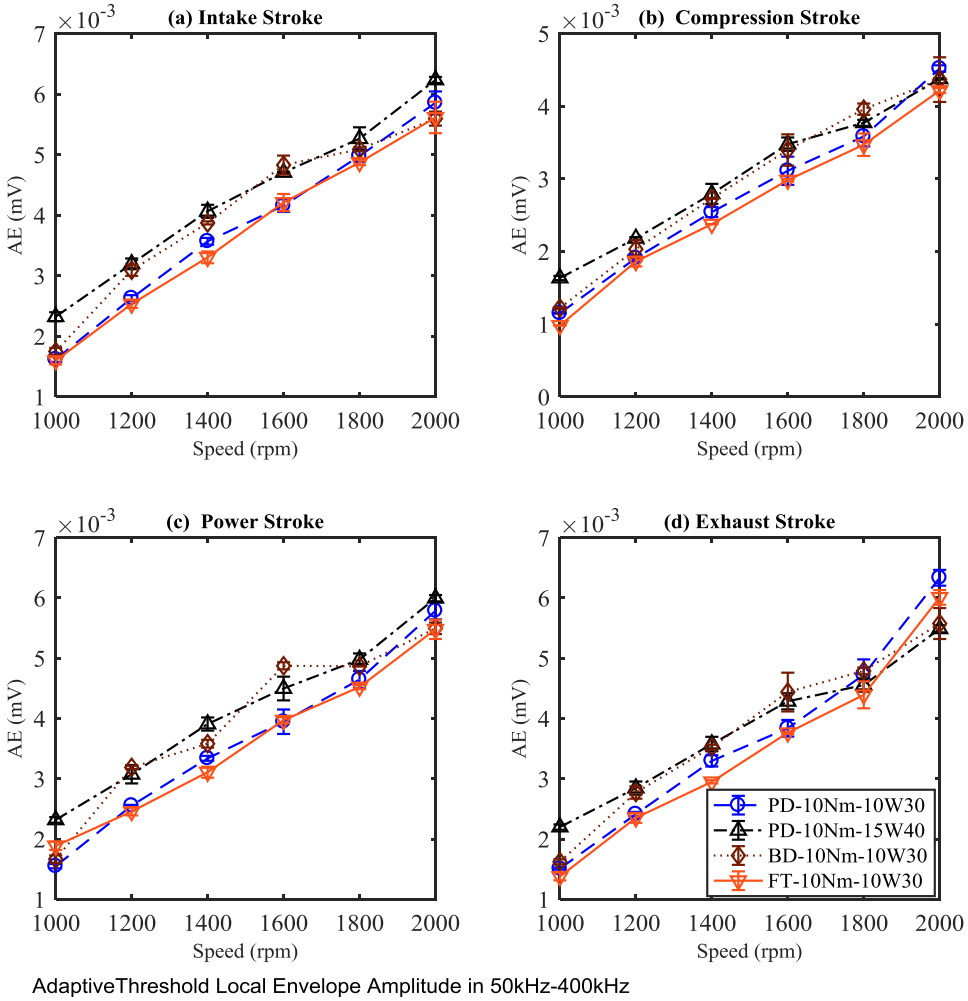

Figure 8-11 Impacts of different alternative fuels with LEA from adaptive threshold under low load

Figure 8-11 and Figure 8-12 show the comparison of LEA values between different fuels under the two engine loads respectively. This optimised LEA produces speed trends with very similar values for all fuels and oils. Therefore, it can be concluded that the two alternative fuels behaviours very similar to the two lubricants during all four strokes, it means that they produce little negative influences on tribological behaviour based on the standpoint of FAI effects for most of operating conditions.

However, during the exhaust stroke, FT diesel exhibits fast increasing LEA at 2000rpm probably indicates abnormal tribological behaviours resulted from additional AAC effects.

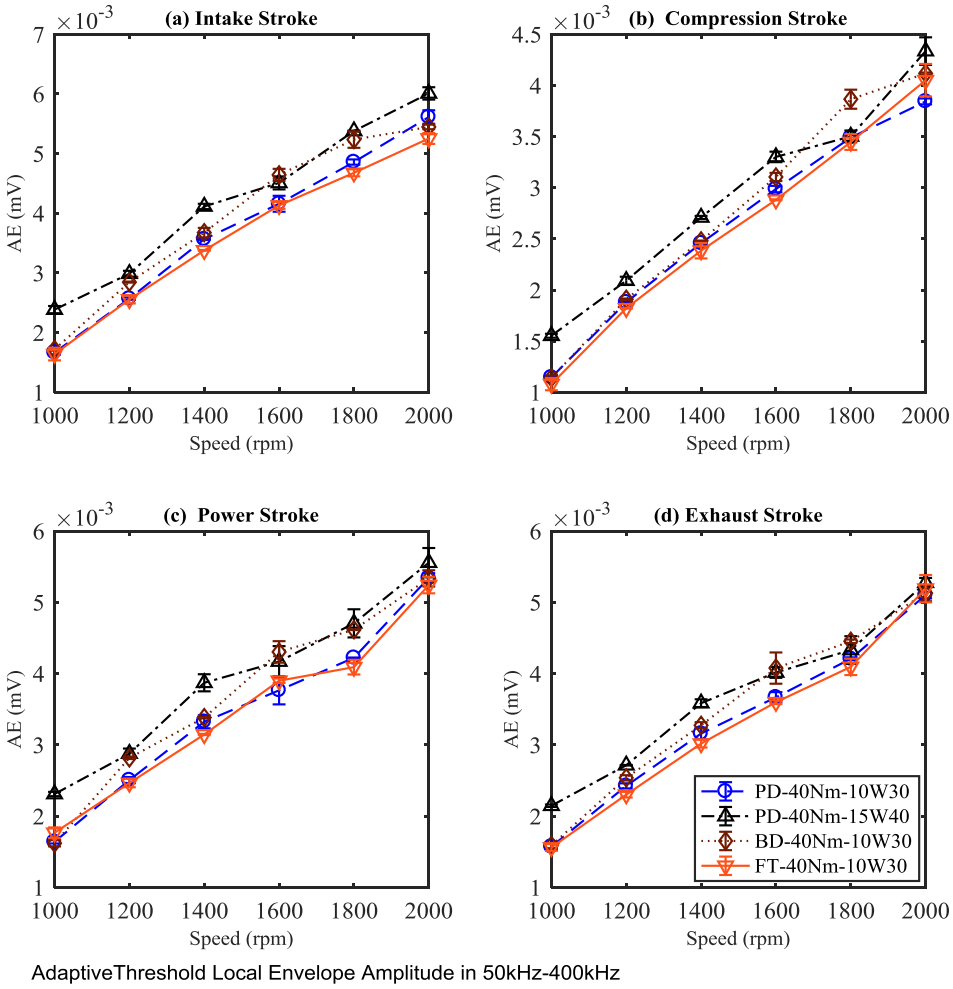

Figure 8-12 Impacts of different alternative fuels with LEA from adaptive threshold under high load

8.5.2 Diagnosis with ARWC

Interestingly, according to ARWC behaviours, shown in Figure 8-12 and Figure 8-13, two alternative fuels are considered to have certain influences on the tribological behaviours. Firstly ARWC trends are unsteady at speeds. This can indicate that the combustions of these alternative fuels are less perfect, which produces more particles that can be adhered to the lubrication surfaces and create more AAC effects. It has more significantly appeared in the exhaust stroke and high-speed operations when more particles can exist immediately after the power stroke in which the instantaneous temperatures are relatively higher [183].

Between the two alternative fuels, the biodiesel produces more impacts as it has higher ARWC values which happen at more speed settings due to high temperatures.

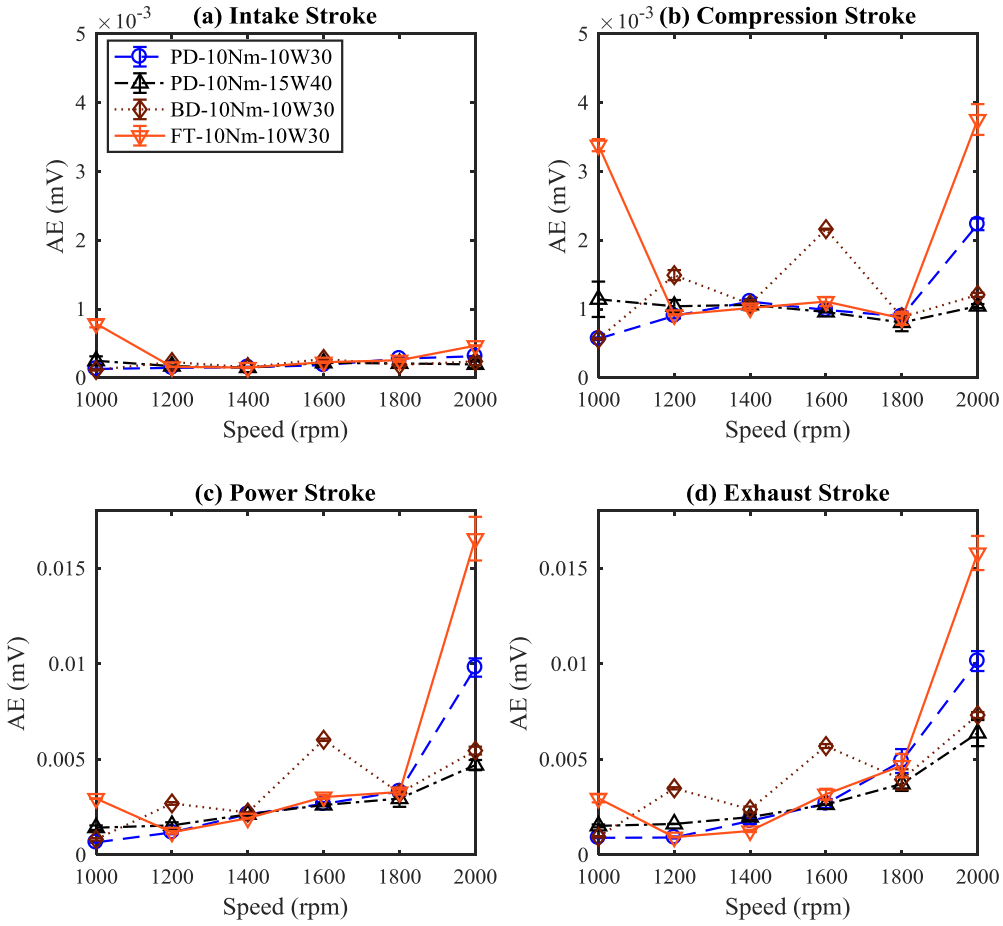

Figure 8-13 Impact of different alternative fuels with ARWC under low load

This diagnostic results demonstrate further the effectiveness of ARWC in detecting subtle abnormalities in tribological behaviours and therefore shows the feasibility of using AE for investigating potential impacts of alternative fuels in an prompt way, avoiding any clear damages to test engines, which often the consequences using the offline methods such as oil analysis and wear mark inspections.

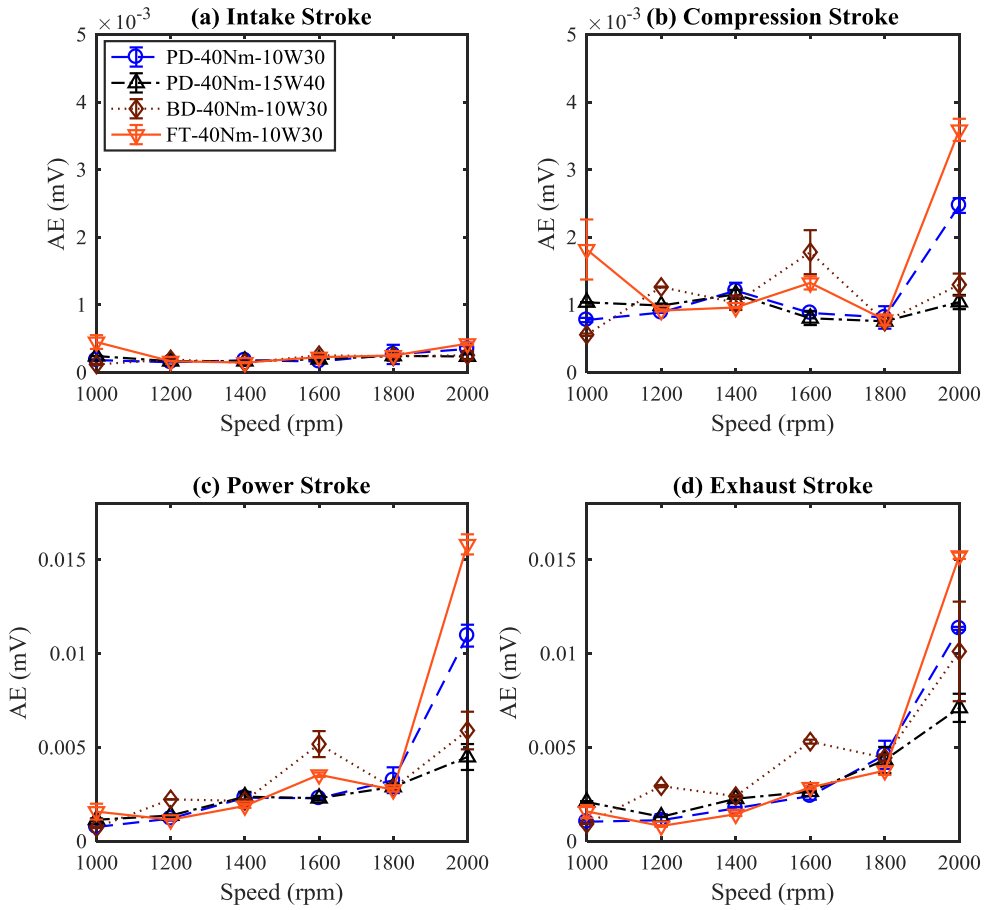

Figure 8-14 Impact of different alternative fuels with ARWC under high load

8.6 Key Findings of Chapter 8

To achieve more comprehensive diagnostics, this chapter has developed an adaptive threshold approach to select wavelet coefficients that are correlated more with FAI effect. The adaptation is achieved by constraining the selection with a modified velocity of the piston motion. Consequently, the adaptive selection produces three diagnostic parameters: improved LEA, GEA and ARWC to reflect FAI and AAC effects respectively and result in more accurate and consistent diagnosis.

Both the improved LEA and the newly established GEA are able to produce correct induction for FAI effects. However, LEA is regarded more reliable as it is from only a portion envelope with higher SNR.

In diagnosing different new lubricants the improved LEA show more stable and consistent results in all engine strokes and operating conditions. However, in diagnosing the used oil, it shows the more significant increase in for only speeds from 1400 rpm to 1800rpm under low loads.

The reason for not being able to separate it under other operating conditions is that the LEA is not very effective in reflecting the unsteady locally non-stationary AE bursts. Such bursts happen due to the AAC effects induced by large numbers solid particles of different sizes in the used oils. In addition, the non-uniformity of the suspended particles in oil this types of AAC happen randomly in some of engine cycles and strokes. Nevertheless, ARWC is particularly sensitive to such bursts and produces accurate and consistent diagnostics for differentiating not only the used oils but also the impacts of different alternative fuels.

CHAPTER 9 OPTIMISED WAVELET PACKET ANALYSIS AND THE DIAGNOSTICS OF TRIBOLOGICAL BEHAVIOUR

To suppression random noise more for improved diagnostics, this chapter details the development and evaluation of using wavelet packet analysis to diagnose tribological behaviour of the piston ring-cylinder liner lubrication conditions. Firstly, a novel scheme is developed to determine optimally the decomposition level and wavelet orders based on the minimisation the overlaps in both the time and frequency directions. Then, it calculates the mean coefficients in narrow frequency bands and a local angular duration which are determined from wavelet spectrum characteristics. Finally, the performance of diagnosing different types of lubricants and alternative fuels are evaluated under a wide range of engine operating conditions.

9.1 Introduction

As shown in [26], [27] and in Chapter 7 and 8, WMRA can result in several broad bands that contain more content of the weak AE relating to the tribological behaviours associated with both AAC and FAI. Based on AE amplitudes in these bands it achieves acceptable separation between different lubrication conditions which have large differences in lube properties such as viscosity difference in two new lubricating oils under majority operating conditions[24]. However, it produces less accurate diagnostic results for the small differences in lubricating oils and light operating conditions. One of the main reasons behind this is that the broad signals can include more noise influences arisen from measurement process i.e. the signal to noise ratio (SNR) is still not sufficiently high. In addition, other potential unidentified AE interferences that exhibit different characteristics from the tribological AE of the ring-line such as the asperity collisions between the cam and flower in valve trains can also contribute the measured AE and cause inconsistent diagnostics. Therefore, WPT is employed in this study to refine the frequency band and time durations with an attempt to minimise different noise influences and achieve better diagnostics.

The WPT spectrum can effectively present the wavelet coefficients of terminal nodes of the binary wavelet packet tree in the frequency or time ordered [192]. As a result, WPT spectrum shows more flexible and finer time-frequency resolutions which can be more effective and efficient for characterising AE signals with complicated contents along with large data volumes, compared with conventional DWT which provides too coarse frequency resolution. The CWT, which is implemented with high computational complexity and classic Fourier basis based representations, such as STFT, which is much less efficient to represent the AE signals with strong non-stationarity.

Moreover, WPT allows characterising AE responses in a finer frequency band in which the influence of random noise can be reduced, and thus potentially give new features to isolate the medium and large bursts better. Consequently, an improved diagnostics can be achieved.

Based on WMRA for tribological diagnostics, the weak and locally stationary AE activities in the middle of strokes have been revealed effectively, these AE contents provide with wide band features and show larger amplitudes during the higher part of

the low frequency than others. Previous studies [193] and [194] show that WMRA technique has the shortage that it cannot provide a high-frequency resolution in low-requency bands. Although the wavelet multi-resolution analysis (WMRA) has been produced some promising results to identify the small frictional AE signals. Nevertheless, the frequency characteristics of the weak tribological AE events are ambiguous, mainly because the WMRA analysis does not highlight the interesting contents sufficiently as it has insufficiently high-frequency resolution over the entire frequency band.

Wavelet packet transform (WPT) can divide the frequency space into finer components acquire better time–frequency localisation of signals than WT[39]. In other words, the WPT can decompose the signal both on the high frequency and low-frequency band simultaneously with constant frequency intervals. This method has been used widely for condition monitoring and fault diagnosing in rotary mechanical systems such as engines [43, 44], gears[39, 195]and bearings[41, 42] recently. Particularly, reference [196] applied WPT analysis to diagnose the AE reposes of tribological systems based on multiresolution analysis theory. Therefore, the wavelet packets analysis which allows the high-frequency resolution is examined in the following investigation for the tribological AE signal feature extraction in the optimal bandwidth, which simultaneously highlights the frictional AE activities and minimises the interferences.

Like WMRA, an optimisation of key analysis parameters should be carried out based on the signal characteristics in order to rigorously utilise the merit of WPT. Specifically, the adequate wavelet basis and decomposition level need to be examined along with taking into account the efficiency of computational realisation.

9.2 WPT Optimisation by Minimising the Time-Frequency Overlaps

9.2.1 WP Spectrum and Optimal Decomposition Level

Based on previous studies in [43, 44, 195, 196], the Daubechies and Symlets wavelets family often used for processing nonstationary vibration and AE signals. This wavelet selection rule is based on a widely accepted principle that its asymmetric and gradual attenuation profile can highlight effectively the weak nonstationary AE contents with the similar asymmetric characteristics which are illustrated in the magnified graph in

Figure 6-7 (in Section 6.3 Chapter 6). Especially, the Daubechies wavelets have been demonstrated to be effective in processing vibration and AE signals for data compression, denoising, classification, and feature fusions [186]. In addition, these previous studies also recommended using higher orders of the wavelet to obtain better filter characteristics for implementing WPT. Therefore, the Daubechies wavelets with an order of 35 were selected to calculate WPT and then its corresponding spectrum.

It is worth highlighting that Symlets have very similar properties with Daubechies but with increased symmetry. However, the high orders of Symlets wavelet need the significantly high cost of computation which is not efficient to process the AE signals with the large volume of data samples for the optimisation and online implementation. Therefore, only Daubechies wavelets are examined in this study.

With the recommended high orders of Daubechies, it is easy to use a trial and error approach to find an adequate decomposition level for processing current AE signals. Figure 9-1 presents a representative WPT spectrum for the baseline lubricating oils of 15W40 when the engine operates at different speeds under the load of 40Nm. They are obtained using a Daubechies wavelet with order 35 (denoted as db35) and at decomposition level 8.

It can be seen that Figure 9-1 allows more details of AE characteristics to be observed. Firstly, it shows the five distinguished peaks to be observed in several discrete frequency bands around 40kHz, 80kHz, 145kHz, 180kHz and 250kHz. These bands are examined to correspond more to the peaks of the sensor's dynamic responses which are shown as the frequency characteristic curve of the AE sensor (SR800) in Figure 5-6. As these peak responses present in the middle of the power and exhaust strokes, they are also more pronounced and exhibit significant increases with engine speeds, which agrees with the tribological behaviours predicted by the FAI and AAC models. Therefore, they are regarded as the main AE contents for indicating lubrication conditions and will be elaborated in exceeding contents.

In addition, Figure 9-1 also shows clearly that the combustion and valve opening and closing impacts induced AE spread continuously over much wider frequency bands with high amplitudes, which fully reflect the feature of short duration impact process as predicted by AAC model. In particular, the combustion shows much stronger AE

responses and spreads wider bands which are used to separate it from the others in implementing combustion diagnosis.

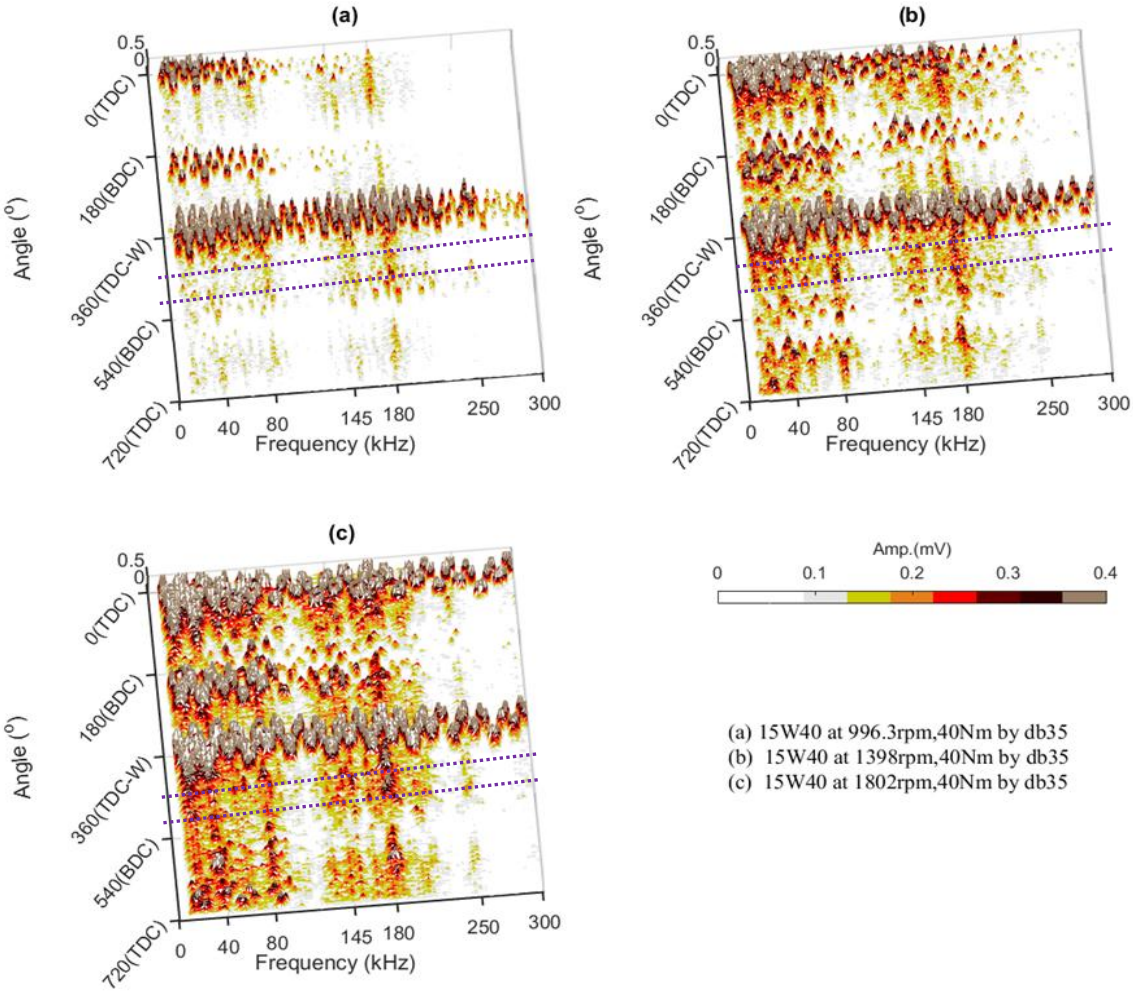

Figure 9-1. WPT spectrum comparison with db35 wavelet for 15W40 oil

However, in the low-frequency range, less than 30 kHz, there are also many discrete AE spikes. They may be attributed more from other excitations such as the cam-follower, the valve-rocker and main bearing as these excitations are relatively far from the AE sensor and their AE shows less significant in the middle of the strokes. They are less correlated with the tribological AE between the ring and the liner. Obviously, the inclusion of such components for quantitative indication of the tribological conditions is not very reliable. This may be one of the reasons that DWT analysis in a broadband could not produce a consistent result in differentiating the lubricating conditions over the entire engine operations [16, 17].

The WPT can provide the detail coefficients of the given signals by more subband filters at higher decomposition level. At level j, the frequency axis can be divided into 2^j subbands. Hence, too high decomposition level of WPT needs more computation time. Based on the comprehensive observations achieved from WPT spectra, it can be drawn that the decomposition at level 8 is sufficient to reveal the frequency characteristics of the FAI AE which is stated in Chapter 4. The WPT spectrums at 8 level around the middle of each stroke were started from a lower frequency and spread in a narrower band. Nevertheless, a further increase of the level results in spectral peaks with too many details or spikes localised in the time-frequency plane and makes it difficult to find the definitive characteristics for proceeding a trend analysis. In addition, the computational cost is too high for implementing an optimisation to refine the wavelet basis.

9.2.2 Optimal Wavelet Basis

In Daubechies wavelet family there are many smaller wavelets available for different types of signal analysis. These wavelets are ordered according to an incremental integer number. Theoretically, the higher order number or vanishing moment, the more accurate it will approximate a signal. However, the higher order needs a greater amount of computation, which is an important factor influencing the performance of the online implementation.

From the point of view of time-frequency analysis, the transition band and side lobe suppression become better as wavelet orders increase [197]. It will reduce the effect of frequency-overlapping and result in a better estimate to reflect more accurately the spectral amplitude in the interested frequency bands. However, as the order exceeds certain values, which is largely dependent on the content of the signal, the time resolution can be reduced due to the longer filter used. This can be also understood to be the effect of time overlapping which can lead to an over-estimate on the spectrum amplitudes in the time interval interested.

According to these critical understandings upon WPT spectrum analysis, a novel scheme can be formulated to determine an optimal order in Daubechies wavelet family in conjunction with both the AE signal characteristics predicted by models and the WPT spectrum characteristics. Principally, it examines the variation of the spectral amplitude

with wavelet orders in a time-frequency plane interested. For doing so, an average amplitude criterion is established in the time-frequency plane of a WPT spectrum as:

$$\bar{W} = \frac{1}{K}\sum_{k=1}^{K}\frac{1}{NM}\sum_{n=1}^{N}\sum_{m}^{M}|W_k(n,m)| \tag{9-1}$$

where n is the time or angle index. In this study, it runs for 50 °of crank angles around the middle of the power stroke where FAI induced tribological AE responses are more significant, as illustrated by the angular interval between the two dotted lines in Figure 9-1, which is the same interval for obtaining LEA in Chapter 7 and 8. m is the frequency index which covers a frequency range from 30kHz to 200kHz within which the spectral amplitudes at the four frequencies are more significant, and k is the index for engine cycles which runs to 20 for more reliable results. This average amplitude will exhibit a decrease with the increase of wavelet orders because the effect of time overlapping is gradually reduced with improved transition bands and side lobes. It also means that the frequency resolution becomes better. Consequently, it gives a more accurate and stable estimate of the deterministic frequency components shown in Figure 9-1. However, as the order is further increased, the average amplitude will increase again because more overlapping presents in the frequency direction due to the use of longer filter and decreased time resolution.

The effects of these two types of overlaps can be seen by comparing WPT spectra in Figure 9-1 with that of Figure 9-2. Clearly, there appears more frequency smearing in the WPT spectra of Figure 9-2 obtained by using db6 wavelet, whereas the db35 in Figure 9-1 exhibits more time smearing. In addition, both types of overlaps can give a even more incorrect estimation of AE strength as the random and small noise components can be added on and taken into account in calculating diagnostic features.

To obtain an accurate characterisation of AE amplitudes, the optimal order is selected by finding an optimal order for AE responses for all speeds tested. Figure 9-3 shows the optimal wavelet basis selection from the baseline case using diesel 15W40 oil under 40Nm. Figure 9-3 (a) shows the variation of the average amplitudes with wavelet orders, in which the highest order is up to 45 that is available in Matlab software package, and the amplitude trend is normalised by the corresponding maximum amplitude at each speed for a more effective comparison between speeds. Moreover, the average

amplitude for the AE responses in the power stroke is only in which the lubrication condition is severe due to high pressure and temperature. It can be seen that there is minimal amplitude for each speed, which stands for an optimal amplitude estimate because the effects of overlapping in time and frequency directions are minimised, and therefore allows the optimal order to be identified. Moreover, the turning point at which the amplitude starts to increase again or exhibit very slight decrease can be observed at the orders above 35 for all speeds. In addition, as shown in Figure 9-3 (b), CPU usages increase linearly with wavelet orders for all speeds. Especially the CPU, the time is about 20% higher for the low speed cases due to the finer frequency bands achieved by resampling the original time data into the angular domain with equal angle intervals. Nevertheless, by compromising the high accuracy of amplitude estimate and the demand for efficient computation, an optimal order 35, is determined for calculating WPT spectra for all test cases as it enables to achieve sufficient accuracy along with fewer demands for computing resources.

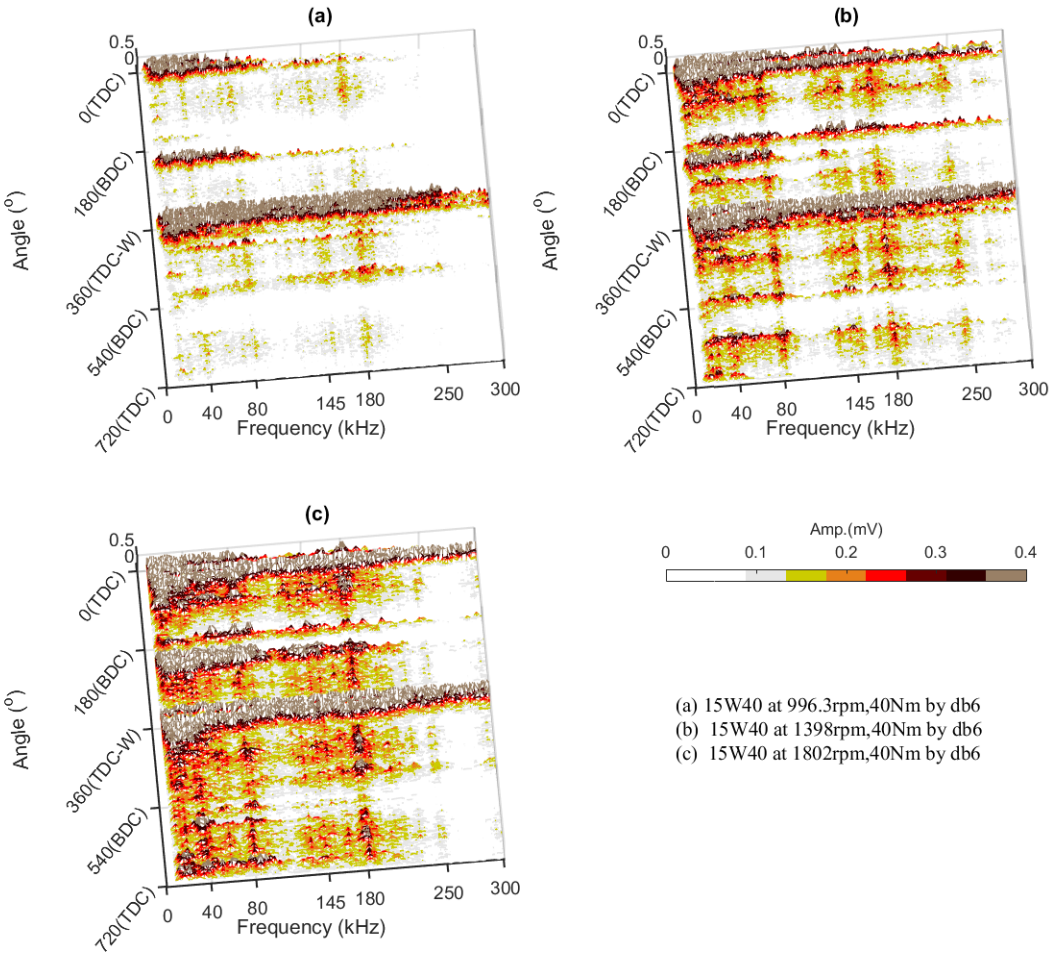

Figure 9-2 WPT Spectra with db6 wavelet for 15W40 oil

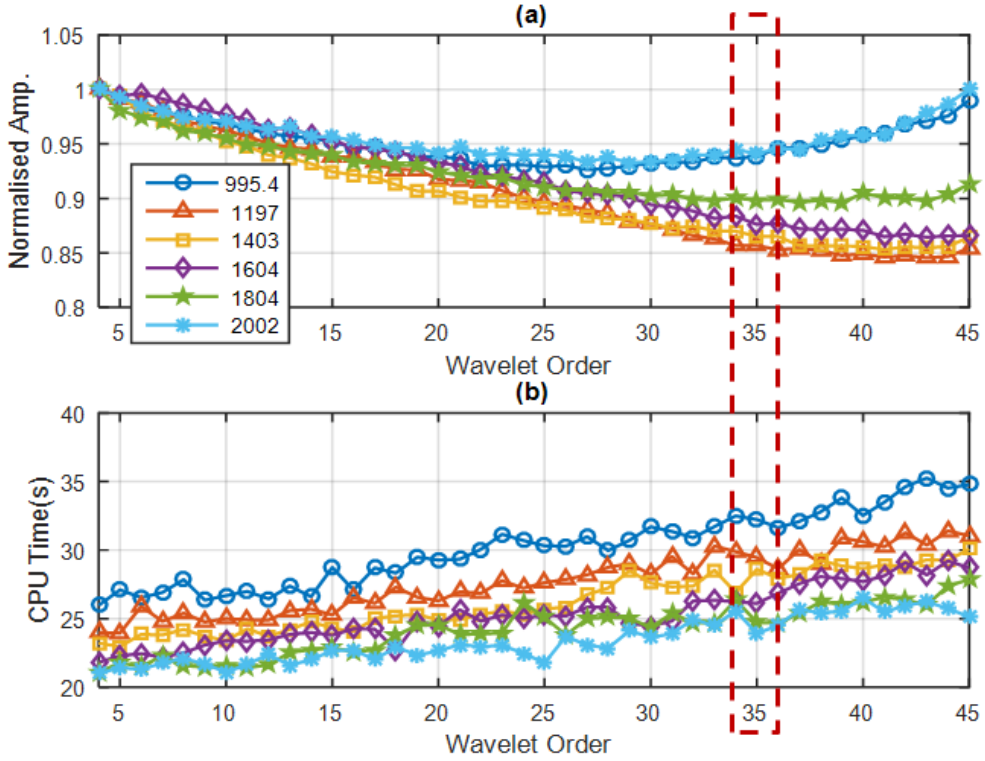

Figure 9-3. Optimal wavelet basis selection: (a) Spectral amplitude variation, and (b) CPU usages

9.3 Diagnosis of Different Lubricants

To verify the optimised wavelet for diagnosing lubrication conditions, WPT spectra are calculated for all different tested oil cases and operating conditions using the db35 wavelet. The average wavelet coefficient amplitudes, denoted as WPT-LEA for brevity, are then calculated as the diagnostic features for representing tribological behaviours and lubrication conditions in four characteristic bands: 30kHz-50kHz, 70kHz-80kHz, 140kHz-160kHz and 174kHz-186kHz. These bands are identified based on the time-frequency characteristics in Figure 9-1 and Figure 9-2 because their amplitudes exhibit the speed related friction profiles more significantly. Specifically, because the AE amplitudes are more significant in these four narrower frequency bands, they allows the tribological behaviours to be quantified with better accuracy as the noise to signal ratio (SNR) is higher, in comparison with the band around 250kHz and the broad bands of DWT transforms employed in Chapter 7 and 8.

In addition, considering that locally stationary AE amplitudes in the power stroke are the more evident, WPT-LEA indicator extracted from this stoke is focused on the

diagnosing analysis. This indicator is calculated within the angular periods in which the tribological AE contents are understood to be more significant and less interfered with major AE events of valve impacts and other potential AE including cam-follower frictions etc. In the meantime, WPT-LEA indicators for other three strokes are also calculated. Not only do they be examined for the suitability for diagnostics but also they can be used as references for an evaluation of the optimised indicator obtained in the power stroke.

9.3.1 Differences between New Lubricating Oils

Figure 9-4 and Figure 9-5 show the differences of WPT-LEA indicators between two tested new oils: 15W40 and 10W30 in two frequency bands: 70kHz-90kHz and 140kHz-160kHz respectively in which the indicator show better performance in differentiating different oils. In addition, they show slightly better and smoother trends, compared to that of Figure 7-12 (c) and Figure 7-13 (c)

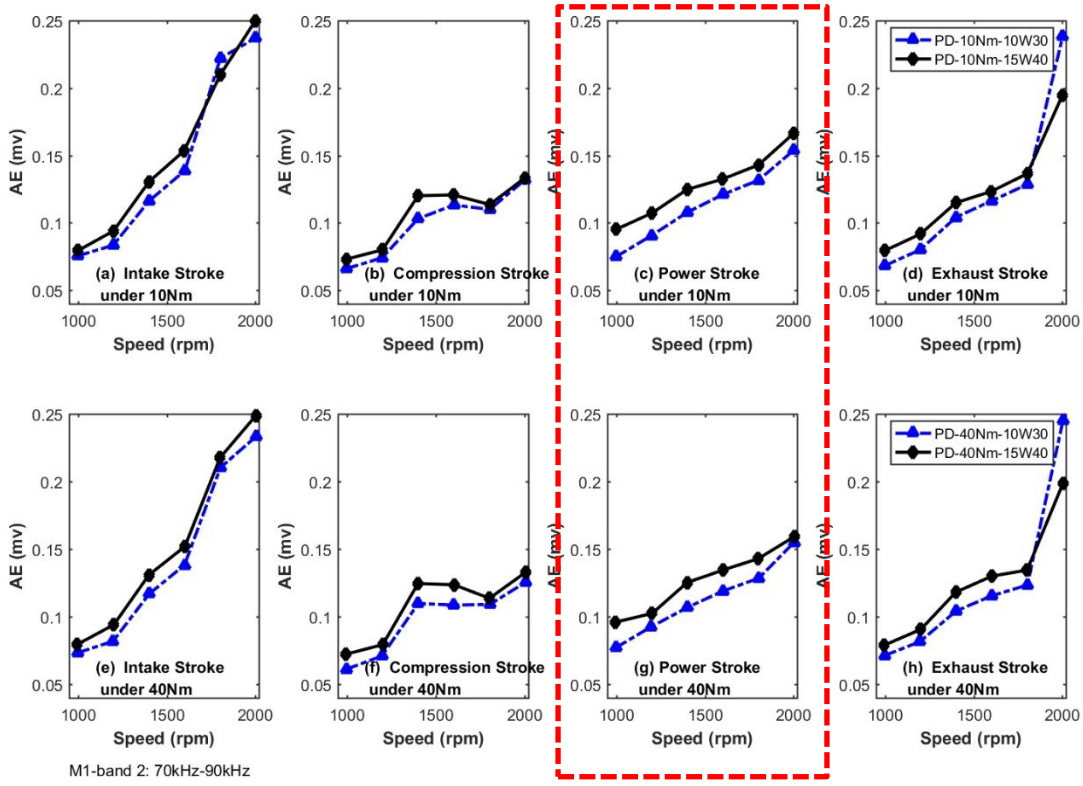

Figure 9-4. AE indicators from 70kHz to 90 kHz under different operating conditions

It can be seen in these two bands that AE responses increase with engine speeds monotonically, showing the agreeable connection with model predictions and engine viscous friction characteristics. Particularly, the AE indicator in the power stroke shows

the better linear connection. These results show a higher degree of agreement with the prediction from the FAI model in conjunction between ring and liner.

Moreover, AE responses in the power stroke for 15W40 oil with higher viscosity exhibit greater amplitudes than 10W30 with lower viscosity. This indicates further that AE responses behave very close to the model prediction, demonstrating that the externally measured AE signals are sufficiently sensitive to small changes in the properties of lubricants. In particular, both bands give consistent results. Therefore, they can be based to detect and diagnose the deterioration of lubricating oils.

However, AE responses in other strokes present more fluctuating increases with speed and give smaller differences between two oils. The main reason for lack of diagnostic capabilities in these strokes is that the wavelet used is not very optimal for these strokes. WPT-LEA can be more erroneous because different degrees of overlap effects can happen under different operating conditions.

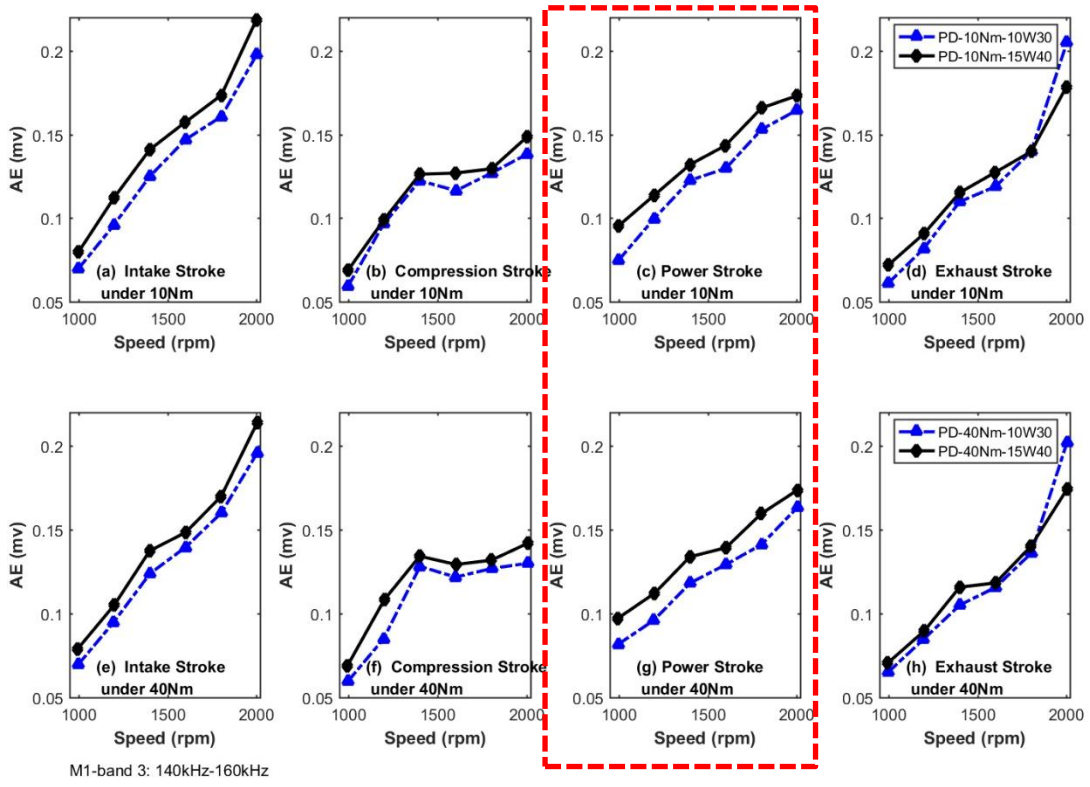

Figure 9-5. AE indicators from 140kHz to 160 kHz for four strokes under different load

Another possible influence is that AE responses in these strokes can be more influenced by the tribological dynamics of other lubrication conjunctions which include the valve landing impacts, and AACs from the conjunctions of the cam-follower and the

valve-rocker. Nevertheless, these results show potential for using AE to diagnose the condition of valve trains, which can be a challenge research subject for future in expanding AE diagnostic capabilities.

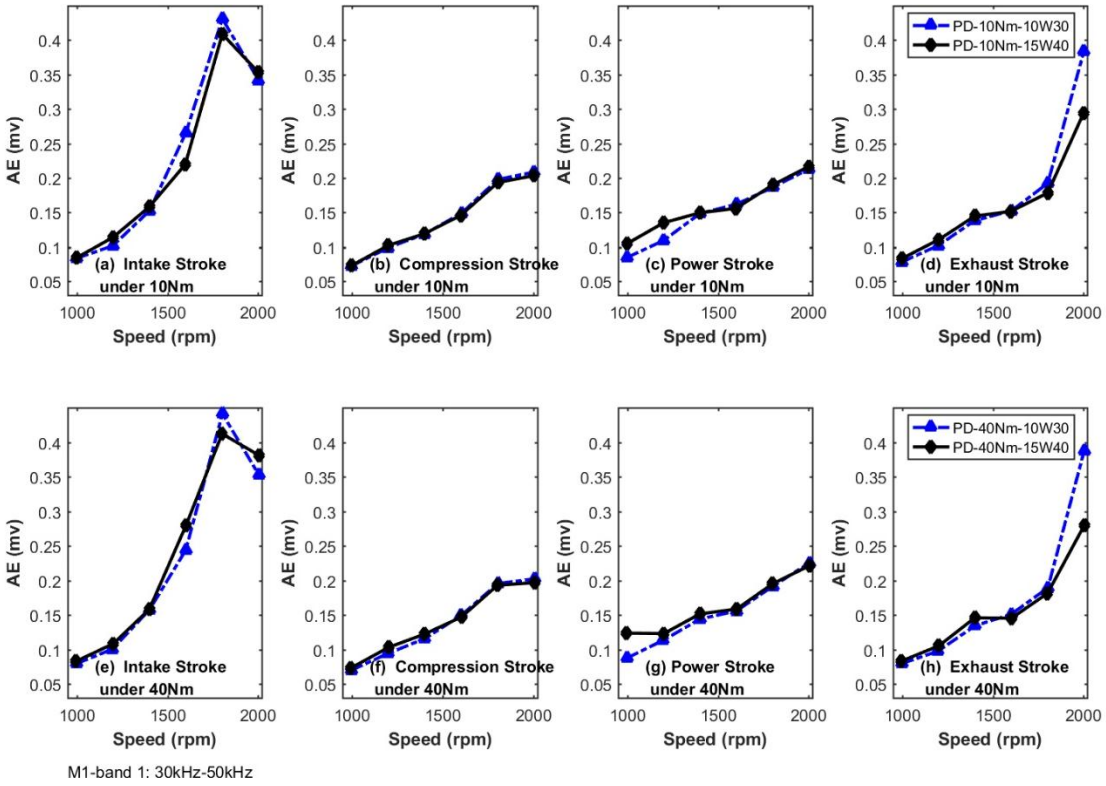

Figure 9-6. AE indicators from 30kHz to 50 kHz for four strokes under different load

Figure 9-6 and Figure 9-7 present AE amplitude comparisons between the two tested new oils in the other two frequency bands: 30kHz-50kHz and 174kHz-186kHz respectively.

It can be seen that there is a marginal increase in the higher viscosity oil in the power stroke although they all exhibit increasingly with all engine operating conditions, showing less sensitivity to oil changes. This observation, especially the less sensitivity to variation of oil viscosities, cannot be sufficiently explained by current AE models which are developed based on ideal flows and linear deflections of asperities with very simple shapes. However, it may be understood that the change in viscosity is not sufficiently large to alter the dynamics of such sized asperities that contribute more to AE responses in these two bands.

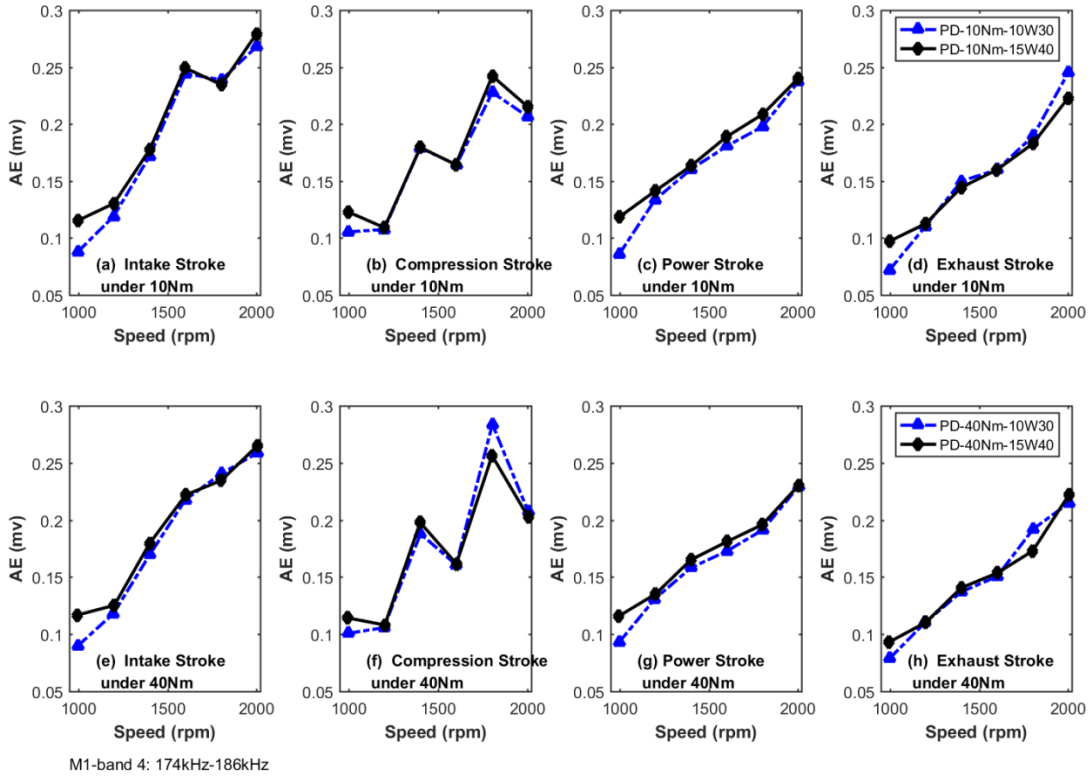

Figure 9-7 AE indicators from 174kHz to 186 kHz for four strokes under different load

In general, the AE responses extracted in the power stroke by the optimized WPT allow the small changes in oil viscosity to be consistently and reliably differentiated in two narrow frequency bands. This achievement can be satisfactory for monitoring the tribological behaviours of the ring-liner conjunction and hence oil conditions for entire engine lubrication. For more extended diagnostics, AE signals should be further analysed with more effective methods which reflect the dynamics corresponding to the intake valve, exhaust valve, fuel injection and combustion processes respectively. For more insights of the tribological behaviours, especially oils with different additives, the nonlinearity of asperity deflections and flows with turbulences and cavitation have to be included in the AE models.

9.3.2 Diagnostics of Used Oils

To further verify the diagnostic performance of AE responses extracted by optimised WPT spectrum, a comparison of WPT-LEA in the power strokes is made between all different tested lubricating oils. Figure 9-8 presents the comparison results for all interested frequency bands. Inherently, the AE responses for used oils show a higher values in the frequency bands of 30kHz-50kHz and 140kHz-160kHz whereas, in the

other two bands 70kHz-90kHz and 174kHz-186kHz, the AE responses of used oils show lower amplitudes than 15W40, additionally, the AE amplitudes in these two bands even slightly lower under the high load than under low load. That is the inconsistency to the prediction that the FAI induced AE amplitudes increase with viscosity values. Because the used CH-4 oil has the highest viscosity than the other new oils confirmed by the offline measurements as shown in Table 3-2 (section 3.4.1 chapter 3).

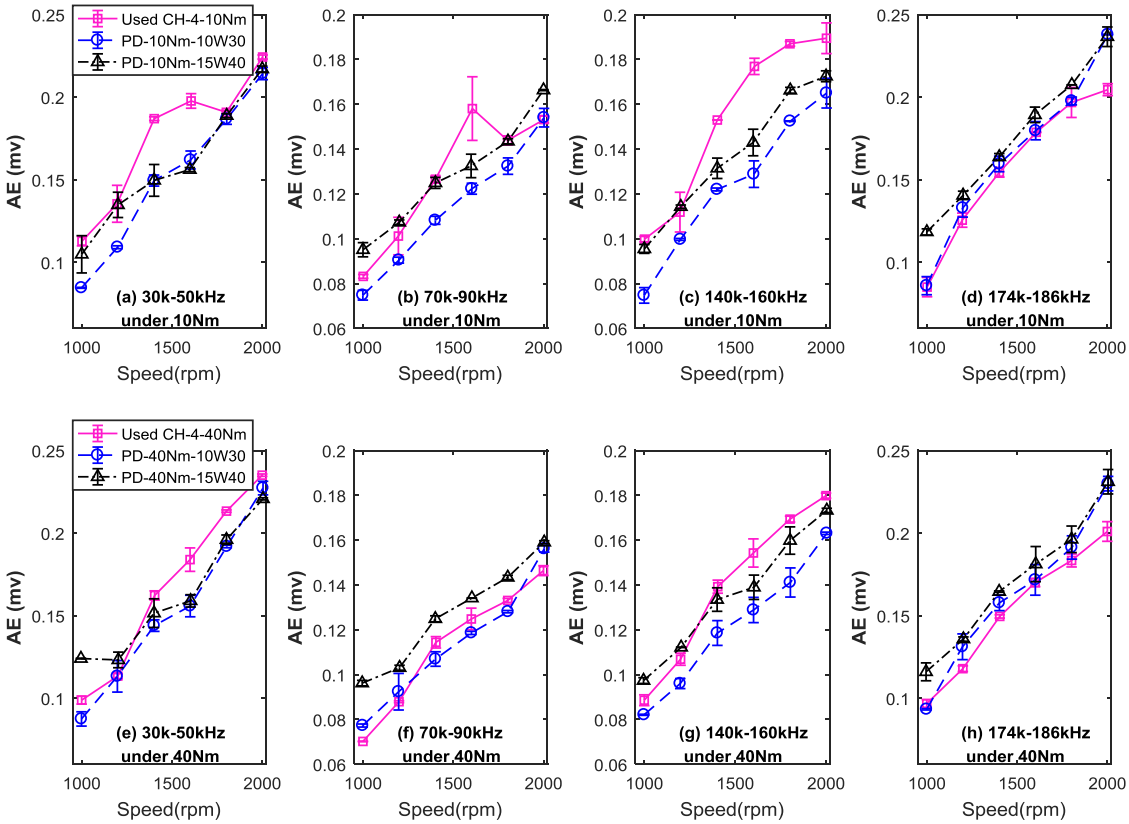

Figure 9-8 AE indicators of the power stroke for different oils and operating conditions

To find the reason for the low amplitude around these frequency bands, Figure 9-9 and Figure 9-10 show a direct comparison of the AE WPT spectra between the used CH-4 oils and 15W40 in power stroke at different speeds under high load. The angular interval selected for AE indicators calculation is illustrated between the two dotted lines in these two figures.

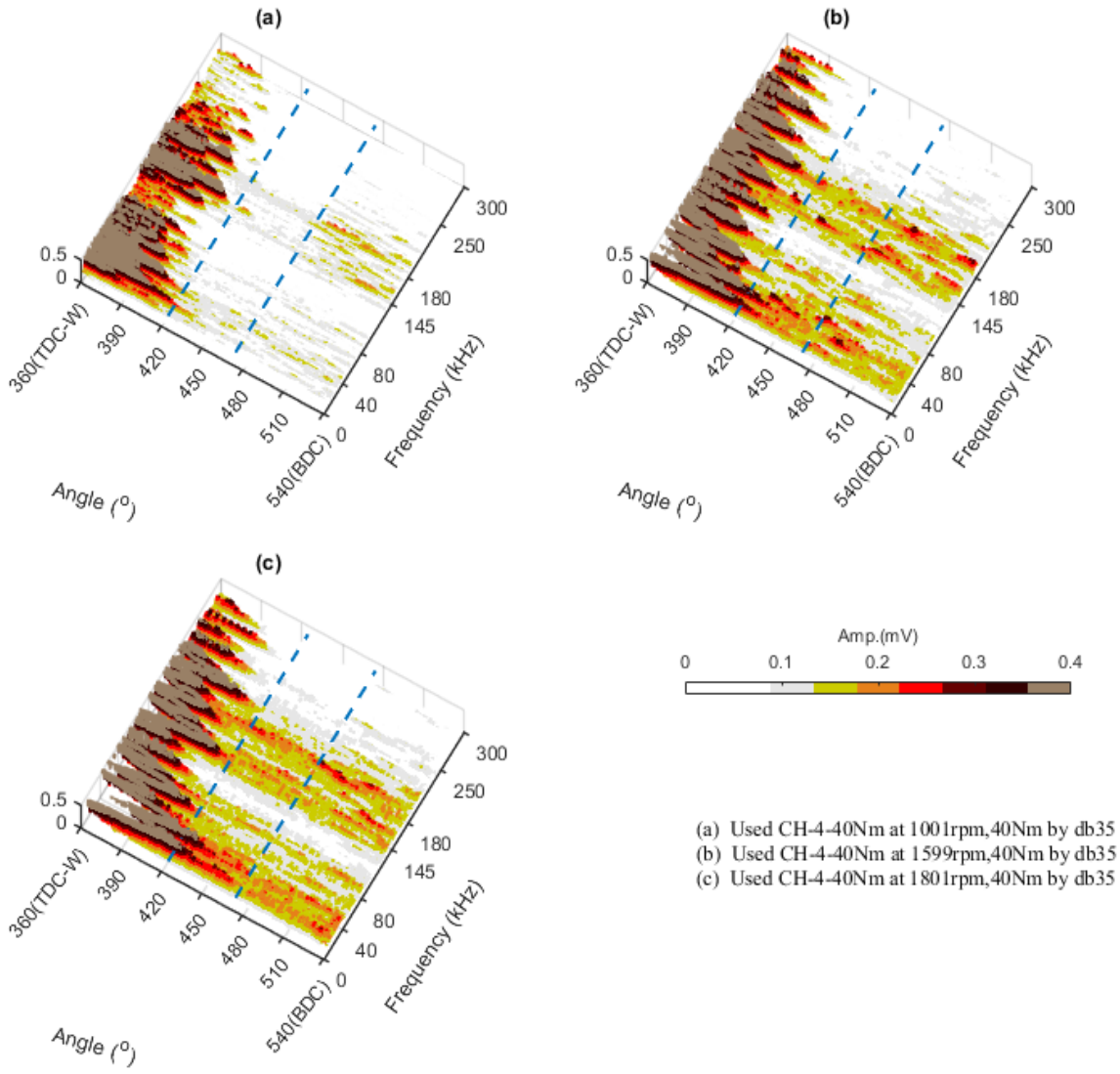

Figure 9-9. The AE WPT spectra in power stroke for the used CH-4 oils at different speeds under high load

The WPT spectra for new 15W40 oil show some distinguished semi-continuous peaks clearly emerged around the 40kHz, 80 kHz, 145 kHz, 180kHz respectively. However, the weak peaks of the used CH-4 oil can be observed with less continuity in the angular domain, particularly, in the frequency domain, these localised district weak peaks occurred more occasionally and showed lower concentration in effects in the target frequency band compared to new oils.

This is probably because the adhesive strength at higher temperature due to higher engine loads decreases more significantly and thus the FAI effect is not consistent with the offline viscosity as discussed in Chapter 7. Whereas the AE responses of used oil

are higher than the other two oils in the band 140kHz-160kHz, it is probably due to the AAC induced AE is increasing with the engine speed along with FAI effects.

These diversities of changes obviously need to be investigated theoretically with the inclusion of more dynamic details of the tribofilm and asperities interactions under high temperature and high load. Nevertheless, they provide additional information for differentiating it from the new oils and between the used ones more reliably.

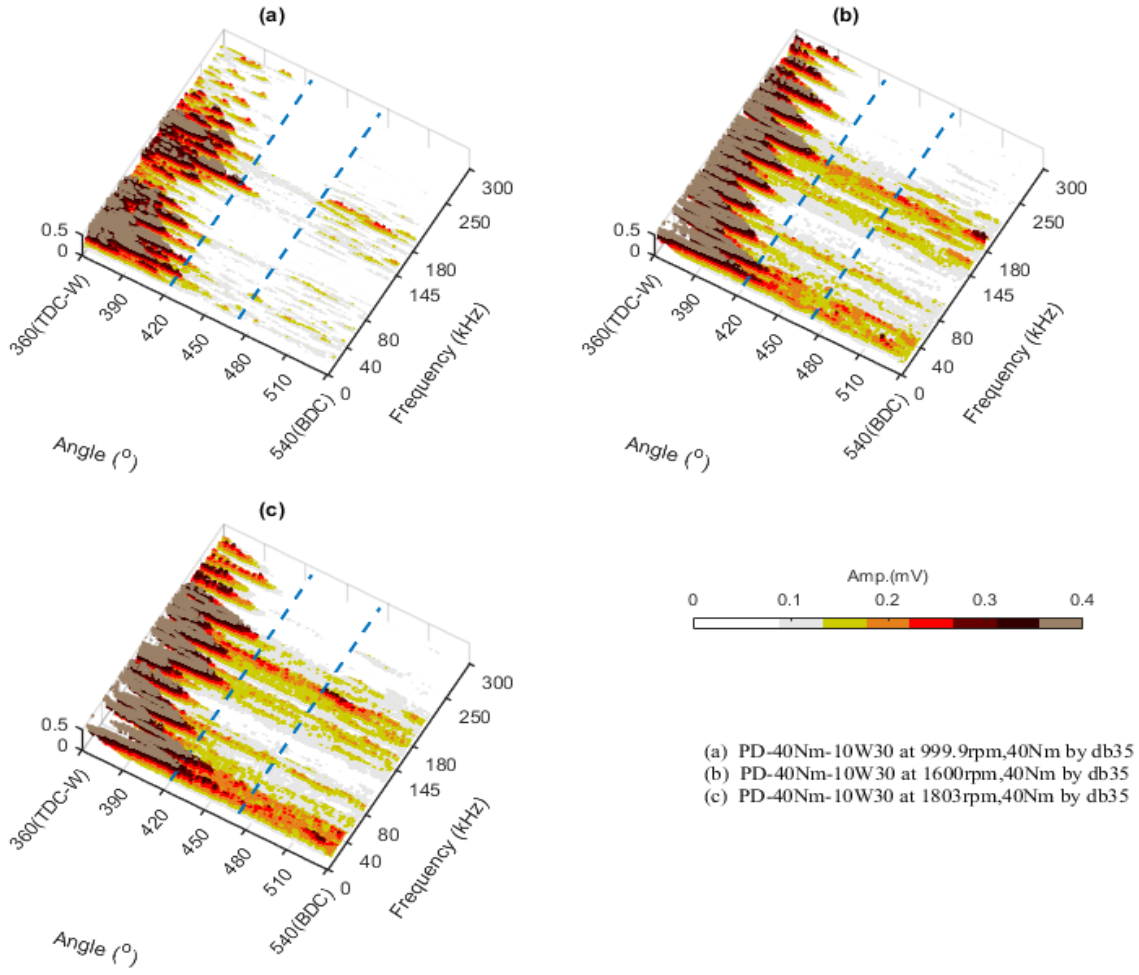

Figure 9-10. The AE WPT spectra in power stroke for the 15W40 oils at different speeds under high load

9.4 Impacts of Different Alternative Fuels on Tribological Behaviours

Although the bio-diesel and F-T fuel are proved as the most potential substitute fuels with progressive effects on the emissions, they still encounter the new challenges in the engine tribology. To promptly and accurately evaluate the influences of these two

alternative fuels, WPT-LEA were calculated for two alternative fuels and then compared to the baseline diesel under same lubricating oils.

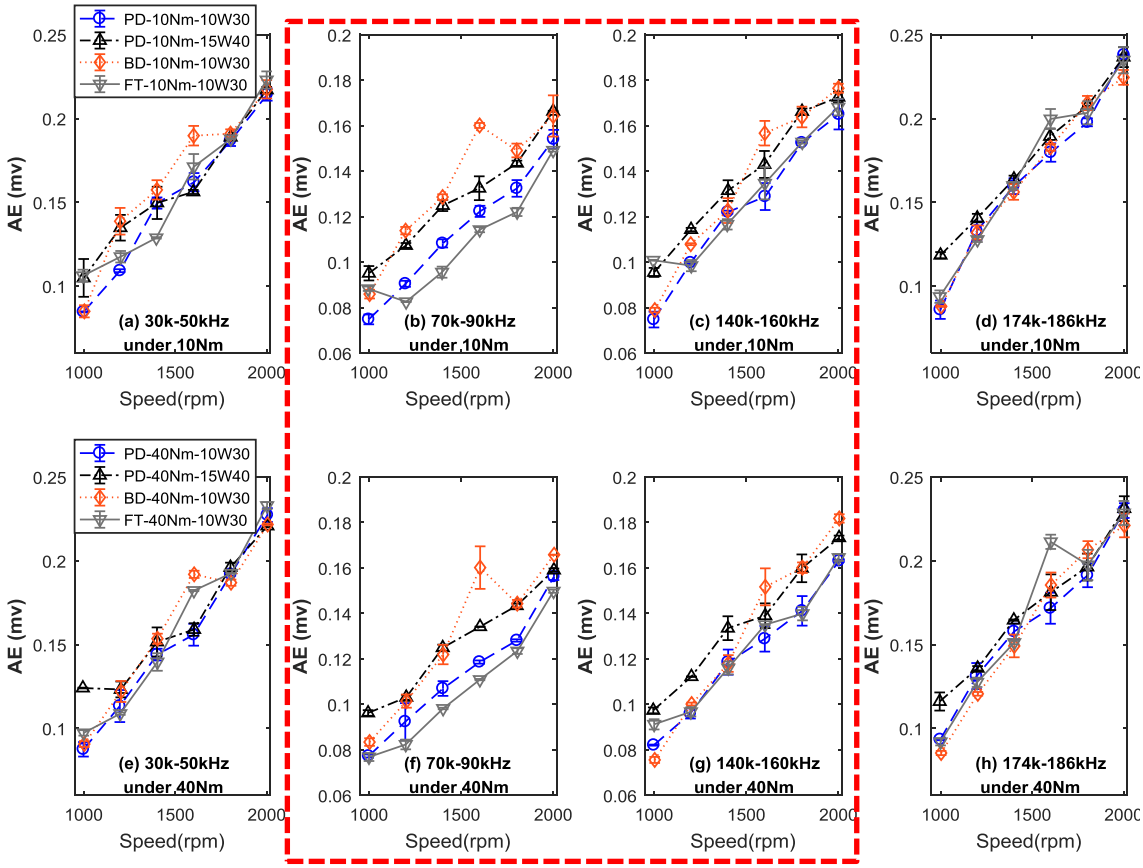

Figure 9-11. WPT-LEA indicators in power stroke for different fuels, and compared to pure diesel with 15W40 and 10W30

Figure 9-11 shows WPT-LEA of AE signals when the engine operates with two alternative fuels. For benchmarking, it also presents WPT-LEA values for operating with diesel fuels but lubricated with 15W40 and 10W30 lubricants. It can be seen that AE magnitudes of biodiesel are basically close to that of diesel fuel using lubricated with higher viscosity oils. This leads to a diagnosis that burning biodiesel causes the ring-liner system are suffered slightly higher viscous friction in the middle of stroke than diesel, whereas the ring-liner system fuelling with the F-T fuel presents the same friction properties or even a tiny lower viscus friction characteristic during the middle of strokes.

The possible reason for differences is due to the differences in the lower heating value of three fuels as listed in Table 5-8 (Section 5.3.2 Chapter 5). The higher lower heating value means higher combustion temperature. It is believed that the higher temperature

leads to lower viscosity of film. Therefore, the biodiesel with the most minimal lower heating value of the three shows a little higher viscous AE responses in the middle of the stroke. Because the lower heating value of the F-T fuel is marginally lower than the diesel's, hence, the AE indicators for these two fuels show basically similar amplitudes.

However, AAC effects revealed by ARWC indicators in Chapter 8 are less observable by WPT-LEA. This shows that the local locally non-stationary AE bursts are smoothed out by using the higher order wavelet (db35), leading to less insensitive to the AAC effect caused by more solid particles and combustion soot when burning the two alternative fuels. Principally, an adaptive procedure similar to Chapter 8 can be adapted to extract the AAC effects. However, the high commotional cost involved in optimising WPT results can be a major limitation for online applications.

9.5 Key Findings of Chapter 9

Based on the study presented in Chapter 9, wavelet packet analysis is shown to be an effective tool for extracting the tribological AE from the ring-liner conjunction with more details. With these details, narrower frequency bands are determined for constructing a WPT-LEA which are subsequently evaluated for diagnosing lubricant conditions with different lubricants as well as the used oil and assessing the impacts of alternative fuels based on AE analysis and AE indicators.

Around the middle of each stroke, significantly higher velocity leads to hydrodynamic lubrication process in which asperity collisions can occur from time to time but the significant AE activities arise mainly from asperity bending deflections driven by fluid shearing forces. This asperity–fluid interaction induced AE are more proportionally connecting to the relative velocity and oil viscosity but less to the load.

The developed WPT-AE indicator i.e. the average spectral amplitude, which is calculated in the lower frequency band of 70kHz-90kHz and 140kHz-160kHz corresponding to the middle of power stroke in the optimised WPT spectrum from a wavelet basis db35, allows the small changes in the viscosities of both the new and used oils to be differentiated consistently and reliably over wide operating conditions, and therefore accurate information for monitoring the tribological behaviours of the ring-liner conjunction and hence lubrication conditions for an entire engine.

Interestingly, AE indicators for used oils exhibit different changes in different frequency bands. These diversities of changes can be based on differentiating the details of oil deteriorations in terms of different contaminants. Obviously, the insights into these diversities of change need to be investigated further with inclusions of more dynamic details around fluid flows, asperities and their interactions that are induced by oil additives, water in oil, solid contaminants, soot, dust, wear debris and oxidation products.

WPT-LEA indicators from AE signals for biodiesel and F-T fuel show a tiny difference, compared to the baseline diesel with the same lubricant 10W30 and the with the higher viscosity oil 15W40. This shows that these two alternatives hardly cause any impacts upon tribological behaviour which is the same diagnosis as that drawn from DWT-LEA.

However, WPT-LEA is not so sensitive to locally non-stationary AE bursts around the middle of the stroke and thus give less indication of AAC effects due to additional particles reused from less perfect combustions of two alternative fuels at high operating conditions. Commotional cost can be too high to optimise WPT for extracting AAC effect when using the adaptive approach developed in DWT.

CHAPTER 10 CONCLUSIONS AND FUTURE WORKS

The chapter concludes the contributions and achievements of this work, finally, the future trends and opportunities of research into non-intrusive measurement improvements to the lubrication system of the engine using acoustic emission are listed.

10.1 Review of Research Objectives and Achievements

This research aims at developing a reliable online method to diagnose engine lubrication conditions based on non-intrusive AE measurements. The main achievements attained by carrying out this research are presented below in the same order as they appear in Section 1.3.

Objective 1: To investigate and develop the AE generation mechanisms for the piston-liner friction and lubrication.

Achievement 1:

The AE generation mechanisms during the sliding friction progress are mainly excited by the elastic deformation during the asperity-asperity collection and asperity-fluid interaction. Most part of the deformation energy is transferred into thermal energy and the others are representing as the elastic waves which generate AE.

Objective 2: To develop frictional AE models for the AE characterisation analysis of the tribological behaviour of the ring-liner system.

Achievement 2:

Conclude the AE mechanisms of lubricated surfaces as the dynamic behaviours of asperity-asperity collisions (AAC) and fluid-asperity interactions (FAI). Fill the gap of the AE modelling investigation under the lubricating conditions to decipher the AE generation mechanisms during fluid-asperity interactions (FAI)

Objective 3: To verify and evaluate AE characteristics through experimental studies.

Achievement 3:

The experimental results show coherence with the AE model and friction simulation results. The AE indicators are demonstrated to increase with velocity and viscosity as both the AE model and friction model predict.

Objective 4: To develop wavelet based de-noising techniques to suppression interfering AE events and enhance frictional AE signals.

Achievement 4:

The de-noising techniques based on wavelet transform and wavelet packets transform are both developed to enhance the frictional AE signals

Objective 5: To develop AE based techniques to diagnose lubrication conditions.

Achievement 5:

An accurate extraction method is developed to compute AE indicators base on optimised Daubechies wavelet. The AE indicators were demonstrated to be sensitive to variations in lubrication conditions.

Objective 6: To develop AE based techniques to diagnose abnormalities of an engine valve and the tribological impacts of alternative fuels.

Objective 6: To develop AE based techniques to diagnose abnormalities of an engine valve and the tribological impacts of alternative fuels.

Achievement 6:

The abnormalities of engine valves are demonstrated to have the influence on the AE indicators in the middle of strokes except for power stroke. The tribological AE indicators of the two alternative fuels can differ from the baseline diesel. Nevertheless, the difference between three fuels is no less than the range of AE indicators variation between two oils with different viscosity.

10.2 Conclusions

The research has carried out the investigation into AE responses from the cylinder body surface in order to reflect the engine tribological behaviours. AE responses from the tribological conjunction of the ring-liner have been modelled analytically according to dynamic elastic deflections of micro asperities. It shows that, around all engine dead centres, the boundary and mixed lubrication conditions contain more asperities collisions to generate AE activities. However, because of very low relative velocity, these collisions induced AE responses are less significant. Around the middle of each stroke, significantly higher velocity leads to more hydrodynamic lubrication in which little asperity collisions can occur but high AE activities arise mainly from asperity bending deflections driven by fluid shearing forces. This asperity–fluid interaction induced AE are more proportionally connecting to the relative velocity and oil viscosity

but less to the load. In addition, in the time domain, it will exhibit a quasi-continuous behaviour as the dynamic deflections on millions of asperities are stimulated by the velocity of the piston which is more continuous in the middle of a stroke. In the frequency domain, FAI induced AE can start from a lower frequency (tens of Kilohertz) and spread in a narrower band as the impulse period is associated with ring height, whereas the AAC induced AE can have extremely wide bands as its characteristic time relates to asperity sizes which are far less than ring height.

In line with the time-varying behaviour of other engine AE sources, AE signals measured externally will be highly nonstationary and noisy along with a large volume of data. As such, wavelet packet analysis is an effective tool for extracting the tribological AE from the ring-liner conjunction. Especially, optimal wavelet analyses can be achieved by adaptively selecting wavelets with constraints of the modified velocity of the piston motion. Furthermore, the proposed scheme of minimising the time and frequency overlaps in WPT spectrum can present more details regarding the tribological behaviour in multiple narrow frequency bands.

The hard threshold method based on LED results have been corrected as show in Section 7.4 and 7.5 from the Figure 10-1 to Figure 10-2. The hard threshold results showed tiny but consistent differences between two new lubricants in downward strokes whereas they separate the used oils better in the upward strokes. The hard threshold-LEA values for the two alternative fuels exhibit very similar behaviours to the two lubricants during all four strokes.

In diagnosing different new lubricants (10W30 oil and 15W40 oil), the improved adaptive threshold-LEA show more stable and consistent results in all engine strokes and operating conditions. However, the improved adaptive threshold-LEA is not very effective in reflecting the unsteady locally non-stationary AE bursts. Based on the AE model analysis, such bursts happen due to the AAC effects induced by large numbers solid particles of different sizes in the used oils. The ARWC based on the adaptive threshold is particularly sensitive to such bursts and produces accurate and consistent diagnostics for differentiating not only the used oils, but also the impacts of different alternative fuels.

The wavelet packet analysis is shown to be an effective tool for extracting the tribological AE from the ring-liner conjunction with more details. With these details,

narrower frequency bands are determined for constructing a WPT-LEA which is subsequently evaluated for diagnosing lubricant conditions with different lubricants as well as the used oil and assessing the impacts of alternative fuels based on AE analysis and AE indicators. The developed AE indicator i.e. the average spectral amplitude, which is calculated in two lower frequency bands in 70kHz-90kHz and 140kHz-160kHz corresponding to the middle of power stroke from the optimised WPT spectrum with a wavelet basis db35, allows the small changes in the viscosities of both the new and used oils to be differentiated consistently and reliably over wide operating conditions, and therefore provides accurate information for monitoring the tribological behaviours of the ring-liner conjunction and thus lubrication conditions for engines.

AE indicators for used oils exhibit different changes in different frequency bands. These diversities of changes can be based on differentiating the details of oil deteriorations in terms of different contaminants. Obviously, the insights into these diversities of change need to be investigated further with inclusions of more dynamic details around fluid flows, asperities and their interactions that are induced by oil additives, water in oil, solid contaminants, soot, dust, wear debris and oxidation products.

The AE indicators for alternative fuels, biodiesel and F-T fuel, displayed a tiny difference compared to the baseline diesel with the same lubricating oil of 10W30 and with the higher viscosity oil 15W40. The main reason is probably due to that the different lower heating value of three fuels means different tribofilm temperature under the running conditions, which leads to a minor difference in the viscosity of tribofilm. These results demonstrate that these two alternative fuels exhibit the acceptable tribological properties to be taken as the substitute fuels of diesel.

10.3 Contributions to Knowledge

The main contributions to knowledge made by this research project are:

1. It has improved the acoustic emission generation mechanisms and analytic models between two sliding surface under different lubrication regimes that allow AE characteristics from the tribological conjunction of the piston ring-cylinder liner to be predicted. In particular, based on the model available for asperity-asperity collision (AAC) induced AE responses, A new analytic model for asperity-fluid

interaction (FAI) induced AE is developed for explaining AE responses from the tribological conjunction of the piston ring-cylinder liner.

2. Three novel approaches have been developed for achieving optimised wavelet analysis of AE signals. They are all based on the AE characteristics predicted by the models which are reflected by the modified velocity of the piston motion. Especially, the adaptive threshold based MWRA allows two different AE effects: AAC and FAC to be separated to a great degree and subsequently used to diagnose the abnormal tribological behaviours. Also the minimisation of time-frequency overlaps for WPT analysis is firstly introduced and show high effectiveness to estimate the weak AE contents for oil condition diagnostics.

3. It shows for the first time that AE signatures extracted by optimised wavelet analysis are able to diagnose subtle changes in tribological behaviours. The improved local envelope amplitudes (LEA) allows the changes between different lubricants and different alternative fuels to be differentiated over a wide range of engine operations. In the meantime, the average residual wavelet coefficient (ARWC) can be used to diagnose any abnormal behaviours of lubrication such as the medium AE burst resulted from occasional collisions between asperities and particles.

4. Finally, these achievements have provided sufficient theoretical fundamentals and experimental supports to demonstrate that AE signals along with wavelet analytics can be an effective technique for on-line monitoring of engine tribological processes.

10.4 Future Work

On the other hand, dynamic effects associated with real operation have not been fully taken into account in this study. For this reason, future studies are recommended in addressing issues as follows:

1. Modify and perform the AE modelling and simulation studies by considering the turbulences or un-smoothness of the tribofilm flows and the particle collisions in more detail.

2. Perform modelling and simulation studies by taking into account influences such as the waviness, dynamic deflections of cylinder liner and distortion of rings, and piston slaps.

3. Study oil cavitation effects and impurity influences on AE contents.

4. Based on AE generation models, the frequency bands can be estimated according to the parameters of the engine. Then, perform the wavelet analysis algorithm in the signal pre-processing hardware based on target frequency bands according to the AE model, thereby improving the efficiency of signal processing for on-line monitoring.

In addition, it also needs continuous efforts to develop faster and simplified way to achieve the optimal results so that AE based analysis can be implemented more efficiently online.

REFERENCES

[1] Jost, Peter, ‘Lubrication (Tribology) - A report on the present position and industry’s needs’, Department of Education and Science, H. M. Stationary Office, London, UK., 1966.

[2] F. Sundus, M. A. Fazal, and H. H. Masjuki, ‘Tribology with biodiesel: A study on enhancing biodiesel stability and its fuel properties’, *Renew. Sustain. Energy Rev.*, vol. 70, no. Supplement C, pp. 399–412, Apr. 2017.

[3] K. Holmberg, P. Andersson, and A. Erdemir, ‘Global energy consumption due to friction in passenger cars’, *Tribol. Int.*, vol. 47, pp. 221–234, Mar. 2012.

[4] Y.-R. Jeng, ‘Friction and Lubrication Analysis of a Piston- Ring Pack’, Feb. 1992.

[5] M. Priest, D. Dowson, and C. . Taylor, ‘Predictive wear modelling of lubricated piston rings in a diesel engine’, *Wear*, vol. 231, no. 1, pp. 89–101, 1999.

[6] N. Patir and H. S. Cheng, ‘An Average Flow Model for Determining Effects of Three-Dimensional Roughness on Partial Hydrodynamic Lubrication’, *J. Lubr. Technol.*, vol. 100, no. 1, pp. 12–17, Jan. 1978.

[7] N. Patir and H. S. Cheng, ‘Application of Average Flow Model to Lubrication Between Rough Sliding Surfaces’, *J. Lubr. Technol.*, vol. 101, no. 2, pp. 220–229, Apr. 1979.

[8] M.-T. Ma, I. Sherrington, and E. H. Smith, ‘Analysis of lubrication and friction for a complete piston-ring pack with an improved oil availability model: Part 1: Circumferentially uniform film’, *Proc. Inst. Mech. Eng. Part J J. Eng. Tribol.*, vol. 211, no. 1, pp. 1–15, Jan. 1997.

[9] L. L. Ting and J. Mayer J. E., ‘Piston Ring Lubrication and Cylinder Bore Wear Analyses, Part II—Theory Verification’, *J. Lubr. Technol.*, vol. 96, no. 2, pp. 258–266, Apr. 1974.

[10] L. L. Ting and J. Mayer J. E., ‘Piston Ring Lubrication and Cylinder Bore Wear Analysis, Part I—Theory’, *J. Lubr. Technol.*, vol. 96, no. 3, pp. 305–313, Jul. 1974.

[11] S. C. TUNG and Y. HUANG, ‘Modeling of Abrasive Wear in a Piston Ring and Engine Cylinder Bore System©’, *Tribol. Trans.*, vol. 47, no. 1, pp. 17–22, Jan. 2004.

[12] ‘Condition monitoring’, *Wikipedia*. 03-Dec-2017.

[13] S. Kaboli and H. Oraee, *Reliability in Power Electronics and Electrical Machines: Industrial Applications and Performance Models*. IGI Global, 2001.

[14] K. Mthis and F. Chmelk, ‘Exploring Plastic Deformation of Metallic Materials by the Acoustic Emission Technique’, in *Acoustic Emission*, W. Sikorski, Ed. InTech, 2012.

[15] S. Lingard and K. K. Ng, ‘An investigation of acoustic emission in sliding friction and wear of metals’, *Wear*, vol. 130, no. 2, pp. 367–379, Apr. 1989.

[16] C. L. Jiaa and D. A. Dornfeld, ‘Experimental studies of sliding friction and wear via acoustic emission signal analysis’, *Wear*, vol. 139, no. 2, pp. 403–424, 1990.

[17] J. Miettinen and V. Siekkinen, ‘Acoustic emission in monitoring sliding contact behaviour’, *Wear*, vol. 181, pp. 897–900, Mar. 1995.
[18] H. S. Benabdallah and D. A. Aguilar, ‘Acoustic Emission and Its Relationship with Friction and Wear for Sliding Contact’, *Tribol. Trans.*, vol. 51, no. 6, pp. 738–747, 2008.
[19] C. K. Mechefske, G. Sun, and J. Sheasby, ‘Using acoustic emission to monitor sliding wear’, *Insight*, vol. 44, no. 8, pp. 490–497, Jan. 2014.
[20] L. Wang and R. J. K. Wood, ‘Acoustic emissions from lubricated hybrid contacts’, *Tribol. Int.*, vol. 42, no. 11–12, pp. 1629–1637, Dec. 2009.
[21] G. Sheng and B. Liu, ‘A theoretical model of slider–disk interaction and AE sensing process for studying interface phenomena and estimating unknown parameters’, *Tribol. Lett.*, vol. 6, no. 3–4, pp. 233–239, May 1999.
[22] A. I. F. Robertson, R. M. Douglas, P. Nivesrangsan, E. R. Brown, J. A. Steel, and R. Reuben, ‘SOURCE IDENTIFICATION USING ACOUSTIC EMISSION ON LARGE BORE CYLINDER LINERS’, Jan. 2004.
[23] R. M. Douglas, J. A. Steel, and R. L. Reuben, ‘A study of the tribological behaviour of piston ring/cylinder liner interaction in diesel engines using acoustic emission’, *Tribol. Int.*, vol. 39, no. 12, pp. 1634–1642, 2006.
[24] N. Wei *et al.*, ‘Characterisation of acoustic emissions for the frictional effect in engines using wavelets based multi-resolution analysis’, in *2015 21st International Conference on Automation and Computing (ICAC)*, 2015, pp. 1–6.
[25] J. D. Turner and L. Austin, ‘Electrical techniques for monitoring the condition of lubrication oil’, *Meas. Sci. Technol.*, vol. 14, no. 10, p. 1794, 2003.
[26] F. Elamin, F. Gu, and A. Ball, ‘Online Monitoring of Engine Oil Quality Based on AE Signal Analysis’, in *Future Technologies in Computing and Engineering: Proceedings of Computing and Engineering Annual Researchers’ Conference 2010: CEARC’10*, G. Lucas and Z. Xu, Eds. Huddersfield: University of Huddersfield, 2010, pp. 116–123.
[27] F. Elamin, F. Gu, and A. Ball, ‘Diesel engine lubricating oil condition and performance monitoring using acoustic emission measurements’, presented at the 24th International Congress on Condition Monitoring and Diagnostics Engineering Management (COMADEM 2011), Stavanger, Norway, May-2011.
[28] F. Sundus, M. A. Fazal, and H. H. Masjuki, ‘Tribology with biodiesel: A study on enhancing biodiesel stability and its fuel properties’, *Renew. Sustain. Energy Rev.*, vol. 70, pp. 399–412, Apr. 2017.
[29] ‘Non-Stationary Nature of Speech Signal (Theory) : Speech Signal Processing Laboratory : Electronics & Communications : IIT GUWAHATI Virtual Lab’. [Online]. Available: http://iitg.vlab.co.in/?sub=59&brch=164&sim=371&cnt=1104. [Accessed: 16-Jan-2018].
[30] D. Zhen, ‘A Study of Non-stationary Signal Processing for Machinery Condition Monitoring’, doctoral, University of Huddersfield, 2012.
[31] A. K. S. Jardine, D. Lin, and D. Banjevic, ‘A review on machinery diagnostics and prognostics implementing condition-based maintenance’, *Mech. Syst. Signal Process.*, vol. 20, no. 7, pp. 1483–1510, 2006.

[32] ‘Rotating machinery fault diagnosis using Wigner distribution’, *Mech. Syst. Signal Process.*, vol. 5, no. 3, pp. 155–166, May 1991.
[33] G. K. Singh and S. A. K. Sa’ad Ahmed, ‘Vibration signal analysis using wavelet transform for isolation and identification of electrical faults in induction machine’, *Electr. Power Syst. Res.*, vol. 68, no. 2, pp. 119–136, Feb. 2004.
[34] J. Chen *et al.*, ‘Wavelet transform based on inner product in fault diagnosis of rotating machinery: A review’, *Mech. Syst. Signal Process.*, vol. 70–71, pp. 1–35, Mar. 2016.
[35] I. Daubechies, ‘The wavelet transform, time-frequency localization and signal analysis’, *IEEE Trans. Inf. Theory*, vol. 36, no. 5, pp. 961–1005, Sep. 1990.
[36] A. Datta, C. Mavroidis, J. Krishnasamy, and M. Hosek, ‘Neural Netowrk Based Fault Diagnostics of Industrial Robots using Wavelt Multi-Resolution Analysis’, in *American Control Conference, 2007. ACC ’07*, 2007, pp. 1858–1863.
[37] S. G. Mallat, ‘A theory for multiresolution signal decomposition: the wavelet representation’, *IEEE Trans. Pattern Anal. Mach. Intell.*, vol. 11, no. 7, pp. 674–693, Jul. 1989.
[38] M. J. Gómez, C. Castejón, and J. C. García-Prada, ‘Review of Recent Advances in the Application of the Wavelet Transform to Diagnose Cracked Rotors’, *Algorithms*, vol. 9, no. 1, p. 19, Mar. 2016.
[39] X. Fan and M. J. Zuo, ‘Gearbox fault detection using Hilbert and wavelet packet transform’, *Mech. Syst. Signal Process.*, vol. 20, no. 4, pp. 966–982, May 2006.
[40] F. Combet, L. Gelman, and G. LaPayne, ‘Novel detection of local tooth damage in gears by the wavelet bicoherence’, *Mech. Syst. Signal Process.*, vol. 26, pp. 218–228, 2012.
[41] N. G. Nikolaou and I. A. Antoniadis, ‘Rolling element bearing fault diagnosis using wavelet packets’, *NDT E Int.*, vol. 35, no. 3, pp. 197–205, Apr. 2002.
[42] F. Dalvand, A. Kalantar, and M. S. Safizadeh, ‘A Novel Bearing Condition Monitoring Method in Induction Motors Based on Instantaneous Frequency of Motor Voltage’, *IEEE Trans. Ind. Electron.*, vol. 63, no. 1, pp. 364–376, Jan. 2016.
[43] X. Wang, C. Liu, F. Bi, X. Bi, and K. Shao, ‘Fault diagnosis of diesel engine based on adaptive wavelet packets and EEMD-fractal dimension’, *Mech. Syst. Signal Process.*, vol. 41, no. 1–2, pp. 581–597, Dec. 2013.
[44] J.-D. Wu and C.-H. Liu, ‘An expert system for fault diagnosis in internal combustion engines using wavelet packet transform and neural network’, *Expert Syst. Appl.*, vol. 36, no. 3, Part 1, pp. 4278–4286, Apr. 2009.
[45] J.-D. Wu and C.-H. Liu, ‘Investigation of engine fault diagnosis using discrete wavelet transform and neural network’, *Expert Syst. Appl.*, vol. 35, no. 3, pp. 1200–1213, Oct. 2008.
[46] D. Dowson and G. R. Higginson, *Elasto-hydrodynamic lubrication: the fundamentals of roller and gear lubrication*. Pergamon Press, 1966.
[47] S. C. Tung and M. L. McMillan, ‘Automotive tribology overview of current advances and challenges for the future’, *Tribol. Int.*, vol. 37, no. 7, pp. 517–536, 2004.

[48] ‘Friction and wear bench tests of different engine liner surface finishes’, *Tribol. Int.*, vol. 41, no. 11, pp. 1032–1038, Nov. 2008.
[49] ‘T. Hoen, J. Schmid, W. Stumpf, W. (2009). Less wear and oil consumption through helical slide honing of engines by Deutz. MTZ worldwide, 70(4), 46-51.
[50] ‘Surface finish’, *Wikipedia*. 20-Nov-2017.
[51] ‘Surface roughness’, *Wikipedia*. 08-Dec-2017.
[52] Peter Andersson, Jaana Tamminen and Carl-Erik Sandström, ‘Piston ring tribology’, Helsinki University of Technology, Internal Combustion Engine Laboratory, Espoo, 2002.
[53] ‘Honing (metalworking)’, *Wikipedia*. 07-Nov-2017.
[54] W. B. Hardy and I. Doubleday, ‘Boundary Lubrication. The Paraffin Series’, *Proc. R. Soc. Lond. Ser. Contain. Pap. Math. Phys. Character*, vol. 100, no. 707, pp. 550–574, 1922.
[55] K. Komvopoulos, N. Saka, and N. P. Suh, ‘The Mechanism of Friction in Boundary Lubrication’, *J. Tribol.*, vol. 107, no. 4, pp. 452–462, Oct. 1985.
[56] O. Reynolds, ‘On the Theory of Lubrication and Its Application to Mr. Beauchamp Tower’s Experiments, Including an Experimental Determination of the Viscosity of Olive Oil.’, *Proc. R. Soc. Lond.*, vol. 40, no. 242–245, pp. 191–203, Jan. 1886.
[57] M. Priest and C. M. Taylor, ‘Automobile engine tribology — approaching the surface’, *Wear*, vol. 241, no. 2, pp. 193–203, Jul. 2000.
[58] R. C. Coy, ‘Practical applications of lubrication models in engines’, *Tribol. Int.*, vol. 31, pp. 563–571, Oct. 1998.
[59] X. Lu, M. M. Khonsari, and E. R. Gelinck, ‘The Stribeck Curve: Experimental Results and Theoretical Prediction’, *J. Tribol.*, vol. 128, no. 4, pp. 789–794, Apr. 2006.
[60] Stribeck, R., ‘Ball bearings for various loads’, *Trans ASME*, vol. 29, pp. 420–463, 1907.
[61] S. M. Rohde, ‘A mixed friction model for dynamically loaded contacts with application to piston ring lubrication’, *ResearchGate*, pp. 262–278, Jan. 1981.
[62] ‘Tribology’, *Wikipedia, the free encyclopedia*. 24-Nov-2014.
[63] H. Rahnejat, *Tribology and dynamics of engine and powertrain: fundamentals, applications and future trends*. Oxford: Woodhead, 2010.
[64] J. A. Mcgeehan, ‘A Literature Review of the Effects of Piston and Ring Friction and Lubricating Oil Viscosity on Fuel Economy’, 1978.
[65] B. S. Andersson, ‘Paper XVIII (iii) Company Perspectives in Vehicle Tribology - Volvo’, in *Tribology Series*, vol. 18, C. M. T. and M. G. D. Dowson, Ed. Elsevier, 1991, pp. 503–506.
[66] Spearot JA., ‘Friction, wear, health, and environmental impacts— tribology in the new millennium’, Nashville, Tennessee, A keynote lecture at the STLE Annual Meeting, May 2000.
[67] Schwaderlapp, M., Koch, D., and Dohmen, D., ‘Friction Reduction - the Engine’s Mechanical Contribution to Saving Fuel’, SAE Technical Paper 2000-05–0160, 2000.
[68] R. A. C. Jr, ‘A Hydrodynamical Theory of Piston Ring Lubrication’, *J. Appl. Phys.*, vol. 7, no. 9, pp. 364–367, Sep. 1936.

[69] J. A. Greenwood and J. H. Tripp, ‘The Contact of Two Nominally Flat Rough Surfaces’, *Proc. Inst. Mech. Eng.*, vol. 185, no. 1, pp. 625–633, Jun. 1970.
[70] O. Akalin and G. M. Newaz, ‘Piston Ring-Cylinder Bore Friction Modeling in Mixed Lubrication Regime: Part I—Analytical Results’, *J. Tribol.*, vol. 123, no. 1, pp. 211–218, Dec. 1999.
[71] N. Morris, R. Rahmani, H. Rahnejat, P. D. King, and B. Fitzsimons, ‘Tribology of piston compression ring conjunction under transient thermal mixed regime of lubrication’, *Tribol. Int.*, vol. 59, pp. 248–258, Mar. 2013.
[72] O. Akalin and G. M. Newaz, ‘Piston Ring-Cylinder Bore Friction Modeling in Mixed Lubrication Regime: Part II—Correlation With Bench Test Data’, *J. Tribol.*, vol. 123, no. 1, pp. 219–223, Dec. 1999.
[73] Y. Hu, H. S. Cheng, T. Arai, Y. Kobayashi, and S. Aoyama, ‘Numerical Simulation of Piston Ring in Mixed Lubrication—A Nonaxisymmetrical Analysis’, *J. Tribol.*, vol. 116, no. 3, pp. 470–478, Jul. 1994.
[74] M.-T. Ma, I. Sherrington, E. H. Smith, and N. Grice, ‘Development of a detailed model for piston-ring lubrication in IC engines with circular and non-circular cylinder Bores’, *Tribol. Int.*, vol. 30, no. 11, pp. 779–788, Nov. 1997.
[75] A. Usman, T. A. Cheema, and C. W. Park, ‘Tribological performance evaluation and sensitivity analysis of piston ring lubricating film with deformed cylinder liner’, *Proc. Inst. Mech. Eng. Part J J. Eng. Tribol.*, p. 1350650115581029, Apr. 2015.
[76] A. Usman and C. W. Park, ‘Modeling and simulation of frictional energy loss in mixed lubrication of a textured piston compression ring during warm-up of spark ignition engine’, *Int. J. Engine Res.*, p. 1468087416656676, Jul. 2016.
[77] E. Tomanik, ‘Modelling the hydrodynamic support of cylinder bore and piston rings with laser textured surfaces’, *Tribol. Int.*, vol. 59, pp. 90–96, Mar. 2013.
[78] T. Tian, L. B. Noordzij, V. W. Wong, and J. B. Heywood, ‘Modeling Piston-Ring Dynamics, Blowby, and Ring-Twist Effects’, *J. Eng. Gas Turbines Power*, vol. 120, no. 4, pp. 843–854, Oct. 1998.
[79] M. Priest, D. Dowson, and C. M. Taylor, ‘Theoretical modelling of cavitation in piston ring lubrication’, *Proc. Inst. Mech. Eng. Part C J. Mech. Eng. Sci.*, vol. 214, no. 3, pp. 435–447, Mar. 2000.
[80] R. F. Ausas, M. Jai, I. S. Ciuperca, and G. C. Buscaglia, ‘Conservative one-dimensional finite volume discretization of a new cavitation model for piston–ring lubrication’, *Tribol. Int.*, vol. 57, pp. 54–66, Jan. 2013.
[81] D. J. Radakovic and M. M. Khonsari, ‘Heat Transfer in a Thin-Film Flow in the Presence of Squeeze and Shear Thinning: Application to Piston Rings’, *J. Heat Transf.*, vol. 119, no. 2, pp. 249–257, May 1997.
[82] Y. Harigaya, M. Suzuki, F. Toda, and M. Takiguchi, ‘Analysis of Oil Film Thickness and Heat Transfer on a Piston Ring of a Diesel Engine: Effect of Lubricant Viscosity’, *J. Eng. Gas Turbines Power*, vol. 128, no. 3, pp. 685–693, Sep. 2004.
[83] D. E. Richardson, ‘Review of Power Cylinder Friction for Diesel Engines’, *J. Eng. Gas Turbines Power*, vol. 122, no. 4, pp. 506–519, 2000.

[84] R. A. Mufti and M. Priest, ‘Experimental Evaluation of Piston-Assembly Friction Under Motored and Fired Conditions in a Gasoline Engine’, *J. Tribol.*, vol. 127, no. 4, pp. 826–836, Aug. 2004.
[85] G. Smedley, ‘Piston ring design for reduced friction in modern internal combustion engines’, Thesis, Massachusetts Institute of Technology, 2004.
[86] K. Liao, H. Chen, and T. Tian, ‘The Study of Friction between Piston Ring and Different Cylinder Liners using Floating Liner Engine - Part 1’, 2012.
[87] B. O’Rourke, D. Radford, and R. Stanglmaier, ‘Tri-Axial Force Measurements on the Cylinder of a Motored SI Engine Operated on Lubricants of Differing Viscosity’, *J. Eng. Gas Turbines Power*, vol. 132, no. 9, pp. 092807–092807, Jun. 2010.
[88] ‘Lubricating oil conditioning sensors for online machine health monitoring – A review’, *Tribol. Int.*, vol. 109, pp. 473–484, May 2017.
[89] J. Zhu, D. He, and E. Bechhoefer, *Survey of lubrication oil condition monitoring, diagnostics, prognostics techniques and systems*, vol. 2. 2013.
[90] A. Mujahid and F. L. Dickert, ‘Monitoring automotive oil degradation: analytical tools and onboard sensing technologies’, *Anal. Bioanal. Chem.*, vol. 404, no. 4, pp. 1197–1209, Sep. 2012.
[91] B. E. A. Jacobs, *Design of Slurry Transport Systems*, 1 edition. London: CRC Press, 1998.
[92] R. S. Dwyer-Joyce, B. W. Drinkwater, and C. J. Donohoe, ‘The measurement of lubricant–film thickness using ultrasound’, *Proc. R. Soc. Lond. Math. Phys. Eng. Sci.*, vol. 459, no. 2032, pp. 957–976, Apr. 2003.
[93] ‘Ultrasonic echo waveshape features extraction based on QPSO-matching pursuit for online wear debris discrimination’, *Mech. Syst. Signal Process.*, vol. 60–61, pp. 301–315, Aug. 2015.
[94] L. Du and J. Zhe, ‘An integrated ultrasonic–inductive pulse sensor for wear debris detection’, *Smart Mater. Struct.*, vol. 22, no. 2, p. 025003, 2013.
[95] R. S. Mills, E. Y. Avan, and R. S. Dwyer-Joyce, ‘Piezoelectric sensors to monitor lubricant film thickness at piston–cylinder contacts in a fired engine’, *Proc. Inst. Mech. Eng. Part J J. Eng. Tribol.*, Nov. 2012.
[96] M. A. Fazal, A. S. M. A. Haseeb, and H. H. Masjuki, ‘Investigation of friction and wear characteristics of palm biodiesel’, *Energy Convers. Manag.*, vol. 67, pp. 251–256, Mar. 2013.
[97] T. L. Alleman and R. L. Mccormick, ‘Fischer-Tropsch Diesel Fuels - Properties and Exhaust Emissions: A Literature Review’, SAE International, Warrendale, PA, SAE Technical Paper 2003-01–0763, Mar. 2003.
[98] ‘Elobio: Fischer-Tropsch diesel’. [Online]. Available: http://www.elobio.eu/biofuels/fischer-tropsch-diesel/. [Accessed: 10-Nov-2013].
[99] P. W. Schaberg, I. S. Myburgh, J. J. Botha, and I. A. Khalek, ‘Comparative Emissions Performance of Sasol Fischer-Tropsch Diesel Fuel in Current and Older Technology Heavy-Duty Engines’, SAE Technical Paper, Warrendale, PA, SAE Technical Paper 2000-01–1912, Jun. 2000.

[100] A. S. Cheng and R. W. Dibble, ‘Emissions Performance of Oxygenate-in-Diesel Blends and Fischer-Tropsch Diesel in a Compression Ignition Engine’, SAE Technical Paper, Warrendale, PA, SAE Technical Paper 1999-01–3606, Oct. 1999.
[101] T. L. Alleman and R. L. Mccormick, ‘Fischer-Tropsch Diesel Fuels - Properties and Exhaust Emissions: A Literature Review’, SAE International, Warrendale, PA, SAE Technical Paper 2003-01–0763, Mar. 2003.
[102] Y. Huang, L. Zhou, and K. Pan, ‘Combustion characteristics of a direct-injection diesel engine fueled with Fischer-Tropsch diesel’, *Front. Energy Power Eng. China*, vol. 1, no. 2, pp. 239–244, May 2007.
[103] A. de Klerk, *Fischer-Tropsch Refining*. John Wiley & Sons, 2012.
[104] O. O. Ajayi and M. F. Alzoubi, A. Erdemir , G. R. Fenske, ‘Effect of Carbon Coating on Scuffing performance in Diesel Fuels’, *Tribol. Trans.*, vol. 44, no. 2, pp. 298–304, Mar. 2008.
[105] S. S. Gill, A. Tsolakis, K. D. Dearn, and J. Rodr ́guez-Fernández, ‘Combustion characteristics and emissions of Fischer–Tropsch diesel fuels in IC engines’, *Prog. Energy Combust. Sci.*, vol. 37, no. 4, pp. 503–523, Aug. 2011.
[106] B. Tesfa, F. Gu, R. Mishra, and A. Ball, ‘Emission Characteristics of a CI Engine Running with a Range of Biodiesel Feedstocks’, *Energies*, vol. 7, no. 1, pp. 334–350, Jan. 2014.
[107] A. S. Ramadhas, C. Muraleedharan, and S. Jayaraj, ‘Performance and emission evaluation of a diesel engine fueled with methyl esters of rubber seed oil’, *Renew. Energy*, vol. 30, no. 12, pp. 1789–1800, Oct. 2005.
[108] M. Shahabuddin, H. H. Masjuki, M. A. Kalam, M. Mofijur, M. A. Hazrat, and A. M. Liaquat, ‘Effect of Additive on Performance of C.I. Engine Fuelled with Bio Diesel’, *Energy Procedia*, vol. 14, pp. 1624–1629, Jan. 2012.
[109] A. K. Agarwal and L. M. Das, ‘Biodiesel Development and Characterization for Use as a Fuel in Compression Ignition Engines’, *J. Eng. Gas Turbines Power*, vol. 123, no. 2, pp. 440–447, Dec. 2000.
[110] C. Carraretto, A. Macor, A. Mirandola, A. Stoppato, and S. Tonon, ‘Biodiesel as alternative fuel: Experimental analysis and energetic evaluations’, *Energy*, vol. 29, no. 12, pp. 2195–2211, Oct. 2004.
[111] D. H. Qi, L. M. Geng, H. Chen, Y. Z. Bian, J. Liu, and X. C. Ren, ‘Combustion and performance evaluation of a diesel engine fueled with biodiesel produced from soybean crude oil’, *Renew. Energy*, vol. 34, no. 12, pp. 2706–2713, Dec. 2009.
[112] B. Kegl, ‘Experimental Investigation of Optimal Timing of the Diesel Engine Injection Pump Using Biodiesel Fuel’, *Energy Fuels*, vol. 20, no. 4, pp. 1460–1470, 2006.
[113] C. S. Lee, S. W. Park, and S. I. Kwon, ‘An Experimental Study on the Atomization and Combustion Characteristics of Biodiesel-Blended Fuels’, *Energy Fuels*, vol. 19, no. 5, pp. 2201–2208, 2005.
[114] K. Yamane, A. Ueta, and Y. Shimamoto, ‘Influence of physical and chemical properties of biodiesel fuels on injection, combustin and exhaust emission characteristics in a direct injection compression ignition engine’, *Int. J. Engine Res.*, vol. 2, no. 4, pp. 249–261, Aug. 2001.

[115] Haseeb ASMA, Sia SY, Fazal MA, Masjuki HH, 'Effect of temperature on tribological properties of palm biodiesel', *Energy*, vol. 35, pp. 1460–4, 2010.
[116] J. Hu, Z. Du, C. Li, and E. Min, 'Study on the lubrication properties of biodiesel as fuel lubricity enhancers', *Fuel*, vol. 84, no. 12–13, pp. 1601–1606, Sep. 2005.
[117] G. Knothe and K. R. Steidley, 'Kinematic viscosity of biodiesel components (fatty acid alkyl esters) and related compounds at low temperatures', *Fuel*, vol. 86, no. 16, pp. 2560–2567, 2007.
[118] A. Banerji, M. J. Lukitsch, and A. T. Alpas, 'Friction reduction mechanisms in cast iron sliding against DLC: Effect of biofuel (E85) diluted engine oil', *Wear*, vol. 368–369, pp. 196–209, Dec. 2016.
[119] A. K. Agarwal, 'Experimental investigations of the effect of biodiesel utilization on lubricating oil tribology in diesel engines', *Proc. Inst. Mech. Eng. Part J. Automob. Eng.*, vol. 219, no. 5, pp. 703–713, May 2005.
[120] Peterson CL RD, Thompson JL, Zhang X, Hammond BL, Beck S, 'development of eapeseed biodiesel for use in high speed disesl engines', University of Idaho Department of Biological and Agricultural Engineering, ID83844-2337, May 1996.
[121] R. Fraer, H. Dinh, K. Proc, R. L. McCormick, K. Chandler, and B. Buchholz, 'Operating Experience and Teardown Analysis for Engines Operated on Biodiesel Blends (B20)', SAE Technical Paper, Warrendale, PA, SAE Technical Paper 2005-01–3641, Nov. 2005.
[122] E. Hu, Y. Xu, X. Hu, L. Pan, and S. Jiang, 'Corrosion behaviors of metals in biodiesel from rapeseed oil and methanol', *Renew. Energy*, vol. 37, no. 1, pp. 371–378, Jan. 2012.
[123] M. B. H. HASSAN, 'Comparative corrosive characteristics of petroleum diesel and palm biodiesel for automotive materials', *Fuel Process. Technol.*, vol. 91, Feb. 2010.
[124] A. S. M. A. Haseeb, H. H. Masjuki, L. J. Ann, and M. A. Fazal, 'Corrosion characteristics of copper and leaded bronze in palm biodiesel', *Fuel Process. Technol.*, vol. 91, no. 3, pp. 329–334, Mar. 2010.
[125] C. B. Scruby, 'An introduction to acoustic emission', *J. Phys. [E]*, vol. 20, no. 8, p. 946, Aug. 1987.
[126] Miinshiou Huang, Liang Jiang, Peter K. Liaw, Charlie R. Brooks, Rodger Seeley, and Dwaine L. Klarstrom., 'Using Acoustic Emission in Fatigue and Fracture Materials Research'. [Online]. Available: http://www.tms.org/pubs/journals/jom/9811/huang/huang-9811.html. [Accessed: 25-Nov-2015].
[127] V. M. Baranov, E. M. Kudryavtsev, G. A. Sarychev, and V. M. Schavelin, *Acoustic Emission in Friction*. Elsevier, 2011.
[128] 'AE Sources'. [Online]. Available: https://www.nde-ed.org/EducationResources/CommunityCollege/Other%20Methods/AE/AE_Theory-Sources.htm. [Accessed: 13-Aug-2015].
[129] J. T. Broch, *Mechanical vibration and shock measurements*. Brüel & Kjaer, 1980.
[130] P. Nivesrangsan, 'Multi-source, multi-sensor approaches to diesel engine monitoring using acoustic emission', thesis, Heriot-Watt University, 2004.

[131] N. P. Suh, *Tribophysics*. Englewood Cliffs, N.J: Prentice-Hall, 1986.
[132] R. V. Williams, *Acoustic Emission*. A. Hilger, 1980.
[133] J. Sun, R. J. K. Wood, L. Wang, I. Care, and H. E. G. Powrie, 'Wear monitoring of bearing steel using electrostatic and acoustic emission techniques', *Wear*, vol. 259, no. 7–12, pp. 1482–1489, 2005.
[134] J. Kannatey-Asibu Elijah and D. A. Dornfeld, 'Quantitative Relationships for Acoustic Emission from Orthogonal Metal Cutting', *J. Eng. Ind.*, vol. 103, no. 3, pp. 330–340, Aug. 1981.
[135] C. Beggan, M. Woulfe, P. Young, and G. Byrne, 'Using Acoustic Emission to Predict Surface Quality', *Int. J. Adv. Manuf. Technol.*, vol. 15, no. 10, pp. 737–742, Sep. 1999.
[136] X. Li, 'A brief review: acoustic emission method for tool wear monitoring during turning', *Int. J. Mach. Tools Manuf.*, vol. 42, no. 2, pp. 157–165, 2002.
[137] 'Tool wear monitoring of micro-milling operations', *J. Mater. Process. Technol.*, vol. 209, no. 10, pp. 4903–4914, Jun. 2009.
[138] 'Tool wear detection in dry high-speed milling based upon the analysis of machine internal signals', *Mechatronics*, vol. 18, no. 10, pp. 627–633, Dec. 2008.
[139] 'Direct adaptive control of plunge grinding process using acoustic emission (AE) sensor', *Int. J. Mach. Tools Manuf.*, vol. 35, no. 10, pp. 1445–1457, Oct. 1995.
[140] 'Acoustic emission spikes at workpiece edges in grinding: Origin and applications', *Int. J. Mach. Tools Manuf.*, vol. 64, pp. 96–101, Jan. 2013.
[141] S. Lingard, C. W. Yu, and C. F. Yau, 'Sliding wear studies using acoustic emission', *Wear*, vol. 162â€"164, Part A, pp. 597–604, Apr. 1993.
[142] T. Kita, K. Kogure, Y. Mitsuya, and T. Nakanishi, 'New method of detecting contact between floating-head and disk', *IEEE Trans. Magn.*, vol. 16, no. 5, pp. 873–875, Sep. 1980.
[143] A. G. Khurshudov and F. E. Talke, 'A Study of Subambient Pressure Tri-Pad Sliders Using Acoustic Emission', *J. Tribol.*, vol. 120, no. 1, pp. 54–59, Jan. 1998.
[144] D.-Y. Lee, J. Lee, J. Hwang, and S.-H. Choa, 'Effect of relative humidity and disk acceleration on tribocharge build-up at a slider–disk interface', *Tribol. Int.*, vol. 40, no. 8, pp. 1253–1257, Aug. 2007.
[145] S. Suzuki and H. Nishihira, 'Study of Slider Dynamics Over Very Smooth Magnetic Disks', *J. Tribol.*, vol. 118, no. 2, pp. 382–387, Apr. 1996.
[146] V. M. Baranov, E. M. Kudryavtsev, and G. A. Sarychev, 'Modelling of the parameters of acoustic emission under sliding friction of solids', *Wear*, vol. 202, no. 2, pp. 125–133, Jan. 1997.
[147] Y. Fan, F. Gu, and A. Ball, 'Modelling acoustic emissions generated by sliding friction', *Wear*, vol. 268, no. 5–6, pp. 811–815, Feb. 2010.
[148] P. C. Mishra, H. Rahnejat, and P. D. King, 'Tribology of the ring–bore conjunction subject to a mixed regime of lubrication', *Proc. Inst. Mech. Eng. Part C J. Mech. Eng. Sci.*, vol. 223, no. 4, pp. 987–998, Apr. 2009.

[149] A. I. F. Robertson, R. M. Douglas, P. Nivesrangsan, E. R. Brown, J. A. Steel, and R. L. Reuben, 'Source identification using acoustic emission on large bore cylinder liners', *ResearchGate*, Jan. 2004.
[150] M. El-Ghamry, J. A. Steel, R. L. Reuben, and T. L. Fog, 'Indirect measurement of cylinder pressure from diesel engines using acoustic emission', *Mech. Syst. Signal Process.*, vol. 19, no. 4, pp. 751–765, Jul. 2005.
[151] 'Impact (mechanics)', *Wikipedia*. 16-Jun-2017.
[152] F. Elamin, Y. Fan, F. Gu, and A. Ball, 'Diesel Engine Valve Clearance Detection Using Acoustic Emission', *Adv. Mech. Eng.*, vol. 2010, Jun. 2010.
[153] F. Elamin, Y. Fan, F. Gu, and A. Ball, 'Detection of diesel engine valve clearance by acoustic emission.', in *Proceedings of Computing and Engineering Annual Researchers' Conference 2009: CEARC'09*, G. Lucas and Z. Xu, Eds. Huddersfield: University of Huddersfield, 2009, pp. 7–13.
[154] F. Elamin, Y. Fan, F. Gu, and A. Ball, 'Detection of Diesel Engine Injector Faults Using Acoustic Emissions', presented at the COMADEM 2010: Advances in Maintenance and Condition Diagnosis Technologies towards Sustainable Society, Nara, Japan, Jun-2010.
[155] A. Albarbar, F. Gu, and A. D. Ball, 'Diesel engine fuel injection monitoring using acoustic measurements and independent component analysis', *Measurement*, vol. 43, no. 10, pp. 1376–1386, 2010.
[156] R. M. Douglas, 'Monitoring of the piston ring-pack and cylinder liner interface in diesel engines through acoustic emission measurements', Thesis, Heriot-Watt University, 2007.
[157] N. Wei, A. Ball, and F. Gu, 'A Study of Alternative Fuels Potential Effects on the Combustion Engines using acoustic emission', in *Proceedings of Computing and Engineering Annual Researchers' Conference 2013 : CEARC'13*, Huddersfield, 2013, p. 239.
[158] M. H. El-Ghamry, R. L. Reubrn, and J. A. Steel, 'The Development of Automated Pattern Recognition and Statistical Feature Isolation Techniques for The Diagnosis of Reciprocating Machinery Faults using Acoustic Emission', *Mech. Syst. Signal Process.*, vol. 17, no. 4, pp. 805–823, 2003.
[159] N. Cavina, S. Sgatti, F. Cavanna, and G. Bisanti, 'Combustion Monitoring Based on Engine Acoustic Emission Signal Processing', 2009.
[160] F. Elamin, Y. Fan, F. Gu, and A. Ball, 'Diesel Engine Valve Clearance Detection Using Acoustic Emission', *Adv. Mech. Eng.*, vol. 2010, Jun. 2010.
[161] J. D. Gill, R. L. Reuben, and J. Steel, 'A study of small HSDI diesel engine fuel injection equipment faults using acoustic emission', *J. Acoust. Emiss.*, vol. 18, 2000.
[162] J. D. Gill, R. L. Reuben, and J. Steel, 'A study of small HSDI diesel engine fuel injection equipment faults using acoustic emission', *J. Acoust. Emiss.*, vol. 18, 2000.
[163] M. Shuster, D. Combs, K. Karrip, and D. Burke, 'Piston Ring Cylinder Liner Scuffing Phenomenon Studies Using Acoustic Emission Technique', SAE International, Warrendale, PA, SAE Technical Paper 2000-01–1782, Jun. 2000.

[164] Y. Harigaya, M. Suzuki, and M. Takiguchi, ‘Analysis of Oil Film Thickness on a Piston Ring of Diesel Engine: Effect of Oil Film Temperature’, *J. Eng. Gas Turbines Power*, vol. 125, no. 2, pp. 596–603, Apr. 2003.
[165] C. J. A. Roelands, J. C. Vlugter and H. I. Waterman, ‘The Viscosity-Temperature-Pressure Relationship of Lubricating Oils and Its Correlation With Chemical Constitution’, *J. Basic Eng.*, vol. 85, no. 4, pp. 601–607, Dec. 1963.
[166] R. Gohar, *Fundamentals Of Tribology*. London: Imperial College Press, 2008.
[167] H. Shahmohamadi, R. Rahmani, H. Rahnejat, P. King, and C. Garner, ‘Cavitating Flow in Engine Piston Ring-Cylinder Liner Conjunction’, p. V07AT08A056, Nov. 2013.
[168] D. Dowson and G. R. Higginson, *Elasto-hydrodynamic lubrication: the fundamentals of roller and gear lubrication*. Pergamon Press, 1966.
[169] Y. Harigaya, M. Suzuki, F. Toda, and M. Takiguchi, ‘Analysis of Oil Film Thickness and Heat Transfer on a Piston Ring of a Diesel Engine: Effect of Lubricant Viscosity’, *J. Eng. Gas Turbines Power*, vol. 128, no. 3, pp. 685–693, Sep. 2004.
[170] C. Wu and L. Zheng, ‘An Average Reynolds Equation for Partial Film Lubrication With a Contact Factor’, *J. Tribol.*, vol. 111, no. 1, pp. 188–191, Jan. 1989.
[171] S. B. M, D. V. Bhatt, and M. K. N, ‘Simulation and Modeling of Friction Force and Oil Film Thickness in Piston Ring - Cylinder Liner Assembly of an I. C. Engine’, *ResearchGate*, vol. 2177, no. 1, Jul. 2009.
[172] V. W. Wong and S. C. Tung, ‘Overview of automotive engine friction and reduction trends–Effects of surface, material, and lubricant-additive technologies’, *Friction*, vol. 4, no. 1, pp. 1–28, Mar. 2016.
[173] R. J. Boness and S. L. McBride, ‘Adhesive and abrasive wear studies using acoustic emission techniques’, *Wear*, vol. 149, no. 1, pp. 41–53, Sep. 1991.
[174] A. Ravikiran, T. Liew, and T. S. Low, ‘Effect of disk acceleration on the generation of acoustic emission signal at the head–disk interface’, *J. Appl. Phys.*, vol. 85, no. 8, pp. 5612–5614, Apr. 1999.
[175] H. Tanaka, S. Yonemura, and H. Tokisue, ‘Slider dynamics during continuous contact with textured and smooth disks in ultra low flying height’, in *2000 Asia-Pacific Magnetic Recording Conference. Digests of APMRC2000 on Mechanical and Manufacturing Aspects of HDD (Cat. No.00EX395)*, 2000, p. TB3/1-TB3/2.
[176] Yibo Edward Fan, ‘The Condition Monitoring of Mechanical Seals Using Acoustic Emissions’, Thesis, the University of Manchester, 2007.
[177] ‘Plastic deformation and sliding friction of metals’, *Wear*, vol. 53, no. 2, pp. 345–370, Apr. 1979.
[178] W. R. Chang, I. Etsion, and D. B. Bogy, ‘An Elastic-Plastic Model for the Contact of Rough Surfaces’, *J. Tribol.*, vol. 109, no. 2, pp. 257–263, Apr. 1987.
[179] *Theory of Elasticity, Third Edition: Volume 7*, 3 edition. Butterworth-Heinemann, 1986.
[180] A. Majumdar and B. Bhushan, ‘Fractal Model of Elastic-Plastic Contact Between Rough Surfaces’, *J. Tribol.*, vol. 113, no. 1, pp. 1–11, Jan. 1991.
[181] M. Anand, M. Hadfield, B. Thomas, and R. Cantrill, ‘The depletion of ZDDP additives within marine lubricants and associated cylinder liner wear in RNLI lifeboat

engines', *Proc. Inst. Mech. Eng. Part J. Mater. Des. Appl.*, vol. 231, no. 1–2, pp. 162–170, Feb. 2017.
[182] C. Hellier, *Handbook of Nondestructive Evaluation*. McGraw Hill Professional, 2001.
[183] N. Wei *et al.*, 'Characterisation of acoustic emissions for the frictional effect in engines using wavelets based multi-resolution analysis', in *2015 21st International Conference on Automation and Computing (ICAC)*, 2015, pp. 1–6.
[184] R. K. Young, *Wavelet theory and its applications*. Boston: Kluwer Academic Publishers, 1993.
[185] T.-Y. Yang and L. Leu, 'Study of transition velocities from bubbling to turbulent fluidization by statistic and wavelet multi-resolution analysis on absolute pressure fluctuations', *Chem. Eng. Sci.*, vol. 63, no. 7, pp. 1950–1970, Apr. 2008.
[186] C. Vonesch, T. Blu, and M. Unser, 'Generalized Daubechies Wavelet Families', *IEEE Trans. Signal Process.*, vol. 55, no. 9, pp. 4415–4429, Sep. 2007.
[187] A. M. Gaouda, E. F. El-Saadany, M. M. A. Salama, V. K. Sood, and A. Y. Chikhani, 'Monitoring HVDC systems using wavelet multi-resolution analysis', *IEEE Trans. Power Syst.*, vol. 16, no. 4, pp. 662–670, Nov. 2001.
[188] H. Zang, Z. Wang, and Y. Zheng, 'Analysis of signal de-noising method based on an improved wavelet thresholding', in *9th International Conference on Electronic Measurement Instruments, 2009. ICEMI '09*, 2009, pp. 1-987-1–990.
[189] S. Mallat and W. L. Hwang, 'Singularity detection and processing with wavelets', *IEEE Trans. Inf. Theory*, vol. 38, no. 2, pp. 617–643, Mar. 1992.
[190] L. Su and G. Zhao, 'De-Noising of ECG Signal Using Translation- Invariant Wavelet De-Noising Method with Improved Thresholding', in *Engineering in Medicine and Biology Society, 2005. IEEE-EMBS 2005. 27th Annual International Conference of the*, 2005, pp. 5946–5949.
[191] Y.M. Chen, Y.Y. Zi, and H.R. Cao, 'A data-driven threshold for wavelet sliding window denoising in mechanical fault detection', *Sci. China Technol. Sci.*, vol. 57, no. 3, pp. 589–597, 2014.
[192] M. V. Wickerhauser, *Lectures on Wavelet Packet Algorithms*. 1992.
[193] X. Liu, P. Liu, and S. Cheng, 'A wavelet transform based scheme for power transformer inrush identification', in *IEEE Power Engineering Society Winter Meeting, 2000*, 2000, vol. 3, pp. 1862–1867 vol.3.
[194] Y. F. Xing, Y. S. Wang, L. Shi, H. Guo, and H. Chen, 'Sound quality recognition using optimal wavelet-packet transform and artificial neural network methods', *Mech. Syst. Signal Process.*, vol. 66–67, pp. 875–892, Jan. 2016.
[195] Y. Liu, X. Wang, J. Lin, and W. Zhao, 'Early chatter detection in gear grinding process using servo feed motor current', *Int. J. Adv. Manuf. Technol.*, vol. 83, no. 9–12, pp. 1801–1810, Apr. 2016.
[196] D. Bianchi, E. Mayrhofer, M. Gröschl, G. Betz, and A. Vernes, 'Wavelet packet transform for detection of single events in acoustic emission signals', *Mech. Syst. Signal Process.*, vol. 64–65, pp. 441–451, Dec. 2015.

[197] D. D. Ariananda, M. K. Lakshmanan, and H. Nikookar, ‘A study on the application of wavelet packet transforms to Cognitive Radio spectrum estimation’, in *2009 4th International Conference on Cognitive Radio Oriented Wireless Networks and Communications*, 2009, pp. 1–6.

APPENDIX A THE COMPARISON OF PARTICLE CONTENT IN TESTED OILS

This appendix shows that the used oil contains significantly more particles with larger sizes than the new 15w40 oils, which was measured using Q230 particle analyser after the tests.

2017/11/6 15:46

Customer / Site: Unknown
Machine: Unknown
Equipment Name:
Port Sample Loc: Unknown
Notes:

Sample Date: 2017/11/6
Analysis Date: 2017/11/6 15:41:32
Sample #: CH-4
Operator: LUXINGCHEN
Fluid Type:
Seq#: 4
Operating Hrs/miles: 0
Hrs/mile Overhaul: 0
Hrs/mile oil Change: 0

Address

Phone:
Fax

Wear Debris

Wear Debris Summary:

ISO 4406 (1999)		NAS 1638			NAVAIR 01-1A-17		
Part/1 ml		Part/100 ml		12	Part/100 ml		>6
>4um(c): 42,573.9	23	5-15um	6-14um(c): 1,081,654	12	5-10um	6-10um(c): 926,408	>6
>6um(c): 11,530.7	21	15-25um	14-21um(c): 54,336	11	10-25um	10-21um(c): 209,582	>6
>14um(c): 714.1	17	25-50um	21-38um(c): 15,525	11	25-50um	21-38um(c): 15,525	>6
		50-100um	38-70um(c): 1,552	11	50-100um	38-70um(c): 1,552	>6
		>100um	>70um(c):	00	>100um	>70um(c):	0

Max Diameter Method	(Part/ml)	Max(um)	Mean(um)	20-25um	25-50um	50-100um	>100um
Cutting Wear	31.0	59.7	40.1	15.5	0.0	15.5	0.0
Severe Sliding Wear	186.3	55.2	29.6	93.1	77.6	15.5	0.0
Fatigue Wear	465.7	82.5	27.7	310.5	139.7	15.5	0.0
Non Metallic Wear	62.1	39.1	29.2	15.5	46.6	0.0	0.0
Unclassified Wear	0.0	0.0	0.0	0.0	0.0	0.0	0.0

Free Water (ppm) 0 Viscosity (cP) 1.38

Wear Particle Map - Representative Selection

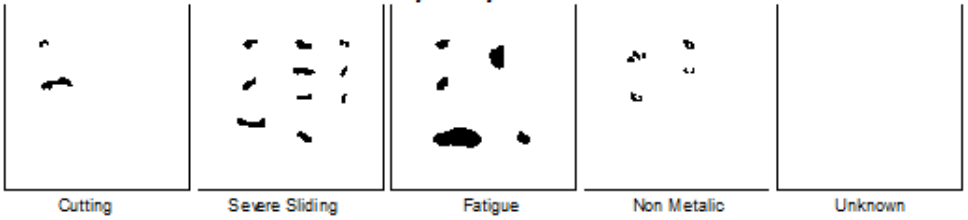

Cutting Severe Sliding Fatigue Non Metalic Unknown

Customer / Site: Unknown
Machine: Unknown
Equipment Name:
Port Sample Loc: Unknown
Notes:

Sample Date: 2017/11/6
Analysis Date: 2017/11/6 20:57:27
Sample #: 15W-40
Operator: LUXINGCHEN
Fluid Type:
Seq#: 8
Operating Hrs/miles: 0
Hrs/mile Overhaul: 0
Hrs/mile oil Change: 0

Address

Phone:
Fax

Wear Debris

Wear Debris Summary:

ISO 4406 (1999)			NAS 1638			NAVAIR 01-1A-17		
Part/1 ml			Part/100 ml		12	Part/100 ml		>6
>4um(c):	33,568.6	22	5-15um	6-14um(c): 978,875	12	5-10um	6-10um(c): 905,910	>6
>6um(c):	10,083.7	21	15-25um	14-21um(c): 29,497	10	10-25um	10-21um(c): 102,462	>6
>14um(c):	295.0	15	25-50um	21-38um(c):	00	25-50um	21-38um(c):	0
			50-100um	38-70um(c):	00	50-100um	38-70um(c):	0
			>100um	>70um(c):	00	>100um	>70um(c):	0

Max Diameter Method	(Part/ml)	Max(um)	Mean(um)	20-25um	25-50um	50-100um	>100um
Cutting Wear	15.5	31.2	31.2	0.0	15.5	0.0	0.0
Severe Sliding Wear	62.1	31.3	26.9	15.5	46.6	0.0	0.0
Fatigue Wear	93.1	25.1	23.5	62.1	31.0	0.0	0.0
Non Metallic Wear	15.5	25.8	25.8	0.0	15.5	0.0	0.0
Unclassified Wear	0.0	0.0	0.0	0.0	0.0	0.0	0.0

Free Water (ppm) 0 Viscosity (cP) 1.33

Wear Particle Map - Representative Selection

Cutting | Severe Sliding | Fatigue | Non Metalic | Unknown